

Charles University
Faculty of Science

Study programme: Developmental and Cell Biology



Mgr. Jakub Gemperle

Analyzing the role of the p130Cas SH3 domain in
p130Cas-mediated signaling

Analýza úlohy SH3 domény proteinu p130Cas v jeho signalizaci

Doctoral thesis

Supervisor: Doc. Daniel Rösler, PhD

Co-supervisor: Doc. Jan Brábek, PhD

Prague, 2018

I hereby declare that I have carried out this work and have written the thesis independently based on my best knowledge and under the guidance of my supervisor. All sources and literature used have been cited properly and this work has not been used to obtain any other academic degree.

Prague, August 2018

.....

Mgr. Jakub Gemperle

I further declare that I have truthfully stated my contribution to the works published with collective authorship in the chapter “Description of research results and their discussion“.

.....

Mgr. Jakub Gemperle

Prague, August 2018

.....

Supervisor: Doc. Daniel Rösel, PhD

ACKNOWLEDGEMENTS

I would like to thank my supervisors Doc. Daniel Rösel, Ph.D. and Doc. Jan Brábek, Ph.D. for the guidance and support they have been providing me during my 9 years-long work in Laboratory of Cancer Cell Invasion. Furthermore, I would like to thank Mgr. Marian Novotný, Ph.D. and Mgr. Martin Lepšík, Ph.D. and Ing. Václav Veverka, Ph.D. for their help with bioinformatics, computational and structural biology.

My many thanks belong to my parents for their love and support. Finally, I would like to thank all my friends and colleagues which went along with me during my studies.

This work was supported by the Grant Agency of The Charles University grants 642012 and 674612, by Czech Science Foundation grants 15-17419S, and by the Ministry of Education, Youth and Sports of CR within the LQ1604 National Sustainability Program II (Project BIOCEV-FAR).

TABLE OF CONTENTS

ACKNOWLEDGEMENTS	3
TABLE OF CONTENTS	4
LIST OF ABBREVIATIONS.....	5
SUMMARY.....	7
SUMMARY IN CZECH	8
1. INTRODUCTION	9
1.1. PROTEIN P130CAS	10
1.1.1. <i>Structure of p130Cas and its interaction partners.....</i>	<i>10</i>
1.2. SH3 DOMAIN	13
1.2.1.1. Structure of the p130Cas SH3 domain.....	16
1.2.1.2. Importance and function of the p130Cas SH3 domain.....	18
1.2.1.2.1. Interaction with kinases (FAK, PYK2, Ack1 and PKN3).....	20
1.2.1.2.2. Interaction with phosphatases (PTP-PEST, PTP-1B).....	22
1.2.1.2.3. Interaction with GEF proteins (C3G, Dock180) and GTPase (Dynamin I)	23
1.2.1.2.4. Interaction with transcription factors CIZ and GLIS2	24
1.2.1.2.5. Interaction with cytoskeletal and adaptor proteins	25
1.2.1.3. Tyr (and Ser/Thr) phosphorylation of p130Cas.....	27
1.2.1.4. Ser/Thr (and Tyr) phosphorylation of p130Cas.....	30
1.2.2. <i>p130Cas function and signaling</i>	<i>34</i>
1.2.2.1. Cellular localization of p130Cas.....	35
1.2.2.2. Mechanotransduction.....	38
1.2.2.3. Cell migration and invasion.....	40
1.2.2.3.1. Role of p130Cas and its SH3 domain in ECM degradation.....	43
1.2.2.4. Malignant growth, cancer progression and drug resistance.....	45
1.2.2.5. Angiogenesis and vascular remodeling.....	50
1.2.2.6. Bone homeostasis	53
2. DESCRIPTION OF RESEARCH RESULTS AND THEIR DISCUSSION.....	55
2.1. CAS DIRECTLY INTERACTS WITH VINCULIN TO CONTROL MECHANOSENSING AND FA DYNAMICS.....	55
2.2. STRUCTURAL CHARACTERIZATION OF CAS SH3 DOMAIN SELECTIVITY AND REGULATION REVEALS NEW CAS INTERACTION PARTNERS.....	57
2.3. NOVEL FRET-BASED SRC BIOSENSOR REVEALS MECHANISMS OF SRC ACTIVATION AND ITS DYNAMICS IN FOCAL ADHESIONS	60
2.4. THE INTERACTION OF PKN3 WITH P130CAS PROMOTES MALIGNANT GROWTH.....	62
3. CONCLUDING REMARKS	65
4. REFERENCES	67
5. APPENDIX: REPRINTS OF THE PUBLICATIONS/PREPRINTS DESCRIBED IN THE THESIS	90
5.1. THE 1 ST PUBLICATION	91
5.2. THE 2 ND PUBLICATION	110
5.3. THE 3 RD PUBLICATION/PREPRINT	129
5.4. THE 4 TH PUBLICATION/PREPRINT	157

LIST OF ABBREVIATIONS

2D	Two d imensional
3D	Three d imensional
Aa	Amino acid
BCAR1	B reast c ancer a nti-estrogen r esistance 1
BCAR3	B reast c ancer a nti-estrogen r esistance 3
CCH domain	Cas family C -terminal h omology domain
Dox	D oxycycline
EC	E ndothelial c ells
ECM	E xtracelullar m atrix
EGF	E pidermal g rowth f actor
EGFR	E pidermal g rowth f actor r eceptor
ER +/-	Estrogen receptor positive (+), negative (-)
ErbB2	V - e rb- b 2 erythroblastic leukemia viral oncogene homolog 2
FA	F ocal a dhesion(s)
FAK	F ocal a dhesion k inase
FAT domain	F ocal a dhesion t argeting domain
FRET	F örster r esonance e nergy t ransfer
GAP	G TPase a ccelerating p rotein
GEF	G uanine n ucleotide e xchange f actor
GTP/GDP	G uanosine t riphosphate/ d iphosphate
GTPase	Epidermal growth factor receptor
HLH	H elix- l oop- h elix
JNK	c - J un N -terminal k inase
Kd	D issociation c onstant
KD	K inase d ead
kDa	k ilo D alton
LPA	L ysophosphatidic a cid
MEFs	Mouse embryonic fibroblasts
MMP	M atrix m etallo p rotease
mPR	mutations disrupting binding to p130Cas
Nedd9	N eural precursor cell expressed, d evelopmentally d own-regulated 9
NGR1	N egative g rowth r egulatory protein 1
NLS	N uclear l ocalization s equence
NMR	N uclear m agnetic r esonance
p130Cas	C rk- a ssociated substrate (130 kDa)
PDB	P rotein d ata b ank
PDGF	P latelet- D erived g rowth f actor
PI3K	activated phosphoinositide 3-kinase
PKN3	P rotein k inase N 3
PNSS	Vinculin mutation disrupting binding to p130Cas
PPII	P olyproline h elix type II
PTP	P rotein tyrosine p hosphatase

PxxP	SH3 core binding motif (P-proline, x- any Aa)
SB region	Src binding region
SC cells	SrcF- transformed p130Cas ^{-/-} MEFs re-expressing p130Cas
SD	Substrate domain
SDE	Short distance element
SDS-PAGE	Sodium dodecyl sulfate–polyacrylamide gel electrophoresis
SFK	Src family kinase
SH2 domain	Src homology 2 domain
SH3 domain	Src homology 3 domain
SRD	Serine rich domain
SRE	Serum response element
VEGF	Vascular endothelial growth factor
VEGFR	Vascular endothelial growth factor receptor
VSMC	Vascular smooth muscle cell(s)
WT	Wild type
Y12E	p130Cas SH3 phosphomimicking mutation in motif ALYD
YxxP	15x repeated YxxP motif rich in p130Cas SD

SUMMARY

The adaptor protein p130Cas (CAS, BCAR1) represents a nodal signaling platform for integrin and growth factor receptor signaling, and influences normal development and tissue homeostasis. Its altered expression drives many pathological conditions including tumor growth, metastasis and drug resistance in many cancer types. How p130Cas contributes to many of these pathologies is still poorly understood. Therefore, the overall aim of my PhD work was to provide new insights to p130Cas signaling and its regulation.

The SH3 domain is indispensable for p130Cas signaling, but the ligand binding characteristics of the p130Cas SH3 domain, and the structural determinants of its regulation were not well understood. To be able to study various aspects of p130Cas signaling we identified an atypical binding motif in p130Cas SH3 domain by establishing collaborations with Dr Veverka (Structural biology) and Dr Lepšík (Computational biochemistry; Academy of Sciences, CZ) which gave new insight into this binding interface. Through these collaborations I generated chimeras of p130Cas SH3 domain with its ligands for structural NMR analysis and learned how to visualize and analyze structures. Furthermore, my work expanded our knowledge of p130Cas SH3 ligand binding regulation and led to a novel model of Src-p130Cas-FAK binding ([see 2.2](#)). Our efforts to monitor Src kinase activity and conformation, which influence how Src phosphorylates p130Cas, led us to construct a novel FRET-based Src biosensor and allowed me to use cutting edge FRET imaging ([see 2.3](#)).

In addition, I developed a bioinformatic workflow to identify novel direct p130Cas binding partners that led to identification DOK7, GLIS2 and PKN3, and helped to validate direct binding to Vinculin. Vinculin-p130Cas interaction was further demonstrated to have a crucial role in mechanosensing and focal adhesion dynamics ([see 2.1](#)), and the interaction with DOK7 and GLIS2 gave insight into neuromuscular and kidney pathologies ([see 2.2](#)). Finally, I helped to demonstrate that p130Cas interacts with Ser/Thr kinase PKN3 in pro-invasive cell invadopodia/lamellipodia and showed that this interaction is important for mouse embryonic fibroblast growth and invasiveness independent of Src transformation, indicating a mechanism distinct from that previously suggested for p130Cas. I further showed the relevance of this work to human breast cancer combining in vitro work with analysis of proteomic data to provide evidence that PKN3 phosphorylates p130Cas in invasive breast tumors ([see 2.4](#)).

SUMMARY IN CZECH

Adaptorový protein p130Cas (CAS, BCAR1) propojuje signalizaci od integrinových receptorů s receptory růstových faktorů a ovlivňuje správný embryonální vývoj a tkáňovou homeostázu. Jeho změněná exprese může vyvolat mnoho patologických stavů, včetně nádorového bujení, metastazování a rezistence vůči různým protinádorovým lékům. Molekulární mechanismy, jakými p130Cas přispívá k různým patologickým stavům nejsou zatím jednoznačně popsány. Cílem mé doktorské práce bylo tedy poskytnout nové poznatky o signalizaci p130Cas a o její regulaci.

Doména SH3 je nepostradatelná pro signalizaci proteinu p130Cas, ale její vazebné preference/regulace nebyly dosud přesně charakterizovány ani strukturně popsány. Proto jsme začali spolupracovat se skupinou Dr. Veverky (Strukturní biologie) a Dr. Lepšíkem (Výpočetní biochemie, AV ČR). S jejich pomocí jsme pak připravili fúzní chiméry SH3 domény proteinu p130Cas se svými ligandy a provedli strukturní analýzu NMR, která nám pomohla strukturně popsat atypický vazebný motiv SH3 domény proteinu p130Cas. Díky této spolupráci jsem se navíc naučil, jak tyto struktury vizualizovat a analyzovat. Tato práce rozšířila naše znalosti o regulaci vazby mezi p130Cas SH3 a jejími ligandy a dále vedla k vylepšenému modelu vazby mezi Src-p130Cas-FAK (see 2.2). Naše snaha sledovat aktivitu kinázy Src a její konformaci, která ovlivňuje, jak Src fosforilyje p130Cas, vedla k vytvoření nového biosenzoru Src na bázi FRET. Díky tomu jsem si vyzkoušel pokročilou zobrazovací mikroskopickou techniku FRET (see 2.3).

Navíc jsem vyvinul pracovní postup, který nám umožnil nalézt nové přímé vazebné partnery p130Cas a identifikovat DOK7, GLIS2 a PKN3, a také pomohl validovat přímou vazbu s Vinculinem. U interakce p130Cas-Vinculin jsme dále prokázali, že má důležitou roli v přenosu mechanického napětí a na dynamiku fokálních adhezí. Interakce s DOK7 a GLIS2 přinesla nový vhled do možných procesů vedoucích k neuromuskulárním a ledvinovým patologiím (see 2.2). Na závěr jsem pomohl prokázat, že p130Cas interaguje se Ser/Thr kinázou PKN3 v pro-invazivních buněčných invadopódiích/lamellipodiích a ukázal, že tato interakce je důležitá pro růst a invazivitu myších embryonálních fibroblastů. Oboje bylo nezávislé na transformaci kinázou Src, což poukazuje na nový mechanismus, který je odlišný od dříve prokázaného pro p130Cas. Fyziologický význam těchto zjištění jsem dále podpořil analýzou proteomických dat z nádorů od pacientů s rakovinou prsu, která poskytla důkaz, že PKN3 fosforilyje p130Cas u invazivních nádorů prsu (see 2.4).

1. INTRODUCTION

Cell interaction with their surrounding environment are governed by signaling cascades emanating from the cell surface receptors. Such signaling circuits must be tightly regulated to ensure proper development, tissue homeostasis and to avoid pathological conditions like cancer. The adaptor protein p130Cas represents a nodal signaling platform for integrin and growth factor receptor signaling, and influences normal development and tissue homeostasis (Tikhmyanova et al., 2010). Its altered expression drives many pathological conditions including tumor growth, metastasis and drug resistance in many cancer types (Camacho Leal et al., 2015). Therefore, new insights into the p130Cas regulation mechanism will not only shed more light on p130Cas signaling but may help to find treatment or prevention to many pathologies related to p130Cas.

This thesis will review the current state of understanding of p130Cas protein biology as in “Table of Contents”, including results of my PhD work, with a strong emphasis on the p130Cas SH3 domain.

1.1. Protein p130Cas

Protein p130Cas was originally described as one of the major proteins phosphorylated on tyrosines in v-Crk (Matsuda et al., 1990) and v-Src-transformed cells (Reynolds et al., 1989). Later, its human ortholog, called BCAR1 (breast cancer resistance 1), was identified. This name reflects its ability to promote resistance of breast cancer patients to tamoxifen treatment (Brinkman et al., 2000).

Protein **p130Cas** (p130 Crk-associated substrate, CAS, BCAR1) is part of the CAS (Crk-associated substrate) family of adaptor proteins. The other family members are **Nedd9** (Neural precursor cell expressed, developmentally down-regulated 9; also known as HEF1 or Cas-L), **EFS** (Embryonal Fyn-associated substrate; also known as SIN) and **CASS4** (Cas scaffolding protein family member 4; also known as HEPL). Although these proteins have high structural and sequence homology, especially in their SH3 domain and the C-terminal domain ([see chapter 1.1.1](#)), their temporal expression, tissue distribution and functional roles are distinct (summarized in Defilippi et al., 2006; Tikhmyanova et al., 2010). Here, I focus on p130Cas, which is ubiquitously expressed and its deletion in mice is embryonic lethal (Honda et al., 1998). Although p130Cas is devoid of any enzymatic or transcriptional activity, its phosphorylation drives formation of multi-protein signaling complexes with pleiotropic effects on cell motility (chemotaxis and migration), cell adhesion, mechanosensing and cytoskeleton remodeling, invasion, survival, proliferation and cell death (summarized in Camacho Leal et al., 2015; Defilippi et al., 2006; Tikhmyanova et al., 2010).

1.1.1. Structure of p130Cas and its interaction partners

Thanks to its modular structure (Defilippi et al., 2006), p130Cas can form many multiprotein signaling complexes ([see Table 1](#)). Analysis of the p130Cas interactome revealed that actin-binding and cytoskeletal-associated proteins represent a major class of p130Cas-interacting proteins and also indicated previously unsuspected p130Cas functions such as regulation of mRNA stability (Evans et al., 2017). Protein p130Cas structure contains an amino-terminal Src homology (SH3) domain, polyproline region, substrate domain (SD), serine rich (SR) domain followed by Src binding region (SB) and the CAS family C-terminal homology domain (CCH).

	Interactor	Significance	Reference
SH3 3-65	FAK	p130Cas phosphorylation	(Polte et al., 1995)
	FRNK	p130Cas phosphorylation	(Harte et al., 1996)
	PYK2	p130Cas phosphorylation	(Li and Earp, 1997)
	Ack1	p130Cas phosphorylation	(Modzelewska et al., 2006)
	PTP1B	p130Cas de-phosphorylation	(Liu et al., 1996)
	PTP-PEST	p130Cas de-phosphorylation	(Garton et al., 1997)
	C3G	Rap1, Ras activation	(Kirsch et al., 1998)
	Dock180	Rac1 activation	(Hsia et al., 2003)
	CD2AP/CMS	Actin cytoskeleton regulation	(Kirsch et al., 1999)
	MICA1	Intermediate filament connection	(Suzuki et al., 2002)
	Dynamin1	EGFR internalization inhibition	(Kang et al., 2011)
	CIZ	MMPs transcription activation	(Nakamoto et al., 2000)
	Vinculin	Mechanosensing	(Janoštiak et al., 2014a)
	DOK7	Neuromuscular synapsis?	(Gemperle et al., 2017)
	GLIS2	Kidney homeostasis?	(Gemperle et al., 2017)
PKN3	Malignant growth, phosphorylation	(Gemperle et al., 2018)	
P 74-87	?	?	?
SD 115-416	IQGAP1?	VEGF-induced cell migration	(Evans et al., 2017)
	Crk family	C3G, Dock180 activation	(Klemke et al., 1998; Sakai et al., 1994)
	Nck	MAPK and Cdc42 signaling	(Schlaepfer et al., 1997)
	SHIP2	Membrane ruffling	(Prasad et al., 2001)
	Abl	p130Cas phosphorylation	(Mayer et al., 1995)
	Zyxin, TRIP6	Cell motility	(Yi et al., 2002)
	CRP2	Inhibiting migration of VSMC	(Chen et al., 2013)
SRD 422-614	14-3-3 proteins	MAPK signaling pathway?	(Garcia-Guzman et al., 1999)
SB 635-667	Src kinase family	p130Cas phosphorylation, invasion, metastasis, bone resorption	(Burnham et al., 1996; Nakamoto et al., 1996; Sakai et al., 1994)
	Bmx/Etk	p130Cas phosphorylation	(Abassi et al., 2003)
	PI3K	p130Cas phosphorylation regulation, Rac1 activation	(Li et al., 2000; Riggins et al., 2003a)
	Grb2	MAPK pathway	(Hakak and Martin, 1999)
	Nephrocystin	Epithelial cell polarity control	(Donaldson et al., 2000)
CCH 730-870	NSP protein family	p130Cas phosphorylation regulation	(Cai et al., 1999; Gotoh et al., 2000)
	Ajuba	Cell motility	(Pratt et al., 2005)
	E2A/E47/E12	p21 transcription repression	(Kim et al., 2004)
	Id2	Transcriptional activity control?	(Law et al., 1999)
	Smad2/3	TRE transcription repression	(Kim et al., 2008)
	CAS family	dimerization	(Braniš et al., 2017; Law et al., 1999)
	Paxillin?	P130Cas targeting to focal adhesion?	(Zhang et al., 2017)
	P140Cap	Inhibits Src kinase activity	(Di Stefano et al., 2004; Di Stefano et al., 2011)

Table 1: Direct (presumably) interaction partners of p130Cas. Besides proteins in table, additional associations with p130Cas (potentially direct) are reported without determining the p130Cas binding site : **Tensin** (Salgia et al., 1996), **MMP14** (Gingras et al., 2008), **SHP-2** (Manie et al., 1997), **ER** (Cabodi et al., 2004), **PLC γ** (Vuori et al., 1996) and **PP2A** (Yokoyama and Miller, 2001a), **Lmo7** (Wozniak et al., 2013), **Vimentin** (Wang et al., 2007), **Nephrocystin 4** (Mollet et al., 2005), **Profilin** and **MRCK β** (Evans et al., 2017).

Note.: Aa numbering according to human p130Cas; TRE (Transcriptional response element), MMPs (matrix metalloproteases).

The **SH3** domain of the p130Cas protein interacts with the polyproline sequences present in many proteins, with the most studied FAK and PYK2 kinases, PTP-PEST phosphatase or C3G protein (references in Table 1 and Table 2, also see chapter 1.2.1.2). In addition, we demonstrated novel direct interactions with Vinculin (Janoštiak et al., 2014a), DOK7 and GLIS2 (Gemperle et al., 2017) and Ser/Thr kinase PKN3 (Gemperle et al., 2018). The structure of p130Cas SH3 domain and function of such interactions will be described in detail in separate chapters (see chapter 1.2.1.1 and 1.2.1.2).

In the **SD** (substrate domain) is the most notable feature the presence of a 15 repetitions of tyrosine-rich YxxP motif, a main site of tyrosine phosphorylation on p130Cas molecule (Mayer et al., 1995). Once phosphorylated, they serve as docking sites for the SH2 domains of adaptor proteins Nck and Crk, SHP-2 phosphatase and Abl kinase (references in Table 1). Among others, it is also assumed that SD is responsible for binding Zyxin family proteins (Yi et al., 2002). Extensive biophysical studies suggest that this region is intrinsically disordered (unstructured), and that mechanical forces associated with stretching of SD may induce an opening that allows phosphorylations by regulatory kinases and association with binding partners (Hotta et al., 2014; Sawada et al., 2006). It is therefore believed that these phosphorylations induced by mechanical tension/stimulation are responsible for the mechanosensitive effects of p130Cas (Sawada et al., 2006). Details will be presented in a separate chapter (see chapter 1.2.2.2).

Next to the SD is the **SR** domain which is characteristically serine-rich (eleven conserved Ser/Thr residues in total). Although SR domain has relatively low sequence homology among other CAS family members, its structure always folds a four-helix bundle (Briknarová et al., 2005). Computational modeling of this structure and biochemical experiments suggest that phosphorylation of rat p130Cas SR domain on Ser592 inside RxxS₅₉₂xP motif (R...Arg, P...Pro, x any Aa) creates a docking sites for 14-3-3 proteins (Briknarová et al., 2005; Garcia-Guzman et al., 1999). This interaction is promoted by cell adhesion to fibronectin and disrupted by phosphatase treatment, but part of this interaction is localized outside SR domain (and SD) and the exact role of this

complex is not determined (Garcia-Guzman et al., 1999). The SR domain of p130Cas is also proved to be important for the transcriptional activation of the serum response element downstream of Src kinase and to support p130Cas SD in anti-estrogen resistant proliferation, but the mechanisms are unclear (Brinkman et al., 2010; Hakak and Martin, 1999). Although p130Cas SR domain is highly phosphorylated on Ser/Thr residues (see [chapter 1.2.1.4](#) and Table 3), their effect on p130Cas signaling and responsible kinases are not known. We have recently identified PKN3 as the first Ser/Thr kinase which is able to both directly bind and phosphorylate p130Cas (on mouse Ser428; see [chapter 1.2.1.2.1](#)) (Gemperle et al., 2018). In addition, Evans et al. have reported p130Cas association with Ser/Thr kinase MRCK β , a regulator of cytoskeleton reorganization and cell migration (Evans et al., 2017).

The **C-terminus** of protein p130Cas is well conserved among the CAS protein family and can be divided into the **SB** region and the **CCH** domain. The **SB** region contains the YDYVHL sequence, which is phosphorylated in response to various stimuli, and the polyproline sequence RPLPSPP (summarized in Tikhmyanova et al., 2010). These two sequences mediate interactions with SH2 and/or SH3 domains of a large number of kinases, such as the Src family (Src, Fyn, Lyn, Lck), Bmx / Etk and PI3K, and of protein Nephrocystin and adaptor protein Grb2 (for reference see Table 1). The **CCH** domain adopts the four-helix bundle fold similar to focal adhesion targeting (FAT) domain (Mace et al., 2011). This feature allows p130Cas to homo / heterodimerize with p130Cas / Nedd9 and interact with Ajuba, Smad3 and HLH transcription factors, and with NSP family proteins (3 members: NSP1, NSP2 / BCAR3 / AND-34 and NSP3 / CHAT(-H) / SHEP1) (for reference see Table 1). NSP protein family interacts with the p130Cas CCH domain by their C-terminal domain which has Cdc25-homology fold of Ras GTPase exchange factors incapable of enzymatic activity. The lack of enzymatic activity is caused by 'closed' conformation that revealed to be required for high affinity interaction with p130Cas (Mace et al., 2011).

1.2. SH3 domain

The SH3 domain is an important interaction module that is conserved from yeast to mammals, and their numbers roughly correlate with genome complexity - human genome encodes around 650 and *Saccharomyces cerevisiae* (yeast) around 165 of individual SH3 domains (Pfam database). SH3 domains are about 60-70 amino acids and

are found in many actin-regulated cytoskeleton proteins, proteins involved in endocytosis, signal transduction and cell death (Carducci et al., 2012). They may also influence protein localization, such as in the case of the p130Cas protein (see chapter 1.2.2.1), or influence kinase activity by intramolecular interactions such as in Src kinase (Nakamoto et al., 1996; Nakamoto et al., 1997). SH3 domains have a very conserved compact β -sandwich architecture formed by 5-6 anti-parallel β -strands arranged in two β -sheets that are approximately right-angled. β -strands are connected by a short 3_{10} -helix and loops of different lengths, of which RT, n-Src and distal loops are functionally the most significant (see Figure 1).

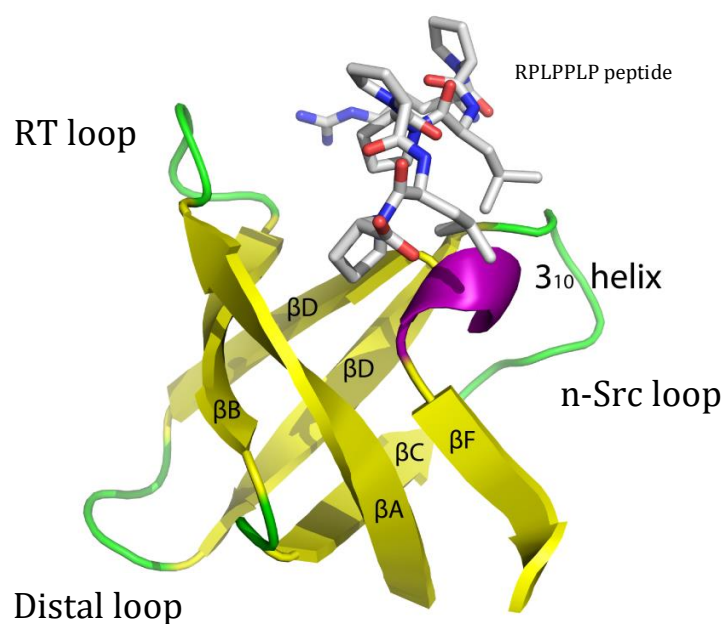


Figure 1: The schematic representation of the SH3 domain binding shown on the Src SH3 domain with RPLPPLP peptide (PDB 1QWF). β -chains are yellow, 3_{10} helix is purple and loops are green. The structure is visualized by PyMOL version 1.4.1 (DeLano, 2002).

SH3 ligands are characterized, in very simplified version, by pseudo-symmetrical PxxP core motif (P - proline, x - any Aa) that assume polyproline helix type II when bound to an SH3 domain. The binding surface of most SH3 domains comprise three discrete patches: two hydrophobic grooves (S1, S2) lined mainly by aromatic amino acid residues that accommodate xP dipeptides, and a groove formed primarily by the RT and n-Src loops to provide the specificity (S3 called “the specificity pocket”). Because these loops are generally sequentially variable among different SH3 domains, they play an important role in determining the recognized binding sequence. Besides hydrophobic amino acids, they usually contain negatively charged residues allowing electrostatic interactions with basic residue of the ligand, such as arginine (R) and lysine (K). These

positively charged Aa have proved to be important for binding to SH3 domains, not only by providing additional binding energy but also by orienting the ligand with respect to the binding groove on the SH3 domain. R/K flanking the core motif PxxP from one side or the other is called “an anchoring amino acid”. Generally, most SH3 domains therefore bind sequences that contain a motif (“Classical”) of either **type I** (R/K)₋₃X₋₂X₋₁P₀X₁X₂P₃ or **type II** P₀X₁X₂P₃X₄(R/K)₅ (see Figure 2)(Li, 2005; Posern et al., 1998). Based on the Aa composition changes in the binding groove, some SH3 domains prefer peptides having one of these motifs, while others accept both and there are ligands completely devoid of this characteristic motif (“Atypical”). These atypical motifs may differ in the sequential preference of a basic Aa or even in their requirement for SH3 binding at all (e.g. PxRP; PxxxPR; PppPppP; RxxKp; PxxDY)(Carducci et al., 2012).

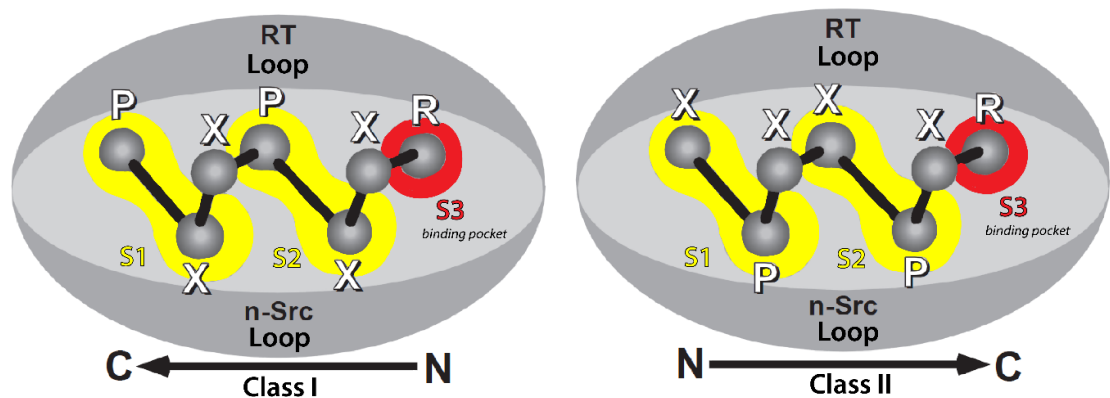


Figure 2: Determination of ligand orientation binding to the SH3 domain. Hydrophobic pockets S1 and S2 are shown in yellow, S3 in red (P represents proline, R anchoring Arginine, X any Aa). Figure is adapted and modified from (Mayer, 2001)

The specificity/affinity of the recognized ligand can be further increased by the additional binding of sequences flanking the primary 6-7 amino acid long binding motif, also known as short distance elements (SDEs), that bind to less conserved portions of the SH3 surface (Agrawal and Kishan, 2002; Gemperle et al., 2017; Wisniewska et al., 2005). Nevertheless, the affinity of SH3 domains is relatively low for its interaction partners, with a dissociation constants (K_d) in the 100 nM - 200 μM range and with margin selectivity, typically common for classical motifs (Li, 2005; Posern et al., 1998). Surprisingly, the interaction of SH3 domains with binding partners can be controlled/regulated by tyrosine phosphorylation on Tyr7 (numbering from N-terminus of SH3; Tyr12 in case of p130Cas SH3) present in the highly conserved motif of ALY₇D (see Figure 3; Tatárová et al., 2012).

1.2.1.1. Structure of the p130Cas SH3 domain

The p130Cas SH3 domain shares the general properties of SH3 domains (Wisniewska et al., 2005) but as we have shown has some very unique features that provide specificity to p130Cas signaling (see Figure 3; Gemperle et al., 2017). First, besides to the typical hydrophobic residues (Tyr12, Val15, Trp43, and pro56) which accommodate the ligand in the hydrophobic grooves S1 and S2, p130Cas SH3 binding pocket S2 is also lined by charged Aa (Asn14, Glu21, Glu17, Arg59) making S2 very polar (Gemperle et al., 2017). This p130Cas SH3 domain atypical property is especially obvious in comparison with SH3 domains of proteins involved in the same signaling circuit, such as the well-defined SH3 domains of Crk, Src, and Grb2 (see Figure 3), and leads to strong electrostatic interactions with Lys (K) of PxK₂P core motif (Gemperle et al., 2017). Furthermore, the specificity pocket S3 (green circle), usually very polar, selectively bind two rather dissimilar optional anchoring residues, leucine (L₅) and arginine (R₅), at position +5. This surprising observation is possible due to the unique presence of Glu17 in the RT loop in combination with Ser18, Asp20, Glu21 (R₅ binding) and Leu40 in the n-Src loop that cooperates with Trp43, Ile54 (L₅ binding). The p130Cas SH3 final high-affinity binding motif is then determined as an atypical motif of class II: (A/P)₋₁P₀X₁K₂P₃X₄(L/R)₅ (Gemperle et al., 2017). The binding specificity and affinity of this motif can be further increased by binding of the flanking ligand residues (SDEs; „short distance elements“) to the p130Cas SH3 domain surface located in the vicinity of the S1 and S3 binding pockets (Gemperle et al., 2017; Wisniewska et al., 2005). Interestingly, N-terminal SDEs (flanking S1) of known p130Cas SH3 ligands are enriched of negatively charged amino acid residues that form transient and strong electrostatic interactions with Lys26 (see Figure 3E, F; Gemperle et al., 2017). This lysine not only contributes to ligand binding affinity, but also play a significant role in the regulation of p130Cas SH3 domain binding negatively controlled by Src-mediated phosphorylation of Tyr12 (Gemperle et al., 2017; Janoštiak et al., 2011; Luo et al., 2008). Phosphorylated Tyr12, which normally attracts ligand's P₀ and P/A₋₁ by CH/π interactions, forms a salt bridge with Lys26 and thus displacing/disrupting the native salt bridges (Lys26:ligand) and CH/π interactions (Tyr12:ligand) (Gemperle et al., 2017).

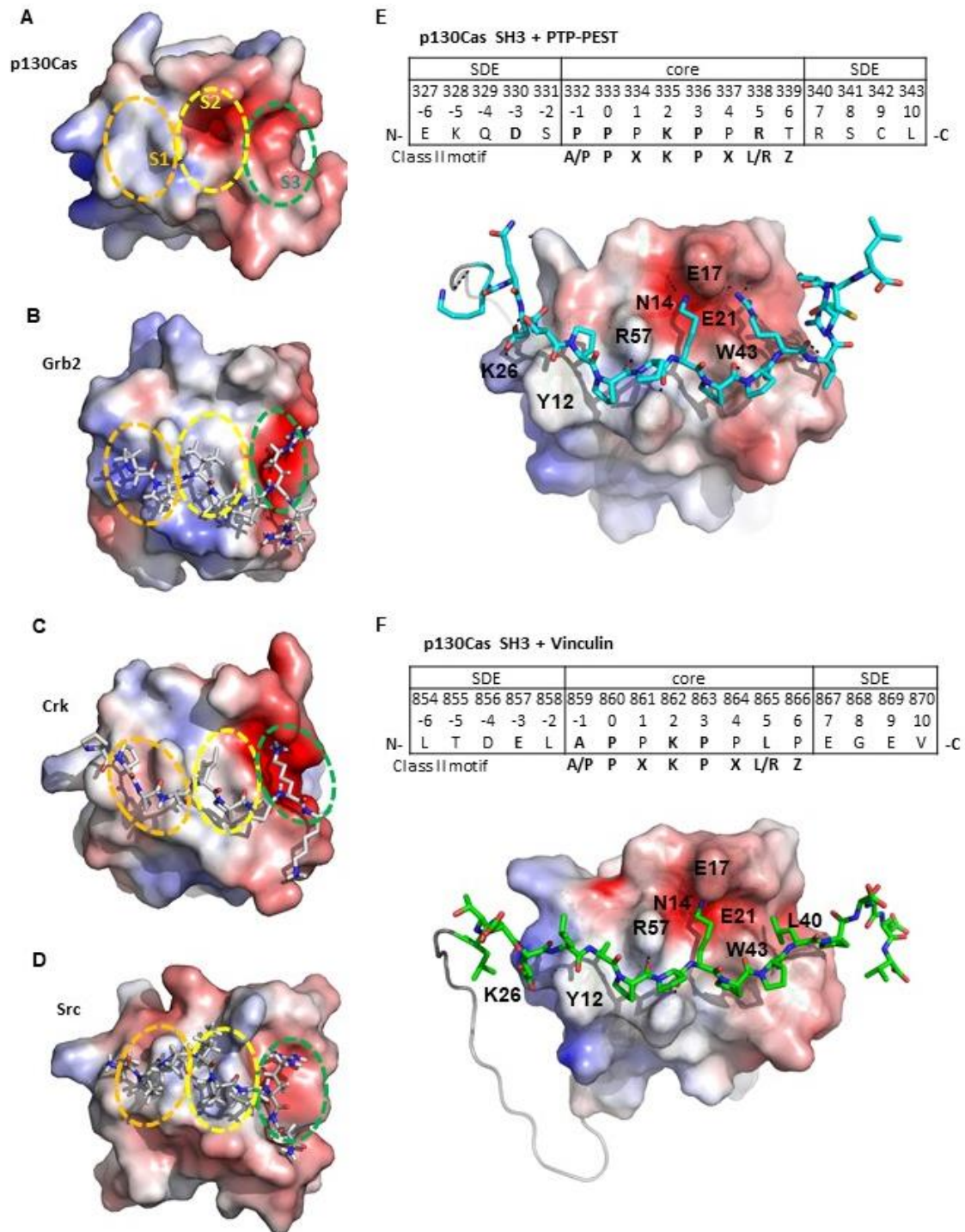


Figure 3: The p130Cas SH3 domain unique properties and its binding to Vinculin and PTP-PEST. (A-D) SH3 domains of proteins involved in the p130Cas signaling circuit. (A) (p130Cas, PDB code 1WYX), (B) (Grb2, PDB code 1AZE), (C) (Crk, PDB code 1CKA), (D) (Src, PDB code 1QWE). The first S1 and second S2 xP dipeptide-binding pockets are highlighted with orange and yellow circles, respectively. The third pocket/zone S3 is highlighted with a green circle. (E) p130Cas SH3 – PTP-PEST chimera (PDB code 5O2P), (F) p130Cas SH3 – Vinculin chimera (PDB code 5O2Q). SH3 domains are shown in electrostatic potential surface representation (APBS colored in the range from -5 to $+5$). Structures are visualized by PyMOL version 1.4.1 (DeLano, 2002). Similar models were used in (Gemperle et al., 2017).

1.2.1.2. Importance and function of the p130Cas SH3 domain

The SH3 domain of p130Cas mediates interactions with many different proteins (see Table 2), thus affects many p130Cas functions (see Figure 4) and in many cases is indispensable for p130Cas signaling as shown by genetic engineering; mice lacking only the p130Cas SH3 domain (*p130Cas SH3^{-/-}*) die in the uterus, as well as mice with the deletion of the whole p130Cas gene (*p130Cas^{-/-}*) (Honda et al., 1998; Tazaki et al., 2008). Besides embryonic development, the p130Cas SH3 domain has a crucial role in mechanosensing by localizing p130Cas to focal adhesions (FA) (see chapter 1.2.2.1) where it regulates focal adhesion dynamics (Janoštiak et al., 2011; Janoštiak et al., 2014a). Furthermore the p130Cas SH3 domain regulates p130Cas Ser/Thr (see chapter 1.2.1.4) and Tyr (see chapter 1.2.1.3) phosphorylation and thus is also implicated in cell invasiveness and cancer progression (see chapter 1.2.2.3 and 1.2.2.4). The SH3 domain of p130Cas can promote cell invasion by stimulating the expression or activation of matrix metalloproteases (MMPs) in both direct and indirect manner (see chapter 1.2.2.3.1). There are also evidences that the p130Cas SH3 domain is also involved in many other pathologies included of a kidney (see chapter 1.2.1.2.5), bones (see chapter 1.2.2.6) and blood vessels (see chapter 1.2.2.5).

	Interactor		Binding motif	Reference
The p130Cas SH3 domain	FAK/FRNK	✓	A ₇₁₁ PPKPSRP P ₈₇₄ PKKPPRP	(Harte, 1996; Ohba et al., 1998; Polte, 1995).
	PYK2	✓	P ₇₁₃ PPKPSRP P ₈₅₅ PQKPPRL	(Li and Earp, 1997; Ohba et al., 1998)
	PTP-PEST	✓	P ₃₃₃ PPKPPRT	(Garton et al., 1997)
	PKN3	✓	P ₅₀₀ PPKPPRL	(Gemperle et al., 2018)
	GLIS2	✓	P ₃₃₃ PPKPPLP	(Gemperle et al., 2017)
	DOK7	✓	P ₅₀₉ PPKPLRP	(Gemperle et al., 2017)
	MICA1	✓	P ₈₂₉ PPKPPRS	(Suzuki et al., 2002)
	CIZ/ZNF384	✓	A ₁₈₇ PPKPPRG	(Nakamoto et al., 2000)
	C3G	✓	A ₂₆₆ PPKPPLP	(Kirsch et al., 1998)
	Vinculin	✓	A ₈₅₉ PPKPPLP	(Janoštiak et al., 2014a)
	PTP1B	✓ *	P ₃₀₈ PPRPPKR	(Liu, 1996)
	CD2AP/CMS	*	Y ₄₀₉ PKRPEKP	(Kirsch et al., 1999)
	Ack1	*	I ₇₄₅ PPRPTRP	(Modzelewska et al., 2006)
	Dynamin1	*	V ₈₃₂ PSRPNRA	(Kang et al., 2011)
	Dock180	*	S ₁₇₃₄ PLRPQRP	(Hsia et al., 2003)

Table 2: The CAS SH3 domain binding interaction partners with their respective binding motifs. ✓ or/and * indicates high or low p130Cas SH3 domain binding motif according to (Gemperle et al., 2017).

As is described in detail in the [chapter 1.2.1.3](#), the most well-known p130Cas SH3 domain role is in both positive and negative regulation of p130Cas SB phosphorylation by interaction with many kinases (e.g. FAK, PYK2, Ack1) and phosphatases (e.g. PTP1B, PTP-PEST; see [Figure 4](#)). Dynamic phosphorylation and dephosphorylation of the p130Cas substrate domain (SD) promoted by functional p130Cas SH3 domain has been shown to be the key to promoting cell migration and invasion (Brábek et al., 2005; Janoštiak et al., 2011; Meenderink et al., 2010). In addition, the p130Cas SH3 domain can promote cell invasion also without change of SD phosphorylation status (Hsia et al., 2003; see [chapter 1.2.2.3.1](#)). Surprisingly, protein p130Cas has six variants encoded by additional alternative first exons generating p130Cas proteins, which differ in the length/sequence preceding SH3 domain and consequently in the expression pattern in the tissues. The longer is the N-terminal linker preceding SH3 domain, the better is the binding to SH3 ligand FAK resulting in changes of cell migration and invasion (Kumbrink et al., 2015). Consistently, p130Cas with a truncated alternatively spliced p130Cas leading to a non-functional SH3 domain has, similarly to p130Cas with deleted SH3 domain (*p130Cas SH3^{-/-}*), reduced binding to FAK, decreased p130Cas SD Tyr phosphorylation and therefore a defect in Crk protein binding and stress fibers formation (Kumbrink et al., 2015; Tazaki et al., 2010).

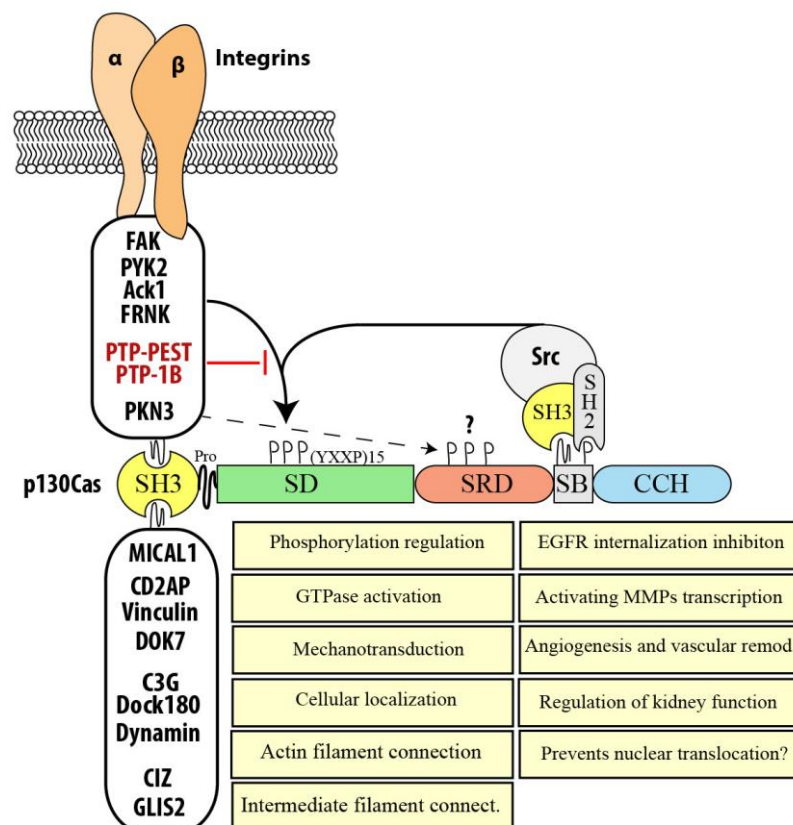


Figure 4: Importance of the p130Cas SH3 domain for p130Cas signaling. Different p130Cas SH3 functions mediated by various interactions are displayed in yellow boxes. Picture drawn in Adobe Illustrator.

In addition, the binding of p130Cas SH3 domain to its interactors, and thus p130Cas localization in cells, can be regulated by Tyr12 phosphorylation (see Figure 3 E, F) which has been identified in the proteome of Src transformed cells (Luo et al., 2008). The Phosphomimicking mutation of Tyr12 to Glu leads to disruption of p130Cas SH3-mediated interactions (e.g. with FAK or PTP-PEST) and to the relocalization of the p130Cas molecule from FA to podosome rosettes resulting in an increase of gelatin degradation of Src transformed mouse embryonic fibroblasts (MEFs) (Janoštiak et al., 2011).

In the following chapters, I will review the individual details of p130Cas SH3 domain interactions, including their potential role in pathological conditions, particularly renal malfunctions. In addition, a summary of current knowledge of p130Cas signaling will be followed, especially relevant for cancer progression and bone homeostasis.

1.2.1.2.1. Interaction with kinases (FAK, PYK2, Ack1 and PKN3)

Interaction of p130Cas with non-receptor tyrosine kinase FAK, its related PYK2 (PTK2B), and dual Tyr-Ser / Thr kinase Ack1 mediated by the p130Cas SH3 domain leads to phosphorylation of the p130Cas SD and hence increased cell migration and/or invasiveness (see chapter 1.2.1.3). In addition, these interactions are important for the localization of p130Cas to the plasma membrane, especially FA (see chapter 1.2.2.1).

FAK kinase binds to the SH3 domain of p130Cas via two binding sequences. A first sequence APPKPSR is located between amino acid residues 711-717 (numbered by human FAK) and has a higher affinity than the other. The second PPKKPPR sequence lies between 874-880 (Harte et al., 1996; Ohba et al., 1998; Polte et al., 1995). A peptide synthesized from FAK kinase (sequence EAPPKPSRP) binds p130Cas SH3 domain with a ca 6 μ M affinity as shown by fluorescence correlation spectroscopy and this affinity is increased to 2 μ M by additional flanking amino acids (sequence EAPPKPSRPGYPS₇₂₂P) that bind to less conserved portions of the SH3 surface (Wisniewska et al., 2005). Ser722 present at the C-terminal SDE of the longer FAK peptide can be phosphorylated during cell adhesion and spreading on fibronectin and this phosphorylation was suggested to negatively regulate FAK activity through decrease p130Cas SH3 binding (Bianchi et al., 2005; Ma et al., 2001). Serine phosphorylation of both FAK and p130Cas is profoundly

evident during mitosis and leads to complete disruption of FAK/p130Cas/Src ternary complex (Yamakita et al., 1999). This complex is further regulated by Src activity itself, because the inhibition of Src kinase prevents p130Cas-FAK dissociation induced by p130Cas Tyr12 phosphorylation (see Figure 7) (Gemperle et al., 2017).

PYK2 kinase (the FAK paralog) shares a 45% sequence identity with the FAK kinase, and interacts with the p130Cas SH3 domain also through two sequences: P₇₁₃PPKPSRP and P₈₅₅PQKPPRL (Ohba et al., 1998). Due to the high sequence homology, PYK2 can partially compensate for the loss of FAK in FAK-mediated signaling events (Lahlou et al., 2012; Sieg et al., 1998). But, unlike FAK, PYK2 is Ca²⁺ dependent and specific functions relevant to p130Cas has been proposed in angiogenesis (see chapter 1.2.2.5), osteoclastic bone resorption (see chapter 1.2.2.6) and even pathological renal diseases (see Figure 5) (Benzing et al., 2001; Ruffanova et al., 2009).

Ack1 belongs to tyrosine kinases, but surprisingly, this kinase is also capable of effective phosphorylation of Ser242 on the protein WASP (Yokoyama et al., 2005). Ack1 is downstream effector of Cdc42 GTPase increasing cell migration on a collagen matrix by Tyr phosphorylation of p130Cas. Cell attachment to collagen stimulates Ack1-p130Cas interaction, but independently of Ack1 kinase activity. The predicted polyproline binding sequence I₇₄₅PPRPTRP of Ack1 does not represent the high-affinity p130Cas SH3 binding motif but both the p130Cas and Ack1 SH3 domains appear to be independently involved in the Ack1-p130Cas association, possibly stabilizing this interaction. Surprisingly, the formation of this complex is strongly stimulated by the deletion of the p130Cas SD, independent of cell adhesion to collagen. This indicates an inhibitory effect of the substrate domain on the constitutive association of p130Cas with Ack1 (Modzelewska et al., 2006).

In addition to these known Tyr kinases, we have recently identified the first Ser/Thr kinase PKN3 which binds directly to p130Cas and phosphorylates p130Cas on Ser432 (Gemperle et al., 2018). PKN3 expression is dispensable for embryonic development (Kraus et al., 2015), but has significant role in progression of different cancer types (Leenders et al., 2004; Unsal-Kacmaz et al., 2011). Interestingly, a therapeutic agent that targets PKN3 by RNA interference (siRNA Atu027) has already completed Phase I clinical trials in a study with patients exhibiting different solid advanced and metastatic tumors, showing very promising results without any adverse effects (Schultheis et al., 2014). PKN3 binds to p130Cas via a central proline-rich sequence of P₅₀₀PPKPPRL and the p130Cas SH3 domain (Gemperle et al., 2018). This

sequence (a synthesized peptide PPPKPPRL) binds the p130Cas SH3 domain with a ca 5 μ M affinity as shown by Isothermal titration calorimetry (Gemperle et al., 2017). This proline-rich motif is well conserved in mammals. Moreover, in humans is almost functionally duplicated (P₅₀₉PPKPPRL; P₅₄₉TRKPPRL). This suggests that this motif has an important role for PKN3. Indeed, we have shown that the interaction of p130Cas with PKN3 mediated by this functional proline-rich motif is necessary for PKN3-induced malignant growth and invasiveness of mouse embryonic fibroblasts independent of Src transformation. Mechanism is unclear, but PKN3 can remodel actin cytoskeleton, binds Actin and Src in p130Cas dependent manner and colocalizes with p130Cas in lamellipodia of MEFs and podosome rosettes of Src transformed MEFs (Gemperle et al., 2018). Furthermore, PKN3 regulate malignant prostate and breast cell growth downstream of activated phosphoinositide 3-kinase (PI3K) independent of Akt (Leenders et al., 2004; Unsal-Kacmaz et al., 2011). Apart from this, literature suggests strong connections with p130Cas in angiogenesis (see chapter 1.2.2.5) and osteoclastic bone resorption (see chapter 1.2.2.6).

1.2.1.2.2. Interaction with phosphatases (PTP-PEST, PTP-1B)

Tyrosine phosphatases PTP-PEST and PTP-1B interact with the p130Cas SH3 domain and this interaction is necessary for efficient dephosphorylation of the p130Cas substrate domain. This, in general, leads to inhibition of cell migration (Garton and Tonks, 1999; Garton et al., 1996; Garton et al., 1997; Liu et al., 1996; Liu et al., 1998), although not always and the resulted outcome depends on the context and expression levels of PTP-PEST and PTP-1B (see below).

We have structurally characterized the complex of p130Cas SH3 with PTP-PEST derived molecule (PDB code 5O2P) containing the sequence corresponding to residues 327-343 (E₃₂₇KQDS-PPKPPRT-R₃₄₀SCL) where interaction of the core binding motif PPPKPPRT is further stabilized by hydrogen bonds formed between both SDEs and less conserved part of the SH3 domain (Gemperle et al., 2017). The p130Cas SH3 domain binds PTP-PEST with a relatively high affinity, much higher (approx. 5-50x) than other SH3 domains binding PTP-PEST. The specificity of p130Cas / PTP-PEST association is further enhanced by strong preference of PTP-PEST for phosphorylated p130Cas due to additional catalytic domain-mediated interaction (Garton et al., 1996; Garton et al., 1997). Recently, a novel regulatory mechanism has been published, involving PTP-PEST,

p130Cas and Vcp (another PTP-PEST substrate) that dynamically balances phosphorylation-dependent ubiquitination of focal p130Cas involved in glioblastoma cell invasion (Chen et al., 2018).

PTP-1B phosphatase is associated with an endoplasmic reticulum and a plasma membrane. This phosphatase binds the p130Cas SH3 domain via the PPPRPPKR sequence, but unlike PTP-PEST, it does not distinguish between phosphorylated and unphosphorylated state of p130Cas. Substrate selectivity is achieved by limited cellular localization of PTP-1B (Flint et al., 1997; Liu et al., 1996). The effect of PTP-1B on p130Cas signaling is more complex (as in PTP-PEST) and involves dynamic interplay between multiple PTP-1B substrates (p130Cas and Crk). PTP-1B phosphatase regulates the binding capacity of p130Cas SD and Crk SH2 domain. In the first case, it dephosphorylates p130Cas and thus prevents binding of the Crk SH2 domain (negative regulation of cell migration), and in the second paradoxically dephosphorylates the Crk SH2 domain, thus potentiate Crk binding to the p130Cas SD. Crk is the preferential substrate of PTP1-B, and the effect, either positive or negative, of PTP-1B on cell migration depends on the correct Crk / PTP1B / p130Cas ratio in the cell (Dadke and Chernoff, 2002; Liu et al., 1996; Liu et al., 1998; Takino et al., 2003).

1.2.1.2.3. Interaction with GEF proteins (C3G, Dock180) and GTPase (Dynamin I)

The adaptor protein p130Cas is functionally associated with interacting partner Crk that binds to p130Cas via its SH2 domain (Chodniewicz and Klemke, 2004). Both p130Cas and Crk have SH3 domain(s) which cooperate to bind GTP / GDP exchange factors (GEF) C3G and Dock180 to promote cell migration, invasion or proliferation ([see chapter 1.2.2.3, Figure 8](#)). Protein C3G contains several proline-rich sequences, most of which are responsible for the interaction with the Crk SH3 domain. The sequence A₂₆₆PPKPPLP with an anchoring leucine at position +5 specifically binds only to the p130Cas SH3 domain (Gemperle et al., 2017; Kirsch et al., 1998).

Crk / p130Cas complex also binds to protein Dock180 through SH3 domains. The sequence S₁₇₃₄PLRPQRP of Dock180 predicted for p130Cas SH3 binding does not possess a high affinity binding motif and therefore a cooperative binding to Crk is probably necessary for the stabilization of p130Cas / Dock180 complex (Gemperle et al., 2017; Hsia et al., 2003; Kiyokawa et al., 1998a).

Interactions of p130Cas with GEFs (e.g. C3G, Dock180) or other proteins (e.g. BCAR3, Grb2...) leads to the activation of small GTPases such as Rac, Ras, Cdc42 and Rap (see Figure 12). In addition, there is evidence that p130Cas SH3 domain is involved in the regulation of GTPase function of Dynamin I. This GTPase is one of the critical regulators of endocytic internalization of the epidermal growth factor receptor (EGFR) and catalyzes membrane fission and vesicle budding (summarized in Praefcke and McMahon, 2004). It was proposed that p130Cas enhances EGFR stabilization at the cell surface in response to cell adhesion by reducing EGFR internalization and degradation through a p130Cas SH3-dependent interaction with proline-rich domain of Dynamin (Kang et al., 2011). The most likely binding site is V₈₃₂PSRPNRA, which does not match the high affinity binding motif, and therefore indirect binding via the third protein is more probable (Gemperle et al., 2017; Kang et al., 2011).

1.2.1.2.4. Interaction with transcription factors CIZ and GLIS2

The p130Cas SH3 domain binds and transactivates transcription factor CIZ (Zinc finger protein 384). This nucleocytoplasmic shuttle protein activates transcription of MMP-1, MMP-3, MMP-7 (Nakamoto et al., 2000). Rat protein CIZ / ZNF384 interacts with the p130Cas SH3 domain directly via the A₁₈₇PPKPPR sequence, whereas the human lacks one key proline and does not interact with the SH3 domain of p130Cas. However, this deficiency bridges another nucleocytoplasmic protein, the protein Zyxin, which interacts with p130Cas and CIZ, thus linking these two proteins (Janssen and Marynen, 2006).

We have demonstrated that GLIS2, a zinc finger transcription factor also referred to as Nephrocystin 7, interacts directly with the p130Cas SH3 domain via P₃₃₃PPKPPLP sequence (Gemperle et al., 2017). The importance of this interaction is not yet clear, but both proteins are implicated in kidney function regulation (see Figure 5) and may regulate kidney cell planar polarity (Attanasio et al., 2007; Donaldson et al., 2000). Loss of GLIS2 function in humans and mice leads to development of nephronophthisis, a recessive cystic kidney disease (Attanasio et al., 2007) caused by a mutation in one of the nine nephrocystin genes (only related by function). Interestingly, Nephrocystin 1 and 4 also interact with p130Cas (Donaldson et al., 2000; Mollet et al., 2005).

1.2.1.2.5. Interaction with cytoskeletal and adaptor proteins

It has been shown that the SH3 domain of p130Cas protein is important for the remodeling of actin cytoskeleton (Tazaki et al., 2008). Therefore, it is not surprising that adaptor protein p130Cas interacts via its SH3 domain with cytoskeletal proteins or other adaptor proteins with potential role in this process. So far have been identified CD2AP, MICA1, Vinculin and recently adaptor protein DOK7 (see Table 1 for references).

CD2AP (CMS) is a multifunctional adapter molecule that mediates interaction between membrane proteins and actin cytoskeleton and contributes to the polymerization of F-actin (Bruck et al., 2006; Lehtonen et al., 2002). Although the interaction between p130Cas SH3 and CD2AP has been proved to be direct, CD2AP contains in its central part only an unsatisfactory binding motif I₄₀₉PKRPEKP (Gemperle et al., 2017; Kirsch et al., 1999). Nevertheless, both CD2AP and p130Cas support renal function (Donaldson et al., 2000; Shih et al., 1999; Welsch et al., 2001) similarly to other p130Cas SH3 domain binding proteins, thereby generating a vast signaling interaction network of proteins implicated in regulation of kidney function (see Figure 5). Moreover, alterations in both proteins are correlated with renal malfunction (Bains et al., 1997; Shih et al., 1999). In detail, mutations in the *CD2AP* gene are associated with sporadic nephrotic syndrome and focal segmental glomerulosclerosis (Gigante et al., 2009). Furthermore, *CD2AP*-deficient mice die at 6 to 7 weeks of age from renal failure as a result of improper formation of a specialized cell-cell junction called the slit diaphragm (Shih et al., 1999).

MICA1 is monooxygenase that promotes depolymerization of F-actin and acts as a cytoskeletal regulator that connects CAS family members (p130Cas or Nedd9) to intermediate filaments (Suzuki et al., 2002; Zucchini et al., 2011). For the p130Cas SH3 binding is responsible a high affinity binding sequence P₈₂₉PPKPPRS of MICA1 (Suzuki et al., 2002).

We have shown that p130Cas forms a direct interaction with Vinculin, an actin filament binding protein and that this binding is mediated by the p130Cas SH3 domain and a proline-rich sequence A₈₅₉PPKPPLP in the hinge region of Vinculin. This interaction have a crucial role in mechanosensing (see 1.2.2.2) and focal adhesion dynamics (Janoštiak et al., 2014a). A peptide synthesized from Vinculin (sequence APPKPPLP) binds the p130Cas SH3 domain with a ca 15 μ M affinity, as shown by Isothermal titration calorimetry. This sequence extended from both sides (L₈₅₄TDEL-APPKPPLP-E₈₆₇GEV) in complex with p130Cas SH3 domain (chimera) is structurally

characterized (PDB code 5O2Q; (Gemperle et al., 2017). In addition to the strong binding of the core motif, N-terminal SDE (LTDEL) makes a significant contribution to binding (Gemperle et al., 2017).

We have experimentally validated that DOK7, which is preferentially expressed in skeletal muscle and heart, interacts directly with the p130Cas SH3 domain via a high affinity binding motif P₅₀₉PPKPLRP (Gemperle et al., 2017). The importance of this interaction is not yet known, but the binding of Crk to DOK7 is similarly as binding of Crk to p130Cas dependent on phosphorylation and Crk-DOK7 complex is important for neuromuscular synapsis formation (Hallock et al., 2010; Vuori et al., 1996). Furthermore, p130Cas is essential in organization of myofibrils, in maintaining integrity of Z-disks in cardiomyocytes (Honda et al., 1998), in regulation smooth muscle contraction (see chapter 1) and associates with Lmo7 transcription factor that has been implicated in the expression of muscle relevant genes (Wozniak et al., 2013). DOK7 has also been implicated in the exercise-stimulated expansion of muscle fibers, which could be related to the mechanosensing function of p130Cas (Haramizu et al., 2014) (see chapter 1.2.2.2).

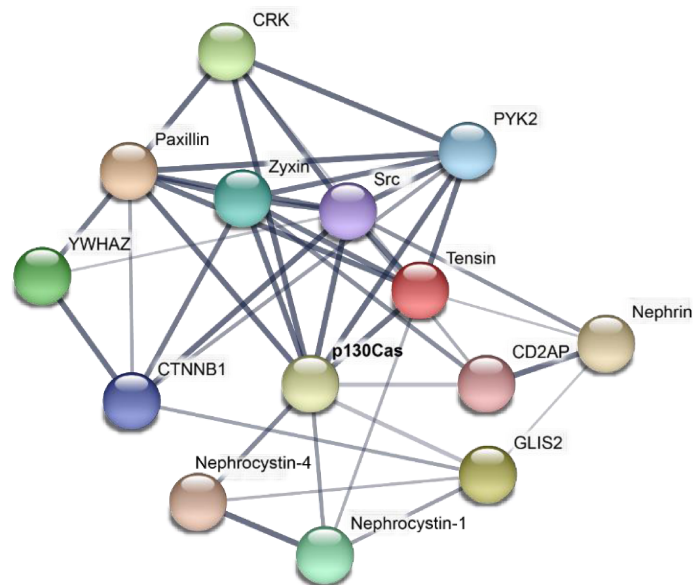


Figure 5: Signaling interaction network of protein implicated in regulation of kidney function. Crosstalk is illustrated with STRING 10 (http://version_10.string-db.org/). Line thickness indicates the strength of data support.

1.2.1.3. Tyr (and Ser/Thr) phosphorylation of p130Cas

Protein p130Cas is composed of 870 amino acids, corresponding to a molecular weight of 93.5 kDa (human; mouse 874 amino acids). On SDS-PAGE, however, p130Cas migrates at 130 kDa. This apparently higher molecular weight reflects the extensive p130Cas phosphorylation, in particular tyrosine and serine phosphorylation (Kanner et al., 1991). Phosphorylation of protein p130Cas rapidly changes in response to many/various internal and external signals. These phosphorylation events affect p130Cas conformation, protein binding ability, cell localization and even stability by regulating p130Cas susceptibility to caspase cleavage (summarized in Bouton et al., 2001). Among the most studied events that lead to p130Cas tyrosine phosphorylation are the binding of integrins to extracellular matrix (ECM), activation of receptors by growth factors (e.g. EGF, PDGF, VEGF), hormones (e.g. antidiuretic hormone, endothelin) or other biologically active molecules (e.g. glucose, LPA) and mechanical stress (Bouton et al., 2001; Konrad et al., 2003; Sawada et al., 2006). Similarly, p130Cas tyrosine phosphorylation plays a crucial role in signaling originating from many mutated or amplified oncogenes such as Ras, PI3K, ErbB2, Crk and Src (Brábek et al., 2004; Cabodi et al., 2010a; Matsuda et al., 1990; Pylayeva et al., 2009; Reynolds et al., 1989). Taken together, such evidences clearly underline a role for p130Cas as a general/universal transmitter of various signaling inputs. Specific cellular responses are achieved by the presence of different multiprotein complexes associated with phosphorylated p130Cas (see chapter 1.2.2).

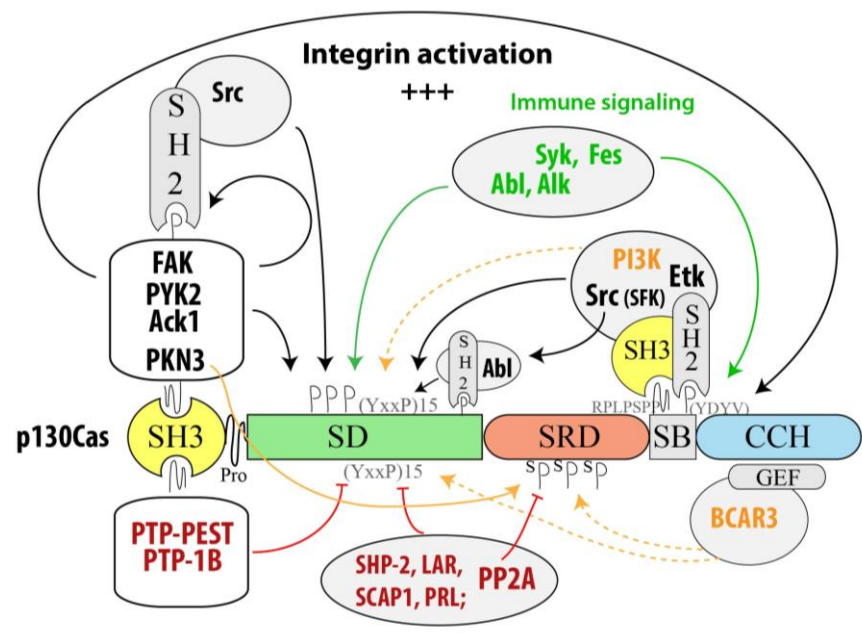


Figure 6: Mechanisms of p130Cas phosphorylation. The scheme describes the p130Cas phosphorylation mechanisms (SD – Tyr, SRD – Ser) and the way the various p130Cas domains are involved in this process. Black arrows indicate direct phosphorylation (integrin signaling), green immune signaling. Orange arrows show the unexplained effect of PKN3, PI3K and BCAR3 on p130Cas phosphorylation (dotted lines – undirect, full lines – direct), while red lines indicate p130Cas dephosphorylation. Scheme drawn by Adobe Illustrator version CS5. *Note: PI3K can bind to p130Cas as well as Src through the SH2 and SH3 domain (Etk via SH2).*

Up to date, 4 regions of protein p130Cas have been detected to be post-translationally modified by Ser/Thr (see chapter 1.2.1.4) or Tyr phosphorylation: SH3 domain (see chapter 1.2.1.1), SR domain, SD and SB region. The mechanism of phosphorylation of the YxxP motifs in the SD mostly involves co-ordination between SH3 and SB domain/region-associated kinases and phosphatases (see Figure 6). The SH3 domain binds FAK and PYK2 kinases which can either directly phosphorylate the YxxP motif or indirectly through Etk / Bmx and Src family kinases (SFK) that associate with p130Cas SB region (YDYVHL motif) in FAK/PYK2 phosphorylation status-dependent manner (Abassi et al., 2003; Nakamoto et al., 1996; Ruest et al., 2001; Tachibana et al., 1997). FAK kinase plays a major role in regulating p130Cas phosphorylation but has only a limited capacity to phosphorylate p130Cas as compared to Src kinase. However, in our lab we have shown that under specific condition of p130Cas localization to a lower topographical layer within the 3D nanostructure of focal adhesions, FAK can represent an effective kinase of p130Cas (Braniš et al., 2017). Nevertheless, the proposed main role of FAK in p130Cas phosphorylation is to function as a docking or scaffolding protein needed for recruitment of Src which afterwards phosphorylates p130Cas. In detail, FAK binding to the p130Cas SH3 domain leads to FAK autophosphorylation (Tyr397) that stimulates Src binding (via SH2 domain) and phosphorylation activity towards p130Cas (Ruest et al., 2001). Recently, we updated this model for Src-mediated regulation of p130Cas-FAK association (see Figure 7). Upon activation, Src associates with both FAK and p130Cas through its SH2 and SH3 domains, respectively. This brings Src kinase catalytic domain into close contact with p130Cas SD, promoting its phosphorylation and stimulation of downstream signaling. Src also phosphorylates Tyr12 (Y12) within p130Cas SH3 domain with lower dynamics (see Figure 3 E, F) that prevents its further binding to FAK and potentially leads to dissociation of the ternary p130Cas-FAK-Src complex. In contrast, Src kinase inhibition enhances the formation/stabilization of this ternary complex (Gemperle et al., 2017).

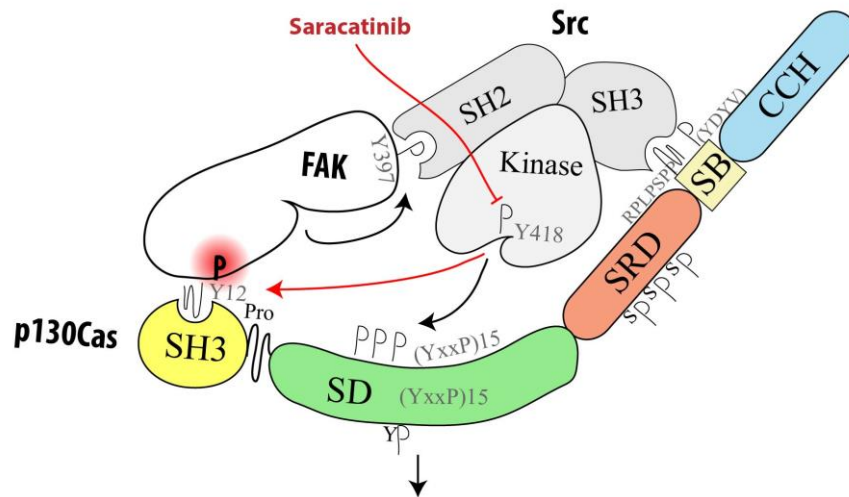


Figure 7: Upgraded model of Src and FAK mediated phosphorylation of p130Cas. In this model, Src upon activation forms a ternary complex p130Cas-FAK-Src that stabilizes the recruitment of each component. This brings Src kinase catalytic domain into close proximity with p130Cas SD resulting in its phosphorylation and activation of downstream signaling. With lower dynamics, Src also phosphorylates Tyr12 (Y12) within p130Cas SH3 domain that disrupts its further binding to FAK potentially resulting in dissociation of the ternary p130Cas-FAK-Src complex. In contrast, Src kinase inhibition enhances the formation/stabilization of this ternary complex. Model was drawn by Adobe Illustrator version CS5 and published in (Gemperle et al., 2017).

Mass spectrometry, directed mutagenesis and phospho-peptide map analysis revealed that Src phosphorylates at least ten YxxP sites (total 15) located between Tyr238 and Tyr414 (Luo et al., 2008; Tikhmyanova et al., 2010; see Table 3). Various kinases may substitute each other in the p130Cas phosphorylation (e.g. Src family kinases or FAK/PYK2), the choice of the particular responsible kinase depends on the cell type and signaling input (Bouton et al., 2001; Klinghoffer et al., 1999).

For leukocytes, in addition to FAK and SFK kinases, p130Cas is recognized and phosphorylated by SYK and FES kinases known primarily in macrophage, B and T lymphocytes signaling (Jucker et al., 1997; Kim et al., 2011; see Figure 6). Similarly to adherent cells (described above), here, the p130Cas protein acts as transmitting scaffold downstream of the cell adhesion. Unbalance of this signaling can lead to SD hyperphosphorylation of YxxP motifs by Abl or Alk kinase, and to the formation of lymphomas or leukemias (Ambrogio et al., 2005; Bazzoni et al., 1996; Salgia et al., 1996). Independently of all described kinases here so far, p130Cas can be also phosphorylated by Ack1 kinase binding to the p130Cas SH3 domain (see chapter 1.2.1.2.1; Modzelewska et al., 2006) and there is another unexplained mechanism leading to the phosphorylation of p30Cas requiring activity of lipid kinase PI3K, but not FAK or Src kinase (see Figure 6) (Armulik et al., 2004).

Besides different signaling inputs and cell types, p130Cas phosphorylation is regulated spatially and temporally by association with various binding partners. For example, NSP proteins affect p130Cas phosphorylation and thus cell migration by inducing p130Cas translocation from cytosol to FA and lamellipodia (Makkinje et al., 2009; Riggins et al., 2003b; Schrecengost et al., 2007). NSP proteins, mainly BCAR3, bridge receptors ErbB, Eph and EGFR (Dodelet et al., 1999; Kim et al., 2009) present at the plasma membrane with p130Cas and Src kinase which leads to stimulation of p130Cas tyrosine phosphorylation (Riggins et al., 2003b; Schuh et al., 2010). Surprisingly, BCAR3 also promotes p130Cas serine phosphorylation ([see 1.2.1.4](#)) (Makkinje et al., 2009).

Tyrosine dephosphorylation of p130Cas executes tyrosine phosphatases PTP-1B, PTP-PEST, SHP-2, LAR, SCAP1 and PRL (Manie et al., 1997; summarized in Tikhmyanova et al., 2010). Of these, PTP-PEST and PTP-1B directly bind to the p130Cas SH3 domain (Garton et al., 1997; Liu et al., 1996; [see chapter 1.2.1.2.2](#)). Generally, tyrosine phosphorylation of p130Cas leads to induction of cell migration, whereas dephosphorylation interferes with it and often leads to degradation of p130Cas and apoptosis (summarized in Tikhmyanova et al., 2010).

1.2.1.4. Ser/Thr (and Tyr) phosphorylation of p130Cas

Protein p130Cas was first identified as a pTyr-containing 130 kDa protein in cells transformed by v-src (Reynolds et al., 1989) and v-crk oncogenes (Matsuda et al., 1990). This discovery triggered a new era of investigation of the importance of tyrosine phosphorylation and p130Cas protein function. Although, soon after Reynolds's and Matsuda's findings, Kanner et al. demonstrated that the p130Cas phosphorylation resembles the most serine phosphorylation (more than tyrosine), only little progress has been made in understanding p130Cas Ser/Thr phosphorylation compared to Tyr. This can be nicely demonstrated by the Phosphonet database, repository of known and by P-Site algorithm predicted phosphorylation sites (<http://www.phosphonet.ca/>) that predict p130Cas phosphorylation on 27 tyrosines, 21 threonines and 37 serines. Of these phosphosites, most of Tyr were verified, but only a few of Ser/Thr ([see Table 3](#)). That suggests that many phosphorylated serine and threonine residues remain unidentified -

especially in the Serine-rich domain. Furthermore, tens of tyrosine kinases have been reported to phosphorylate p130Cas (see 1.2.1.3). In contrast, we have recently identified the first Ser/Thr kinase, pro-malignant PKN3, able to directly bind and phosphorylate p130Cas (Gemperle et al., 2017; Gemperle et al., 2018).

Domain	Nedd9	p130Cas				Importance of the phosphorylation	
	Human	Human	Mouse	Rat	iso2		
SH3	Y12-p	Y12-p	Y12-p	Y106	Y12	Disrupts binding	
SD	Y112-p	Y128-p	Y132-p	Y226-p	Y132-p	Allows Crk binding	
SD	Q127	S134-p	N138	N232	N138	Induced by BCAR3; effect?	
SD	V134	S139-p	S143-p	S237	S143-p	Allows binding of SH2 containing proteins such as Crk, Nck, SHIP2, Abl	
SD	T156	Y165-p	Y169-p	Y263-p	Y169-p		
SD	Y166-p	Y179	Y183	Y277-p	Y183-p		
SD	Y177-p	Y192-p	Y196-p	Y290-p	Y196-p		
SD	P199	Y222-p	Y226-p	Y320	Y226		
SD	F201	Y224-p	Y228-p	Y322	Y228		
SD	/	Y234-p	Y238-p	Y332-p	Y238-p		
SD	Y214-p	Y249-p	Y253-p	Y347-p	Y253-p		
SD	Y223-p	Y267-p	Y271-p	Y365-p	Y271-p		
SD	I225	T269-p	T273-p	T367	T273		
SD	Y241-p	Y287-p	Y291-p	Y385-p	Y291-p		
SD	P246	S292-p	S296	S390	S296		
SD	Y261-p	Y306-p	Y310-p	Y404-p	Y310-p		
SD	T268	S313	S317	S411	S313		Prevents cleavage by Caspase 3
SD	N280	T326-p	T330-p	T424	T330		Allows binding of Crk, Nck, SHIP2, Abl
SD	C281	Y327-p	Y331-p	Y425	Y331		Disrupts Aurora A binding to Nedd9
SD	S296-p	P345	P349	P443	P349	Allows binding of SH2 containing proteins such as Crk, Nck, SHIP2, Abl	
SD	G307	Y362-p	Y366-p	Y460	Y366		
SD	Y317-p	Y372-p	Y376-p	Y470	Y376		
SD	/	T385-p	T389-p	T483	T389		
SD	P329	Y387-p	Y391-p	Y485-p	Y391-p		
SD	H350	Y410-p	Y414-p	Y508-p	Y414-p		
SRD	S369-p	S428-p	S432	S526	S432	Nedd9 degradation by proteasome p130Cas phosphor. by PKN3; effect?	
SRD	S378	S437-p	S441	S535	S441-p	Induced by BCAR3; effect?	
SRD	G439	S494	S498	S592	S498	14-3-3 binding	
SRD	H496	H552	Y556-p	Y650-p	Y556	?	
SRD	S503	G568	S572-p	G666	G572	?	
SRD	P521	S569	P573	P667	P573	?	
SB	/	S639-p	S643	S737	S643-p	Induced by BCAR3, Src binding?	
SB	K609	S645	S649	S743	S649	Prevents cleavage by Caspase 3	
SB	S618	Y653-p	Y657	Y751-p	Y657		
SB	Y629-p	Y664-p	Y668-p	Y762-p	Y668	Allows binding of Grb2, Src family kinases and kinase FES	
SB	Y631-p	Y666-p	Y670-p	Y764-p	Y670		
CCH	S667	K702-u	K706	K800	K706	?	

Table 3: Verified p130Cas phosphorylation sites or predicted by analogy/homology with Nedd9. Phosphorylated amino acid residues verified by MS analysis are in blue. Note: Iso2 is shorter isoform of rat p130Cas. *Phosphorylation* = -p; *Ubiquitylation*= -u. Data obtained from <http://www.phosphonet.ca/> and <https://www.phosphosite.org>

Here, I will summarize the current knowledge about the p130Cas Ser phosphorylation and compare it to p130Cas Tyr. Both Ser and Tyr phosphorylation of p130Cas appears to be regulated by the cell cycle or cell adhesion and affects the sensitivity to caspase cleavage (Tikhmyanova et al., 2010). Although these two types of phosphorylation are likely to predetermine p130Cas to a different function (Pugacheva et al., 2006), in some cases they regulate the same signaling events, and it appears that tyrosine phosphorylation affects Ser and vice versa (Kanner et al., 1991; Yokoyama and Miller, 2001b). During mitosis, p130Cas is similarly as other proteins of FA complex (e.g., FAK) dephosphorylated on tyrosines followed by Ser phosphorylation. This Ser phosphorylation disrupts the interaction of FAK with p130Cas, resulting in the prevention of FAK dependent p130Cas tyrosine phosphorylation and functional integrin signaling (Yamakita et al., 1999). At the end of mitosis, the original ratio is restored in part by the Ser/Thr phosphatase PP2A that associates with protein p130Cas. This association is dependent on the activity of tyrosine kinase Src, which stimulates the association (Yokoyama and Miller, 2001b). The loss of cell adhesion occurs not only during mitosis but also during apoptosis where Caspase 3 generates 74 kDa and 31 kDa fragments of p130Cas. The apoptosis is stimulated by p130Cas Tyr and Ser dephosphorylation while serine and tyrosine phosphomimicking mutations (S411, S743, Y751 rat numbering), neighboring to the p130Cas cleavage sites, prevent cell death (Hoon Kim et al., 2003).

Ser phosphorylation of the p130Cas protein, similarly as Tyr, can be stimulated by seeding cells on fibronectin, and therefore part of Ser phosphorylation is dependent on cell adhesion (Schlaepfer et al., 1997). Compared to Tyr, Ser phosphorylation has different dynamics. Suspension MDA-231B cells restore p130Cas tyrosine phosphorylation to the original level after attachment to fibronectin within minutes, while serine after several hours (Makkinje et al., 2009). This adhesion-dependent p130Cas Ser phosphorylation can be stimulated by mouse CHAT-H and human BCAR3/NSP2 proteins (but not NSP1 or NSP3) from the NSP family although mechanism is not clear. This Ser phosphorylation was mainly dependent on the p130Cas SH3 domain, required proline/serine-rich domains of BCAR3 and N-terminal part of BCAR3 and CHAT-H (Makkinje et al., 2009; Regelman et al., 2006). Makkinje et al. further suggested that BCAR3 induced p130Cas Ser phosphorylation correlates with invasive MDA-231MB

cell phenotype (Makkinje et al., 2009) and Regelmann et al. demonstrated (on Nedd9 – close member of CAS family) that Ser/Thr localized in SR domain are even necessary for T-lymphocytes migration and integrin mediated adhesion (Regelmann et al., 2006). In addition, a rat p130Cas has been shown to interact with 14-3-3 proteins in a phosphoserine-dependent manner (rat Ser592 corresponds to human Ser494), which occurs mainly at lamellipodia during integrin-mediated cell attachment to the extracellular matrix (ECM) (Garcia-Guzman et al., 1999).

Protein p130Cas, similarly to Nedd9, exists in cells in two main isoforms, which are attributed to different Ser/Thr phosphorylation (Hivert et al., 2009; Makkinje et al., 2009). Depending on the cell type, p130Cas protein is present upon SDS-PAGE as a single protein or detected as a doublet with the increased proportional representation of the upper band correlating with cell aggressive properties (Janoštiak et al., 2011; Makkinje et al., 2009). The resolution of p130Cas migration profile on SDS-PAGE can be further improved using an acrylamide/bisacrylamide ratio of 30:0.2 (Gemperle et al., 2018; Hivert et al., 2009) to two pairs of migrating doublets. In MEFs, p130Cas migrates on SDS-PAGE as 4 bands with the most pronounced form migrating the slowest. Mutation of all 15 Ser/Thr inside p130Cas SR domain, similarly to the single mutation of Ser432, lead p130Cas to migrate only in the form of two fastest (lower doublet) migrating bands (Gemperle et al., 2018). The SH3 (also partly CCH) domain of p130Cas seems to be important for this phosphorylation (Gemperle et al., 2018; Makkinje et al., 2009). Consistently, we have shown that phosphorylation of p130Cas Ser432 (homologous to human Ser428) can be catalyzed by PKN3 kinase which binds to the p130Cas SH3 domain ([see 1.2.1.2.1](#)) and is enriched in breast carcinoma tumors where it correlates with PKN3 activity (Gemperle et al., 2018). The effect of this phosphorylation is, however, not clear, although literature can offer some suggestions. Notably, p130Cas paralog Nedd9 was found to be phosphorylated on Ser369, which is homologous to p130Cas Ser432. Mutation of Ser369 to alanine, similarly to mutation of p130Cas Ser432, induces p130Cas mobility shift upon SDS-PAGE from 4 bands to two faster migrating bands. Although the kinase responsible for Nedd9 Ser369 phosphorylation is unknown, this modification was shown to induce Nedd9 proteasomal degradation (Hivert et al., 2009). Protein levels of p130Cas, however, are stable during the cell cycle and exhibit a constant expression levels in cells under non-pathological settings (Tikhmyanova et al., 2010). Therefore, the effect of p130Cas Ser432 phosphorylation is likely different from that of Ser369 in Nedd9.

1.2.2. p130Cas function and signaling

As described in (chapter 1.1), protein p130Cas represents a nodal signaling platform mediating crosstalk from many different inputs and therefore, p130Cas exerts many various functions like cell migration and invasion (see chapter 1.2.2.3), cell survival (see chapter 1.2.2.4) and have far-reaching implications like regulation bone homeostasis (see chapter 1.2.2.6) and angiogenesis (see chapter 1.2.2.5). Its altered expression drives tumor growth, metastasis and drug resistance in many cancer types (see chapter 1.2.2.4; (Camacho Leal et al., 2015) and its unique biophysical properties allows to act as mechanosensor (see chapter 1.2.2.2). In following chapters I will address these functions in detail and start with the p130Cas cellular localization as it reflects different p130Cas functions.

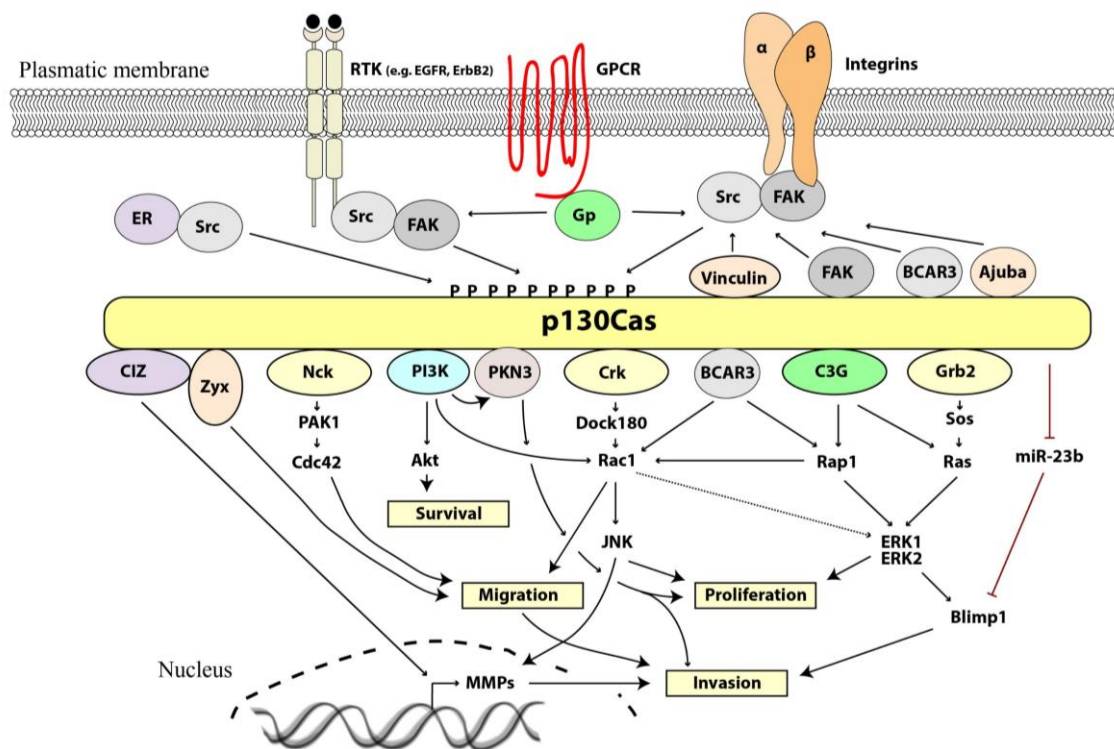


Figure 8: Summary of signaling pathways involving p130Cas. Estrogen receptors (ER), Receptors tyrosine kinases (RTK), G protein-coupled receptors (GPCR), heterotrimeric G protein complex (Gp), MMPs (Matrix Metalloproteases). Adapter proteins (Nck, Crk, Grb2 in yellow) bind to p130Cas only after phosphorylation. See text for details.

Note: FAK, BCAR3, Vinculin and Ajuba also support p130Cas localization near the plasma membrane. JNK and transcription factor CIZ may translocate to the nucleus after stimulation. Figure drawn in Adobe Illustrator version CS5.

1.2.2.1. Cellular localization of p130Cas

Protein p130Cas is spatiotemporally regulated and its localization reflects/permits its function and signaling (see Figure 9; for details see Tikhmyanova et al., 2010). The most studied p130Cas localization is at focal adhesions (FA) and at the edge of lamellipodia, structures that mediate cell attachment to the extracellular matrix (Fonseca et al., 2004; Nakamoto et al., 1997; Polte and Hanks, 1997) and allow cell migration (see chapter 1.2.2.3 and Figure 13). Protein p130Cas concentrates at FAs mainly via its SH3 domain (see chapter 1.2.2.2). Here, FAK or Src kinase phosphorylate p130Cas on YxxP motifs (p130Cas SD) and subsequently on Tyr12 (SH3 domain) leading to increase of focal adhesion turnover (Janoštiak et al., 2011).

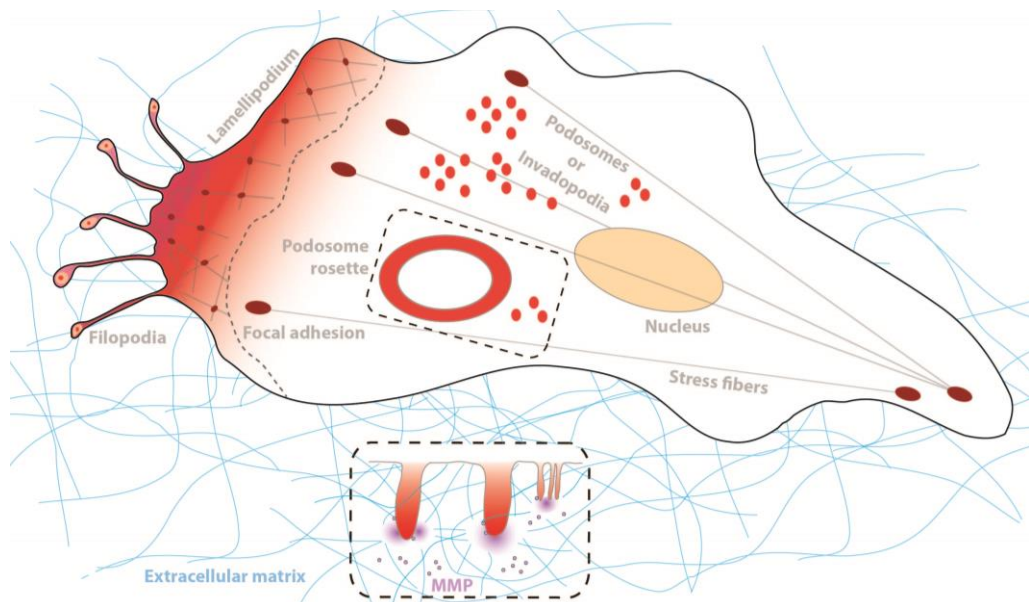


Figure 9: Different cellular structures where p130Cas is localized. Protein p130Cas activates multiple downstream effectors to promote formation of filopodia, lamellipodia, podosomes/invadopodia/podosome rosettes and induce additional changes in the cytoskeleton that support migration. Cellular structures where p130Cas localizes are visualized in orange-red colors. See text for details.

Protein p130Cas is also enriched in podosomes/invadosomes (podosome rosettes; see Figure 9), where the focal adhesion proteins are assembled, of invasive carcinoma cells (see chapter 1.2.2.3.1), Src-transformed MEFs, osteoclasts (see chapter 1.2.2.6) and endothelial cells (see chapter 1.2.2.5) and therefore contributes to the extracellular matrix degradation (See chapter 1.2.2.3.1) (Honda et al., 1999; Lakkakorpi C et al., 1999; Nakamoto et al., 1997). Although p130Cas is not required for focal adhesion formation, it is necessary for podosome rosette assembly (Brábek et al., 2004; Honda et al., 1999; Lakkakorpi C et al., 1999; Nakamoto et al., 1997). While p130Cas YxxP motifs are essential for podosome rosettes formation of Src transformed MEFs and p130Cas SH3 is

involved only partly (Brábek et al., 2005; Pan et al., 2011), for osteoclast, the p130Cas SH3 domain is critical, by binding PYK2 kinase (Lakkakorpi C et al., 1999; Nagai et al., 2013). Surprisingly, functional SH3 domain is not necessary for p130Cas targeting to podosomes (in contrast to FAs) (Janoštiak et al., 2011). The protein composition of podosomes and FAs, thought very similar, differs in several critical components (e.g. PKN3 and Cortactin are only in podosomes/rosettes while FAK, Vinculin or Paxillin are in both structures (Bowden et al., 1999; Gemperle et al., 2018; Linder and Aepfelbacher, 2003).

In contrast to FAK, Vinculin and Paxillin, protein p130Cas is also part of adhesive complexes in filopodia which extend from the cell leading edge and create new dynamic adhesions. At filopodial tips, p130Cas is hyperphosphorylated (Brábek et al., 2004; Gustavsson et al., 2004). This phosphorylation has been demonstrated by an elegant technical approach with specific p130Cas-dependent activation of membrane-anchored Src that leads to lengthened filopodial adhesions (and their number), increased cell spreading and produces a limited burst of cell protrusions as (Karginov et al., 2014). This effect is probably promoted by Src-p130Cas-Crk-Dock180-Rac pathway (Gustavsson et al., 2004) that also supports cell migration (see chapter 1.2.2.3) through lamellipodia. A number of proteins has proved to be important for targeting p130Cas to lamellipodia (Fonseca et al., 2004), allowing its efficient phosphorylation by Src or FAK: e.g BCAR3 (Riggins et al., 2003b; Schrecengost et al., 2007) and Ajuba protein (Pratt et al., 2005) that bind to the p130Cas CCH domain (see Table 1).

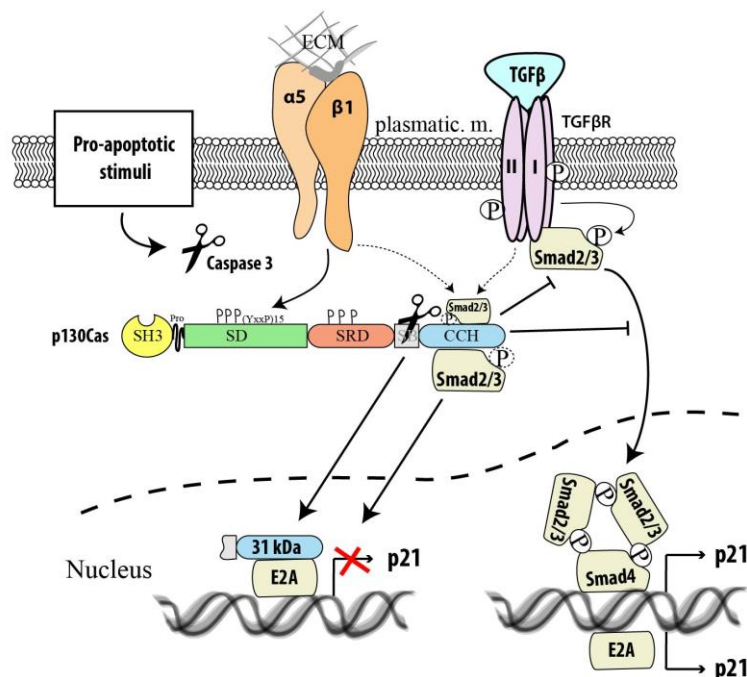


Figure 10: Protein p130Cas in nucleus acts as negative transcription regulator. During apoptosis, caspase 3 cleaves protein p130Cas on 31 kDa C-terminal fragment which binds transcription factor E2A and translocates to the nucleus. This prevents E2A from heterodimerizing with its coactivators on the promoter of *p21* gene. Furthermore, p130Cas inhibits TGF β -mediated growth arrest: Once tyrosine-phosphorylated via integrin signaling, p130Cas binds to and sequesters Smad3 and thus reduces its phosphorylation. That in turn leads to inhibition of p15 and p21 expression and facilitation of cell cycle progression. *Figure drawn in Adobe Illustrator version CS5.*

Phosphorylation of p130Cas also appears to be enriched in the nucleus, unlike unphosphorylated p130Cas molecules that are diffusely distributed in the cytosol (Kanner et al., 1991; Sakai et al., 1994). The p130Cas function in the nucleus is still little explored, but it has been shown that p130Cas can be cleaved by caspase 3 to 31 kDa fragment (CCH with part of the SB region) which is then enriched in the nucleus (see Figure 10). Excess of this C-terminal fragment is likely to cause disruption of FAs and leads to cell apoptosis or anoikis (Casanova et al., 2006; Kim et al., 2004). The ability of p130Cas to translocate between the nucleus and the cytoplasm suggests that p130Cas may act as a direct transcriptional regulator. Indeed, it can directly interact with transcription factors to prevent the activation of p21, a cyclin-dependent kinase inhibitor that cause growth arrest. Following integrin stimulation, protein p130Cas binds and sequesters Smad2/3 proteins in the cytoplasm, thus preventing their phosphorylation-dependent transactivation and translocation into the nucleus to activate the expression of p21 (Kim et al., 2008; Wendt et al., 2009). This explains one of many mechanisms by which p130Cas regulates cell proliferation (for further details see chapter 1.2.2.4). On the other hand, the expression of p21 can also be induced by E2A / E47 transcription factors which prevents cell apoptosis. The 31 kDa fragment of p130Cas heterodimerizes with E2A / E47 proteins in the nucleus and prevents their binding to DNA (Kim et al., 2004). Protein p130Cas lacks its own nuclear localization signal (NLS), so its nuclear transport is completely dependent on proteins that have it. The truncated form of p130Cas enters the nucleus by heterodimerization with E2A / E47 (Kim et al., 2004). The nuclear translocation mechanism of full version of p130Cas remains unclear, but microscopic experiments with p130Cas deletion mutants suggest that the p130Cas SH3 domain may have a negative effect on its nuclear localization (Donato et al., 2010; Kim et al., 2008; Tazaki et al., 2008; our observation). Given this observation, it is interesting to note that a deficiency of p130Cas exon 2 (encodes the SH3 domain) in primary fibroblasts leads to augmented I κ B α nuclear activity and up-regulation expression of CXC Chemokine Receptor-4 and CC Chemokine Receptor-5 (Tazaki et al., 2008).

1.2.2.2. Mechanotransduction

Cellular responses to mechanical force/fluid flow underlie many critical functions from normal morphogenesis to carcinogenesis (see chapter 1.2.2.4), wound healing, sensory receptors (hair cells), glomerulo-tubular balance in renal epithelial cells (Weinbaum et al., 2011), cardiac hypertrophy and vascular remodeling (see chapter 1.2.2.5), and bone homeostasis (see chapter 1.2.2.6). Cells form FAs and podosomes/invadosomes (see Figure 9) that are responsible for bi-directional information exchange between the cell and its surroundings (ECM). These structures transfer external forces via integrin receptors to cytoskeletal and signaling proteins inside the cell (called mechanosensing). Cells convert physical stimuli that convey information about the cell's environment to biochemical signaling (called mechanotransduction) by force-induced conformational changes of mechanosensors like Talin and p130Cas (summarized in Janoštiak et al., 2014b).

Protein p130Cas is upon integrin engagement/activation translocated to FAs (podosomes) and phosphorylated in SD on tyrosines (Fonseca et al., 2004). This phosphorylation is increased in response to mechanical stretch (see Figure 11) both in intact cells and in vitro and is crucial for mechanotransduction signaling (Sawada et al., 2006). Luo et al. and Hotta et al. demonstrated by extensive biophysical experiments that the substrate domain forms a compact folded structure in non-stretched conditions (Hotta et al., 2014; Lu et al., 2013). In addition, Hotta et al. speculate that this tightly packed fold is further stabilized by LIM domain containing proteins such as Zyxin (Yi et al., 2002), which bind to unphosphorylated SD and thus physically protect p130Cas SD from phosphorylation (Hotta et al., 2014). In all models the compact SD structure (possibly with Zyxin) blocks the accessibility of tyrosine residues to phosphorylation and is after mechanical stretching unfolded (Zyxin released) and exposed tyrosines phosphorylated by Src-family kinases (Hotta et al., 2014; Lu et al., 2013; Sawada et al., 2006). The stretch-induced SD phosphorylation stimulates the binding of Crk/C3G complex that activates Rap1 GTPase to potentiate ERK/p38 signaling (Sawada et al., 2006; Tamada et al., 2004). This p130Cas/Crk/C3G-Rap1-ERK pathway could promote the cancer cell growth as tumor-surrounding tissue is stiffer than the tumor cells themselves and ECM rigidity stimulate cell proliferation (Tilghman et al., 2010).

Moreover, invasive cells sense ECM-rigidity through invadopodia by myosin II-FAK/p130Cas pathway and this signaling leads to increased matrix-degrading activity

(Alexander et al., 2008). Similarly, FAs or/and podosomes of vascular smooth muscle/endothelial cells (see chapter 1.2.2.5) and osteoclasts (see chapter 1.2.2.6) are able to sense and respond to the physical properties of the surrounding environment (Geblinger et al., 2010; Juin et al., 2013).

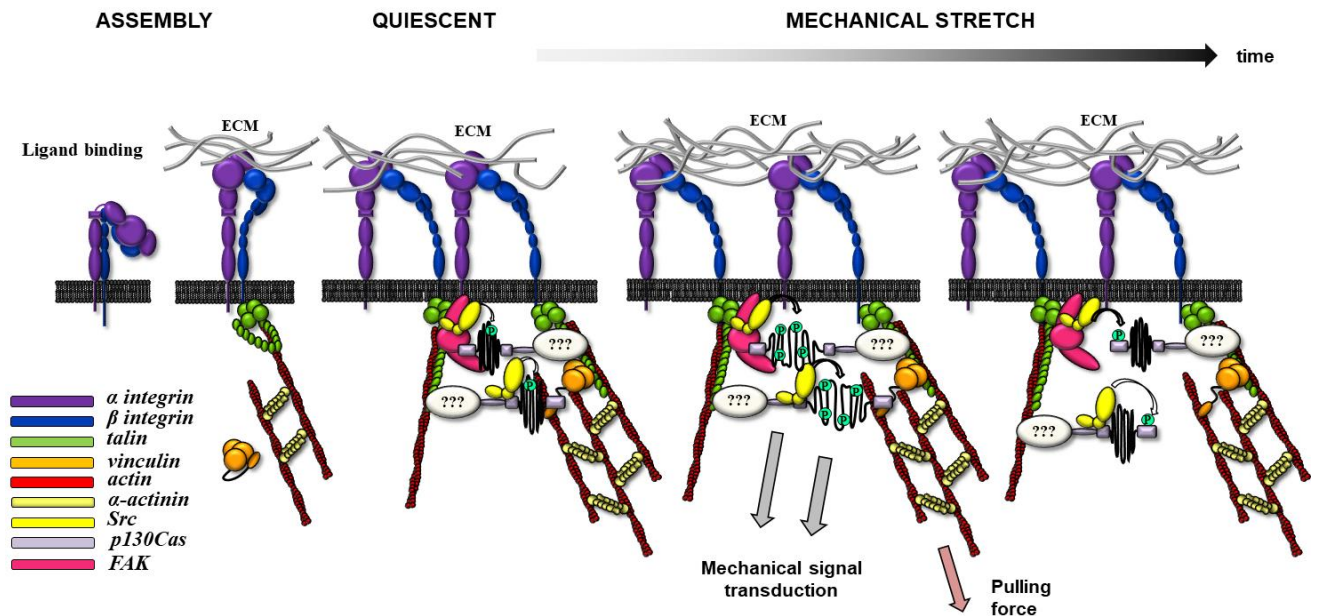


Figure 11: The structural basis of p130Cas-dependent mechanotransduction. Integrin binding to ECM allows cell movement. Cell migration or mechanical stretching generates a tension that reinforces integrin-actin cytoskeleton linkages and triggers conformational changes in several molecules including p130Cas. In the presence of mechanical force, the p130Cas substrate domain is refolded from a compact organized state with hidden/inaccessible tyrosines for phosphorylation into an extended disordered state, thereby exposing cryptic tyrosines. Subsequently, Src-family kinases phosphorylate those tyrosine residues and trigger the transduction of mechanical stimuli. Overtime, Src phosphorylates also Tyr12 within p130Cas SH3 to release the tension on the substrate domain and to attenuate the mechanotransduction. See text and (Janoštiak et al., 2014b) for details. Figure is adapted and modified from (Janoštiak et al., 2014b).

In order to work as mechanosensor, p130Cas SD has to be physically anchored in FAs on two sites. Both the p130Cas SH3 and CCH domain are important for p130Cas targeting to FAs (Harte et al., 2000). By combining chimeric constructs Braniš et al. demonstrated that the p130Cas SH3 domain (SH3 from both sides) can functionally substitute the C-terminal CCH domain to preserve p130Cas-dependent mechanotransduction (Braniš et al., 2017). The p130Cas SH3 domain binds two focal adhesion components, FAK (Polte et al., 1995) and Vinculin (Janoštiak et al., 2014a). Both are important for p130Cas targeting to FAs (Donato et al., 2010; Janoštiak et al., 2014a), but they differ in the position of the functional and topographical layer of FAs (Kanchanawong et al., 2010). While FAK-p130Cas binding triggers classical p130Cas signaling, Vinculin serves as a mechano-coupling protein and Vinculin-p130Cas

interaction probably occurs in the force transduction layer of focal adhesions (Braniš et al., 2017; Janoštiak et al., 2014a; Janoštiak et al., 2014b). Disruption of p130Cas binding to Vinculin impairs both p130Cas phosphorylation and traction force generation (Janoštiak et al., 2014a).

How p130Cas translocates to FAs via CCH domain is not yet clear. Among p130Cas CCH interaction partners, there are some candidates like focal adhesion component Paxillin (Zhang et al., 2017), BCAR3 (Cai et al., 1999; Gotoh et al., 2000) or p130Cas via dimerization itself (Braniš et al., 2017). For instance, Cross et al. demonstrated that p130Cas not only colocalizes with BCAR3 in dynamic FAs, but also showed that p130Cas-BCAR3 interaction stimulates FAs turnover and promotes cell invasion (Cross et al., 2016). This study, however, did not address whether p130Cas targeting to FAs is dependent on BCAR3 and despite the fact that the CCH domain is exceptionally well conserved among the CAS protein family, they are not functionally interchangeable among CAS members (Bradbury et al., 2017).

1.2.2.3. Cell migration and invasion

Cell migration is functionally coupled with actin cytoskeleton remodeling and cell interactions with ECM via FAs (or podosomes/invadosomes). The migrating cells have FAs that are highly dynamic and allow the formation of traction forces necessary for movement (see chapter 1.2.2.2). Protein p130Cas mediates binding between actin cytoskeleton complexes and kinases important for focal adhesion assembly and disassembly, and is therefore important for FAs and cytoskeletal dynamics (Defilippi et al., 2006; Janoštiak et al., 2014b). The relevance of p130Cas for the actin cytoskeleton was first documented by experiments with *p130Cas*^{-/-} fibroblasts. These cells showed defects in stress fibers formation, cell migration, and decreased basal and serum-induced invasiveness. This phenotype was rescued by the addition of the exogenous p130Cas protein (Brábek et al., 2004; Honda et al., 1998; Honda et al., 1999).

Spatiotemporally-regulated polymerization and depolymerization of the actin cytoskeleton is critical for cell migration and is controlled by small GTPases like Rac, Rho and Cdc42, which mostly differ in their localization and effects (summarized in Guilluy et al., 2011). These GTPases communicate with p130Cas in reciprocal manner (Figure 12 and Figure 13, see text below).

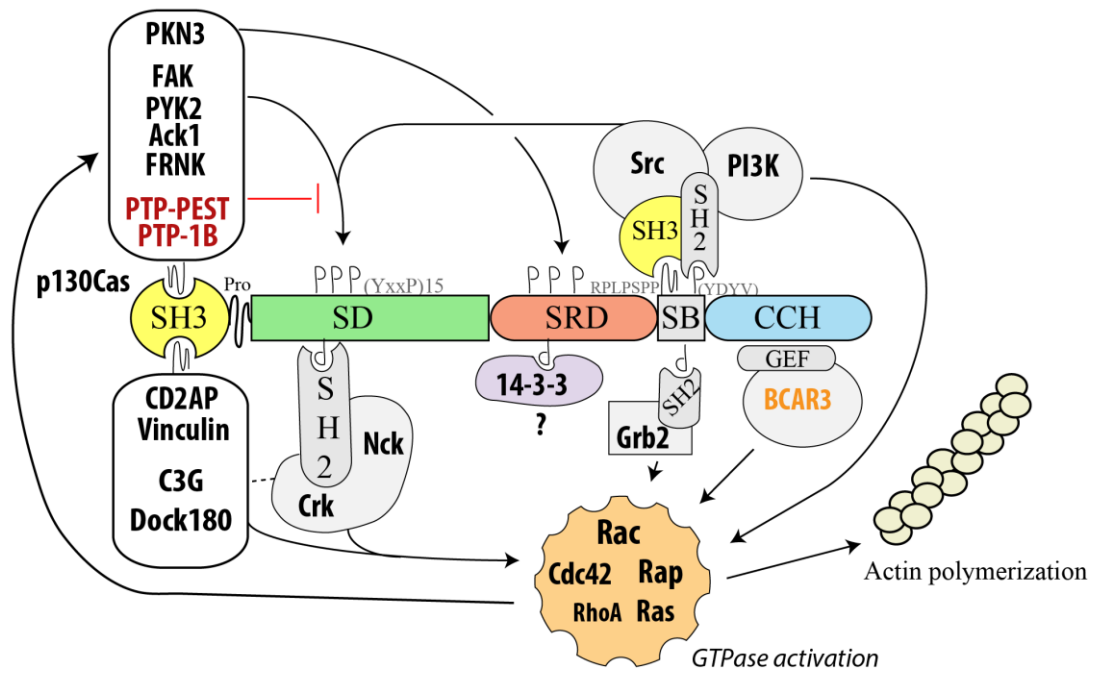


Figure 12: Protein p130Cas and small GTPases. Simplified signaling pathway with p130Cas. Phosphorylation of p130Cas as well as the binding of GTP / GDP exchange factors leads to the activation of small GTPases important for the remodeling of the actin cytoskeleton. See text for details. *Diagram drawn in Adobe Illustrator version CS5.*

The ability of p130Cas to support cell migration correlates to some extent with its increased tyrosine phosphorylation (Cary et al., 1998; Garton and Tonks, 1999; Klinghoffer et al., 1999) [see 1.2.2.3](#)). Tyrosine phosphorylation of the p130Cas substrate domain promotes the formation of p130Cas/Crk complex which stimulates the function of the GTP / GDP exchange factor Dock180 to activate Rac1 GTPase (Chodniewicz and Klemke, 2004; Hsia et al., 2003; Kiyokawa et al., 1998a). This GTPase stimulates the Arp2/3 complex nucleating actin filaments, PAK1 kinase and is necessary for the formation of lamellipodia and membrane protrusions (Kiyokawa et al., 1998b; Nobes and Hall, 1995). In addition, p130Cas binds to a GTPase-binding scaffold protein called IQGAP1 in response to vascular endothelial growth factor (VEGF) and induces polarization and migration of endothelial cell presumably in Rac1 or/and Akt dependent manner ([see chapter 1](#); Evans et al., 2017).

GTPase Cdc42 promotes membrane protrusions called filopodia and in addition determines cell polarity (Guilluy et al., 2011). Cell attachment to collagen leads to Cdc42-dependent activation of kinase Ack1 ([see chapter 1.2.1.2.1](#)) which binds to the SH3 domain of p130Cas (similarly as FAK), phosphorylates p130Cas in the substrate domain and induces cell migration via the p130Cas / Crk complex (Modzelewska et al., 2006).

Similarly, cell binding to fibronectin leads to Src dependent formation of p130Cas / Nck2 complex that activates Cdc42 GTPase to induce cell polarization during cell migration (Funasaka et al., 2010). Protein p130Cas co-operates to activate Rac1 or Cdc42 GTPase not only with Crk and Nck proteins but also with PI3K (Hawkins et al., 1995; Ojaniemi and Vuori, 1997; Figure 12), and BCAR3 (Cai et al., 2003; Cross et al., 2016; Wallez et al., 2014).

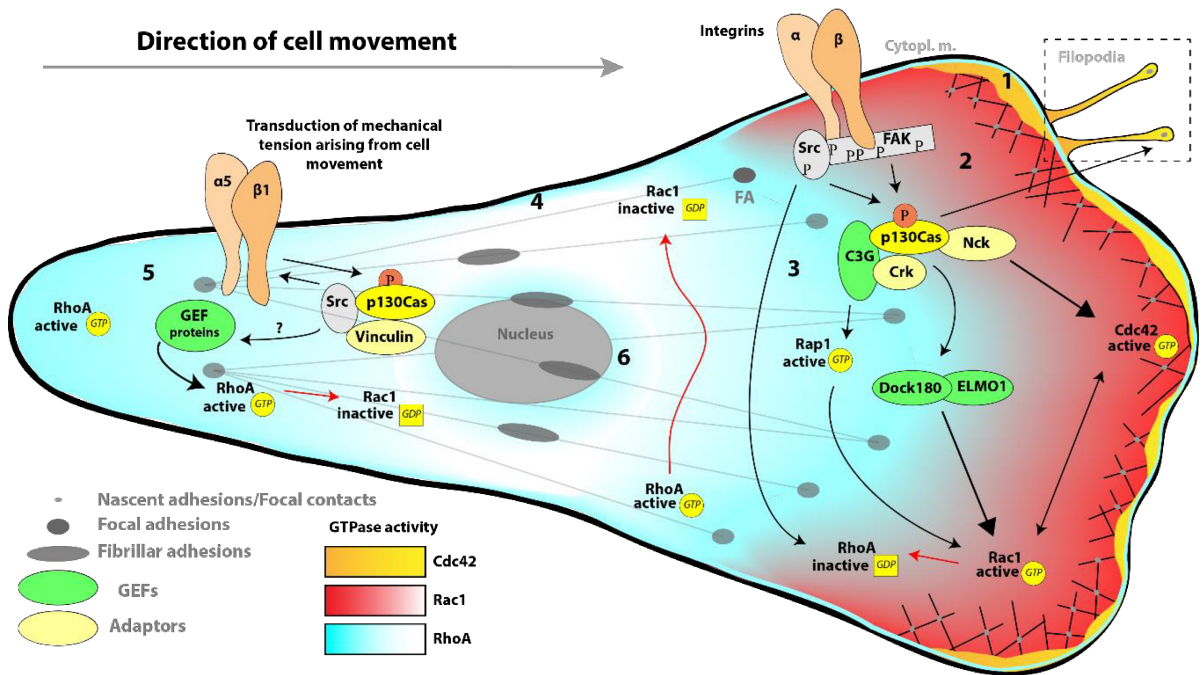


Figure 13: GTPases, p130Cas and cell migration. Cell migration requires precise spatiotemporal coordinated activation and inactivation of Rho GTPases. Individual cells can migrate in a lamellipodium-based manner (**shown here**) with actin polymerization (Rac1-Arp2/3-dependent) driving formation of lamellipodia and filopodia at the front of the cell, and actomyosin contractility promoting retraction at the cell rear or in a pseudopodium-based manner (not shown here) with actin spikes and filopodial bundles promoted by high RhoA activity at the cell front (RhoA-FHOD3-dependent) (Paul et al., 2015). The figure shows seven depicting zones of Rho proteins activation and crosstalk in the lamellipodium-based migrating cell.:

1. RhoA (light blue) and Cdc42 (orange) are localized and active at the front edge of the cell, drive membrane ruffling, and Cdc42 also promotes filopodia formation. RhoA activity is tightly controlled here, is only max 2 μm wide and rapidly decays from the leading edge.
2. A wider zone of Rac1 (red) activity that may arise downstream from integrin engagement. Indeed, integrins binding to ECM leads to the Src / FAK mediated phosphorylation of p130Cas followed by Crk, Nck binding and Rap1, Rac1 or Cdc42 activation through GEF proteins (green). This, in turn, inhibits RhoA and promotes nascent adhesion formation associated with actin-based protrusion.
3. In this part, RhoA generates contractility and inhibits Rac1, leading to focal adhesion maturation.
4. RhoA prevents inappropriate lateral protrusion by inhibiting Rac1.
5. During cell movement, a mechanical tension is generated at the cell body. Integrins A5 β 1 transfer this force through p130Cas to activate RhoA and promote cell body retraction.
6. RhoA GTPase activity has also been observed in the perinuclear region and in the nucleus.

Diagram was drawn using Adobe Illustrator version CS5 largely based on information from (Guilluy et al., 2011; Huvneers and Danen, 2009).

The activity of RhoA GTPase mainly increases in later stages of cell adhesion, presumably due to the resulting tension, and leads to the inactivation of Rac1 and Cdc42. This tension between ECM and actin cytoskeleton is transmitted by integrins and causes conformational changes of protein p130Cas leading to the binding and activity of Src kinase (see Figure 13), resulting in a subsequent retraction of the rear of the cell. Src is primarily known to mediate activation of Rac1 GTPase (RhoA inactivation), but in the case of mechanical force transfer from $\alpha 5\beta 1$ integrins, Src activates RhoA at the cell rear, probably by phosphorylation of its GEF activators (summarized in Huveneers and Danen, 2009). The importance of p130Cas in RhoA-dependent mechanotransduction is supported by a study showing that ROCK kinase (RhoA effector) inhibition significantly suppresses migration of MCF-7 cells induced by CAS family proteins (Bargon et al., 2005). In addition, there are another links between RhoA and p130Cas independent of the actin cytoskeleton remodeling. Cell stimulation by bombesin, LPA, fibronectin, or v-Crk induced transformation of rat fibroblasts results in tyrosine phosphorylation of p130Cas in RhoA GTPase activity-dependent manner, since the inhibition of RhoA or its kinase effector ROCK significantly reduces this phosphorylation (Altun-Gultekin et al., 1998; Flinn and Ridley, 1996; Kumagai et al., 1993; Tsuda et al., 2002).

Cancer cell invasiveness is fundamental process of tumor cell metastasis and is promoted by enhanced cell motility and/or ECM degradation capacity (see next chapter). Protein p130Cas is upregulated in cancer (see chapter 1.2.2.4) and stimulates cell invasion by both mentioned ways. The ability of p130Cas to induce cell invasion by enhanced cellular motility correlates to some extent with pathways described above and as a consequence of p130Cas hyperphosphorylation (see chapter 1.2.1.3) or over-expression (see chapter 1.2.2.4).

1.2.2.3.1. Role of p130Cas and its SH3 domain in ECM degradation

Matrix metalloproteases (MMPs) are responsible for the degradation of ECM, which allows cells to invade surrounding tissues, and is therefore one of the key factors of cellular invasiveness (DeClerck, 2000). Secretion of MMPs is tightly linked to cell structures called podosomes/invadosomes or their Src-induced fused super-structures, podosome rosettes. Protein p130Cas localizes to these structures and regulates assembly (podosome fusion) of podosome rosettes (see chapter 1.2.2.1). While the contribution of the p130Cas SH3 domain to podosome rosettes formation differs between cell types, the

p130Cas SH3 domain is absolutely necessary for JNK-dependent MMP2 activation and MMP9 secretion/expression (see Figure 14), and thus Matrigel invasion of *FAK*^{-/-} Src transformed MEFs (Hsia et al., 2003). This effect was surprisingly not attributed to the decrease of p130Cas SD (YxxP) phosphorylation (almost unchanged), but to the p130Cas SH3-mediated binding of Dock180 (see chapter 1.2.1.2.3). In the excess of Src kinase (expression level higher than FAK; Src over-expressing MEFs), the p130Cas SH3 domain is much less important than its SB (Src binding) region for the phosphorylation of p130Cas YxxP motifs (see Figure 6) that are critical for the invasion of Src transformed MEFs (Brábek et al., 2005; Hsia et al., 2003; Ruest et al., 2001). However, deletion of the p130Cas SH3 domain or the SB region decreases Matrigel invasion of Src transformed MEFs to similar extent (50 % of the original capacity) and the p130Cas SH3 domain is for MMP2 activation the most important structural part of p130Cas (more than YxxP motifs) (Brábek et al., 2005). In summary, the p130Cas SH3 domain can support cell invasiveness not only by promoting p130Cas SD phosphorylation but also by SH3 domain function “itself” without change of p130Cas SD phosphorylation. Another example, the p130Cas SH3 domain binds transcription factor CIZ (see chapter 1.2.1.2.4) which activates the transcription of MMP-1, MMP-3, MMP-7 (Nakamoto et al., 2000). Moreover, we have recently shown that p130Cas binds Ser/Thr kinase PKN3 by the p130Cas SH3 domain and this interaction was important to increase cell invasion in 3D collagen independent of Src transformation (Gemperle et al., 2018).

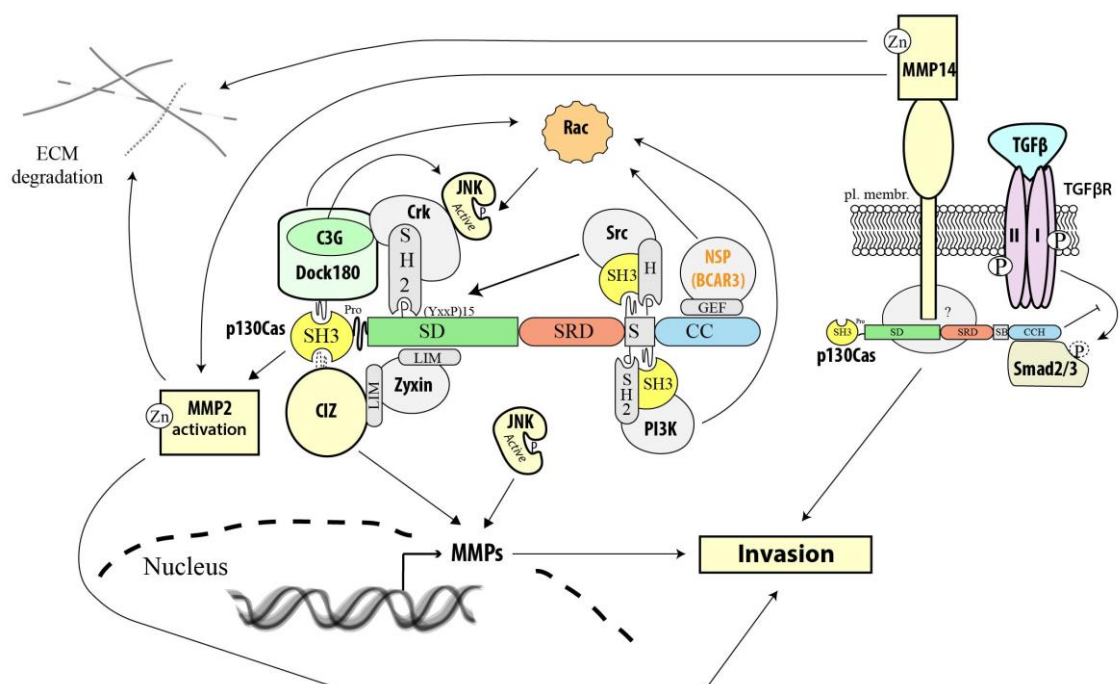


Figure 14: Role of the p130Cas SH3 domain in ECM degradation. See text for details. *Diagram drawn in Adobe Illustrator version CS5.*

In addition, p130Cas associates with MMP-14 (MT1-MMP) at the leading edge of sphingosine-1 phosphate-treated endothelial cells and thus promotes their invasive migration (Gingras et al., 2008). Furthermore, in ErbB2-positive breast cancer is p130Cas required to induce invasion by supporting and amplifying ErbB2 downstream signals, triggering MMP9 secretion and modulating several coding and non-coding genes (Cabodi et al., 2010a; Pincini et al., 2013; Sciortino et al., 2017; Tornillo et al., 2011). For instance, Sciortino et. al demonstrated that p130Cas can increase breast cancer cell invasion (and metastasis; see Figure 8) by de-repressing expression of transcriptional repressor Blimp1 in ErBb2-overexpressing cells by methylation-dependent downregulation of miR-23b which targets Blimp1 (Sciortino et al., 2017). Surprisingly, p130Cas can be target of miRNA itself and their (miR-24-3p, microRNA-362-3p and microRNA-329) ectopic expression suppress the cell proliferation/tumor growth (see chapter 1.2.2.4), migration and invasion/metastasis. These miRNA, therefore, perform a tumor-suppressive function and are downregulated in human breast cancer (Kang et al., 2015; Kang et al., 2017).

1.2.2.4. Malignant growth, cancer progression and drug resistance

For a growing number of cancers, it is known that p130Cas is upregulated by hyperphosphorylation, amplification, transcriptional upregulation, or stability changes. The sustained presence of upregulated p130Cas drives not only cell migration and invasion (see chapter 1.2.2.3), but also promotes cell survival (blocks anoikis, apoptosis and autophagy), proliferation/tumor growth, cancer progression and drug resistance (Brinkman et al., 2000; Camacho Leal et al., 2015; Nikonova et al., 2014; Tikhmyanova et al., 2010; Tornillo et al., 2014). Correspondingly, elevated expression of p130Cas in human patients is associated with early disease recurrence and poor prognosis in several cancer types, including lung, mammary, pancreas, prostate, and ovarian cancers (Cabodi et al., 2010b; Camacho Leal et al., 2015; Defilippi et al., 2006; Fromont and Cussenot, 2011; Fromont et al., 2007; Nick et al., 2011; Nikonova et al., 2014; Tikhmyanova et al., 2010). This section summarizes the current knowledge of p130Cas signaling leading to p130Cas upregulation and its involvement in malignant cell growth and drug resistance and cell sensitivity to cytotoxic drugs.

Protein p130Cas is required for cell survival/growth mediated by integrin activation, growth factors, and peptides. Its phosphorylation and/or binding to phosphorylation-independent interactors (such as C3G, Dock180, BCAR3) activates small GTPases Ras/Rap1 and Rac1 as well as JNK, Erk1/2, mTOR/p70S6K and Akt (see Figure 8), which are known to trigger gene expression for cell growth or survival, respectively (Cross et al., 2016; Hakak and Martin, 1999; Hsia et al., 2003; Kirsch et al., 1998; Oktay et al., 1999; Tikhmyanova et al., 2010; Tornillo et al., 2011; Wallez et al., 2014). Furthermore, protein p130Cas plays a crucial role downstream of many amplified or mutated oncogenes such as *KRAS*, *BRAF*, *PIK3CA*, *PTEN*, *ErbB2* or *Src*, as p130Cas knockdown leads to proliferative arrest in cancer cell lines dependent on these oncogenes or failure to induce metastases in mice (Brábek et al., 2004; Cabodi et al., 2006; Cabodi et al., 2010a; Pylayeva et al., 2009).

Surprisingly, protein p130Cas also regulates different modes of cell death induced by cytotoxic drugs. Besides cell death (anoikis/apoptosis) initiated by rapid dephosphorylation of p130Cas SD in response to cell detachment or the withdrawal of growth factors (Wei et al., 2002; Wei et al., 2004), cells can be also sensitized to apoptosis triggered by anti-cancer drugs or UV irradiation through mechanism involving Caspase 3-dependent cleavage of p130Cas (see Figure 10; (Hoon Kim et al., 2003; Kook et al., 2000)). In response to proteasome inhibition, Abl phosphorylates Crk to disassembly Crk/p130Cas complex and thus induces apoptosis (Holcomb et al., 2006). Furthermore, protein p130Cas increases cell sensitivity to proteasome inhibition by inhibiting autophagy (Zhao and Vuori, 2011). In breast cancer cells, p130Cas regulates their sensitivity to autophagy by protecting the ErbB2 oncogene from ubiquitination and degradation. This p130Cas-dependent protection of ErbB2 is likely to contribute to resistance to the humanized monoclonal antibody trastuzumab used to treat patients with ErbB2-overexpressing aggressive breast tumors (Bisaro et al., 2015). In addition, p130Cas also positively modulate levels of EGFR, a driver of breast and lung tumorigenesis, by blocking its endocytic internalization (see chapter 1.2.1.2.3). In contrast, p130Cas negatively regulates E-Cadherin membrane localization and promotes its lysosomal degradation. E-cadherin is often downregulated during epithelial-mesenchymal transition (EMT) prior to metastasis and this p130Cas activity (see Figure 15) can further explain how p130Cas promotes aggressive tumor behavior. Consistent with this, p130Cas further supports mesenchymal traits of breast cancer cells by sustaining Src, JNK activities, and expression of Cyclooxygenase-2, resulting in tumor

growth (Bisaro et al., 2012). Besides, during breast cancer progression, p130Cas acts as a molecular rheostat that switches transforming growth factor- β (TGF- β) from a tumor suppressor to a pro-metastatic molecule by diminishing the ability of TGF- β 1 to activate Smad2/3 (see Figure 10) and by increasing its coupling to p38 MAPK (Wendt et al., 2009). In addition to this, there are multiple other studies further supporting the role of p130Cas in tumor growth and cancer progression. First, p130Cas silencing in ERBB2-transformed breast cancer cells is sufficient to inhibit tumor growth in vivo and correlates with the downregulation of proliferative and survival pathways, such as Src and Akt activation, FAK phosphorylation and cyclin D1 expression (Cabodi et al., 2010a). Second, p130Cas is functionally coupled with Ser/Thr kinase PKN3 or BCAR3 to promote malignant (tumor) growth. In the case of PKN3, it is independent of Akt, and Erk1/2 signaling and Src transformation, unlike BCAR3/BCAR1 complex that activates Erk1/2 and Rac1 GTPase (Cross et al., 2016; Gemperle et al., 2018; Wallez et al., 2014). Furthermore, p130Cas silencing in ovarian carcinoma effects ovarian cancer growth not only by decreased tumor cell proliferation, but also by reduced angiogenesis and increased tumor cell death via induction of apoptosis and a toxic form of autophagy (Nick et al., 2011).

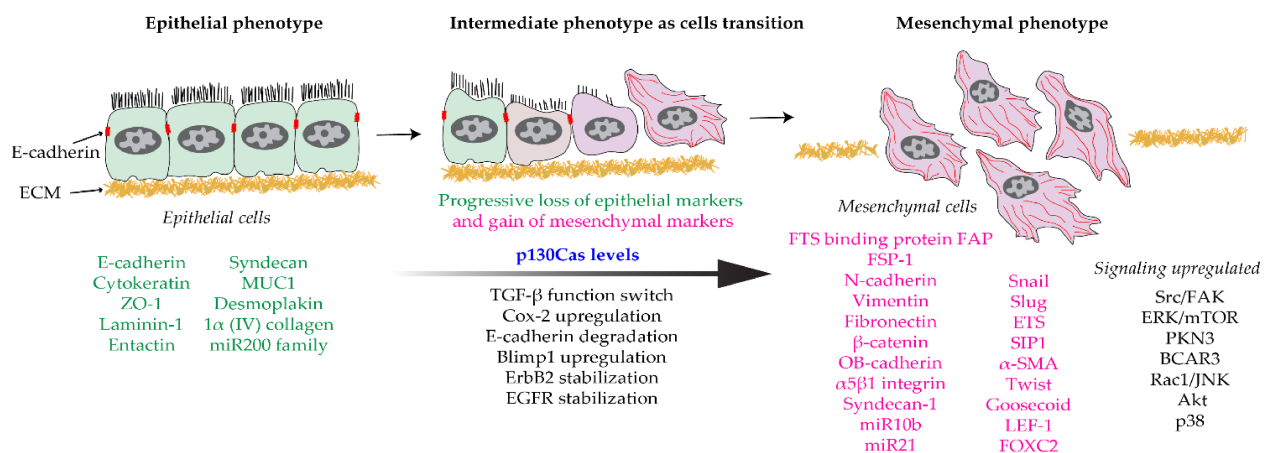


Figure 15: Protein p130Cas and epithelial-mesenchymal transition. Schematic model is illustrating the role of p130Cas in promoting mesenchymal cell features that leads to tumor growth. *Extracellular matrix (ECM)*. Diagram drawn in Adobe Illustrator version CS5.

Expression of protein p130Cas is tightly associated with hormone deprivation-mediated resistance to anti-tumor drugs (standard therapeutics) such as adriamycin (doxorubicin) and tamoxifen (Dorssers et al., 2001; Ta et al., 2008). Anti-estrogens, such as tamoxifen, are most commonly used in the treatment of estrogen receptor positive breast cancer patients (ER, ER⁺ cells). Tamoxifen binds in vivo to ER and inhibits

estrogen-induced cell proliferation. During therapy, however, many initially responding patients acquire resistance to this treatment, mostly due to the loss of ER expression (ER-cells) or increased activation of the ER signaling pathway even in the absence of the ligand (summarized in Ring and Dowsett, 2004). Protein p130Cas has been identified as a gene (*BCAR1* = Breast Cancer Anti-estrogen protein 1) responsible for the resistance to the anti-proliferative effects of tamoxifen (Brinkman et al., 2000; Dorssers et al., 1993) and its high levels correlate with earlier relapse and shorter overall survival (Dorssers et al., 2004). There are few studies underlying the p130Cas role in tamoxifen resistance by p130Cas expression up-regulation (see Figure 16). Tamoxifen-resistant cells have increased expression of the NAB2 which transactivates transcription factor EGR1 to bind *BCAR1* promoter and induce p130Cas over-expression (Kumbrink and Kirsch, 2012). Apart from this, p130Cas mRNA has been recently demonstrated to be negatively regulated by three microRNA: miR-362-3p, miR-329 and miR-24-3p. These miRNAs are downregulated in human breast cancer by enhanced DNA methylation and act as tumor suppressors by inhibiting cellular proliferation/tumor growth, invasion/metastasis (Kang et al., 2015; Kang et al., 2017). Their ectopic expression decreased cell viability and sensitized MCF7 (ER+) or/and Hep3B, B16F10 cells to tamoxifen (Kang et al., 2017). In case of miR-24-3p, also to anti-cancer drugs such as 5-fluorouracil, CDDP, and doxorubicin which further underlines the fundamental role of p130Cas in regulating the growth of cancer cells (Kang et al., 2017).

A major determinant of p130Cas-dependent increased cell proliferation in the presence of tamoxifen is the tyrosine phosphorylation of p130Cas SD. This is indeed specific to the p130Cas SD because chimera p130Cas with SD replaced from Nedd9 fails to induce ant-estrogen resistance. Another chimeras further indicate that p130Cas SR domain is also somehow partially involved (Brinkman et al., 2010).

Tamoxifen resistance is conferred by activation of growth and survival signaling pathways via phosphoinositide 3-kinase/Akt, ERK1/2, EGFR, Rac1 or Src in p130Cas dependent manner (Tornillo et al., 2014). In ER+ cells, estrogen receptor is in complex with activated Src, PI3K and p130Cas (see Figure 16) to promote ERK1 / 2 activity and the production of cyclin D1 (Cabodi et al., 2004). The addition of tamoxifen to ER+ cells initially reduces the p130Cas SD phosphorylation, but a continuous cell exposure to tamoxifen over time leads to the recurrence of the original phosphorylation level and cell proliferation. The cell sensitivity to tamoxifen can be restored by deletion of the p130Cas SD or after Src kinase inhibition (Cowell et al., 2006). By blocking signaling of the

p130Cas SD, which leads to a decrease in activation of ERK and PI3K / Akt signaling pathways, the anti-proliferative effect of tamoxifen in ER- cells can also be restored (Soni et al., 2009). Other work suggests that tamoxifen resistance induced by p130Cas overexpression is not a result of enhanced response to the partial agonist activity of tamoxifen (cyclin D1 expression), but rather by upregulating alternative proliferation pathways via Cas/c-Src/EGFR(Y845)/STAT5b (Riggins et al., 2006). Last but not least, cellular resistance to tamoxifen can also be induced by transfecting cells with plasmids encoding the ErbB2 for which the p130Cas has indispensable function. Here, cell proliferation (in the presence of tamoxifen) is likely a result of p130Cas-dependent ERK1/2 and GTPase Rac1 activation through PI3K / Akt signaling (Cabodi et al., 2010a; Tornillo et al., 2011).

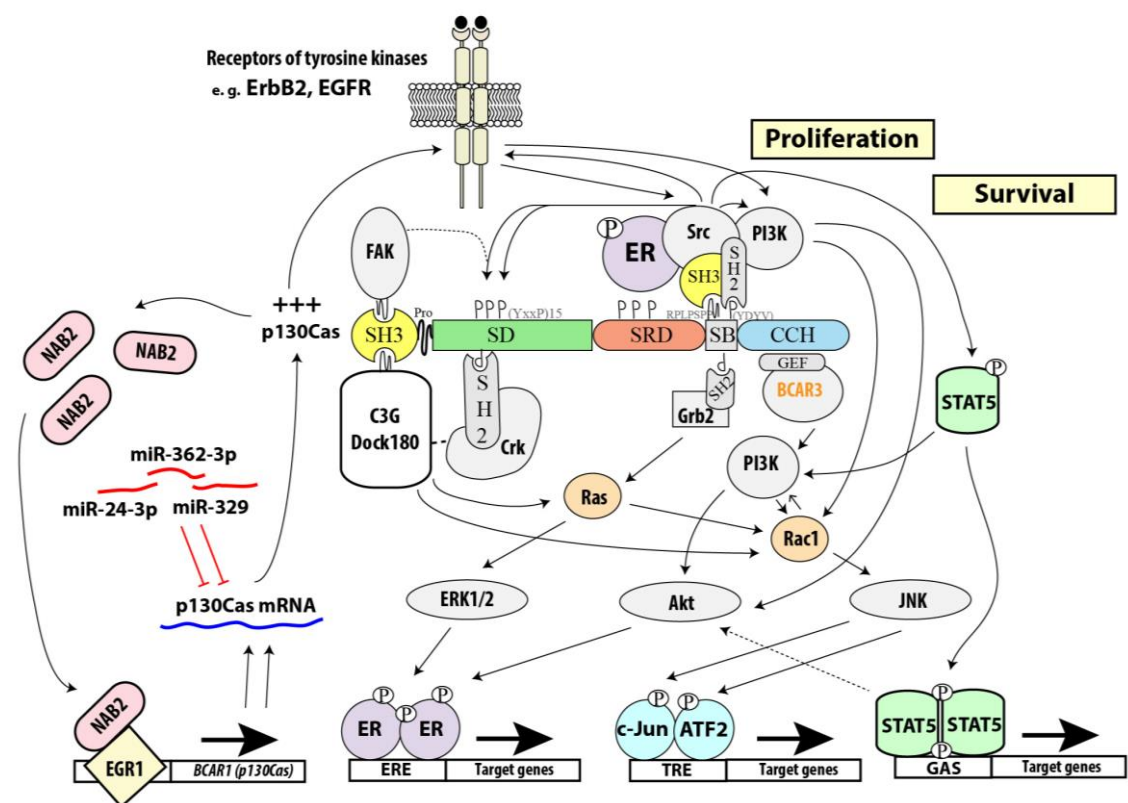


Figure 16: Cellular signaling promoting anti-estrogen resistance. See text for details. *TRE* (*TPA response element*), *ERE* (*estrogen response element*), *GAS* (*Gas - like element*). Diagram drawn in Adobe Illustrator version CS5.

In addition to p130Cas SD, anti-estrogen-resistant cell proliferation assay with p130Cas deletion mutants showed additional importance of the p130Cas SH3 or CCH domain (Brinkman et al., 2010) implicating that further mechanisms are involved in acquiring the tamoxifen resistance. An additional mechanism relies on the interaction between p130Cas and AND-34/ BCAR3, which gene was also identified by a random

search for genes involved in antiestrogen resistance, via the p130Cas CCH domain (van Agthoven et al., 1998; Wallez et al., 2014). There is a clear correlation between the emergence of tamoxifen resistance in breast cancer and the association of BCAR3 with p130Cas (Near et al., 2007) and it has been recently demonstrated that the binding of p130Cas to BCAR3 increases the levels of phosphorylated p130Cas, potentiating Erk1/2 phosphorylation and sustaining p130Cas-dependent anti-estrogen resistance (Wallez et al., 2014).

Since the aberrant activity and expression of p130Cas is associated with tumor cell resistance to chemotherapeutics, it is also interesting to note that radiation induces expression (or phosphorylation) of p130Cas (Beinke et al., 2003) and that cell survival after ionizing radiation is dependent on integrin-mediated p130Cas phosphorylation (Seidler et al., 2005).

Overall these findings indicate that p130Cas plays a key role in the tumor growth and metastasis of several types of cancer and suggest that downregulation of p130Cas might be a valid therapeutic strategy to cure these deadly diseases.

1.2.2.5. Angiogenesis and vascular remodeling

Angiogenesis / vasculogenesis (formation of new blood vessels) plays a central role not only in vascular development and remodeling, but also in tumor growth (Bergers and Benjamin, 2003). Protein p130Cas is critical for both at multiple levels. Particularly, *p130Cas* null mice die in utero with severe defects in the heart and vasculature seen at embryonic days (E) 11.5–12.5 when p130Cas is predominantly expressed in the cardiovascular system of wild type mice (Honda et al., 1998). Similarly, mice lacking only the p130Cas exon 2 (encodes the SH3 domain) died at E 11.5 – 15.5, but due to failure of sinusoidal endothelial cells (sinusoidal blood vessel) in the liver (Tazaki et al., 2010). This observation can be explained by essential role of the p130Cas SH3 domain for the p130Cas SD phosphorylation (see chapter 1.2.1.3). Furthermore, integrin-mediated signaling pathways have been implicated in mechanotransduction especially in cardiovascular cells (Katsumi et al., 2004; Weinbaum et al., 2011). This could be related to the mechanosensing function of p130Cas (see chapter 1.2.2.2).

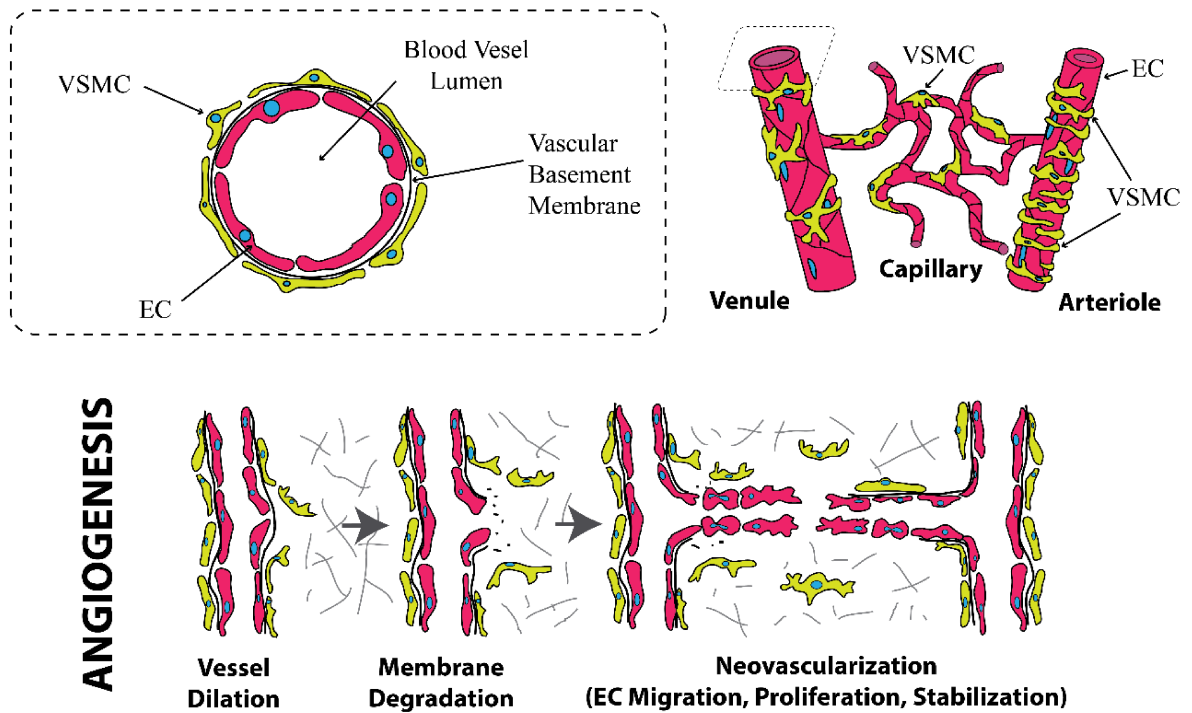


Figure 17: Diagram showing the general composition of blood vessels and angiogenesis. Blood vessels are composed of two interacting cell types: Vascular Smooth Muscle Cells (VSMC) and Endothelial Cells (EC). Different vessel types differ in EC wall thickness and density of circumferentially oriented VSMC (more to withstand higher blood pressure). When vessels form new sprouts (Angiogenesis), the degradation of the basement membrane, VSMC detachment, and loosening of EC junctions occur. This is accompanied by EC proliferation and migration via remodelling extracellular matrix toward an angiogenic stimulus. Then, EC take part in formation of an immature capillary structure by adhering to each other and by deposition of a new complex basement membrane. Finally, VSMC are recruited thereby providing stabilization for the new vessel under normal circumstances. For instance, tumor vessels are primitive and often lack a continuous VSMC layer resulting in a leaky vascular system which promotes metastasis by facilitating the movement of tumor cells into the blood stream. *Diagram drawn in Adobe Illustrator version CS5.*

Blood vessels are mainly composed of vascular smooth muscle cells (VSMC) and endothelial cells (see Figure 17). It has been demonstrated that p130Cas plays a fundamental role in migration and orchestrating VSMC contraction by promoting the actin cytoskeleton remodeling (Pellet-Many et al., 2011; Tang, 2009) and therefore, it is not surprising that p130Cas is involved in Atherosclerosis and pulmonary hypertension (summarized in Camacho Leal et al., 2015). For instance, Abl silencing inhibits p130Cas-mediated multiprotein assembly and constriction in resistance arteries, independent of myosin activation (Anfinogenova et al., 2007). Furthermore, the downregulation of p130Cas in VSMC dramatically attenuates force development and actin polymerization in response to contractile stimulation without affecting myosin regulatory light chain phosphorylation (Tang and Tan, 2003a). Apparently, p130Cas binds to actin binding protein profilin (Evans et al., 2017) and increases the profilin-actin complex in response to contractile stimulation (Tang and Tan, 2003a; Tang and Tan, 2003b). These studies

suggest that p130Cas is critical for smooth muscle tension and contraction development and underlying the p130Cas role in mechanosensing/mechanotransduction ([see chapter 1.2.2.2](#)). The spatial p130Cas redistribution to allow its mechanosensing function can be in VSMC regulated by the vimentin intermediate filament network that is important for contractile response to agonist stimulation (Acetylcholine). Acetylcholine activates p21-activated kinase which phosphorylates vimentin at Ser-55 and thus promotes the dissociation/release of p130Cas from cytoskeletal vimentin, resulting in p130Cas translocation to the membrane (Wang et al., 2007).

Vascular Endothelial Growth Factor (VEGF1 or VEGF-A) is essential for endothelial cell proliferation, migration and angiogenesis during development and in the pathogenesis of human pathologies including cancer and eye diseases (Carmeliet, 2003; Ferrara et al., 2003). In vivo, VEGF binds to VEGF receptor 1 and 2 (VEGFR) and to VEGFR2 coreceptor, protein called Neuropilin-1 (NRP1). NRP1 appears to be largely dispensable for embryonic vascular development, but is required for perinatal retinal vascularization, and for postnatal angiogenesis in pathophysiological settings (Fantin et al., 2014). NRP1 is important for mediating VEGF signaling via PYK2-dependent enhanced p130Cas SD phosphorylation and is strongly implicated in VEGF-induced regulation of directed endothelial cell movement (Evans et al., 2011). Recently, it was published that VEGF promotes assembly of the p130Cas interactome to drive endothelial chemotactic signaling and angiogenesis. Further details of this study showed that p130Cas association of IQGAP1, the GTPase-binding scaffold protein, plays a key role in VEGF signaling, endothelial polarization, VEGF-induced cell migration, and endothelial tube formation (Evans et al., 2017). In addition to IQGAP1, we have recently verified direct interaction of p130Cas with Ser/Thr kinase PKN3 (Gemperle et al., 2018; [see chapter 1.2.1.2.1](#)) which is the major regulator of postnatal angiogenesis and tumor metastasis in mice (Mukai et al., 2016). Although depletion of PKN3 impairs actin organization, adherens junctions dynamics and attenuates endothelial cell activation, probably by decrease of PYK2 activity (Möpert et al., 2012), the role of PKN3/p130Cas association in endothelial cells has not been studied yet.

Neo-vessels, in addition to providing oxygen and nutrient, degrade ECM (by MMPs) to release soluble factors that further promotes angiogenesis and tumor growth (Bergers and Benjamin, 2003; Neve et al., 2014). Protein p130Cas localizes to ECM-degrading structures ([see chapter 1.2.2.1](#)) and associates with MT1-MMP in endothelial

actin-rich membrane ruffles in response to the sphingosine-1-phosphate chemoattractant and thus promote their migration (Gingras et al., 2008).

1.2.2.6. Bone homeostasis

The mechanosensing function of p130Cas (see 1.2.2.2) in osteocytes and also its role in osteoclastic bone resorption have been shown to play an important role in bone tissue homeostasis (Kaneko et al., 2014; Nagai et al., 2013). Kaneko et al. propose that mechanical stimulation of osteoblasts lineage cells/osteocytes with fluid shear stress activates a mechanosensing machinery constitutes of α_v integrin-Src-p130Cas-JNK-YAP/TAZ pathway (Kaneko et al., 2014). Osteocytes play pivotal roles in the sensing and/or transduction of mechanical signals, thereby controlling osteoclast and osteoblast activities on the bone surface. Aberrant activation of osteoclasts (by microgravity, sedentary life style, in osteoporosis,...) causes a rapid bone loss (Tatsumi et al., 2007).

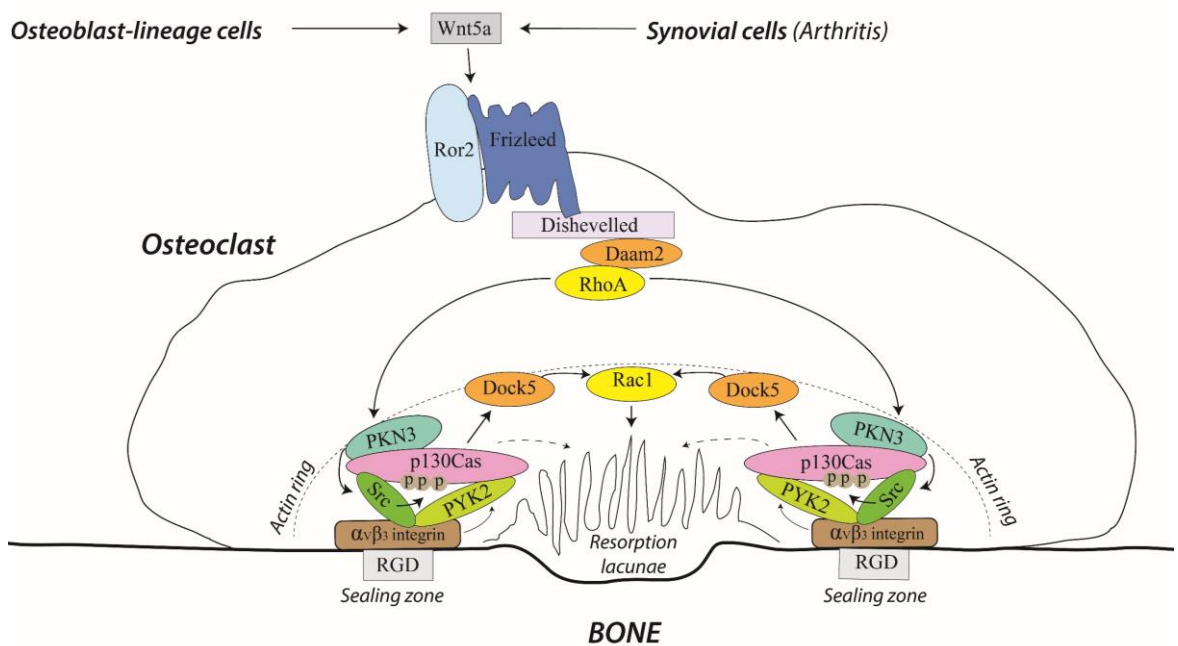


Figure 18: Bone resorption and p130Cas signaling. Hypothetical model of combined PKN3 and p130Cas signaling leading to bone resorption by osteoclasts. Osteoblast-lineage cells or synovial cells secrete Wnt5a which activates osteoclasts via Ror2-Dishevelled-Dam2-RhoA-PKN3 pathway. PKN3 stimulates Src via p130Cas binding. This complex is attached to bone matrix by actin ring which forms sealing zones via integrins. Src dependent p130Cas phosphorylation leads to Rac1-induced ruffled border formation and bone resorption. *Diagram drawn in Adobe Illustrator version CS5.*

Several independent studies highlight p130Cas function in osteoclast-mediated bone resorption that cannot be substituted (see Figure 18). It was reported that Src-

dependent p130Cas phosphorylation is involved in the adhesion-induced actin ring formation that is responsible for bone resorption (Nakamura et al., 1998). In these actin rings p130Cas colocalizes with PYK2 independently of Src-mediated phosphorylation (Lakkakorpi et al., 1999). This interaction is, similarly to p130Cas SD phosphorylation, critical for p130Cas-dependent bone mass resorption as p130Cas mutant lacking SH3 domain is not able to bind PYK2 nor to restore capacity of full p130Cas to induce formation of actin ring and bone mass degradation (Nagai et al., 2013). Protein p130Cas and Rac1 exchange factor called Dock5 have been previously shown to be implicated in Rac1 dependent bone resorption (Vives et al., 2011). Dock5 fails to associate with Src or PYK2 in the absence of p130Cas or in the presence of p130Cas without the SH3 domain indicating that the Src/Pyk2/p130Cas/Dock5 complex regulates osteoclastic bone resorption (Nagai et al., 2013). Subsequently, we identified and characterized direct interaction between p130Cas and PKN3 (see 1.2.1.2.1) (Gemperle et al., 2018). Surprisingly, both proteins are highly expressed in osteoclasts without affecting their differentiation, localize in actin rings and mice with deleted *PKN3* or *p130Cas* in osteoclasts exhibit osteopetrotic phenotype (Nagai et al., 2013; Uehara et al., 2017). PKN3 promotes formation of actin rings, and therefore promotes bone mass resorption, downstream of Wnt5a-Ror2-Daam2-RhoA pathway. Surprisingly, this PKN3 function is performed in the complex with PYK2 and Src. For this multiprotein association, Src activation and bone resorption is necessary an intact polyproline sequence of PKN3 which as we have shown facilitates PKN3-p130Cas binding (Uehara et al., 2017). In our lab, we were able to prove that protein p130Cas is indeed responsible for bridging Src and PKN3 and can mediate PKN3 dependent Src activation (Gemperle et al., 2018). This finding should be further verified in the mice with conditional deletion of *p130Cas* gene in osteoclasts.

These data strengthen the significance of protein p130Cas in bone homeostasis and suggest that the understanding of the precise molecular mechanisms of p130Cas-dependent regulation can be instrumental for the development of new therapeutic approaches to treat bone diseases such as osteoporosis, rheumatoid arthritis, periodontal disease and potentially also bone metastases.

2. DESCRIPTION OF RESEARCH RESULTS AND THEIR DISCUSSION

During my doctoral study in Laboratory of Cancer Cell Invasion, my research focused on mechanisms that control p130Cas and Src signaling in pathological conditions, especially mediated by the p130Cas SH3 domain.

- To study various aspects of p130Cas SH3 domain binding properties, we established collaborations with Dr Veverka (Structural biology) and Dr Lepšík (computational biochemistry; Academy of Sciences, CZ) and structurally characterized the p130Cas SH3 domain-ligand binding interface
- To bring new insight into p130Cas signaling I developed a bioinformatic workflow to identify novel p130Cas direct binding partners that led to identification DOK7, GLIS2 and PKN3, and helped to validate direct binding to Vinculin.
- I helped to functionally characterize p130Cas interaction with Ser/Thr kinase PKN3 and to show that this interaction is important for mouse embryonic fibroblast growth and invasiveness independent of Src transformation
- I contributed to development of a FRET-based Src biosensor that can be used for simultaneous monitoring of Src activity, conformation and localization in cells.

The result of my work were 2 published papers and 2 manuscripts available as preprints in public databases (expected to be accepted as peer-reviewed publications during the autumn of 2018).

2.1. CAS directly interacts with vinculin to control mechanosensing and focal adhesion dynamics (**the 1st publication**)

Janoštiak, R., Brábek, J., Auernheimer, V., Tatárová, Z., Lautscham, L., Dey, T., **Gemperle, J.**, Merkel, R., Goldmann, W., Fabry, B., Rösel, D. (2014). [CAS directly interacts with vinculin to control mechanosensing and focal adhesion dynamics](#). *Cell Mol Life Sci.* 71: 727-744.

In first part of my doctoral study, we performed pull down using the p130Cas SH3 domain and its phosphomimicking variant (Y12E) to identify novel interacting partners

that can differentially bind to a non-phosphorylated p130Cas SH3 domain. Mass spectrometry identified Vinculin, which similarly to p130Cas, localizes to focal adhesions and was shown to be crucial for the ability of cells to transmit mechanical forces and to regulate cytoskeletal tension. We have confirmed that p130Cas-Vinculin interaction is direct and used my preliminary results ([see 2nd publication](#)) determining the p130Cas SH3 binding motif to identify sequence (A₈₅₉PPKPPLP) responsible for p130Cas SH3 binding. Accordingly, mutation A₈₅₉PPKPPLP to A₈₅₉PPNSSLP (called PNSS) disrupted the interaction of Vinculin with p130Cas without significantly affecting Vinculin binding to its main interactors (paxillin or Arp2/3).

Protein p130Cas is targeted to focal adhesions by the interaction of the p130Cas SH3 domain with kinase FAK (Donato et al., 2010; Polte et al., 1995), but is partially present at FAs also in *FAK*-deficient cells (Nakamoto et al., 1997). To test the importance of p130Cas binding to FAK versus to Vinculin for p130Cas FA targeting, we compared p130Cas localization in FAs in *FAK*^{-/-} or *Vinculin*^{-/-} cells with or without re-expression of Vinculin WT or PNSS mutant. In both cells, p130Cas targeting to FAs was significantly impaired compared to WT cells and re-expression of vinculin PNSS mutant in *Vinculin*^{-/-} cells did not restore the p130Cas FA localization. This suggested that both Vinculin and FAK serves as an anchor for p130Cas in FA. Since FAK and Vinculin localize to different layers of FAs (Kanchanawong et al., 2010) and may provide different function ([see chapter Mechanotransduction](#)), we tested the possibility that p130Cas-Vinculin interaction plays a role in mechanotransduction and focal adhesion size and dynamics. Indeed, *Vinculin*^{-/-} or *Vinculin*^{-/-} cells re-expressing vinculin PNSS mutant had much smaller FAs and increased turnover of FAs in comparison to Vinculin WT re-expressing cells. Furthermore, it is known that changes in focal adhesions assembly and disassembly rates are affected by exchange dynamics of protein components within FAs. Therefore, we analyzed the importance of p130Cas-Vinculin interaction on p130Cas and Vinculin exchange rates using FRAP technique. We found that p130Cas and Vinculin mutually affect their dynamics within focal adhesions and this effect was p130Cas-Vinculin interaction-dependent as Vinculin PNSS mutant unable to bind p130Cas or p130Cas Y12E mutant unable to bind Vinculin had significantly faster exchange dynamics in corresponding cells compared to WT (Vinculin or p130Cas) re-expressing cells. Furthermore, to test the role of p130Cas-Vinculin interaction in mechanotransduction, we cultured cells on a stretchable silicon substrate and exposed to uniaxial static stretch. In contrast to Vinculin WT, Vinculin PNSS mutant significantly

reduced stretch-induced phosphorylation of p130Cas substrate domain (SD has mechanosensing properties – see 1.2.2.2). Consistently, *p130Cas*^{-/-} cells re-expressing p130Cas unable to bind Vinculin (Y12E) also prevented stretch-dependent activation of p130Cas. Moreover, mutation Y12F which prevents p130Cas SH3 phosphorylation, thus stabilizing p130Cas-Vinculin association, enhanced stretch-dependent activation of p130Cas SD. Comparison of p130Cas SD and Tyr12 stretch-induced phosphorylation dynamics revealed that p130Cas SD phosphorylation occurs rapidly while Tyr12 phosphorylation is less dynamic. Together these data suggest that the Vinculin-p130Cas interaction is required for stretch-induced SD phosphorylation, and supports our hypothesis that Vinculin serves as a mechanical binding protein that allows p130Cas to transmit mechanical forces within FAs. Finally, we found that p130Cas-Vinculin interaction reduces cell stiffness and traction forces but does not affect adhesion strength, further indicating that p130Cas-Vinculin interaction facilitates generation of traction forces by increasing the actomyosin contractility (probably through phosphorylation of p130Cas SD). Furthermore, our findings have led to a novel model of p130Cas mediated mechanotransduction where Src phosphorylates effectively p130Cas SD domain and with lower dynamics also p130Cas Tyr12 to disassembly p130Cas from FA (see chapter 1.2.1.3 and Figure 7).

My contribution

My task in this publication was to prove that the interaction between Vinculin and p130Cas is direct. At first, I tried to clone and express both components in the bacterial system and perform a binding assay with purified proteins. This method was not optimal. Therefore, I switched to another method called a far-Western-blot analysis which proved to be successful. In addition, my work helped us identify the sequence (A₈₅₉PPKPPLP) of Vinculin responsible for the p130Cas SH3 binding.

2.2. Structural characterization of CAS SH3 domain selectivity and regulation reveals new CAS interaction partners (the 2nd publication)

Gemperle, J., Hexnerová, R., Lepšík, M., Tesina, P., Dibus, M., Novotný, M., Brábek, J., Veverka, V., and Rosel, D. (2017). [Structural characterization of CAS SH3 domain selectivity and regulation reveals new CAS interaction partners](#). *Sci. Rep.* 7: 1–18.

The SH3 domain is indispensable for p130Cas signaling (Janoštiak et al., 2011; [see 1.2.1.2](#)), but the ligand binding characteristics of the p130Cas SH3 domain, and the structural determinants of its regulation were not well understood. To perform a systematic screen for p130Cas SH3 domain ligand preferences, we used Phage Display analysis with a library composed of 10^{12} M13 phages carrying 12-amino-acid degenerate oligopeptides. This revealed an unconventional class II SH3 binding motif ((A/P)₋₁P₀X₁K₂P₃X₄(L/R)₅; [see 1.2.1.1](#)) which was further verified by additional biochemical assays. We found the requirement for an uncommon centrally localized lysine residue at position +2 and two rather dissimilar optional anchoring residues, leucine and arginine, at position +5 ([see chapter 1.2.1.1](#) and Figure 3). To be able to study the structural determinants of the p130Cas SH3 domain, we established collaborations with Dr Veverka (Structural biology) and Dr Lepšík (Computational biochemistry; Academy of Sciences, CZ). Together, we prepared ¹⁵N/¹³C-labeled p130Cas SH3 domain and determined its solution structure by NMR (PDB code 5O2M). Attempts to structurally characterize complexes of p130Cas SH3 with its ligands Vinculin (1st [publication](#); harboring unusual leucine at position +5) and PTP-PEST (harboring conserved arginine at position +5) derived molecules using isotopically labeled recombinant protein and unlabeled synthetic peptides failed due to the polyproline character of the peptides and thus overlapping NMR spectra. Therefore, we designed two chimeras with the peptide sequences located at the C-terminus of the SH3 domain. The NMR analysis of p130Cas-Vinculin and p130Cas-PTP-PEST chimeras containing the sequences corresponding to residues 854–870 and 327–343, respectively, allowed for a detailed characterization of the binding interface between the p130Cas SH3 domain and the studied peptides ([see chapter 1.2.1.1](#) and Figure 3). Notably, centrally localized lysine residue at position +2 has been found as the most critical residue and its unique specificity towards p130Cas SH3 is gained by the presence of non-conserved Aa (Asn14, Glu17, Arg59). Furthermore, the p130Cas SH3 unique ability to selectively bind both Leu or Arg at +5 came from Leu40 or Glu17, respectively. Our chimeric constructs also included nine amino acids corresponding to the sequence flanking the core binding sequence on both sides (SDEs) which showed additional electrostatic interactions with less conserved portion of the p130Cas SH3 domain, especially Lys26 ([see chapter 1.2.1.1](#) and Figure 3).

We have previously shown (Janoštiak et al., 2011; Janoštiak et al., 2014a) that the binding and signaling of the p130Cas SH3 domain is negatively regulated by phosphorylation of Tyr12. Our structural and biochemical data revealed that the aromatic

ring of Tyr12 is involved in nonpolar interactions with P₋₁/ A₋₁ and P₀ of PTP-PEST/Vinculin, while its hydroxyl group remained solvent-exposed. Surprisingly, tyrosine mutation to phenylalanine (Y12F) which differs only in the OH group, reduced p130Cas SH3 ligand binding in biochemical analysis and molecular dynamics and quantum mechanics (QM), probably by decreasing dipole moment of Tyr12 aromatic ring. The introduction of the phosphate group added similarly as the phosphomimicking mutation Y12E a negative charge to the site and prevented to form CH/ π interactions with ligands such as Tyr12. In addition, QM calculations suggested that the main reason of negative contribution of Tyr12 phosphorylation is unexpectedly a formation of a salt bridge with Lys26 within the p130Cas SH3 domain itself.

To confirm our results also in cells and to provide additional experimental evidence that Tyr12 phosphorylation is Src dependent, we compared binding affinities of p130Cas to FAK and Vinculin in MEFs to MEFs overexpressing constitutively active Src (MEFs SrcF) and to MEFs SrcF after Src inhibition. The binding affinity of p130Cas to Vinculin or FAK negatively correlated with Src activity as a function of p130Cas Tyr12 phosphorylation. Moreover, Src inhibition in Src overexpressing cells have led to dramatic increase between FAK and p130Cas association, much higher than in MEFs or between Vinculin and p130Cas. This have led to a novel upgraded model of Src-p130Cas-FAK binding and Src mediated p130Cas phosphorylation ([see Figure 7 and chapter 1.2.1.3 for discussion](#)).

Finally, to increase our understanding of p130Cas signaling and to potentially unravel its novel biological roles, we scanned the identified highly specific p130Cas SH3 domain binding motif in the UNIPROT SWISSPROT human/mouse protein database using PATTINPROT and BLASTP programs and identified 11 potential new interacting partners of p130Cas. Published data allowed us to conduct a thorough evaluation of these potential partners for their possible connection to signaling processes involving p130Cas and narrowed our selection to 7 highly-promising candidates. We tested 5 of them, four successfully: Vinculin ([see 1st publication](#)), PKN3 ([see 4st publication](#)), DOK7 and GLIS2 ([this 2nd publication](#)) and CEP2 (not shown; negative result, but found in interaction with Src). For this publication, we selected and verified a direct interaction with DOK7, which contains the conserved P₅₀₉PPKPLRP motif and GLIS2, with an anchoring leucine at position +5 (P₃₃₃PPKPPLP). DOK7 has suggested a new p130Cas role in neuromuscular synapsis ([see chapter 1.2.1.2.5](#)) and GLIS2 has added another link connecting p130Cas with its underestimated role in kidney pathologies ([see chapter 1.2.1.2.4](#)).

Taken together, these results brought substantial new insight into the mechanisms that control p130Cas signalling and point p130Cas to a new role in neuromuscular synapsis. Furthermore, structural characterization of p130Cas SH3 domain and its binding characteristics support structure-based drug design of inhibitors of p130Cas-ligand interaction.

My contribution

This is my first author's publication and therefore most of the work has been done by me including writing, cloning and protein purifications. Structural assignments, Kd measurements, computational modeling and some sequence alignments were done in collaborations with Václav Veverka (Rozálie Hexnerová and Petr Těšina), Martin Lepšík and Marian Novotný, although most of the structural and bioinformatical figures were prepared/finalized by me including PISA interface analysis. Furthermore, I also performed Phage display analysis and all experiments using Enzyme-linked immunosorbent assays (ELISA). Coimmunoprecipitations and far-Western experiments were done by me and by Michal Dibus.

2.3. Novel FRET-Based Src Biosensor Reveals Mechanisms of Src Activation and Its Dynamics in Focal Adhesions (the 3rd publication/preprint)

Koudelkova, L., Pataki, C., Tolde, O., Pavlik, V., Nobis, M., **Gemperle, J.**, Anderson, K., Brábek, J., Rosel, D., (2018). Novel FRET-Based Src Biosensor Reveals Mechanisms of Src Activation and Its Dynamics in Focal Adhesions. *SSRN*. <https://ssrn.com/abstract=3206266> (Preprint posted July 2, 2018). Under revision at Cell Chemical Biology journal.

Src kinase activity is the main effector of known p130Cas signaling and its deregulation is often found in tumors (Giaccone and Zucali, 2008; Irby and Yeatman, 2000). Therefore, precise control of its activation is necessary to avoid tumor transformation. Our efforts to monitor Src kinase activity led us to construct a novel FRET-based Src biosensor. We took the advantage of determined Src structures showing a negative correlation between structural condensation of the Src backbone and its catalytic activity (Cowan-Jacob et al., 2005). Therefore, we have inserted a FRET pair of fluorescent proteins in the loop between β D and β E strands of SH2 domain (donor; mCFP or mTurquoise2) and at the C-terminus (acceptor; mCit) of Src molecule (WT or its mutants). Hypothetically, Src biosensor should produce an intramolecular FRET in

inactive compact conformation, whereas in active open conformation should be significantly decreased and should therefore effectively monitor structural changes following Src activation. The initial testing measurement with a FRET steady-state approach showed promising results. Src-FRET construct reached ca 73 % of the maximum FRET ratio within the theoretical range, given by the difference in FRET ratio between the positive control and Src-CFP and was significantly higher from FRET ratio of constitutively active Src (Src-FRET527F; ca 33% of the maximum FRET). Furthermore, extensive functional studies revealed that our Src FRET biosensor is functionally equivalent to Src and in cells responsive to EGF or LPA stimulation and even to interaction-based activation (Sin peptide carrying both SH2 and SH3 binding sites). We were able to monitor Src activation dynamics upon mechanical stimulation of p130Cas mechanosensor by measuring the total level of FRET and phosphorylation of p130Cas. Consistently to our previous results ([1st publication](#)), Src reflected the bi-phasic dynamics of p130Cas phosphorylation. Since p130Cas transfers external forces via FAs to cytoskeletal and signaling proteins inside the cell, we also tested the intracellular dynamics of Src activity in focal adhesions by FRET imaging. We found that Src is rapidly activated during FA assembly, its activity remains high and steady throughout the FA life cycle and decreases during FA disassembly.

Since our biosensor reflects Src activity as a function of its conformation change, we tested a whole range of mutations. Our data suggested that activated conformation of the kinase domain forced opened conformation of Src via negative effect on intramolecular SH2- and SH3-binding to kinase domain. And vice versa, mutations affecting SH3-mediated intramolecular interactions of Src also promoted the opening of Src structure.

Having established Src biosensor potential in reflecting Src conformation changes, we then analyzed a panel of Src inhibitors for the effect on compactness of Src-FRET biosensor. All tested inhibitors effectively inhibited Src kinase activity (detected by western blot), but surprisingly ca one half of inhibitors tested paradoxically induced a significant decrease in FRET indicating the open conformation of Src. Strikingly, these inhibitors which induced Src opening also enriched Src biosensor (including endogenous Src) in focal adhesions resembling the localization of the 527F activated Src. This indicates that opened conformation of Src and not its kinase activity is determining Src exchange rates in focal adhesion. Furthermore, it also brings insight to our observation that Src biosensor was only locally activated in focal adhesions and was not enriched.

Taken together, our new Src-FRET biosensor has proofed its potential in providing combined information about the activity and its intracellular conformation changes, which brings a substantial advantage over previously established Src biosensors. Furthermore, it could also contribute to the development of effective therapeutic approaches targeting Src.

My contribution

My role in this publication was to prepare and functionally verify the FRET positive control to estimate the theoretical range of FRET which is possible for our Src-FRET construct. I also tested our Src-FRET biosensor with various linkers between the fluorophores and the kinase using a Varioskan Flash and FRET method based on acceptor photobleaching to find the most optimal version for further experiments. Finally, I helped prepare an illustrative model of Src activation at FAs using Adobe Illustrator version CS5.

2.4. The interaction of PKN3 with p130Cas promotes malignant growth

([4th publication](#)/preprint)

Gemperle, J., Dibus, M., Koudelková, L., Rosel, D., Brábek, J. (2018). The interaction of PKN3 with p130Cas promotes malignant growth. *bioRxiv*. <https://doi.org/10.1101/334425> (Preprint posted June 29, 2018). Under revision at Molecular Oncology journal.

In a screen for new interaction partners of the p130Cas SH3 domain ([see 2nd publication](#)), we predicted also Ser/Thr kinase PKN3 which has significant role in tumorigenesis ([see chapter 1.2.1.2.1](#)). In this study, we verified PKN3-p130Cas interaction and characterized as direct through central PKN3 polyproline motif P₅₀₀PPKPPRL and p130Cas SH3 domain. This interaction did not promote an increase of PKN3 activity, although kinase inactivating mutation significantly reduced its interaction with p130Cas and p130Cas overexpression stimulated PKN3 activity in p130Cas CCH dependent manner. To further assess the p130Cas-PKN3 interaction, we analyzed their co-localization in cells. We observed dynamic colocalization of p130Cas and PKN3 in lamellipodia of MEFs and podosome rosettes of Src transformed MEFs ([see chapter 1.2.2.1](#)). PKN3, similarly as p130Cas, showed involvement in actin cytoskeleton remodeling, but independent of the p130Cas-PKN3 interaction.

Previous studies showed positive correlation between PKN3 or p130Cas protein levels and cancer progression in patients with breast or prostate cancer (Dorssers et al.,

2004; Fromont and Cussenot, 2011; Leenders et al., 2004; Nikonova et al., 2014; Oishi et al., 1999; Schultheis et al., 2014; Strumberg et al., 2012). To test the assumed link between PKN3 and p130Cas signaling, we further performed cross-correlation analysis of publicly available transcriptomic data using the cBio Cancer Genomics Portal (cbioportal.org) (Gao et al., 2013). This analysis showed that elevated expression of PKN3, but not of a paralog PKN2 that do not possess a p130Cas interaction site, significantly positively correlates with the increased expression of p130Cas in both invasive breast carcinoma and prostate adenocarcinoma tumors. In parallel, statistical analysis revealed that PKN3 activity exhibits strong positive correlation with p130Cas phosphorylation at Ser428 (mouse Ser432) in invasive breast human carcinomas. Ser432 of mouse p130Cas has conserved surrounding sequence (KRLSA) and fits well to the known PKN3 phosphorylation motif (Collazos et al., 2011). To test the presumed ability of PKN3 to phosphorylate p130Cas, we prepared a p130Cas mutant for Ser432 (S432A) and p130Cas mutated in all 15 Ser/Thr within SRD (15AN) and performed kinase assays in vitro. This experiment verified that p130Cas Ser432 represents a major PKN3 phosphorylation site and further indicated that PKN3 may phosphorylate p130Cas also outside the SRD domain.

It was previously published that Ser/Thr phosphorylation of p130Cas induces reduction of p130Cas migration profile upon SDS-PAGE (see [chapter 1.2.1.4](#)). Comparison of p130Cas SDS-PAGE migration profiles revealed that p130Cas SH3 and CCH domains are important for p130Cas Ser/Thr phosphorylation and that the presence of the slowest migration form of p130Cas is associated with Ser432 phosphorylation. However, due to the high basal Ser/Thr p130Cas phosphorylation in MEFs, we failed to demonstrate the change of p130Cas WT SDS-PAGE migration pattern by PKN3 overexpression.

Given roles of both PKN3 and p130Cas in the regulation of malignant cell growth (Cabodi et al., 2006; Cabodi et al., 2010a; Leenders et al., 2004), we investigated whether PKN3 regulates cell proliferation in MEFs and whether this is dependent on p130Cas. Indeed, doxycycline (Dox) inducible expression of PKN3 stimulated cell proliferation in p130Cas dependent manner, starting 5 h after the addition of Dox which was the time of initial PKN3 expression. Only the induction of expression of PKN3 WT, but not of mutant unable to binds p130Cas (mPR) or kinase dead variant (KD), led to the increase of cell growth compared to that in non-induced controls. Similarly, PKN3 WT expression (but not mPR or KD) increased MEFs migration in 3D collagen in p130Cas dependent manner.

Having established the importance of the PKN3–p130Cas interaction for proliferation and 3D migration of MEFs, we next analyzed whether this interaction also influences the growth and invasive behavior of SrcF-transformed cells. Surprisingly, cell transformation by a constitutive active Src led to an increase of PKN3 endogenous protein levels, which was dependent on the presence of p130Cas. PKN3 is scarce in normal human adults tissues with some exceptions and it has been found that its protein levels can be increased by several oncogenes, suggesting that PKN3 functions, similarly to p130Cas, as an effector of various signal transduction pathways that mediate cell growth and transformation (Leenders et al., 2004; Unsal-Kacmaz et al., 2011). To reduce the contribution of endogenous PKN3 in subsequent experiments, we inactivated *PKN3* in Src transformed MEFs (SC) using CRISPR/CAS9 system. *PKN3* gene inactivation by CRISPR or PKN3 downregulation using Dox-inducible PKN3 specific shRNA significantly reduced 2D and 3D malignant cell growth and SC cell invasion in 3D and this was rescued by Dox-inducible expression of PKN3 WT, but not mPR. To verify our results in vivo, we subcutaneously injected the modified SC cells to nu/nu mice and compared tumor weight between the four divided groups. Parental SC cells reached the highest weight despite the shorter period of time and *PKN3* gene inactivation strikingly reduced this weight while the re-expression of PKN3 WT, but not PKN3 mpR, rescued tumor growth.

Having established the role of PKN3-p130Cas interaction in malignant growth, we have profoundly tried to elucidate the mechanism. However, PKN3 promoted cell growth and invasion with p130Cas WT and 15AN mutant to a similar level suggesting that p130Cas SRD phosphorylation was not necessary (for deep discussion see 1.2.1.4) and activation status of STAT3, ERK, Akt, MLC and mTOR signaling was also not involved. Although we observed slight p130Cas-dependent PKN3-induced Src activation in MEFs, the mechanism of PKN3-promoted cell growth and invasiveness will probably be different as this effect was similar in MEFs and SC cells with constitutively active Src. Furthermore, PKN3 expression in SC cells did not promote increase in gelatin degradation. Nevertheless, PKN3 has been suggested to promote degradation of osteoclast in Src dependent manner as p130Cas (see chapter 1.2.2.6) and in our system with constitutively active Src, protein p130Cas has bridged association of PKN3 with Src and Actin.

In summary, we suggested that aberrantly expressed PKN3 and p130Cas can cooperate in cancer progression and tumor growth and therefore may represent an attractive target for therapeutic intervention.

My contribution

As the first author of this work I have written the original draft and prepared figures and performed most of the experiments including cloning, stable cell line preparation, characterization of PKN3-p130Cas interaction, microscopy, in silico analysis, proliferation and invasion assays, tumors processing and most of the Western blots. Lenka Koudelková helped to prepare some clonal Dox-inducible stable cell lines and Michal Dibus helped with cloning and performed all kinase assays shown in the work.

3. CONCLUDING REMARKS

This work indicates that protein p130Cas has a much larger set of functions than previously assumed. With every newly-described protein interaction we were able to put p130Cas to new physiological context and even broaden its role in cell biology. Protein p130Cas, thanks to its modular structure, represents a molecular hub for cell signaling originating from many oncogenes. Therefore, high-resolution mapping of the interactions between p130Cas and its pro-growth/pro-migratory binding partners may provide a rationale for the design of novel targeted therapies. Novel therapeutic strategies for many types of p130Cas-linked cancers are needed as current strategies are not effective or cell often acquire resistance over time. Protein p130Cas, in particular, contributes to resistance to chemotherapeutics and also promotes tumor angiogenesis and growth, cancer invasion, aggressiveness and metastasis, and therefore targeting p130Cas by novel therapeutics could mechanistically deal with cancer on multiple levels and even target bone metastases that are difficult to cure.

During my doctoral study, I applied a variety of techniques in imaging, biochemistry/structural biology, bioinformatics, genetic engineering and in vitro cell biology to study p130Cas and Src kinase signaling and their role in pathological diseases and mechanotransduction. To study various aspects of p130Cas I initiated new collaborations, resolved p130Cas SH3 domain binding motif and developed a workflow to identify novel p130Cas direct binding partners that led to identification Vinculin,

DOK7, GLIS2 and PKN3 followed by validation studies. In case of PKN3, I experimentally demonstrated that that PKN3-p130Cas interaction is important for malignant growth and invasiveness independent of Src transformation, indicating a mechanism distinct from that previously characterized for p130Cas. Notably, PKN3 is the first identified Ser/Thr kinase to bind and also phosphorylate p130Cas. Furthermore, I prepared purified chimeras of p130Cas SH3 domain with its ligands for structural NMR analysis. The resolved structure of p130Cas with its ligand could be instructive to drug design of inhibitors targeting p130Cas-ligand interaction. In addition, my work expanded our knowledge of p130Cas SH3 ligand binding regulation (effect of Tyr12 phosphorylation) and led to novel model of Src-p130Cas-FAK binding. Finally, I contributed to development of a FRET-based Src biosensor that can be used for simultaneous monitoring of Src activity, conformation and localization in cells.

Overall, my work brought substantial new insight into the mechanisms that control p130Cas signalling.

4. REFERENCES

- Abassi, Y. A., Rehn, M., Ekman, N., Alitalo, K. and Vuori, K.** (2003). p130Cas Couples the tyrosine kinase Bmx/Etk with regulation of the actin cytoskeleton and cell migration. *J Biol Chem* **278**, 35636–35643.
- Agrawal, V. and Kishan, K. V. R.** (2002). Promiscuous binding nature of SH3 domains to their target proteins. *Protein Pept. Lett.* **9**, 185–193.
- Alexander, N. R., Branch, K. M., Parekh, A., Clark, E. S., Iwueke, I. C., Guelcher, S. A. and Weaver, A. M.** (2008). Extracellular Matrix Rigidity Promotes Invadopodia Activity. *Curr. Biol.* **18**, 1295–1299.
- Altun-Gultekin, Z. F., Chandriani, S., Bougeret, C., Ishizaki, T., Narumiya, S., de Graaf, P., Van Bergen en Henegouwen, P., Hanafusa, H., Wagner, J. A. and Birge, R. B.** (1998). Activation of Rho-dependent cell spreading and focal adhesion biogenesis by the v-Crk adaptor protein. *Mol Cell Biol* **18**, 3044–3058.
- Ambrogio, C., Voena, C., Manazza, A. D., Piva, R., Riera, L., Barberis, L., Costa, C., Tarone, G., Defilippi, P., Hirsch, E., et al.** (2005). p130Cas mediates the transforming properties of the anaplastic lymphoma kinase. *Blood* **106**, 3907–3916.
- Anfinogenova, Y., Wang, R., Li, Q., Spinelli, A. M. and Tang, D. D.** (2007). Abl silencing inhibits CAS-mediated process and constriction in resistance arteries. *Circ. Res.* **101**, 420–8.
- Armulik, A., Velling, T. and Johansson, S.** (2004). The integrin beta1 subunit transmembrane domain regulates phosphatidylinositol 3-kinase-dependent tyrosine phosphorylation of Crk-associated substrate. *Mol Biol Cell* **15**, 2558–2567.
- Attanasio, M., Uhlentaut, N. H., Sousa, V. H., O'Toole, J. F., Otto, E., Anlag, K., Klugmann, C., Treier, A. C., Helou, J., Sayer, J. A., et al.** (2007). Loss of GLIS2 causes nephronophthisis in humans and mice by increased apoptosis and fibrosis. *Nat Genet* **39**, 1018–1024.
- Bains, R., Furness, P. N. and Critchley, D. R.** (1997). A quantitative immunofluorescence study of glomerular cell adhesion proteins in proteinuric states. *J. Pathol.* **183**, 272–280.
- Bargon, S. D., Gunning, P. W. and O'Neill, G. M.** (2005). The Cas family docking protein, HEF1, promotes the formation of neurite-like membrane extensions. *Biochim Biophys Acta* **1746**, 143–154.

- Bazzoni, G., Carlesso, N., Griffin, J. D. and Hemler, M. E.** (1996). Bcr/Abl expression stimulates integrin function in hematopoietic cell lines. *J Clin Invest* **98**, 521–528.
- Beinke, C., Van Beuningen, D. and Cordes, N.** (2003). Ionizing radiation modules of the expression and tyrosine phosphorylation of the focal adhesion-associated proteins focal adhesion kinase (FAK) and its substrates p130cas and paxillin in A549 human lung carcinoma cells in vitro. *Int J Radiat Biol* **79**, 721–731.
- Benzing, T., Gerke, P., Hopker, K., Hildebrandt, F., Kim, E. and Walz, G.** (2001). Nephrocystin interacts with Pyk2, p130(Cas), and tensin and triggers phosphorylation of Pyk2. *Proc Natl Acad Sci U S A* **98**, 9784–9789.
- Bergers, G. and Benjamin, L. E.** (2003). Tumorigenesis and the angiogenic switch. **3**.
- Bianchi, M., De Lucchini, S., Marin, O., Turner, D. L., Hanks, S. K. and Villa-Moruzzi, E.** (2005). Regulation of FAK Ser-722 phosphorylation and kinase activity by GSK3 and PP1 during cell spreading and migration. *Biochem J* **391**, 359–370.
- Bisaro, B., Montani, M., Konstantinidou, G., Marchini, C., Pietrella, L., Iezzi, M., Galiè, M., Orso, F., Camporeale, A., Colombo, S. M., et al.** (2012). p130Cas/Cyclooxygenase-2 axis in the control of mesenchymal plasticity of breast cancer cells. *Breast Cancer Res.* **14**, R137.
- Bisaro, B., Sciortino, M., Colombo, S., Camacho-Leal, M. P., Costamagna, A., Castellano, I., Montemurro, F., Rossi, V., Valabrega, G., Turco, E., et al.** (2015). p130Cas scaffold protein regulates ErbB2 stability by altering breast cancer cell sensitivity to autophagy. *Oncotarget*.
- Bouton, A. H., Riggins, R. B. and Bruce-Staskal, P. J.** (2001). Functions of the adapter protein Cas: signal convergence and the determination of cellular responses. *Oncogene* **20**, 6448–6458.
- Bowden, E. T., Barth, M., Thomas, D., Glazer, R. I. and Mueller, S. C.** (1999). An invasion-related complex of cortactin, paxillin and PKCmu associates with invadopodia at sites of extracellular matrix degradation. *Oncogene* **18**, 4440–9.
- Brábek, J., Constancio, S. S., Shin, N. Y., Pozzi, A., Weaver, A. M. and Hanks, S. K.** (2004). CAS promotes invasiveness of Src-transformed cells. *Oncogene* **23**, 7406–7415.
- Brábek, J., Constancio, S. S., Siesser, P. F., Shin, N. Y., Pozzi, A. and Hanks, S. K.** (2005). Crk-associated substrate tyrosine phosphorylation sites are critical for

- invasion and metastasis of Src-transformed cells. *Mol. Cancer Res.* **3**, 307–315.
- Bradbury, P. M., Turner, K., Mitchell, C., Griffin, K. R., Middlemiss, S., Lau, L., Dagg, R., Taran, E., Cooper-White, J., Fabry, B., et al.** (2017). The focal adhesion targeting domain of p130Cas confers a mechanosensing function. *J. Cell Sci.* **130**, 1263–1273.
- Braniš, J., Pataki, C., Spörrer, M., Gerum, R. C., Mainka, A., Cermak, V., Goldmann, W. H., Fabry, B., Brabek, J. and Rosel, D.** (2017). The role of focal adhesion anchoring domains of CAS in mechanotransduction. *Sci. Rep.* **7**, 46233.
- Briknarová, K., Nasertorabi, F., Havert, M. L., Eggleston, E., Hoyt, D. W., Li, C., Olson, A. J., Vuori, K., Ely, K. R., Briknarova, K., et al.** (2005). The serine-rich domain from Crk-associated substrate (p130cas) is a four-helix bundle. *J. Biol. Chem.* **280**, 21908–21914.
- Brinkman, A., van der Flier, S., Kok, E. M. and Dorssers, L. C.** (2000). BCAR1, a human homologue of the adapter protein p130Cas, and antiestrogen resistance in breast cancer cells. *J Natl Cancer Inst* **92**, 112–120.
- Brinkman, A., de Jong, D., Tuinman, S., Azaouagh, N., van Agthoven, T. and Dorssers, L. C.** (2010). The substrate domain of BCAR1 is essential for anti-estrogen-resistant proliferation of human breast cancer cells. *Breast Cancer Res Treat* **120**, 401–408.
- Bruck, S., Huber, T. B., Ingham, R. J., Kim, K., Niederstrasser, H., Allen, P. M., Pawson, T., Cooper, J. A. and Shaw, A. S.** (2006). Identification of a novel inhibitory actin-capping protein binding motif in CD2-associated protein. *J Biol Chem* **281**, 19196–19203.
- Burnham, M. R., Harte, M. T., Richardson, A., Parsons, J. T. and Bouton, A. H.** (1996). The identification of p130cas-binding proteins and their role in cellular transformation. *Oncogene* **12**, 2467–2472.
- Cabodi, S., Moro, L., Baj, G., Smeriglio, M., Di Stefano, P., Gippone, S., Surico, N., Silengo, L., Turco, E., Tarone, G., et al.** (2004). p130Cas interacts with estrogen receptor alpha and modulates non-genomic estrogen signaling in breast cancer cells. *J Cell Sci* **117**, 1603–1611.
- Cabodi, S., Tinnirello, A., Di Stefano, P., Bisarò, B., Ambrosino, E., Castellano, I., Sapino, A., Arisio, R., Cavallo, F., Forni, G., et al.** (2006). p130Cas as a New Regulator of Mammary Epithelial Cell Proliferation, Survival, and HER2-Neu Oncogene-Dependent Breast Tumorigenesis. *Cancer Res.* **66**, 4672–4680.

- Cabodi, S., Tinnirello, A., Bisaro, B., Tornillo, G., del Pilar Camacho-Leal, M., Forni, G., Cojoca, R., Iezzi, M., Amici, A., Montani, M., et al.** (2010a). p130Cas is an essential transducer element in ErbB2 transformation. *FASEB J* **24**, 3796–3808.
- Cabodi, S., del Pilar Camacho-Leal, M., Di Stefano, P. and Defilippi, P.** (2010b). Integrin signalling adaptors: not only figurants in the cancer story. *Nat Rev Cancer* **10**, 858–870.
- Cai, D., Clayton, L. K., Smolyar, A. and Lerner, A.** (1999). AND-34, a novel p130Cas-binding thymic stromal cell protein regulated by adhesion and inflammatory cytokines. *J Immunol* **163**, 2104–2112.
- Cai, D., Iyer, A., Felekis, K. N., Near, R. I., Luo, Z., Chernoff, J., Albanese, C., Pestell, R. G. and Lerner, A.** (2003). AND-34/BCAR3, a GDP exchange factor whose overexpression confers antiestrogen resistance, activates Rac, PAK1, and the cyclin D1 promoter. *Cancer Res* **63**, 6802–6808.
- Camacho Leal, M. D. P., Sciortino, M., Tornillo, G., Colombo, S., Defilippi, P. and Cabodi, S.** (2015). p130Cas/BCAR1 scaffold protein in tissue homeostasis and pathogenesis. *Gene* **562**, 1–7.
- Carducci, M., Perfetto, L., Briganti, L., Paoluzi, S., Costa, S., Zerweck, J., Schutkowski, M., Castagnoli, L. and Cesareni, G.** (2012). The protein interaction network mediated by human SH3 domains. *Biotechnol Adv* **30**, 4–15.
- Carmeliet, P.** (2003). Angiogenesis in health and disease. *Nat. Med.* **9**, 653–60.
- Cary, L. A., Han, D. C., Polte, T. R., Hanks, S. K. and Guan, J. L.** (1998). Identification of p130Cas as a mediator of focal adhesion kinase-promoted cell migration. *J Cell Biol* **140**, 211–221.
- Casanova, I., Parreno, M., Farre, L., Guerrero, S., Cespedes, M. V, Pavon, M. A., Sancho, F. J., Marcuello, E., Trias, M. and Mangués, R.** (2006). Celecoxib induces anoikis in human colon carcinoma cells associated with the deregulation of focal adhesions and nuclear translocation of p130Cas. *Int J Cancer* **118**, 2381–2389.
- Chen, C.-H., Ho, Y.-C., Ho, H.-H., Chang, I.-C., Kirsch, K. H., Chuang, Y.-J., Layne, M. D. and Yet, S.-F.** (2013). Cysteine-rich protein 2 alters p130Cas localization and inhibits vascular smooth muscle cell migration. *Cardiovasc. Res.* **100**, 461–71.
- Chen, Z., Morales, J. E., Guerrero, P. A., Sun, H. and McCarty, J. H.** (2018).

- PTPN12/PTP-PEST Regulates Phosphorylation-Dependent Ubiquitination and Stability of Focal Adhesion Substrates in Invasive Glioblastoma Cells. *Cancer Res.* **78**, 3809–3822.
- Chodniewicz, D. and Klemke, R. L.** (2004). Regulation of integrin-mediated cellular responses through assembly of a CAS/Crk scaffold. *Biochim Biophys Acta* **1692**, 63–76.
- Collazos, A., Michael, N., Whelan, R. D., Kelly, G., Mellor, H., Pang, L. C., Totty, N. and Parker, P. J.** (2011). Site recognition and substrate screens for PKN family proteins. *Biochem J* **438**, 535–543.
- Cowan-Jacob, S. W., Fendrich, G., Manley, P. W., Jahnke, W., Fabbro, D., Liebetanz, J. and Meyer, T.** (2005). The crystal structure of a c-Src complex in an active conformation suggests possible steps in c-Src activation. *Structure* **13**, 861–71.
- Cowell, L. N., Graham, J. D., Bouton, A. H., Clarke, C. L. and O’Neill, G. M.** (2006). Tamoxifen treatment promotes phosphorylation of the adhesion molecules, p130Cas/BCAR1, FAK and Src, via an adhesion-dependent pathway. *Oncogene* **25**, 7597–7607.
- Cross, A. M., Wilson, A. L., Guerrero, M. S., Thomas, K. S., Bachir, A. I., Kubow, K. E., Horwitz, A. R. and Bouton, A. H.** (2016). Breast cancer antiestrogen resistance 3-p130Cas interactions promote adhesion disassembly and invasion in breast cancer cells. - PubMed - NCBI. *Oncogene* **35**, 5850–5859.
- Dadke, S. and Chernoff, J.** (2002). Interaction of protein tyrosine phosphatase (PTP) 1B with its substrates is influenced by two distinct binding domains. *Biochem J* **364**, 377–383.
- DeClerck, Y. A.** (2000). Interactions between tumour cells and stromal cells and proteolytic modification of the extracellular matrix by metalloproteinases in cancer. *Eur J Cancer* **36**, 1258–1268.
- Defilippi, P., Di Stefano, P. and Cabodi, S.** (2006). p130Cas: a versatile scaffold in signaling networks. *Trends Cell Biol* **16**, 257–263.
- DeLano, W. L.** (2002). The PyMOL Molecular Graphics System. *DeLano Sci. San Carlos, CA, USA*.
- Di Stefano, P., Cabodi, S., Boeri Erba, E., Margaria, V., Bergatto, E., Giuffrida, M. G., Silengo, L., Tarone, G., Turco, E. and Defilippi, P.** (2004). P130Cas-associated protein (p140Cap) as a new tyrosine-phosphorylated protein involved in

cell spreading. *Mol Biol Cell* **15**, 787–800.

- Di Stefano, P., Leal, M. P., Tornillo, G., Bisaro, B., Repetto, D., Pincini, A., Santopietro, E., Sharma, N., Turco, E., Cabodi, S., et al.** (2011). The adaptor proteins p140CAP and p130CAS as molecular hubs in cell migration and invasion of cancer cells. *Am J Cancer Res* **1**, 663–673.
- Dodelet, V. C., Pazzagli, C., Zisch, A. H., Hauser, C. A. and Pasquale, E. B.** (1999). A novel signaling intermediate, SHEP1, directly couples Eph receptors to R-Ras and Rap1A. *J Biol Chem* **274**, 31941–31946.
- Donaldson, J. C., Dempsey, P. J., Reddy, S., Bouton, A. H., Coffey, R. J. and Hanks, S. K.** (2000). Crk-associated substrate p130(Cas) interacts with nephrocystin both proteins localize to cell-cell contacts of polarized epithelial cells. *Exp. Cell Res.* **256**, 168–178.
- Donato, D. M., Ryzhova, L. M., Meenderink, L. M., Kaverina, I. and Hanks, S. K.** (2010). Dynamics and mechanism of p130Cas localization to focal adhesions. *J Biol Chem* **285**, 20769–20779.
- Dorssers, L. C., van Agthoven, T., Dekker, A., van Agthoven, T. L. and Kok, E. M.** (1993). Induction of antiestrogen resistance in human breast cancer cells by random insertional mutagenesis using defective retroviruses: identification of bcar-1, a common integration site. *Mol Endocrinol* **7**, 870–878.
- Dorssers, L. C., Van der Flier, S., Brinkman, A., van Agthoven, T., Veldscholte, J., Berns, E. M., Klijn, J. G., Beex, L. V and Foekens, J. A.** (2001). Tamoxifen resistance in breast cancer: elucidating mechanisms. *Drugs* **61**, 1721–33.
- Dorssers, L. C., Grebenchtchikov, N., Brinkman, A., Look, M. P., van Broekhoven, S. P., de Jong, D., Peters, H. A., Portengen, H., Meijer-van Gelder, M. E., Klijn, J. G., et al.** (2004). The prognostic value of BCAR1 in patients with primary breast cancer. *Clin Cancer Res* **10**, 6194–6202.
- Evans, I. M., Yamaji, M., Britton, G., Pellet-Many, C., Lockie, C., Zachary, I. C. and Frankel, P.** (2011). Neuropilin-1 signaling through p130Cas tyrosine phosphorylation is essential for growth factor-dependent migration of glioma and endothelial cells. *Mol Cell Biol* **31**, 1174–1185.
- Evans, I. M., Kennedy, S. A., Paliashvili, K., Santra, T., Yamaji, M., Lovering, R. C., Britton, G., Frankel, P., Kolch, W. and Zachary, I. C.** (2017). Vascular Endothelial Growth Factor (VEGF) Promotes Assembly of the p130Cas Interactome to Drive Endothelial Chemotactic Signaling and Angiogenesis. *Mol.*

Cell. Proteomics **16**, 168–180.

- Fantin, A., Herzog, B., Mahmoud, M., Yamaji, M., Plein, A., Denti, L., Ruhrberg, C. and Zachary, I.** (2014). Neuropilin 1 (NRP1) hypomorphism combined with defective VEGF-A binding reveals novel roles for NRP1 in developmental and pathological angiogenesis. *Development* **141**, 556–562.
- Ferrara, N., Gerber, H.-P. and LeCouter, J.** (2003). The biology of VEGF and its receptors. *Nat. Med.* **9**, 669–76.
- Flinn, H. M. and Ridley, A. J.** (1996). Rho stimulates tyrosine phosphorylation of focal adhesion kinase, p130 and paxillin. *J Cell Sci* **109** (Pt 5), 1133–1141.
- Flint, A. J., Tiganis, T., Barford, D. and Tonks, N. K.** (1997). Development of “substrate-trapping” mutants to identify physiological substrates of protein tyrosine phosphatases. *Proc Natl Acad Sci U S A* **94**, 1680–1685.
- Fonseca, P. M., Shin, N. Y., Brabek, J., Ryzhova, L., Wu, J. and Hanks, S. K.** (2004). Regulation and localization of CAS substrate domain tyrosine phosphorylation. *Cell Signal* **16**, 621–629.
- Fromont, G. and Cussenot, O.** (2011). The integrin signalling adaptor p130CAS is also a key player in prostate cancer. *Nat Rev Cancer* **11**, 227.
- Fromont, G., Vallancien, G., Validire, P., Levillain, P. and Cussenot, O.** (2007). BCAR1 expression in prostate cancer: Association with 16q23 LOH status, tumor progression and EGFR/KAI1 staining. *Prostate* **67**, 268–273.
- Funasaka, K., Ito, S., Hasegawa, H., Goldberg, G. S., Hirooka, Y., Goto, H., Hamaguchi, M. and Senga, T.** (2010). Cas utilizes Nck2 to activate Cdc42 and regulate cell polarization during cell migration in response to wound healing. *FEBS J* **277**, 3502–3513.
- Gao, J., Aksoy, B. A., Dogrusoz, U., Dresdner, G., Gross, B., Sumer, S. O., Sun, Y., Jacobsen, A., Sinha, R., Larsson, E., et al.** (2013). Integrative Analysis of Complex Cancer Genomics and Clinical Profiles Using the cBioPortal. *Sci. Signal.* **6**, p11-p11.
- Garcia-Guzman, M., Dolfi, F., Russello, M. and Vuori, K.** (1999). Cell adhesion regulates the interaction between the docking protein p130(Cas) and the 14-3-3 proteins. *J Biol Chem* **274**, 5762–5768.
- Garton, A. J. and Tonks, N. K.** (1999). Regulation of fibroblast motility by the protein tyrosine phosphatase PTP-PEST. *J Biol Chem* **274**, 3811–3818.
- Garton, A. J., Flint, A. J. and Tonks, N. K.** (1996). Identification of p130(cas) as a

- substrate for the cytosolic protein tyrosine phosphatase PTP-PEST. *Mol Cell Biol* **16**, 6408–6418.
- Garton, A. J., Burnham, M. R., Bouton, A. H. and Tonks, N. K.** (1997). Association of PTP-PEST with the SH3 domain of p130(cas); A novel mechanism of protein tyrosine phosphatase substrate recognition. *Oncogene* **15**, 877–885.
- Geblinger, D., Addadi, L., Geiger, B., Yamada, K. M., Geiger, B. and Kam, Z.** (2010). Nano-topography sensing by osteoclasts. *J. Cell Sci.* **123**, 1503–10.
- Gemperle, J., Hexnerová, R., Lepšík, M., Tesina, P., Dibus, M., Novotný, M., Brábek, J., Veverka, V. and Rosel, D.** (2017). Structural characterization of CAS SH3 domain selectivity and regulation reveals new CAS interaction partners. *Sci. Rep.* **7**, 1–18.
- Gemperle, J., Dibus, M., Koudelková, L., Rosel, D. and Brábek, J.** (2018). The interaction of p130Cas with PKN3 promotes malignant growth. *bioRxiv*.
- Giaccone, G. and Zucali, P. A.** (2008). Src as a potential therapeutic target in non-small-cell lung cancer. *Ann. Oncol. Off. J. Eur. Soc. Med. Oncol.* **19**, 1219–23.
- Gigante, M., Pontrelli, P., Montemurno, E., Roca, L., Aucella, F., Penza, R., Caridi, G., Ranieri, E., Ghiggeri, G. M. and Gesualdo, L.** (2009). CD2AP mutations are associated with sporadic nephrotic syndrome and focal segmental glomerulosclerosis (FSGS). *Nephrol. Dial. Transplant.* **24**, 1858–1864.
- Gingras, D., Michaud, M., Di Tomasso, G., Beliveau, E., Nyalendo, C. and Beliveau, R.** (2008). Sphingosine-1-phosphate induces the association of membrane-type 1 matrix metalloproteinase with p130Cas in endothelial cells. *FEBS Lett* **582**, 399–404.
- Gotoh, T., Cai, D., Tian, X., Feig, L. A. and Lerner, A.** (2000). p130Cas regulates the activity of AND-34, a novel Ral, Rap1, and R-Ras guanine nucleotide exchange factor. *J Biol Chem* **275**, 30118–30123.
- Guilluy, C., Garcia-Mata, R. and Burridge, K.** (2011). Rho protein crosstalk: another social network? *Trends Cell Biol* **21**, 718–726.
- Gustavsson, A., Yuan, M. and Fallman, M.** (2004). Temporal dissection of beta1-integrin signaling indicates a role for p130Cas-Crk in filopodia formation. *J Biol Chem* **279**, 22893–22901.
- Hakak, Y. and Martin, G. S.** (1999). Cas mediates transcriptional activation of the serum response element by Src. *Mol Cell Biol* **19**, 6953–6962.
- Hallock, P. T., Xu, C.-F. F., Park, T.-J. J., Neubert, T. A., Curran, T. and Burden,**

- S. J.** (2010). Dok-7 regulates neuromuscular synapse formation by recruiting Crk and Crk-L. *Genes Dev* **24**, 2451–2461.
- Haramizu, S., Mori, T., Yano, M., Ota, N., Hashizume, K., Otsuka, A., Hase, T. and Shimotoyodome, A.** (2014). Habitual exercise plus dietary supplementation with milk fat globule membrane improves muscle function deficits via neuromuscular development in senescence-accelerated mice. *Springerplus* **3**, 339.
- Harte, M. T., Hildebrand, J. D., Burnham, M. R., Bouton, A. H. and Parsons, J. T.** (1996). p130Cas, a substrate associated with v-Src and v-Crk, localizes to focal adhesions and binds to focal adhesion kinase. *J Biol Chem* **271**, 13649–13655.
- Harte, M. T., Macklem, M., Weidow, C. L., Parsons, J. T. and Bouton, A. H.** (2000). Identification of two focal adhesion targeting sequences in the adapter molecule p130(Cas). *Biochim Biophys Acta* **1499**, 34–48.
- Hawkins, P. T., Eguinoa, A., Qiu, R. G., Stokoe, D., Cooke, F. T., Walters, R., Wennstrom, S., Claesson-Welsh, L., Evans, T., Symons, M., et al.** (1995). PDGF stimulates an increase in GTP-Rac via activation of phosphoinositide 3-kinase. *Curr Biol* **5**, 393–403.
- Hivert, V., Pierre, J. and Raingeaud, J.** (2009). Phosphorylation of human enhancer of filamentation (HEF1) on serine 369 induces its proteasomal degradation. *Biochem Pharmacol* **78**, 1017–1025.
- Holcomb, M., Rufini, A., Barilà, D. and Klemke, R. L.** (2006). Deregulation of proteasome function induces Abl-mediated cell death by uncoupling p130CAS and c-CrkII. *J. Biol. Chem.* **281**, 2430–40.
- Honda, H., Oda, H., Nakamoto, T., Honda, Z., Sakai, R., Suzuki, T., Saito, T., Nakamura, K., Nakao, K., Ishikawa, T., et al.** (1998). Cardiovascular anomaly, impaired actin bundling and resistance to Src-induced transformation in mice lacking p130Cas. *Nat Genet* **19**, 361–365.
- Honda, H., Nakamoto, T., Sakai, R. and Hirai, H.** (1999). p130(Cas), an assembling molecule of actin filaments, promotes cell movement, cell migration, and cell spreading in fibroblasts. *Biochem Biophys Res Commun* **262**, 25–30.
- Hoon Kim, D., Jeon Choi, S., Kook, S., Kim, W. and Keun Song, W.** (2003). Phosphorylation-dependent cleavage of p130cas in apoptotic rat-1 cells. *Biochem Biophys Res Commun* **300**, 141–148.
- Hotta, K., Ranganathan, S., Liu, R., Wu, F., Machiyama, H., Gao, R., Hirata, H., Soni, N., Ohe, T., Hogue, C. W. V, et al.** (2014). Biophysical properties of

- intrinsically disordered p130Cas substrate domain--implication in mechanosensing. *PLoS Comput. Biol.* **10**, e1003532.
- Hsia, D. A., Mitra, S. K., Hauck, C. R., Streblow, D. N., Nelson, J. A., Ilic, D., Huang, S., Li, E., Nemerow, G. R., Leng, J., et al.** (2003). Differential regulation of cell motility and invasion by FAK. *J Cell Biol* **160**, 753–767.
- Huveneers, S. and Danen, E. H.** (2009). Adhesion signaling - crosstalk between integrins, Src and Rho. *J Cell Sci* **122**, 1059–1069.
- Irby, R. B. and Yeatman, T. J.** (2000). Role of Src expression and activation in human cancer. *Oncogene* **19**, 5636–42.
- Janoštiak, R., Tolde, O., Brůhová, Z., Novotný, M., Hanks, S. K., Rösel, D. and Brábek, J.** (2011). Tyrosine Phosphorylation within the SH3 domain Regulates CAS Subcellular Localization, Cell Migration, and Invasiveness. *Mol Biol Cell* **22**, 4256–4267.
- Janoštiak, R., Brábek, J., Auernheimer, V., Tatárová, Z., Lautscham, L. A., Dey, T., Gemperle, J., Merkel, R., Goldmann, W. H., Fabry, B., et al.** (2014a). CAS directly interacts with vinculin to control mechanosensing and focal adhesion dynamics. *Cell. Mol. Life Sci.* **71**, 727–44.
- Janoštiak, R., Pataki, A. C., Brábek, J. and Rösel, D.** (2014b). *Mechanosensors in integrin signaling: The emerging role of p130Cas.*
- Janssen, H. and Marynen, P.** (2006). Interaction partners for human ZNF384/CIZ/NMP4--zyxin as a mediator for p130CAS signaling? *Exp Cell Res* **312**, 1194–1204.
- Jucker, M., McKenna, K., da Silva, A. J., Rudd, C. E. and Feldman, R. A.** (1997). The Fes protein-tyrosine kinase phosphorylates a subset of macrophage proteins that are involved in cell adhesion and cell-cell signaling. *J Biol Chem* **272**, 2104–2109.
- Juin, A., Planus, E., Guillemot, F., Horakova, P., Albiges-Rizo, C., Génot, E., Rosenbaum, J., Moreau, V. and Saltel, F.** (2013). Extracellular matrix rigidity controls podosome induction in microvascular endothelial cells. *Biol. Cell* **105**, 46–57.
- Kanchanawong, P., Shtengel, G., Pasapera, A. M., Ramko, E. B., Davidson, M. W., Hess, H. F. and Waterman, C. M.** (2010). Nanoscale architecture of integrin-based cell adhesions. *Nature* **468**, 580–584.
- Kaneko, K., Ito, M., Naoe, Y., Lacy-Hulbert, A. and Ikeda, K.** (2014). Integrin α v in

the mechanical response of osteoblast lineage cells. *Biochem. Biophys. Res. Commun.* **447**, 352–7.

- Kang, Y. S., Kim, W., Huh, Y. H., Bae, J., Kim, J. S. and Song, W. K.** (2011). P130Cas attenuates epidermal growth factor (EGF) receptor internalization by modulating EGF-triggered dynamin phosphorylation. *PLoS One* **6**, e20125.
- Kang, H., Kim, C., Lee, H., Rho, J. G., Seo, J.-W., Nam, J.-W., Song, W. K., Nam, S. W., Kim, W. and Lee, E. K.** (2015). Downregulation of microRNA-362-3p and microRNA-329 promotes tumor progression in human breast cancer. *Cell Death Differ.* **23**, 484–495.
- Kang, H., Rho, J. G., Kim, C., Tak, H., Lee, H., Ji, E., Ahn, S., Shin, A.-R., Cho, H.-I., Huh, Y. H., et al.** (2017). The miR-24-3p/p130Cas: a novel axis regulating the migration and invasion of cancer cells. *Sci. Rep.* **7**, 44847.
- Kanner, S. B., Reynolds, A. B., Wang, H. C., Vines, R. R. and Parsons, J. T.** (1991). The SH2 and SH3 domains of pp60src direct stable association with tyrosine phosphorylated proteins p130 and p110. *EMBO J* **10**, 1689–1698.
- Karginov, A. V., Tsygankov, D., Berginski, M., Chu, P.-H., Trudeau, E. D., Yi, J. J., Gomez, S., Elston, T. C. and Hahn, K. M.** (2014). Dissecting motility signaling through activation of specific Src-effector complexes. *Nat. Chem. Biol.* **10**, 286–90.
- Katsumi, A., Orr, A. W., Tzima, E. and Schwartz, M. A.** (2004). Integrins in mechanotransduction. *J. Biol. Chem.* **279**, 12001–4.
- Kim, W., Kook, S., Kim, D. J., Teodorof, C. and Song, W. K.** (2004). The 31-kDa caspase-generated cleavage product of p130cas functions as a transcriptional repressor of E2A in apoptotic cells. *J Biol Chem* **279**, 8333–8342.
- Kim, W., Seok Kang, Y., Soo Kim, J., Shin, N. Y., Hanks, S. K. and Song, W. K.** (2008). The integrin-coupled signaling adaptor p130Cas suppresses Smad3 function in transforming growth factor-beta signaling. *Mol Biol Cell* **19**, 2135–2146.
- Kim, L. C., Song, L. and Haura, E. B.** (2009). Src kinases as therapeutic targets for cancer. *Nat. Rev. Clin. Oncol.* **6**, 587–595.
- Kim, J. Y., Huh, K., Jung, R. and Kim, T. J.** (2011). Identification of BCAR-1 as a new substrate of Syk tyrosine kinase through a determination of amino acid sequence preferences surrounding the substrate tyrosine residue. *Immunol Lett* **135**, 151–157.

- Kirsch, K. H., Georgescu, M. M. and Hanafusa, H.** (1998). Direct binding of p130(Cas) to the guanine nucleotide exchange factor C3G. *J. Biol. Chem.* **273**, 25673–25679.
- Kirsch, K. H., Georgescu, M. M., Ishimaru, S. and Hanafusa, H.** (1999). CMS: an adapter molecule involved in cytoskeletal rearrangements. *Proc Natl Acad Sci U S A* **96**, 6211–6216.
- Kiyokawa, E., Hashimoto, Y., Kurata, T., Sugimura, H. and Matsuda, M.** (1998a). Evidence that DOCK180 up-regulates signals from the CrkII-p130(Cas) complex. *J Biol Chem* **273**, 24479–24484.
- Kiyokawa, E., Hashimoto, Y., Kobayashi, S., Sugimura, H., Kurata, T. and Matsuda, M.** (1998b). Activation of Rac1 by a Crk SH3-binding protein, DOCK180. *Genes Dev* **12**, 3331–3336.
- Klemke, R. L., Leng, J., Molander, R., Brooks, P. C., Vuori, K. and Cheresch, D. A.** (1998). CAS/Crk coupling serves as a “molecular switch” for induction of cell migration. *J Cell Biol* **140**, 961–972.
- Klinghoffer, R. A., Sachsenmaier, C., Cooper, J. A. and Soriano, P.** (1999). Src family kinases are required for integrin but not PDGFR signal transduction. *EMBO J* **18**, 2459–2471.
- Konrad, R. J., Gold, G., Lee, T. N., Workman, R., Broderick, C. L. and Knierman, M. D.** (2003). Glucose stimulates the tyrosine phosphorylation of Crk-associated substrate in pancreatic beta-cells. *J Biol Chem* **278**, 28116–28122.
- Kook, S., Shim, S. R., Choi, S. J., Ahnn, J., Kim, J. I., Eom, S. H., Jung, Y. K., Paik, S. G. and Song, W. K.** (2000). Caspase-mediated cleavage of p130cas in etoposide-induced apoptotic Rat-1 cells. *Mol Biol Cell* **11**, 929–939.
- Kraus, M., Dolinski, B., Rosahl, T. W. and Magee, J. A.** (2015). Protein kinase N3 deficiency impedes PI3-kinase pathway-driven leukemogenesis without affecting normal hematopoiesis. *Leukemia* **29**, 255–258.
- Kumagai, N., Morii, N., Fujisawa, K., Nemoto, Y. and Narumiya, S.** (1993). ADP-ribosylation of rho p21 inhibits lysophosphatidic acid-induced protein tyrosine phosphorylation and phosphatidylinositol 3-kinase activation in cultured Swiss 3T3 cells. *J Biol Chem* **268**, 24535–24538.
- Kumbrink, J. and Kirsch, K. H.** (2012). Regulation of p130(Cas)/BCAR1 expression in tamoxifen-sensitive and tamoxifen-resistant breast cancer cells by EGR1 and NAB2. *Neoplasia* **14**, 108–20.

- Kumbrink, J., Soni, S., Laumbacher, B., Loesch, B. and Kirsch, K. H.** (2015). Identification of Novel Crk-associated Substrate (p130Cas) Variants with Functionally Distinct Focal Adhesion Kinase Binding Activities. *J. Biol. Chem.* **290**, 12247–55.
- Lahlou, H., Sanguin-Gendreau, V., Frame, M. C. and Muller, W. J.** (2012). Focal adhesion kinase contributes to proliferative potential of ErbB2 mammary tumour cells but is dispensable for ErbB2 mammary tumour induction in vivo. *Breast Cancer Res.* **14**, R36.
- Lakkakorpi C, P. T., Nakamura, I., Nagy, R. M., Parsons, J. T., Rodan, G. A. and Duong, L. T.** (1999). Stable association of PYK2 and p130(Cas) in osteoclasts and their co-localization in the sealing zone. *J. Biol. Chem.* **274**, 4900–7.
- Law, S. F., Zhang, Y. Z., Fashena, S. J., Toby, G., Estojak, J. and Golemis, E. A.** (1999). Dimerization of the docking/adaptor protein HEF1 via a carboxy-terminal helix-loop-helix domain. *Exp Cell Res* **252**, 224–235.
- Leenders, F., Möpert, K., Schmiedeknecht, A., Santel, A., Czauderna, F., Aleku, M., Penschuck, S., Dames, S., Sternberger, M., Rohl, T., et al.** (2004). PKN3 is required for malignant prostate cell growth downstream of activated PI 3-kinase. *EMBO J* **23**, 3303–3313.
- Lehtonen, S., Zhao, F. and Lehtonen, E.** (2002). CD2-associated protein directly interacts with the actin cytoskeleton. *Am J Physiol Ren. Physiol* **283**, F734-43.
- Li, S. S.** (2005). Specificity and versatility of SH3 and other proline-recognition domains: structural basis and implications for cellular signal transduction. *Biochem J* **390**, 641–653.
- Li, X. and Earp, H. S.** (1997). Paxillin is tyrosine-phosphorylated by and preferentially associates with the calcium-dependent tyrosine kinase in rat liver epithelial cells. *J Biol Chem* **272**, 14341–14348.
- Li, E., Stupack, D. G., Brown, S. L., Klemke, R., Schlaepfer, D. D. and Nemerow, G. R.** (2000). Association of p130CAS with phosphatidylinositol-3-OH kinase mediates adenovirus cell entry. *J Biol Chem* **275**, 14729–14735.
- Linder, S. and Aepfelbacher, M.** (2003). Podosomes: adhesion hot-spots of invasive cells. *Trends Cell Biol.* **13**, 376–85.
- Liu, F., Hill, D. E. and Chernoff, J.** (1996). Direct binding of the proline-rich region of protein tyrosine phosphatase 1B to the Src homology 3 domain of p130(Cas). *J Biol Chem* **271**, 31290–31295.

- Liu, F., Sells, M. A. and Chernoff, J.** (1998). Protein tyrosine phosphatase 1B negatively regulates integrin signaling. *Curr Biol* **8**, 173–176.
- Lu, C., Wu, F., Qiu, W. and Liu, R.** (2013). P130Cas substrate domain is intrinsically disordered as characterized by single-molecule force measurements. *Biophys. Chem.* **180–181**, 37–43.
- Luo, W., Slebos, R. J., Hill, S., Li, M., Brabek, J., Amanchy, R., Chaerkady, R., Pandey, A., Ham, A. J. L. and Hanks, S. K.** (2008). Global impact of oncogenic Src on a phosphotyrosine proteome. *J. Proteome Res.* **7**, 3447–3460.
- Ma, A., Richardson, A., Schaefer, E. M. and Parsons, J. T.** (2001). Serine phosphorylation of focal adhesion kinase in interphase and mitosis: a possible role in modulating binding to p130(Cas). *Mol Biol Cell* **12**, 1–12.
- Mace, P. D., Wallez, Y., Dobaczewska, M. K., Lee, J. J., Robinson, H., Pasquale, E. B. and Riedl, S. J.** (2011). NSP-Cas protein structures reveal a promiscuous interaction module in cell signaling. *Nat Struct Mol Biol* **18**, 1381–1387.
- Makkinje, A., Near, R. I., Infusini, G., Vanden Borre, P., Bloom, A., Cai, D., Costello, C. E. and Lerner, A.** (2009). AND-34/BCAR3 regulates adhesion-dependent p130Cas serine phosphorylation and breast cancer cell growth pattern. *Cell Signal* **21**, 1423–1435.
- Manie, S. N., Astier, A., Haghayeghi, N., Canty, T., Druker, B. J., Hirai, H. and Freedman, A. S.** (1997). Regulation of integrin-mediated p130(Cas) tyrosine phosphorylation in human B cells. A role for p59(Fyn) and SHP2. *J Biol Chem* **272**, 15636–15641.
- Matsuda, M., Mayer, B. J., Fukui, Y. and Hanafusa, H.** (1990). Binding of transforming protein, P47gag-crk, to a broad range of phosphotyrosine-containing proteins. *Science (80-.)*. **248**, 1537–1539.
- Mayer, B. J.** (2001). SH3 domains: complexity in moderation. *J Cell Sci* **114**, 1253–1263.
- Mayer, B. J., Hirai, H. and Sakai, R.** (1995). Evidence that SH2 domains promote processive phosphorylation by protein-tyrosine kinases. *Curr Biol* **5**, 296–305.
- Meenderink, L. M., Ryzhova, L. M., Donato, D. M., Gochberg, D. F., Kaverina, I. and Hanks, S. K.** (2010). P130Cas Src-binding and substrate domains have distinct roles in sustaining focal adhesion disassembly and promoting cell migration. *PLoS One* **5**, e13412.
- Modzelewska, K., Newman, L. P., Desai, R. and Keely, P. J.** (2006). Ack1 mediates

- Cdc42-dependent cell migration and signaling to p130Cas. *J Biol Chem* **281**, 37527–37535.
- Mollet, G., Silbermann, F., Delous, M., Salomon, R., Antignac, C. and Saunier, S.** (2005). Characterization of the nephrocystin/nephrocystin-4 complex and subcellular localization of nephrocystin-4 to primary cilia and centrosomes. *Hum. Mol. Genet.* **14**, 645–656.
- Möpert, K., Löffler, K., Röder, N., Kaufmann, J. and Santel, A.** (2012). Depletion of protein kinase N3 (PKN3) impairs actin and adherens junctions dynamics and attenuates endothelial cell activation. *Eur J Cell Biol* **91**, 694–705.
- Mukai, H., Muramatsu, A., Mashud, R., Kubouchi, K., Tsujimoto, S., Hongu, T., Kanaho, Y., Tsubaki, M., Nishida, S., Shioi, G., et al.** (2016). PKN3 is the major regulator of angiogenesis and tumor metastasis in mice. *Sci. Rep.* **6**, 18979.
- Nagai, Y., Osawa, K., Fukushima, H., Tamura, Y., Aoki, K., Ohya, K., Yasuda, H., Hikiji, H., Takahashi, M., Seta, Y., et al.** (2013). p130Cas, Crk-associated substrate, plays important roles in osteoclastic bone resorption. *J. Bone Miner. Res.* **28**, 2449–62.
- Nakamoto, T., Sakai, R., Ozawa, K., Yazaki, Y. and Hirai, H.** (1996). Direct binding of C-terminal region of p130Cas to SH2 and SH3 domains of Src kinase. *J Biol Chem* **271**, 8959–8965.
- Nakamoto, T., Sakai, R., Honda, H., Ogawa, S., Ueno, H., Suzuki, T., Aizawa, S., Yazaki, Y. and Hirai, H.** (1997). Requirements for localization of p130cas to focal adhesions. *Mol Cell Biol* **17**, 3884–3897.
- Nakamoto, T., Yamagata, T., Sakai, R., Ogawa, S., Honda, H., Ueno, H., Hirano, N., Yazaki, Y. and Hirai, H.** (2000). CIZ, a zinc finger protein that interacts with p130(cas) and activates the expression of matrix metalloproteinases. *Mol Cell Biol* **20**, 1649–1658.
- Nakamura, I., Jimi, E., Duong, L. T., Sasaki, T., Takahashi, N., Rodan, G. A. and Suda, T.** (1998). Tyrosine phosphorylation of p130Cas is involved in actin organization in osteoclasts. *J Biol Chem* **273**, 11144–11149.
- Near, R. I., Zhang, Y., Makkinje, A., Vanden Borre, P. and Lerner, A.** (2007). AND-34/BCAR3 differs from other NSP homologs in induction of anti-estrogen resistance, cyclin D1 promoter activation and altered breast cancer cell morphology. *J Cell Physiol* **212**, 655–665.
- Neve, A., Cantatore, F. P., Maruotti, N., Corrado, A. and Ribatti, D.** (2014).

Extracellular matrix modulates angiogenesis in physiological and pathological conditions. *Biomed Res. Int.* **2014**,.

- Nick, A. M., Stone, R. L., Armaiz-Pena, G., Ozpolat, B., Tekedereli, I., Graybill, W. S., Landen, C. N., Villares, G., Vivas-Mejia, P., Bottsford-Miller, J., et al.** (2011). Silencing of p130cas in ovarian carcinoma: a novel mechanism for tumor cell death. *J. Natl. Cancer Inst.* **103**, 1596–612.
- Nikonova, A. S., Gaponova, A. V., Kudinov, A. E. and Golemis, E. A.** (2014). CAS proteins in health and disease: An update. *IUBMB Life* **66**, 387–395.
- Nobes, C. D. and Hall, A.** (1995). Rho, rac, and cdc42 GTPases regulate the assembly of multimolecular focal complexes associated with actin stress fibers, lamellipodia, and filopodia. *Cell* **81**, 53–62.
- Ohba, T., Ishino, M., Aoto, H. and Sasaki, T.** (1998). Interaction of two proline-rich sequences of cell adhesion kinase beta with SH3 domains of p130(Cas)-related proteins and a GTPase-activating protein, *Graf. Biochem. J.* **330**, 1249–1254.
- Oishi, K., Mukai, H., Shibata, H., Takahashi, M. and Ona, Y.** (1999). Identification and characterization of PKNbeta, a novel isoform of protein kinase PKN: expression and arachidonic acid dependency are different from those of PKNalpha. *Biochem Biophys Res Commun* **261**, 808–814.
- Ojaniemi, M. and Vuori, K.** (1997). Epidermal growth factor modulates tyrosine phosphorylation of p130Cas. Involvement of phosphatidylinositol 3'-kinase and actin cytoskeleton. *J Biol Chem* **272**, 25993–25998.
- Oktay, M., Wary, K. K., Dans, M., Birge, R. B. and Giancotti, F. G.** (1999). Integrin-mediated activation of focal adhesion kinase is required for signaling to Jun NH2-terminal kinase and progression through the G1 phase of the cell cycle. *J Cell Biol* **145**, 1461–1469.
- Pan, Y.-R. R., Chen, C.-L. L. and Chen, H.-C. C.** (2011). FAK is required for the assembly of podosome rosettes. *J. Cell Biol.* **195**, 113–29.
- Paul, N. R. R., Jacquemet, G. and Caswell, P. T. T.** (2015). Endocytic Trafficking of Integrins in Cell Migration. *Curr. Biol.* **25**, R1092-105.
- Pellet-Many, C., Frankel, P., Evans, I. M., Herzog, B., Junemann-Ramirez, M. and Zachary, I. C.** (2011). Neuropilin-1 mediates PDGF stimulation of vascular smooth muscle cell migration and signalling via p130Cas. *Biochem J* **435**, 609–618.
- Pincini, A., Tornillo, G., Orso, F., Sciortino, M., Bisaro, B., Leal, M. D. P. C.,**

- Lembo, A., Brizzi, M. F., Turco, E., De Pittà, C., et al.** (2013). Identification of p130Cas/ErbB2-dependent invasive signatures in transformed mammary epithelial cells. *Cell Cycle* **12**, 2409–22.
- Polte, T. R. and Hanks, S. K.** (1997). Complexes of focal adhesion kinase (FAK) and Crk-associated substrate (p130(Cas)) are elevated in cytoskeleton-associated fractions following adhesion and Src transformation. Requirements for Src kinase activity and FAK proline-rich motifs. *J Biol Chem* **272**, 5501–5509.
- Polte, T. R., Hanks, S. K. and Polte Hanks, S.K., T. R.** (1995). Interaction between focal adhesion kinase and Crk-associated tyrosine kinase substrate p130Cas. *Proc Natl Acad Sci U S A* **92**, 10678–10682.
- Posern, G., Zheng, J., Knudsen, B. S., Kardinal, C., Müller, K. B., Voss, J., Shishido, T., Cowburn, D., Cheng, G., Wang, B., et al.** (1998). Development of highly selective SH3 binding peptides for Crk and CRKL which disrupt Crk-complexes with DOCK180, SoS and C3G. *Oncogene* **16**, 1903–1912.
- Praefcke, G. J. and McMahon, H. T.** (2004). The dynamin superfamily: universal membrane tubulation and fission molecules? *Nat Rev Mol Cell Biol* **5**, 133–147.
- Prasad, N., Topping, R. S. and Decker, S. J.** (2001). SH2-containing inositol 5'-phosphatase SHIP2 associates with the p130(Cas) adapter protein and regulates cellular adhesion and spreading. *Mol Cell Biol* **21**, 1416–1428.
- Pratt, S. J., Epple, H., Ward, M., Feng, Y., Braga, V. M. and Longmore, G. D.** (2005). The LIM protein Ajuba influences p130Cas localization and Rac1 activity during cell migration. *J Cell Biol* **168**, 813–824.
- Pugacheva, E. N., Roegiers, F. and Golemis, E. A.** (2006). Interdependence of cell attachment and cell cycle signaling. *Curr Opin Cell Biol* **18**, 507–515.
- Pylayeva, Y., Gillen, K. M., Gerald, W., Beggs, H. E., Reichardt, L. F. and Giancotti, F. G.** (2009). Ras- and PI3K-dependent breast tumorigenesis in mice and humans requires focal adhesion kinase signaling. *J Clin Invest* **119**, 252–266.
- Regelmann, A. G., Danzl, N. M., Wanjalla, C. and Alexandropoulos, K.** (2006). The hematopoietic isoform of Cas-Hef1-associated signal transducer regulates chemokine-induced inside-out signaling and T cell trafficking. *Immunity* **25**, 907–918.
- Reynolds, A. B., Kanner, S. B., Wang, H. C. and Parsons, J. T.** (1989). Stable association of activated pp60src with two tyrosine-phosphorylated cellular proteins. *Mol Cell Biol* **9**, 3951–3958.

- Riggins, R. B., DeBerry, R. M., Toosarvandani, M. D. and Bouton, A. H.** (2003a). Src-dependent association of Cas and p85 phosphatidylinositol 3'-kinase in v-crk-transformed cells. *Mol Cancer Res* **1**, 428–437.
- Riggins, R. B., Quilliam, L. A. and Bouton, A. H.** (2003b). Synergistic promotion of c-Src activation and cell migration by Cas and AND-34/BCAR3. *J Biol Chem* **278**, 28264–28273.
- Riggins, R. B., Thomas, K. S., Ta, H. Q., Wen, J., Davis, R. J., Schuh, N. R., Donelan, S. S., Owen, K. A., Gibson, M. A., Shupnik, M. A., et al.** (2006). Physical and functional interactions between Cas and c-Src induce tamoxifen resistance of breast cancer cells through pathways involving epidermal growth factor receptor and signal transducer and activator of transcription 5b. *Cancer Res* **66**, 7007–7015.
- Ring, A. and Dowsett, M.** (2004). Mechanisms of tamoxifen resistance. *Endocr Relat Cancer* **11**, 643–658.
- Ruest, P. J., Shin, N. Y., Polte, T. R., Zhang, X. and Hanks, S. K.** (2001). Mechanisms of CAS substrate domain tyrosine phosphorylation by FAK and Src. *Mol Cell Biol* **21**, 7641–7652.
- Rufanova, V. A., Alexanian, A., Wakatsuki, T., Lerner, A. and Sorokin, A.** (2009). Pyk2 mediates endothelin-1 signaling via p130Cas/BCAR3 cascade and regulates human glomerular mesangial cell adhesion and spreading. *J Cell Physiol* **219**, 45–56.
- Sakai, R., Iwamatsu, A., Hirano, N., Ogawa, S., Tanaka, T., Mano, H., Yazaki, Y. and Hirai, H.** (1994). A novel signaling molecule, p130, forms stable complexes in vivo with v-Crk and v-Src in a tyrosine phosphorylation-dependent manner. *EMBO J* **13**, 3748–3756.
- Salgia, R., Pisick, E., Sattler, M., Li, J. L., Uemura, N., Wong, W. K., Burky, S. A., Hirai, H., Chen, L. B. and Griffin, J. D.** (1996). p130CAS forms a signaling complex with the adapter protein CRKL in hematopoietic cells transformed by the BCR/ABL oncogene. *J Biol Chem* **271**, 25198–25203.
- Sawada, Y., Tamada, M., Dubin-Thaler, B. J., Cherniavskaya, O., Sakai, R., Tanaka, S. and Sheetz, M. P.** (2006). Force sensing by mechanical extension of the Src family kinase substrate p130Cas. *Cell* **127**, 1015–1026.
- Schlaepfer, D. D., Broome, M. A. and Hunter, T.** (1997). Fibronectin-stimulated signaling from a focal adhesion kinase-c-Src complex: involvement of the Grb2,

p130cas, and Nck adaptor proteins. *Mol Cell Biol* **17**, 1702–1713.

- Schrecengost, R. S., Riggins, R. B., Thomas, K. S., Guerrero, M. S. and Bouton, A. H.** (2007). Breast cancer antiestrogen resistance-3 expression regulates breast cancer cell migration through promotion of p130Cas membrane localization and membrane ruffling. *Cancer Res* **67**, 6174–6182.
- Schuh, N. R., Guerrero, M. S., Schrecengost, R. S. and Bouton, A. H.** (2010). BCAR3 regulates Src/p130 Cas association, Src kinase activity, and breast cancer adhesion signaling. *J Biol Chem* **285**, 2309–2317.
- Schultheis, B., Strumberg, D., Santel, A., Vank, C., Gebhardt, F., Keil, O., Lange, C., Giese, K., Kaufmann, J., Khan, M., et al.** (2014). First-in-human phase I study of the liposomal RNA interference therapeutic Atu027 in patients with advanced solid tumors. *J. Clin. Oncol.* **32**, 4141–8.
- Sciortino, M., Camacho-Leal, M. del P., Orso, F., Grassi, E., Costamagna, A., Provero, P., Tam, W., Turco, E., Defilippi, P., Taverna, D., et al.** (2017). Dysregulation of Blimp1 transcriptional repressor unleashes p130Cas/ErbB2 breast cancer invasion. *Sci. Rep.* **7**, 1145.
- Seidler, J., Durzok, R., Brakebusch, C. and Cordes, N.** (2005). Interactions of the integrin subunit β 1A with protein kinase B/Akt, p130Cas and paxillin contribute to regulation of radiation survival. In *Radiotherapy and Oncology*, pp. 129–134.
- Shih, N. Y., Li, J., Karpitskii, V., Nguyen, A., Dustin, M. L., Kanagawa, O., Miner, J. H. and Shaw, A. S.** (1999). Congenital nephrotic syndrome in mice lacking CD2-associated protein. *Science* **286**, 312–5.
- Sieg, D. J., Ilic, D., Jones, K. C., Damsky, C. H., Hunter, T. and Schlaepfer, D. D.** (1998). Pyk2 and Src-family protein-tyrosine kinases compensate for the loss of FAK in fibronectin-stimulated signaling events but Pyk2 does not fully function to enhance FAK- cell migration. *EMBO J* **17**, 5933–5947.
- Soni, S., Lin, B. T., August, A., Nicholson, R. I. and Kirsch, K. H.** (2009). Expression of a phosphorylated p130(Cas) substrate domain attenuates the phosphatidylinositol 3-kinase/Akt survival pathway in tamoxifen resistant breast cancer cells. *J Cell Biochem* **107**, 364–375.
- Strumberg, D., Schultheis, B., Traugott, U., Vank, C., Santel, A., Keil, O., Giese, K., Kaufmann, J. and Drevs, J.** (2012). Phase I clinical development of Atu027, a siRNA formulation targeting PKN3 in patients with advanced solid tumors. *Int J Clin Pharmacol Ther* **50**, 76–78.

- Suzuki, T., Nakamoto, T., Ogawa, S., Seo, S., Matsumura, T., Tachibana, K., Morimoto, C. and Hirai, H.** (2002). MICAL, a novel CasL interacting molecule, associates with vimentin. *J Biol Chem* **277**, 14933–14941.
- Ta, H. Q., Thomas, K. S., Schrecengost, R. S. and Bouton, A. H.** (2008). A Novel Association between p130Cas and Resistance to the Chemotherapeutic Drug Adriamycin in Human Breast Cancer Cells. *Cancer Res.* **68**, 8796–8804.
- Tachibana, K., Urano, T., Fujita, H., Ohashi, Y., Kamiguchi, K., Iwata, S., Hirai, H. and Morimoto, C.** (1997). Tyrosine phosphorylation of Crk-associated substrates by focal adhesion kinase. A putative mechanism for the integrin-mediated tyrosine phosphorylation of Crk-associated substrates. *J Biol Chem* **272**, 29083–29090.
- Takino, T., Tamura, M., Miyamori, H., Araki, M., Matsumoto, K., Sato, H. and Yamada, K. M.** (2003). Tyrosine phosphorylation of the CrkII adaptor protein modulates cell migration. *J Cell Sci* **116**, 3145–3155.
- Tang, D. D.** (2009). p130 Crk-associated substrate (CAS) in vascular smooth muscle. *J Cardiovasc Pharmacol Ther* **14**, 89–98.
- Tang, D. D. and Tan, J.** (2003a). Role of Crk-Associated Substrate in the Regulation of Vascular Smooth Muscle Contraction. *Hypertension* **42**, 858–863.
- Tang, D. D. and Tan, J.** (2003b). Downregulation of profilin with antisense oligodeoxynucleotides inhibits force development during stimulation of smooth muscle. *Am J Physiol Hear. Circ Physiol* **285**, H1528-36.
- Tatárová, Z., Brábek, J., Rösel, D. and Novotný, M.** (2012). SH3 domain tyrosine phosphorylation--sites, role and evolution. *PLoS One* **7**, e36310.
- Tatsumi, S., Ishii, K., Amizuka, N., Li, M., Kobayashi, T., Kohno, K., Ito, M., Takeshita, S. and Ikeda, K.** (2007). Targeted ablation of osteocytes induces osteoporosis with defective mechanotransduction. *Cell Metab.* **5**, 464–75.
- Tazaki, T., Miyazaki, K., Hiyama, E., Nakamoto, T., Sakai, R., Yamasaki, N., Honda, Z., Noda, M., Miyasaka, N., Sueda, T., et al.** (2008). Functional analysis of Src homology 3-encoding exon (exon 2) of p130Cas in primary fibroblasts derived from exon 2-specific knockout mice. *Genes Cells* **13**, 145–157.
- Tazaki, T., Sasaki, T., Uto, K., Yamasaki, N., Tashiro, S., Sakai, R., Tanaka, M., Oda, H., Honda, Z.-I. and Honda, H.** (2010). p130Cas, Crk-associated substrate plays essential roles in liver development by regulating sinusoidal endothelial cell fenestration. *Hepatology* **52**, 1089–1099.

- Tikhmyanova, N., Little, J. L. and Golemis, E. A.** (2010). CAS proteins in normal and pathological cell growth control. *Cell. Mol. Life Sci.* **67**, 1025–1048.
- Tilghman, R. W., Cowan, C. R., Mih, J. D., Koryakina, Y., Gioeli, D., Slack-Davis, J. K., Blackman, B. R., Tschumperlin, D. J. and Parsons, J. T.** (2010). Matrix Rigidity Regulates Cancer Cell Growth and Cellular Phenotype. *PLoS One* **5**, e12905.
- Tornillo, G., Bisaro, B., Camacho-Leal, M. D., Galie, M., Provero, P., Di Stefano, P., Turco, E., Defilippi, P., Cabodi, S., Camacho-Leal Mdel, P., et al.** (2011). p130Cas promotes invasiveness of three-dimensional ErbB2-transformed mammary acinar structures by enhanced activation of mTOR/p70S6K and Rac1. *Eur J Cell Biol* **90**, 237–248.
- Tornillo, G., Defilippi, P. and Cabodi, S.** (2014). Cas proteins: dodgy scaffolding in breast cancer. *Breast Cancer Res.* **16**, 443.
- Tsuda, M., Tanaka, S., Sawa, H., Hanafusa, H. and Nagashima, K.** (2002). Signaling adaptor protein v-Crk activates Rho and regulates cell motility in 3Y1 rat fibroblast cell line. *Cell Growth Differ* **13**, 131–139.
- Uehara, S., Udagawa, N., Mukai, H., Ishihara, A., Maeda, K., Yamashita, T., Murakami, K., Nishita, M., Nakamura, T., Kato, S., et al.** (2017). Protein kinase N3 promotes bone resorption by osteoclasts in response to Wnt5a-Ror2 signaling. *Sci. Signal.* **10**, eaan0023.
- Unsal-Kacmaz, K., Rangunathan, S., Rosfjord, E., Dann, S., Upešlacis, E., Grillo, M., Hernandez, R., Mack, F. and Klippel, A.** (2011). The interaction of PKN3 with RhoC promotes malignant growth. *Mol Oncol.* **6**, 284–98.
- van Agthoven, T. L., van Agthoven, T. L., Dekker, A., van der Spek, P. J., Vreede, L. and Dorsers, L. C.** (1998). Identification of BCAR3 by a random search for genes involved in antiestrogen resistance of human breast cancer cells. *EMBO J* **17**, 2799–2808.
- Vives, V., Laurin, M., Cres, G., Larrousse, P., Morichaud, Z., Noel, D., Cote, J. F. and Blangy, A.** (2011). The Rac1 exchange factor Dock5 is essential for bone resorption by osteoclasts. *J Bone Min. Res* **26**, 1099–1110.
- Vuori, K., Hirai, H., Aizawa, S. and Ruoslahti, E.** (1996). Introduction of p130cas signaling complex formation upon integrin-mediated cell adhesion: a role for Src family kinases. *Mol Cell Biol* **16**, 2606–2613.
- Wallez, Y., Riedl, S. J. and Pasquale, E. B.** (2014). Association of the BCAR1 and

- BCAR3 Scaffolding Proteins in Cell Signaling and Antiestrogen Resistance. *J. Biol. Chem.* **289**, 10431–44.
- Wang, R., Li, Q.-F., Anfinogenova, Y. and Tang, D. D.** (2007). Dissociation of Crk-associated substrate from the vimentin network is regulated by p21-activated kinase on ACh activation of airway smooth muscle. *Am. J. Physiol. Cell. Mol. Physiol.* **292**, L240–L248.
- Wei, L., Yang, Y., Zhang, X. and Yu, Q.** (2002). Anchorage-independent phosphorylation of p130Cas protects lung adenocarcinoma cells from anoikis. *J. Cell. Biochem.* **87**, 439–449.
- Wei, L., Yang, Y., Zhang, X. and Yu, Q.** (2004). Cleavage of p130Cas in anoikis. *J. Cell. Biochem.* **91**, 325–335.
- Weinbaum, S., Duan, Y., Thi, M. M. and You, L.** (2011). An Integrative Review of Mechanotransduction in Endothelial, Epithelial (Renal) and Dendritic Cells (Osteocytes). *Cell. Mol. Bioeng.* **4**, 510–537.
- Welsch, T., Endlich, N., Kriz, W. and Endlich, K.** (2001). CD2AP and p130Cas localize to different F-actin structures in podocytes. *Am J Physiol Ren. Physiol* **281**, F769-77.
- Wendt, M. K., Smith, J. A. and Schiemann, W. P.** (2009). p130Cas is required for mammary tumor growth and transforming growth factor-beta-mediated metastasis through regulation of Smad2/3 activity. *J Biol Chem* **284**, 34145–34156.
- Wisniewska, M., Bossenmaier, B., Georges, G., Hesse, F., Dangl, M., Kunkele, K. P., Ioannidis, I., Huber, R. and Engh, R. A.** (2005). The 1.1 angstrom resolution crystal structure of the p130cas SH3 domain and ramifications for ligand selectivity. *J. Mol. Biol.* **347**, 1005–1014.
- Wozniak, M. A., Baker, B. M., Chen, C. S. and Wilson, K. L.** (2013). The emerin-binding transcription factor Lmo7 is regulated by association with p130Cas at focal adhesions. *PeerJ* **1**,.
- Yamakita, Y., Totsukawa, G., Yamashiro, S., Fry, D., Zhang, X., Hanks, S. K. and Matsumura, F.** (1999). Dissociation of FAK/p130(CAS)/c-Src complex during mitosis: role of mitosis-specific serine phosphorylation of FAK. *J Cell Biol* **144**, 315–324.
- Yi, J., Kloeker, S., Jensen, C. C., Bockholt, S., Honda, H., Hirai, H. and Beckerle, M. C.** (2002). Members of the Zyxin family of LIM proteins interact with members of the p130Cas family of signal transducers. *J Biol Chem* **277**, 9580–

9589.

- Yokoyama, N. and Miller, W. T.** (2001a). Inhibition of Src by direct interaction with protein phosphatase 2A. *FEBS Lett* **505**, 460–464.
- Yokoyama, N. and Miller, W. T.** (2001b). Protein phosphatase 2A interacts with the Src kinase substrate p130(CAS). *Oncogene* **20**, 6057–6065.
- Yokoyama, N., Lougheed, J. and Miller, W. T.** (2005). Phosphorylation of WASP by the Cdc42-associated kinase ACK1: dual hydroxyamino acid specificity in a tyrosine kinase. *J Biol Chem* **280**, 42219–42226.
- Zhang, C., Miller, D. J., Guibao, C. D., Donato, D. M., Hanks, S. K. and Zheng, J. J.** (2017). Structure-functional insights into the interaction between the Cas family scaffolding protein p130Cas and the focal adhesion-associated protein paxillin. *J. Biol. Chem.* jbc.M117.807271.
- Zhao, M. and Vuori, K.** (2011). The docking protein p130Cas regulates cell sensitivity to proteasome inhibition. *BMC Biol* **9**, 73.
- Zucchini, D., Caprini, G., Pasterkamp, R. J., Tedeschi, G. and Vanoni, M. A.** (2011). Kinetic and spectroscopic characterization of the putative monooxygenase domain of human MICAL-1. *Arch Biochem Biophys* **515**, 1–13.

5. Appendix: Reprints of the publications/preprints described in the thesis

The following section contains reprints of four publications/preprints.

Paper I:

Janoštiak, R., Brábek, J., Auernheimer, V., Tatárová, Z., Lautscham, L., Dey, T., **Gemperle, J.**, Merkel, R., Goldmann, W., Fabry, B., Rösel, D. (2014). [CAS directly interacts with vinculin to control mechanosensing and focal adhesion dynamics](#). *Cell Mol Life Sci.* 71: 727-744.

Paper II:

Gemperle, J., Hexnerová, R., Lepšík, M., Tesina, P., Dibus, M., Novotný, M., Brábek, J., Veverka, V., and Rosel, D. (2017). [Structural characterization of CAS SH3 domain selectivity and regulation reveals new CAS interaction partners](#). *Sci. Rep.* 7: 1–18.

Paper III:

Koudelkova, L., Pataki, C., Tolde, O., Pavlik, V., Nobis, M., **Gemperle, J.**, Anderson, K., Brábek, J., Rosel, D., (2018). Novel FRET-Based Src Biosensor Reveals Mechanisms of Src Activation and Its Dynamics in Focal Adhesions. *SSRN*. <https://ssrn.com/abstract=3206266> (Preprint posted July 2, 2018). Under revision at *Cell Chemical Biology* journal.

Paper IV:

Gemperle, J., Dibus, M., Koudelková, L., Rosel, D., Brábek, J. (2018). The interaction of PKN3 with p130Cas promotes malignant growth. *bioRxiv*. <https://doi.org/10.1101/334425> (Preprint posted June 29, 2018). Under revision at *Molecular Oncology* journal.

5.1. The 1st publication

Janoštiak, R., Brábek, J., Auernheimer, V., Tatárová, Z., Lautscham, L., Dey, T.,
Gemperle, J., Merkel, R., Goldmann, W., Fabry, B., Rösel, D.

CAS directly interacts with vinculin to control mechanosensing and focal adhesion dynamics.

Cell Mol Life Sci. (2014), 71: 727-744.

CAS directly interacts with vinculin to control mechanosensing and focal adhesion dynamics

Radoslav Janoštiak · Jan Brábek · Vera Auernheimer · Zuzana Tatárová · Lena A. Lautscham · Tuli Dey · Jakub Gemperle · Rudolf Merkel · Wolfgang H. Goldmann · Ben Fabry · Daniel Rösel

Received: 3 May 2013 / Revised: 19 July 2013 / Accepted: 5 August 2013 / Published online: 25 August 2013
© The Author(s) 2013. This article is published with open access at Springerlink.com

Abstract Focal adhesions are cellular structures through which both mechanical forces and regulatory signals are transmitted. Two focal adhesion-associated proteins, Crk-associated substrate (CAS) and vinculin, were both independently shown to be crucial for the ability of cells to transmit mechanical forces and to regulate cytoskeletal tension. Here, we identify a novel, direct binding interaction between CAS and vinculin. This interaction is mediated by the CAS SRC homology 3 domain and a proline-rich sequence in the hinge region of vinculin. We show that CAS localization in focal adhesions is partially dependent on vinculin, and that CAS–vinculin coupling is required for stretch-induced activation of CAS at the Y410 phosphorylation site. Moreover, CAS–vinculin binding significantly affects the dynamics of CAS and vinculin within focal adhesions as well as the size of focal adhesions. Finally, disruption of CAS binding to vinculin reduces cell stiffness and traction force generation. Taken together, these findings

strongly implicate a crucial role of CAS–vinculin interaction in mechanosensing and focal adhesion dynamics.

Keywords CAS · Focal adhesions · Mechanosensing · Vinculin · Src · Traction forces

Introduction

Crk-associated substrate (CAS) is an important substrate of Src. CAS is dominantly localized in focal adhesions of adherent cells and plays a central role in the integrin-mediated control of cell behavior [1]. The re-expression of CAS in *cas*-deficient mouse embryonic fibroblasts (MEFs) altered by oncogenic Src was shown to elevate cell invasiveness [2] and lung metastasis formation [3]. BCAR1 (breast cancer anti-estrogen resistance), the human equivalent of CAS, was first discovered in a screen for anti-estrogen drug-resistant genes in breast cancer cells [4]. Increased CAS/BCAR1 levels in breast cancer patients are associated with premature disease recurrence, decreased response to tamoxifen treatment, and lower survival rate [5].

The structure of CAS consists of an N-terminal SRC homology 3 (SH3) domain, a C-terminally localized Src-binding domain (SBD), and a Cas-family C-terminal homology (CCH) domain. The CAS central region comprises of a substrate domain (SD), which is characterized by 15 Tyr- X- X- Pro (YxxP) motifs. Src family kinases seem to phosphorylate numerous, if not all, of the CAS SD YxxP tyrosines either by binding directly to the CAS SBD, or by indirect association with CAS via a FAK bridge [6, 7]. CAS SD tyrosine phosphorylation, in untransformed cells, takes place at the integrin-mediated adhesion sites [8], and has been shown to be associated with integrin

Electronic supplementary material The online version of this article (doi:10.1007/s00018-013-1450-x) contains supplementary material, which is available to authorized users.

R. Janoštiak · J. Brábek · Z. Tatárová · J. Gemperle · D. Rösel (✉)
Department of Cell Biology, Faculty of Science, Charles University in Prague, Czech Republic, Vinicna 7, 128 43 Prague, Czech Republic
e-mail: rosel@natur.cuni.cz

V. Auernheimer · L. A. Lautscham · T. Dey · W. H. Goldmann · B. Fabry
Biophysics Group, Department of Physics, University of Erlangen-Nuremberg, Erlangen, Germany

R. Merkel
Forschungszentrum Jülich GmbH, ICS-7, Biomechanics, Jülich, Germany

signaling pathways that regulate cell movement and survival [9–12].

The SH3 domain of CAS is known to interact with polyproline motifs on numerous proteins [13], which include FAK and PYK2/RAFTK kinases [14], FRNK [15], PTP-PEST [16], C3G [17], PTP1B [18], CMS [19], and CIZ [20]. The interaction between the prominent focal adhesion protein, FAK, and the CAS SH3 domain [13, 15, 21] contributes to the phosphorylation of SD tyrosine and is further enhanced by Src that is bound to the FAK autophosphorylation site [6]. Accordingly, CAS SH3 domain deletion diminishes the phosphorylation of CAS SD tyrosine [6] and greatly reduces the localization of CAS to focal adhesions [22]. Detection of CAS in focal adhesions of FAK null cells [23], however, also indicates the presence of other SH3 domain binding partners.

CAS acts as a primary force sensor, transducing forces into mechanical extension of the substrate domain and thereby priming its phosphorylation and subsequent activation of downstream signaling [24]. Stretch-dependent tyrosine phosphorylation of CAS by Src family kinases is involved in force-dependent activation of the MAP kinase cascade and the small GTPase Rap1 [25, 26]. Details of how mechanical forces are coupled to the CAS protein are currently elusive. It has been suggested that mechanical stress leads to force-dependent extension of the CAS substrate domain and enhances its susceptibility to phosphorylation [24].

In this study, we identified a novel direct interaction of CAS with vinculin mediated by the CAS SH3 domain and a proline-rich sequence in the hinge region of vinculin. We found that this interaction is important for CAS localization in focal adhesions, focal adhesion dynamics, mechanosensing, and traction force generation.

Results

CAS SH3 domain interacts with the polyproline motif PPKP on vinculin

The importance of CAS SH3 domain in CAS-mediated signaling is well established. The SH3 domain targets CAS into focal adhesions and significantly contributes to CAS substrate domain phosphorylation and downstream signaling through the CAS/Crk scaffold [8, 22, 23]. We have previously shown that phosphorylation on tyrosine 12 within the SH3 domain of CAS suppresses FAK binding and deactivates CAS-mediated signaling [27, 28]. To identify novel interacting partners that can differentially bind to a non-phosphorylated CAS SH3 domain, we employed peptide mass fingerprinting of proteins differentially pulled-down by a GST fused CAS SH3 domain

from HeLa cell lysates. Apart from known interaction partners of the CAS SH3 domain such as FAK and CMS, we found vinculin as a novel potential binding partner of CAS. CAS–vinculin interaction was confirmed to be specific for non-phosphorylated CAS SH3 domain using a GST pull-down assay with immunoblot analysis (Fig. 1a). Vinculin binding was only present in CAS–SH3 domain constructs with WT tyrosine at position 12 or with a non-phosphorylatable mutation Y12F (Tyr 12 changed to phenylalanine). No vinculin binding was observed in the case of a mutation Y12E (Tyr 12 changed to glutamic acid). The Y12E was previously shown to also abolish specific binding of other CAS–SH3 interacting partners, similarly to Tyr 12 phosphorylation [27]. Even though the Y12E mutation may not truly mimic the structure of phosphorylated Tyr 12, it was clearly shown that substitution of Tyr 12 and analogous Tyr in SH3 domains to Glu in its effect on binding capacity of the SH3 domains mimics phosphorylation [27, 28]. We will thus further refer to this mutation as a phosphomimicking. Results from GST-pull down were further confirmed by immuno-precipitation of full-length CAS tagged with GFP (Fig. 1b).

As the CAS SH3 domain is also known to interact with FAK [13], we investigated whether CAS SH3 interaction with vinculin is independent of FAK. GFP–CAS was immuno-precipitated from FAK–/– cells and Western-blot analysis showed that CAS also interacts with vinculin in FAK-deficient cells (Fig. 1c). Moreover, GST-pull-down assays with the WT CAS SH3 domain were performed with or without FAK depletion using an anti-FAK antibody. FAK depletion in cell lysate did not affect the interaction of WT CAS SH3 domain and vinculin (Fig. S1), suggesting that the CAS–vinculin interaction is FAK independent and potentially direct. In a far-Western experiment, we confirmed that CAS directly interacts with vinculin (Fig. 1d).

We then searched for the binding motif on vinculin that is responsible for CAS SH3 domain binding. We analyzed CAS SH3 binding motifs among known CAS SH3 binding partners and identified as a conserved motif a PXXP sequence (Table S1). In vinculin, the P860PKP sequence in the proline-rich region of vinculin, also known as hinge region [29], is a single potential CAS SH3 binding motif. To abolish the capability of CAS SH3 domain binding to vinculin, the *in silico*-identified SH3 domain-binding motif **PPKPP** was mutated into **PPNSS** (PNSS). The importance of the PPKP motif for vinculin–CAS interaction was verified by co-immunoprecipitation experiments with full-length CAS and vinculin PNSS mutant or vinculin WT. Binding of CAS to vinculin carrying the PNSS mutation was abolished (Fig. 1e). In contrast, the binding of paxillin and Arp2, which bind the tail region of vinculin [30] and proline-rich region surrounding P776 and P878

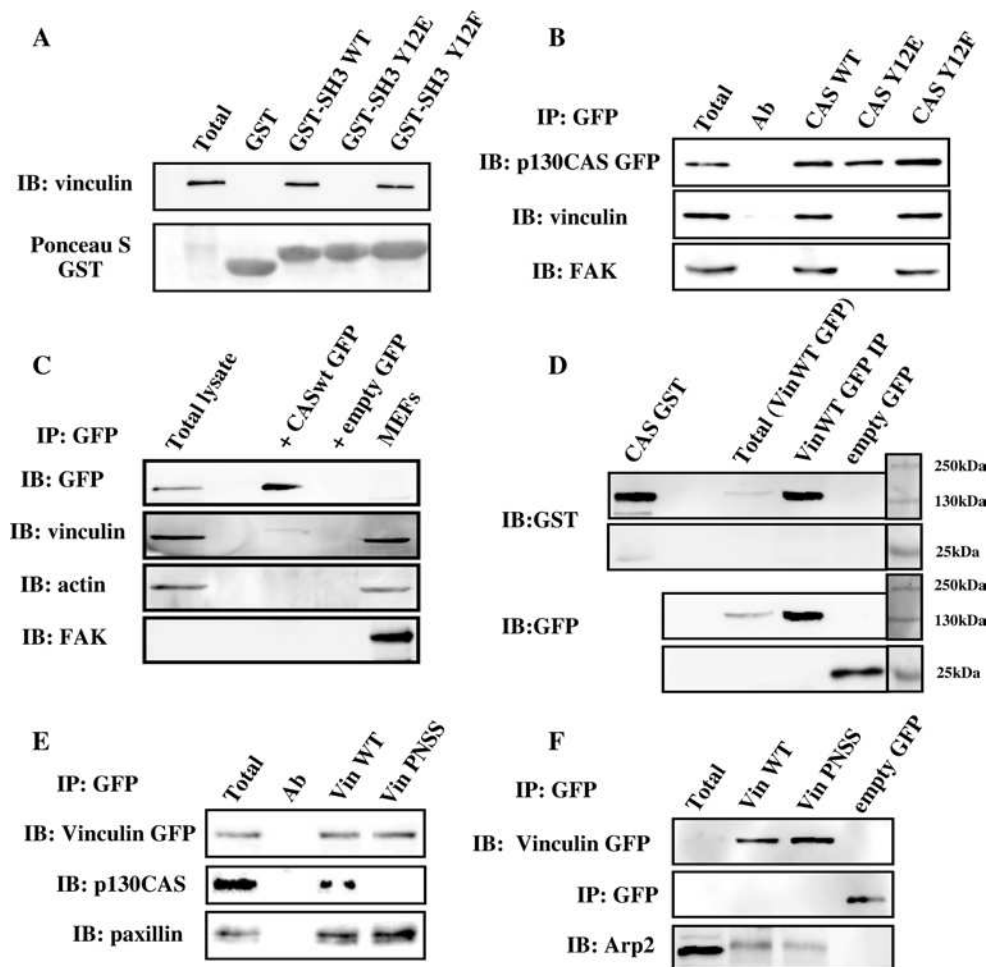


Fig. 1 The CAS SH3 domain interacts with the polyproline region of vinculin. **a** Binding of vinculin to SH3 domains of CAS WT, CAS Y12E, and CAS Y12F fused with GST was analyzed with pull-down assays by immunoblotting. Vinculin was detected with an anti vinculin antibody. GST fused SH3 domains were detected by Ponceau S staining. Aliquots of total cell lysates (total) were used as a control. **b** GFP CAS was immunoprecipitated from CAS^{-/-} MEFs expressing CAS Y12 variants, and binding of vinculin and FAK (as a control) was analyzed using vinculin and FAK antibodies. **c** GFP CAS WT was immunoprecipitated from FAK^{-/-} MEFs and binding of vinculin was analyzed using vinculin antibody. **d** In a far-Western experiment, Vin WT GFP or GFP immunoprecipitated from Vin^{-/-}

MEFs expressing the GFP constructs were transferred to nitrocellulose membranes and incubated with recombinant CAS-GST, followed by detection with anti-GST antibody. Loading controls of GFP constructs were analyzed by anti-GFP antibody. As a positive control for anti-GST reactivity, purified CAS-GST was run alongside. **e** GFP vinculin was immunoprecipitated from Vin^{-/-} MEFs re-expressing GFP-fused Vin WT or Vin PNSS (PKPP sequence in the proline-rich region changed to PNSS), and binding of CAS and paxillin was detected with CAS and paxillin antibodies. **f** GFP vinculin was immunoprecipitated from Vin^{-/-} MEFs re-expressing GFP-fused Vin WT or Vin PNSS (PKPP sequence in proline-rich region changed to PNSS), and binding of Arp2 was detected with Arp2 antibody

[31], respectively, was not significantly affected by this mutation (Fig. 1e, f). This further confirmed that CAS-vinculin interaction is through direct binding, as a potential linker molecule would need to recognize the PPKPP binding motif on vinculin and at the same time would need to bind to the CAS-SH3 domain, and both with higher affinity than a direct CAS-vinculin interaction, which is highly unlikely.

The interaction of CAS with vinculin in living cells was assessed using fluorescent confocal microscopy. CAS^{-/-} cells were transfected with CAS Y12 variants that were

N-terminally tagged with GFP, and the co-localization with vinculin was examined. As expected, CAS WT or Y12F CAS (both interact with vinculin, see Fig. 1b) were found to be co-localized with vinculin. CAS with a phosphomimicking mutation Y12E, that blocks interaction with vinculin, did not co-localize with vinculin in focal adhesions (Fig. S2).

Taken together, these results suggest that CAS directly interacts with vinculin, and that the CAS-vinculin interaction can be potentially regulated by phosphorylation of Tyr12 on the SH3 domain of CAS [27].

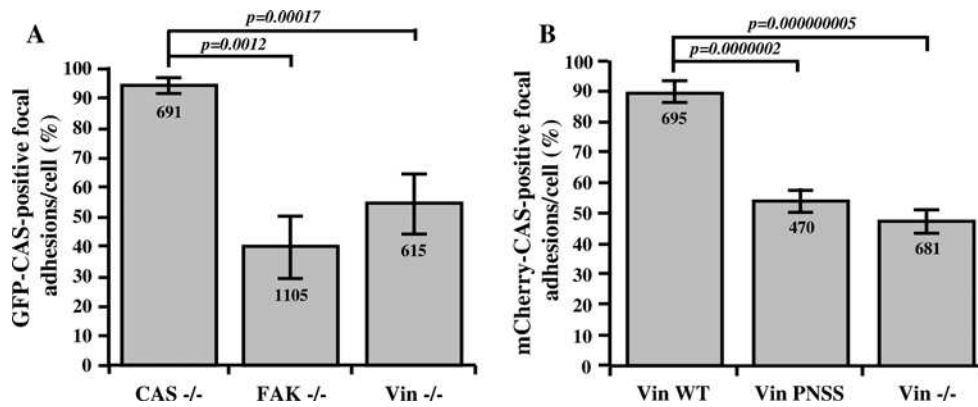


Fig. 2 CAS localization in focal adhesions is dependent on FAK and vinculin. The *bar graphs* show the percentage of focal adhesions stained positive for GFP-CAS (a) or for mCherry-CAS (b). Focal adhesions were considered CAS-positive if the GFP-CAS or

mCherry-CAS signal is at least double the signal in cytoplasm, adjacent to the focal adhesions, indicated by paxillin staining. *Numbers in columns* indicate number of analyzed focal adhesions and *error bars* represent standard deviation

CAS localization in focal adhesion is partially dependent on FAK, but also on vinculin

FAK and vinculin belong to fundamental components of the focal adhesions [32], both interact with CAS, and thus both can be responsible for CAS targeting to focal adhesions. To differentially evaluate the importance of CAS binding to FAK versus vinculin, we tested the dependence of CAS focal adhesion targeting on these two proteins. Full-length GFP-CAS WT was expressed in CAS^{-/-}, FAK^{-/-}, and vinculin^{-/-} cells, and its localization to focal adhesions was assessed by fluorescence confocal microscopy. Localization of GFP-CAS to focal adhesions was examined by differential co-localization with paxillin. Focal adhesions were identified as elongated structures with localization of paxillin and F-actin (Fig. S3A). In CAS^{-/-} cells re-expressing GFP-CAS, CAS was present in nearly all focal adhesions. In FAK^{-/-} cells, GFP-CAS was found only in 40 % of focal adhesions, and in Vin^{-/-} cells, GFP-CAS was found in 54 % of focal adhesions (Fig. 2a). Re-expression of vinculin WT in Vin^{-/-} cells, but not vinculin carrying the PNSS mutation, restored the localization of CAS in focal adhesions (Fig. 2b, Fig. S3B). These results suggest that both FAK and vinculin are responsible for focal adhesion targeting of CAS.

CAS–vinculin interaction is important for focal adhesion dynamics

We have previously shown that phosphorylation of tyrosine 12 within the CAS SH3 domain is important for the dynamics of focal adhesions [27]. Focal adhesions are relatively stable structures, but a continuous exchange of proteins takes place. To explore the influence of CAS–vinculin interaction on focal adhesions, we first analyzed their mean

size using fluorescence microscopy (Fig. 3a). The size of focal adhesions in cells expressing WT vinculin [33] was nearly 2 μm^2 , whereas the size of focal adhesions in cells lacking vinculin or in cells expressing the mutated PNSS vinculin (Vin PNSS) was significantly smaller (Vin^{-/-}: 1,2 μm^2 , VinPNSS: 1,4 μm^2) (Fig. 3b), suggesting that CAS targeting to vinculin is important for the formation of focal adhesions.

Changes in the inner dynamics of focal adhesion proteins are linked to changes in focal adhesions assembly and disassembly rates [34, 35] and maturation [36, 37]. Therefore, we investigated the influence of CAS–vinculin interaction on the exchange dynamics of CAS within focal adhesions using the FRAP technique. The exchange dynamics of CAS in focal adhesions was measured in FAK^{-/-} cells, Vin^{-/-} cells, and Vin^{-/-} cells re-expressing either Vin WT or Vin PNSS mutants. The half-maximum recovery time after photobleaching ($t_{1/2}$) of CAS fused with a Venus variant of GFP was quantified (Fig. 4a) [22]. CAS exchange dynamics in Vin^{-/-} cells ($t_{1/2} = 8.6 \pm 3.3$ s) and cells re-expressing a Vin PNSS mutant ($t_{1/2} = 8.6 \pm 3.6$ s) was significantly faster compared to cells re-expressing Vin WT ($t_{1/2} = 12.7 \pm 4.7$ s) (Fig. 4b). CAS exchange dynamics in FAK^{-/-} cells was also greatly accelerated ($t_{1/2} = 5.2 \pm 1.6$ s) (Fig. 4b). These results indicate that both binding of CAS to FAK and to vinculin slow down CAS exchange dynamics in focal adhesions.

To confirm these results, we tested whether efficient CAS–vinculin binding also slows down the vinculin exchange dynamics in focal adhesions. CAS^{-/-} cells re-expressing the CAS WT or CAS tyrosine 12 variants [27] were transfected to express GFP tagged Vin WT. FRAP experiments revealed a similar, slow dynamics of vinculin in cells expressing vinculin binding proficient CAS Y12F

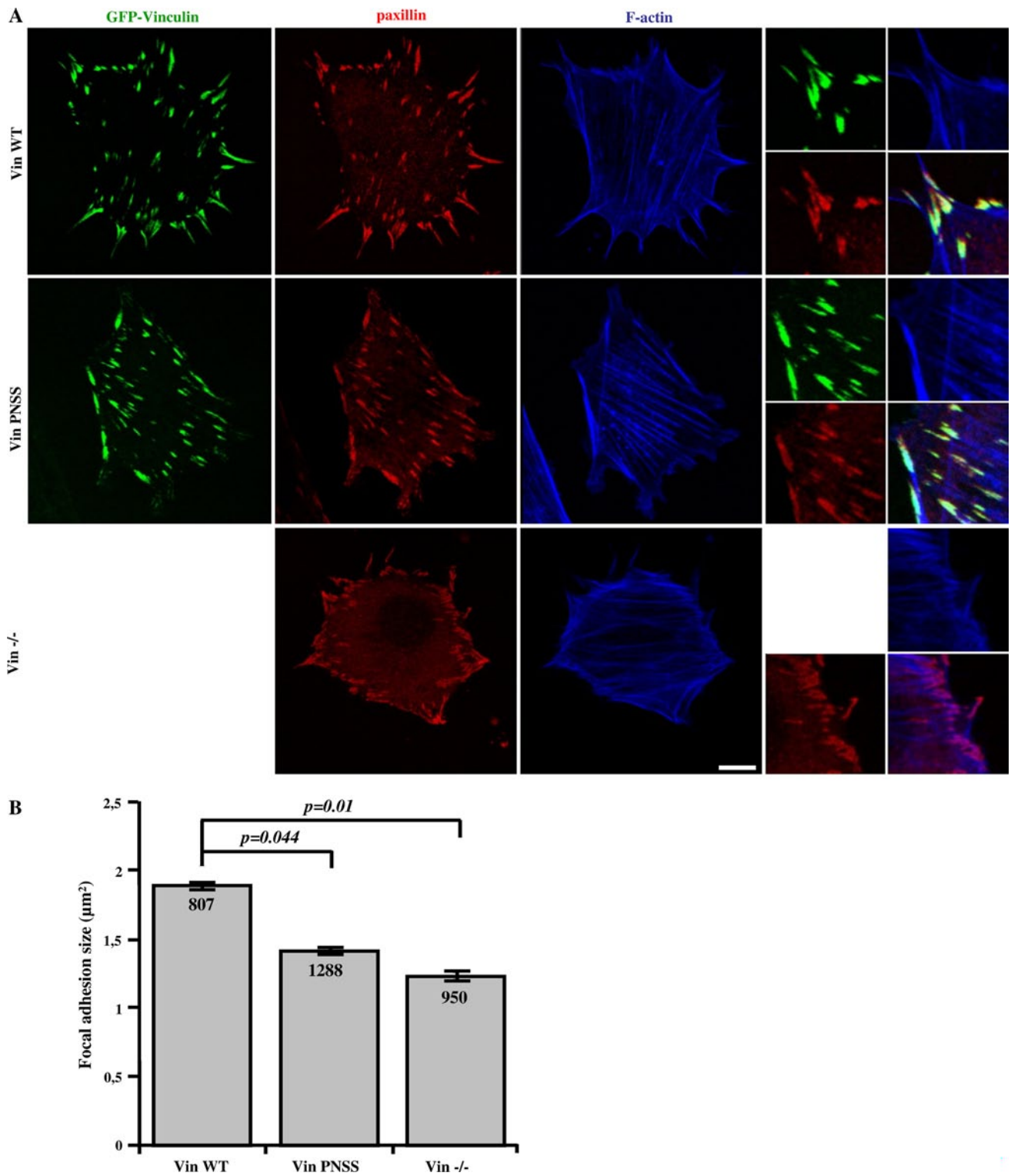
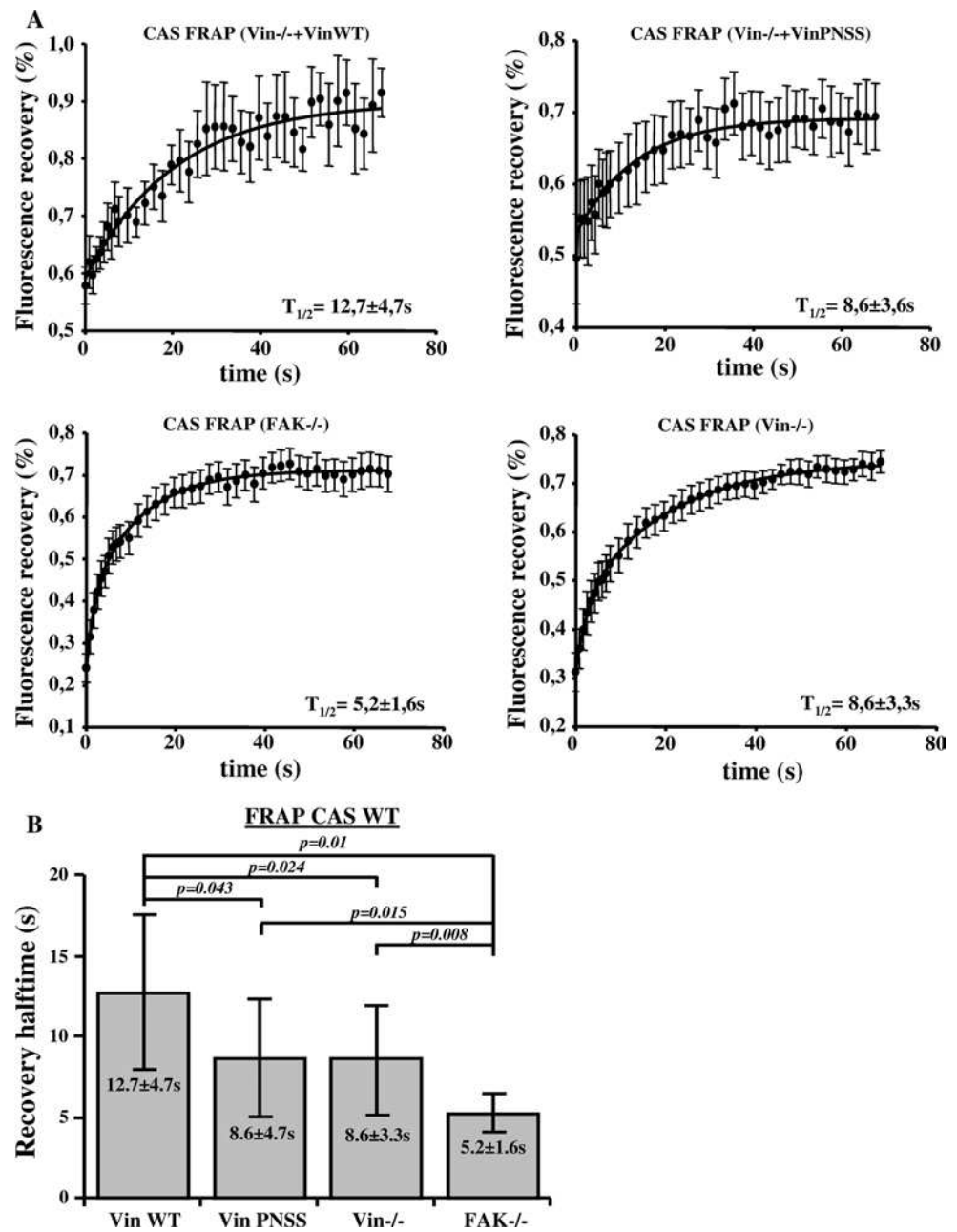


Fig. 3 CAS–vinculin interaction affects focal adhesion size. **a** Vin^{-/-} MEFs re-expressing either Vin WT or Vin PNSS C-terminally fused with GFP were grown on fibronectin-coated coverslips and stained for paxillin (focal adhesion marker) and F-actin. Focal adhesion size was determined using ImageJ software. *Scale bar*

10 μm **(b)**. The *histogram bars* represent average size of adhesion structures in cells deficient in vinculin, or re-expressing either Vin WT or Vin PNSS mutant. *Numbers in columns* indicate number of analyzed focal adhesions

Fig. 4 Dependence of CAS dynamics on FAK and vinculin within focal adhesions. **a** FRAP curves of CAS-Venus associated with focal adhesions in MEFs lacking FAK or vinculin, or re-expressing either Vin WT or mutated Vin PNSS. Numbers indicate average half-maximum recovery times ($t_{1/2}$). **b** The bar plot shows average half-maximum recovery times of CAS-Venus in different MEFs. Error bars represent standard errors



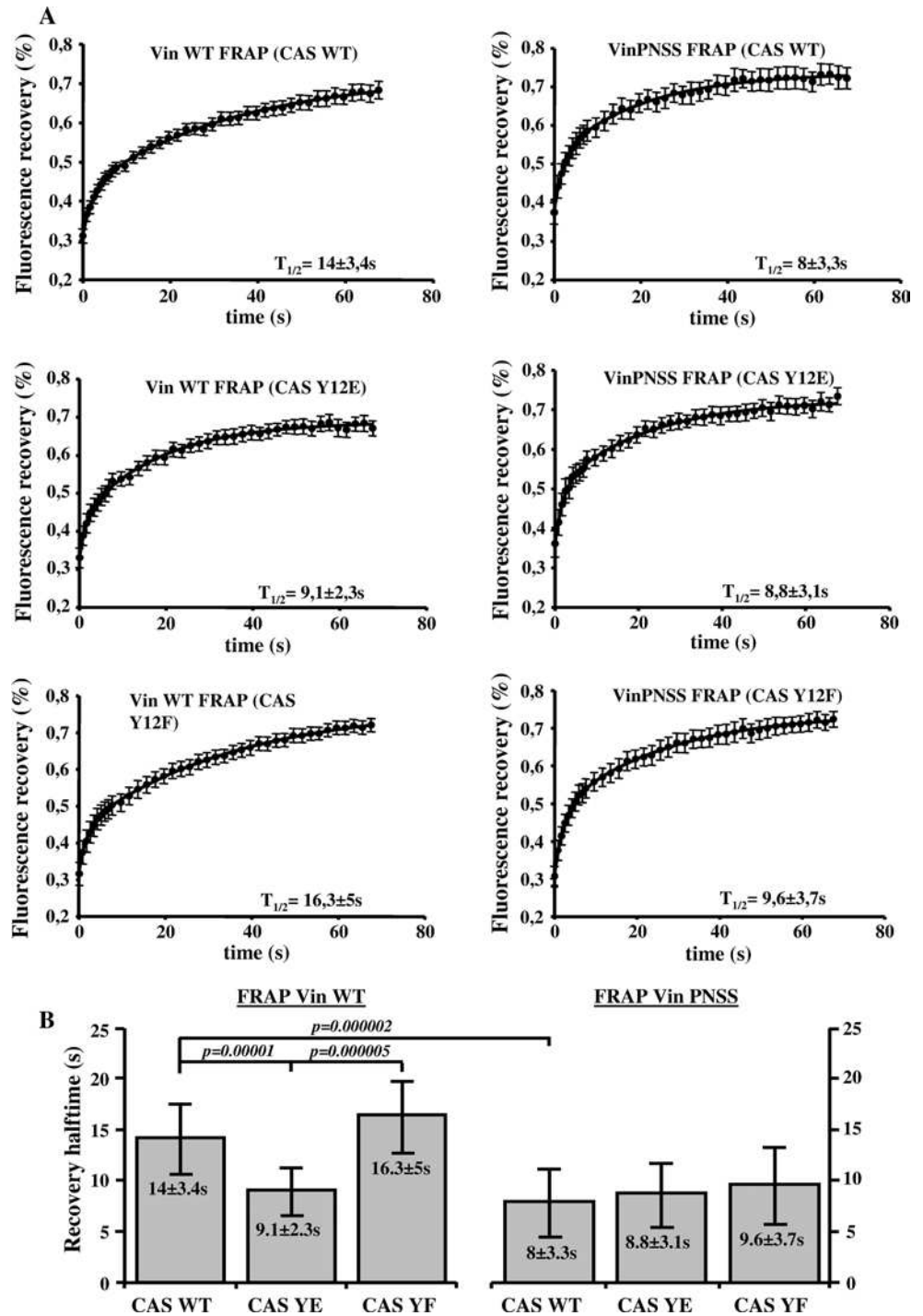
($t_{1/2} = 16.3 \pm 5$ s) and CAS WT ($t_{1/2} = 14 \pm 3.4$ s). However, vinculin dynamics in cells expressing vinculin binding-deficient CAS Y12E was significantly increased ($t_{1/2} = 9.1 \pm 2.3$ s) (Fig. 5a). In contrast to Vin WT, the exchange dynamics of Vin PNSS mutant was not affected by the different CAS tyrosine 12 variants. The half-maximum recovery time after photobleaching GFP-tagged Vin PNSS mutant was 8 ± 3.3 s for CAS WT, 8.8 ± 3.1 s for CAS Y12E, and $9.6 \pm 3,7$ s for CAS Y12F, which is comparable to the dynamics of Vin WT in CAS Y12E cells (Fig. 5b). These findings are consistent with our previous observations of vinculin dynamics in Src-transformed CAS-/- cells expressing CAS tyrosine 12 variants [27]

and suggest that binding to CAS stabilizes vinculin in focal adhesions.

CAS–vinculin interaction is important for stretch-induced phosphorylation of the CAS substrate domain

The CAS substrate domain has been reported to be extensively phosphorylated in response to mechanical extension of the CAS molecule, both in vivo and in vitro [24]. For the CAS molecule to be extended in response to forces or matrix stretch, it needs to be mechanically anchored on at least two distant sites to cytoskeletal or focal adhesion proteins. We hypothesize that vinculin might serve as one

Fig. 5 Dependence of vinculin dynamics on CAS–vinculin interaction. **a** FRAP curves of GFP–vinculin WT (*left side*) or GFP–vinculin PNSS (*right side*) associated with focal adhesions in CAS^{-/-} MEFs re-expressing indicated CAS variants. *Numbers* in plot indicate average half-maximum recovery times (*t*_{1/2}). **b** The *bar plot* shows half-maximum recovery times of GFP-fused Vin WT (*left*) and GFP–vinculin PNSS (*right*) in CAS^{-/-} MEFs re-expressing indicated CAS variants. *Error bars* represent standard errors



of the anchors. To test whether vinculin binding is necessary for a mechanical activation of CAS, mouse embryonic fibroblasts (MEFs) were cultured on a stretchable silicon substrate and exposed to uniaxial static stretch (20 % for 10 min). Stretch-induced activation of CAS was analyzed by measuring the phosphorylation of the CAS substrate domain at position Y410. We observed only a small stretch-induced increase in phosphorylation of CAS Y410 in cells

lacking vinculin or expressing mutated PNSS vinculin that was unable to interact with CAS (Fig. 6a), yet PNSS vinculin retained its ability to reverse high basal phosphorylation of FAK in Vin^{-/-} cells (Fig.S4). The lower FAK phosphorylation at Y397 in PNSS vinculin cells rules out that the stretch-insensitivity of CAS in these cells is an indirect effect mediated by FAK. Moreover, in Vin^{-/-} cells re-expressing WT vinculin, CAS Y410 phosphorylation was

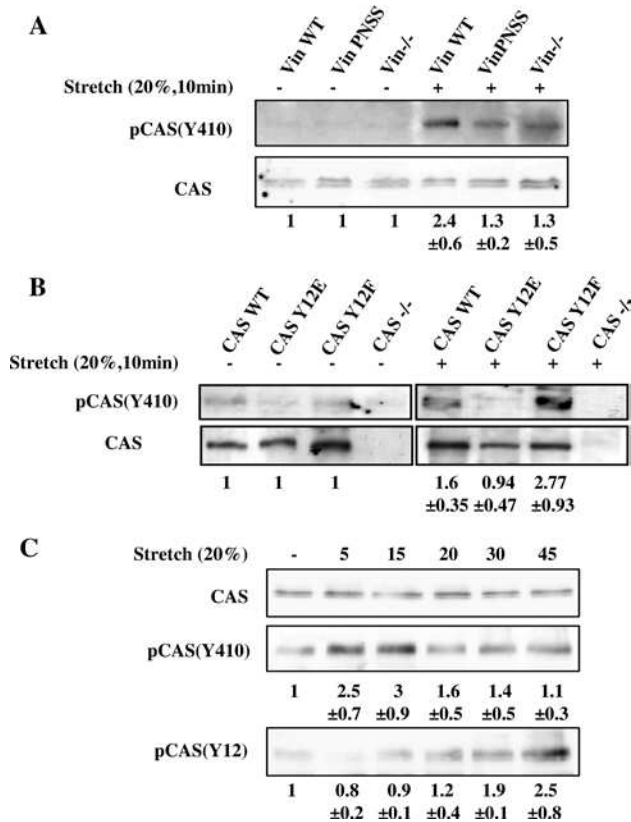


Fig. 6 Stretch-mediated phosphorylation of CAS is dependent on CAS–vinculin interaction. **a** Vin^{-/-} MEFs or Vin^{-/-} MEFs re-expressing indicated vinculin variants, **b** CAS^{-/-} MEFs re-expressing indicated CAS variants and **c** MEFs transformed by constitutively active Src (MEFs + Src527F) were seeded on fibronectin-coated flexible membrane, incubated for 24 h, and then subjected to 20 % static stretch for 10 min (**a**, **b**) or for indicated times (**c**). Subsequently, cells were lysed and analyzed by Western blotting against phosphorylated Y410 in the CAS substrate domain and Y12 in CAS SH3 domain. Numbers indicate fold-change (mean ± SD) in CAS Y410 and Y12 phosphorylation after stretching. The immunoblots are representative of three independent experiments

significantly increased by 2.4-fold after stretch (Fig. 6a). These data suggest that the direct interaction of vinculin with CAS is indispensable for stretch-induced CAS phosphorylation. Consistently, CAS^{-/-} cells re-expressing CAS carrying Y12E mutation, which blocks CAS–vinculin binding, also prevents stretch-dependent activation of CAS. Furthermore, the CAS Y12F mutation, which enhances vinculin–CAS binding, increases the stretch-dependent activation of CAS (Fig. 6b).

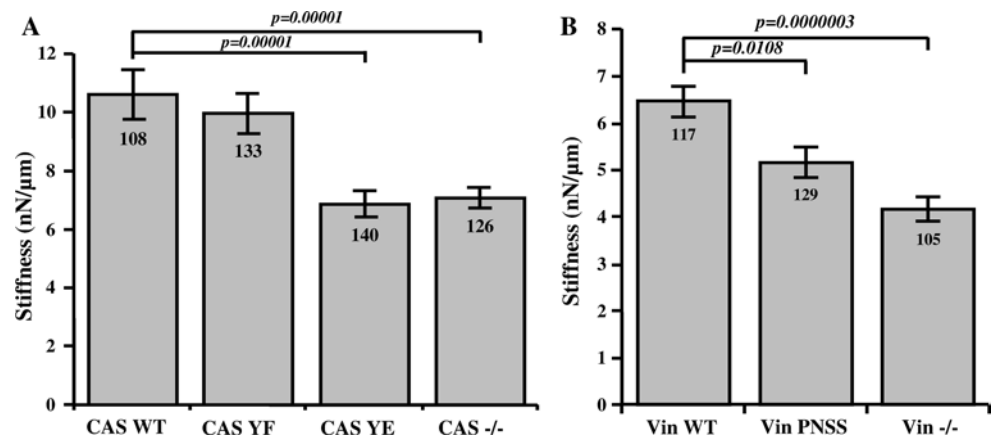
We further analyzed the dynamics of CAS Y410 phosphorylation during stretch. CAS Y410 phosphorylation appears rapidly, peaks after 15 min, and then disappears (Fig. 6c). In contrast, CAS Y12 phosphorylation exhibits different dynamics, characterized by a gradual increase of Y12 phosphorylation during stretch (Fig. 6c).

Taken together, these data indicate that vinculin–CAS interaction is required for stretch-induced CAS substrate domain phosphorylation and supports our hypothesis that vinculin serves as a mechanical coupling protein to transmit forces to the CAS molecule.

Loss of CAS–vinculin interaction reduces cell stiffness and traction forces, but does not affect adhesion strength

Because vinculin is not only a force-coupling protein but has also been implicated in the regulation of cytoskeletal stiffness and pre-stress [38], we hypothesized that the higher turnover dynamics in cells with impaired CAS–vinculin binding leads to changes in cell stiffness and contractile activation. First, we measured the stiffness of CAS^{-/-} MEF cells re-expressing CAS WT or mutated CAS Y12F and Y12E using magnetic beads coated with fibronectin that were attached to integrin cell surface receptors and pulled laterally with magnetic tweezers. Beads on CAS WT and CAS Y12F cells moved significantly ($p < 0.05$) less in

Fig. 7 Effect of CAS–vinculin interaction on cell mechanical properties. Stiffness of MEFs analyzed at 6nN force using magnetic tweezers. The bar plots show stiffness of **a** CAS^{-/-} MEFs re-expressing indicated CAS variants and **b** Vin^{-/-} MEFs re-expressing indicated vinculin variants. Numbers in columns indicate number of analyzed cells, and error bars represent standard error



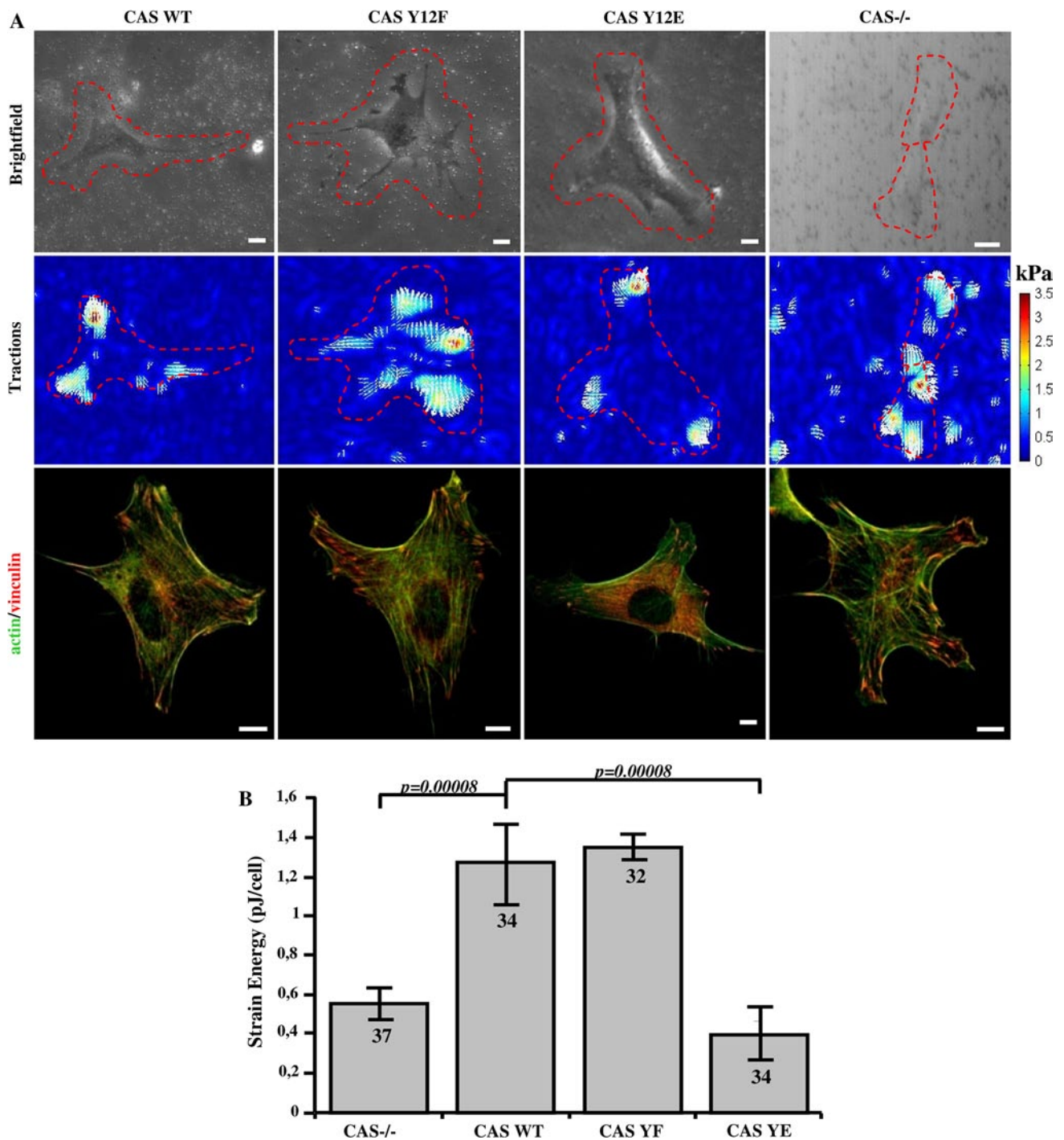


Fig. 8 Traction force generation is modulated by phosphorylation of Y12 in the CAS SH3 domain. **a** Bright field (*upper row*), traction field (*middle row*), and fluorescent (*bottom row*) images of CAS-/- MEFs

re-expressing indicated CAS variants. *Scale bar* 10 μm . **b** The *bar plot* shows the strain energy generated by single cells (mean \pm SE). *Numbers in columns* indicate number of analyzed cells

response to lateral forces compared to CAS Y12E. From the bead displacements, we computed the stiffness of cells. CAS WT and CAS Y12F cells are approximately 1.5 times stiffer compared to CAS Y12E cells (Fig. 7a). Next, we measured also the stiffness of Vin-/- MEFs re-expressing

Vin WT or mutated Vin PNSS. The stiffness of Vin PNSS cells again was significantly reduced in comparison to Vin WT cells (Fig. 7b).

Because stiffness and contractile pre-stress are linearly related in adherent cells [39], we expected that also the

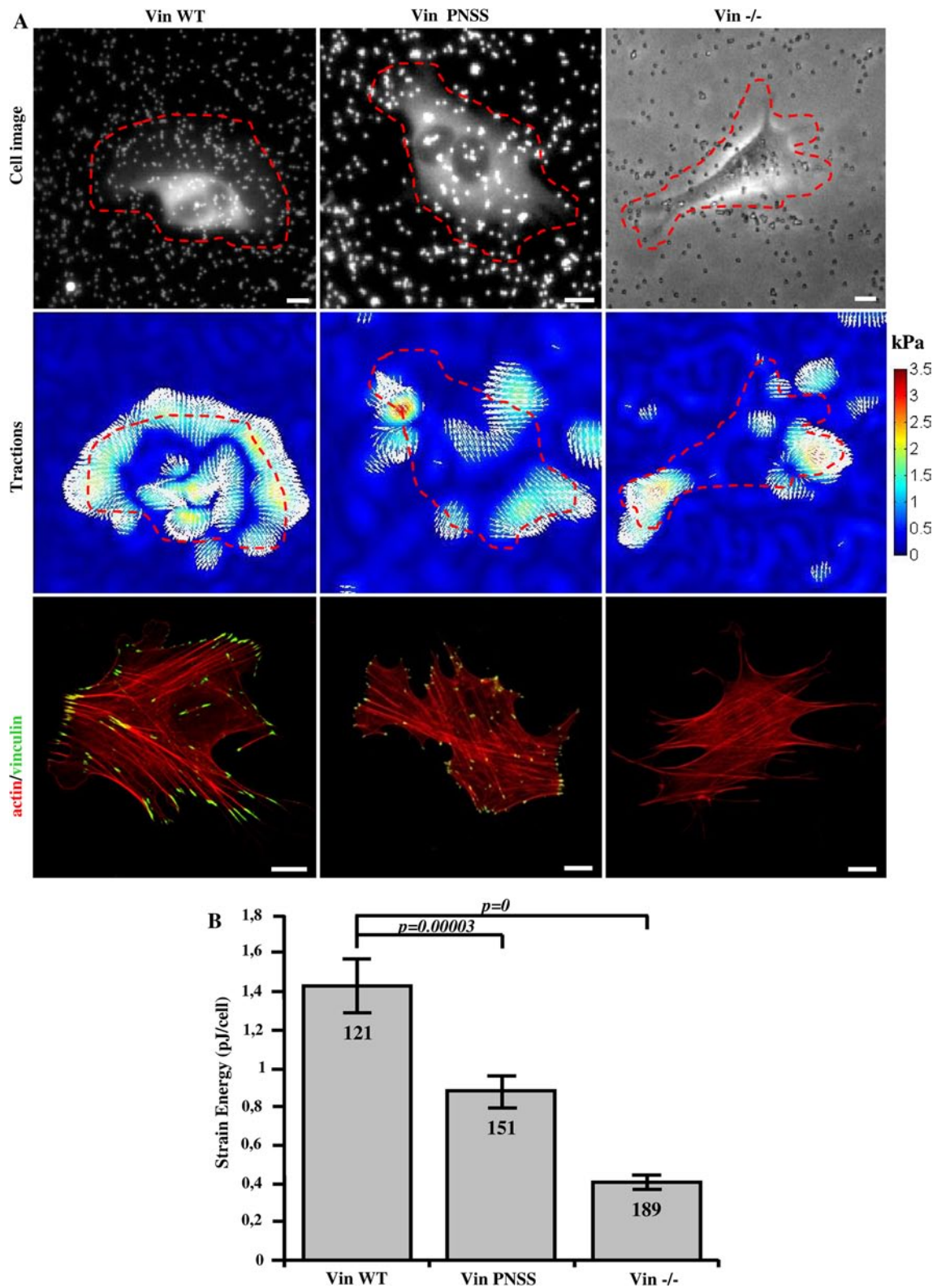


Fig. 9 Disruption of CAS–vinculin interaction results in impaired traction forces generation. **a** Upper row cell image represented by GFP fluorescence (Vin Wt, Vin PNNS) and bright field image (Vin -/-) traction field (middle row), and fluorescent (bottom row)

images of Vin -/- MEFs re-expressing different vinculin variants. Scale bar 10 μ m. **b** The bar plot shows the strain energy generated by single cells (mean \pm SE). Numbers in columns indicate number of analyzed cells

traction forces are reduced in cells with impaired CAS–vinculin binding. The traction field of cells was measured using the Fourier transform traction cytometry method [40] (Fig. 8a). As a scalar value for the traction force magnitude, we computed the elastic strain energy stored in the matrix beneath each cell. The strain energy of vinculin binding-deficient CAS Y12E mutant cells was about three times lower compared to CAS WT and mutant CAS Y12F cells (Fig. 8b). To exclude the possibility that this finding was only due to the impaired FAK-binding to the CAS SH3 domain, we repeated these measurements on CAS binding-deficient Vin PNSS cells and confirmed that traction forces were significantly reduced compared to Vin WT cells (Fig. 9a, b).

To ensure that the lower traction forces of the phosphomimicking CAS mutants are not caused by diminished adhesion strength, we measured with magnetic tweezers the forces that were needed to detach integrin-bound beads from the cells. The bead binding strength was not markedly different between the CAS WT and CAS Y12 mutant (Y12E, Y12F) cells (Fig. S5). Therefore, the reduced traction forces that we observed in the phosphomimicking Y12E mutant are not caused by poor adhesion, but are likely due to diminished contractile activation. Taken together, these findings are in support of our hypothesis that proper CAS–vinculin binding is important for vinculin and/or CAS to fulfill its mechano-regulating function.

Discussion

In this study, we have identified vinculin as a new binding partner of CAS. We have shown that CAS directly interacts with vinculin, and that this interaction is dependent on the CAS SH3 domain and the PKPP sequence of the vinculin's hinge-region. Vinculin affects the dynamics of CAS within focal adhesions and vice versa. Moreover, vinculin is important for proper CAS localization and targeting in focal adhesions. Disruption of CAS–vinculin interaction leads to decreased cell stiffness and impairs traction force generation. These findings suggest that the interaction of CAS–vinculin is important for regulating the mechanical properties of cells.

Vinculin PNSS mutation

To analyze CAS–vinculin interaction, we have mutated vinculin in P860PKPP to P860PNSS and have shown that PNSS mutated vinculin does not bind CAS (Fig. 1e). The P860PKPP motif is located within the hinge region of vinculin. Three proline-rich sequences conserved across species can be identified [41] within the hinge region. Looking

from the N-terminus, the first F842PPPP motif is distinct from sequences generally recognized by SH3 domains and mediates interaction of vinculin with VASP [42]. The third P871PPRPPPP motif was shown to mediate the interaction of vinculin with Arp2/3 [31] and proteins of the vinexin family [41]. The second AP860PKPPLP together with the third motif was suggested to be involved in binding of vinexin family proteins through interaction with a pair of its SH3 domains in tandem [43]. In our study, we identified this second motif as a target binding site of the CAS SH3 domain. The PNSS mutation of the second motif specifically blocks interaction with CAS without significantly affecting the interaction with Arp2/3 or paxillin (Fig. 1e, f). We cannot rule out that mutation of the second motif to PNSS does not affect the binding of proteins of the vinexin family or some unknown vinculin binding partners, however, our results are most consistent with the notion that the inhibition of CAS–vinculin interaction is responsible for the observed phenotypes of the PNSS mutant.

Vinculin influences targeting of CAS to focal adhesions

Correct assembly and disassembly of focal adhesions is required for regulation of cell migration and proliferation [44]. CAS and vinculin are both important focal adhesion proteins. The interaction between them that we report in this study offers a new insight into the regulation of protein dynamics in focal adhesions. CAS is recruited early to the newly formed adhesions and persists throughout their lifetime [22]. It has been previously shown that the CAS SH3 domain is important for its localization to focal adhesions [22, 27] through coupling to FAK [13, 21]. In this study, we identify vinculin as another important CAS SH3 binding partner. The localization of CAS in focal adhesion, either in FAK^{-/-} or Vin^{-/-} cells, is significantly reduced (Fig. 2), demonstrating that both FAK and vinculin are essential for proper localization of CAS. Since FAK and vinculin localize in different layers of focal adhesions [45], we speculate that CAS may be present throughout the entire focal adhesion complex to integrate signals from different layers. In addition, re-expression of vinculin PNSS, unlike re-expression of vinculin WT in Vin^{-/-} cells, was not able to restore CAS localization to focal adhesions (Fig. 2b, Fig. S3B). This suggests that a direct interaction of CAS with vinculin is necessary for proper localization of CAS to focal adhesions. However, when a form of activated vinculin is re-expressed in Vin^{-/-} cells, CAS localization is restored even when the vinculin lacks the CAS-binding region [46]. This suggests that in the case of focal adhesions stabilized by pre-activated vinculin, either FAK can fully restore the CAS localization to focal adhesions, or the second focal adhesions-targeting domain of CAS, the C-terminal CCH domain [22] can in these conditions gain

the ability to compensate for the loss of direct CAS–vinculin interaction.

Dynamics of CAS and vinculin within focal adhesions

Previously, we have shown that substitution of tyrosine 12 in the CAS SH3 domain to phosphomimicking glutamate results in increased cell migration, and this effect is probably caused by increased focal adhesion dynamics [27]. Vinculin stabilizes focal adhesions and slows down migration [47]. Moreover, the dynamics of vinculin in focal adhesions decreases during the maturation of adhesion contacts [37]. Our FRAP experiments indicate that CAS and vinculin mutually affect their dynamics within focal adhesions, and that this effect is dependent on their direct interaction. CAS dynamics in focal adhesions was decreased when WT vinculin was re-expressed in *Vin*^{−/−} cells, whereas re-expression of the mutated (PNSS) vinculin, which can not bind CAS, did not affect CAS dynamics when compared to *Vin*^{−/−} cells (Fig. 4b). Conversely, the exchange rate of vinculin in focal adhesions was increased in cells expressing CAS Y12E, which cannot interact with vinculin, when compared to cells expressing CAS WT (Fig. 5a). Moreover, the dynamics of the mutated (PNSS) vinculin was not sensitive to expression of Tyr12 CAS variants (CAS WT, Y12E, Y12F) and was similar to WT vinculin dynamics expressed in CAS Y12E cells (Fig. 5b). Taken together, the presence of CAS in the cells and its ability to localize to focal adhesions affects vinculin dynamics. However, the dynamics of the vinculin PNSS mutant (no interaction with CAS) in focal adhesions is neither affected by the presence of CAS nor by the ability of CAS to localize to focal adhesions. These observations are most consistent with the notion that CAS directly affects vinculin dynamics in focal adhesions through a direct interaction with vinculin. In addition, the data suggest that phosphorylation of CAS on Tyr 12 can potentially represent a novel mechanism regulating vinculin dynamics in focal adhesions [27].

Changes in the dynamics of focal adhesion proteins are often associated with changes in the size of adhesion structures. In this study, we have shown that disruption of CAS–vinculin interaction in vinculin-deficient cells and in vinculin PNSS mutant cells leads to a decreased size of adhesive structures (Fig. 3). This is consistent with previous findings that vinculin-deficient cells have smaller focal adhesions [48, 49], and also with our observation of smaller focal adhesions in CAS-deficient cells re-expressing the CAS Y12E mutant (Fig. S6). In contrast, *FAK*^{−/−} cells have larger focal adhesions when compared to WT MEFs [50] or *Vin*^{−/−} and *CAS*^{−/−} cells (see Fig. S3A), suggesting that unlike CAS–vinculin, CAS–FAK interaction is probably not directly involved in the regulation of focal adhesion size.

CAS-mediated effects on vinculin dynamics in focal adhesions and size of focal adhesions may be mechanistically explained by CAS interaction with vinculin that leads to stabilization of vinculin in its open conformation. According to Humphries and colleagues, activated vinculin forms exhibit increased residency time in focal adhesions and increase in size of focal adhesions [51].

CAS binding to vinculin regulates mechanosensing

Focal adhesions are cellular structures that sense external and internal forces and mechanical properties of the environment. CAS is one of the mechanosensors that is activated by extension and subsequent phosphorylation of tyrosines in the CAS substrate domain [24]. For proper mechanotransduction, CAS has to be anchored on at least two distant sides of the molecule to other force-transmitting proteins. Because vinculin is one of the main force-transmitting proteins in focal adhesions [38, 52, 53], we tested the role of CAS–vinculin interaction for mechanosensing. Stretching experiments revealed an attenuated CAS substrate domain phosphorylation in CAS Y12E transfected cells and also in vinculin PNSS mutant cells, both of which lack CAS–vinculin binding, strongly suggesting that for stretch-dependent phosphorylation of CAS, the interaction of CAS with vinculin is indispensable (Fig. 6).

Previously, we have shown that phosphomimicking mutation of tyrosine 12 (CAS Y12E) delocalizes CAS from focal adhesions [27]. Consistently, we show here that CAS Y12E does not co-localize with vinculin in focal adhesions and that only the CAS WT and CAS Y12F substrate domain was tyrosine phosphorylated in focal adhesions after stretching (Fig. S7). These findings further support our interpretation that a direct interaction of CAS with vinculin is necessary for mechanical stress-mediated CAS substrate domain phosphorylation.

CAS–vinculin interaction affects cell stiffness and traction force generation

The ability of the cell to resist deformation is important for normal cell function. Cell stiffness is determined by various factors such as number and bond elasticity of force-transmitting and force-generating molecular interactions within the cytoskeleton: between the cytoskeleton and focal adhesions, between cells, and between the cell and the extracellular matrix. We show here that CAS–vinculin interactions participate in these processes through modulating the cytoskeletal prestress. When we applied magnetic pulling forces on CAS Y12E and *Vin* PNSS cells where CAS–vinculin interaction was inhibited, magnetic beads moved more easily compared to wild-type cells, indicating a lower cell stiffness (Fig. 7). We have previously shown that

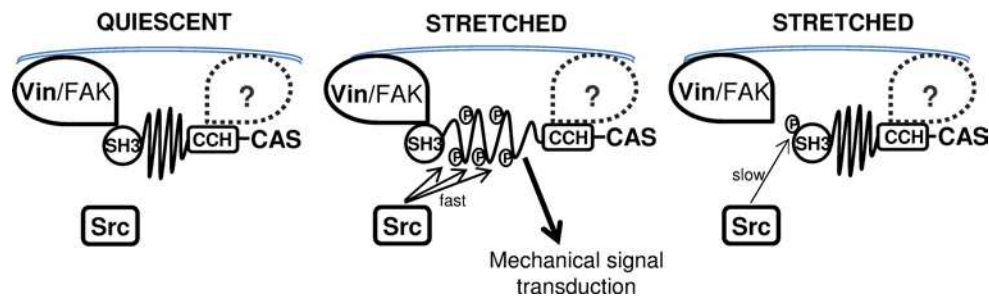


Fig. 10 Model for regulation of CAS-dependent mechanosensing. CAS is anchored in focal adhesions by N-terminal SH3 and C-terminal CCH domains [22, 24]. In quiescent cells, the substrate domain of CAS adopts a compact structure (*left*). Mechanical stretch leads to extension of the CAS substrate domain and subsequent phosphorylation by Src, which activates CAS-mediated mechanotransduction

signals (*middle*). Src phosphorylation of CAS on tyrosine 12 blocks CAS–vinculin binding, and the substrate domain returns to a compact structure. CAS-mediated mechanotransduction is attenuated (*right*) either by a gradual loss of substrate domain phosphorylation or by making the phosphorylated tyrosines in the substrate domain inaccessible for downstream signaling proteins

Src-transformed CAS^{-/-} MEFs expressing CAS Y12E are more invasive in collagen gels than wild-type cells [27], which we attribute to their lower resistance against deformation when navigating through a 3-D environment with a high degree of steric hindrance [54, 55].

In spread cells, cell stiffness is linearly related to cytoskeletal prestress and traction forces [39]. Diminished traction forces can be the result of either reduced actomyosin contractility [56, 57] or reduced adhesion strength [58, 59]. It has been previously shown that loss of vinculin resulted in decreased traction force generation [38, 60], and that the presence of CAS in focal adhesions is crucial for cell contractility [61]. Our data suggest that it is the interaction of both proteins, CAS and vinculin, that is important for traction force generation. CAS–vinculin interactions, however, are not important for maintaining adhesion strength (Fig. S5) even though the size and dynamics of focal adhesions is altered when CAS–vinculin interaction is disrupted. This suggests that the larger traction forces in CAS WT and Y12F cells are facilitated by CAS–vinculin interactions that modulate actomyosin contractility through downstream signaling mechanisms, likely involving the force-dependent activation of CAS.

To summarize, we have identified vinculin as a novel binding partner of CAS, and have shown that CAS–vinculin interactions are important for the internal dynamics of focal adhesion, sensing of mechanical stress, regulating cell stiffness and traction forces.

CAS-dependent mechanosensing: a possible role of CAS and Src in a negative feedback circuit

CAS was proposed to be a primary mechanical force sensor, transducing forces into mechanical extension of the CAS substrate domain and thereby priming the substrate domain for subsequent activation of downstream signaling

[25]. The concept of CAS as a mechanical sensor requires at least two anchoring sites along the CAS structure. The N-terminal SH3 and C-terminal CCH domain, both important for CAS targeting to focal adhesions [22], most likely represent such anchoring domains. Our data suggest that CAS–vinculin interaction is a critical focal adhesion anchoring mechanism for CAS and is essential for CAS-mediated mechanotransduction.

CAS-mediated mechanotransduction in turn requires phosphorylation of the CAS substrate domain by Src [25]. At the same time, Src also phosphorylates CAS on tyrosine 12 and inhibits CAS binding not only to FAK and PTP-PEST [27] but also to vinculin, as demonstrated by the phosphomimicking Y12E mutation (Fig. 1b). Results from a structural modeling study confirm that phosphorylation of tyrosines responsible for substrate binding of SH3 domains (in CAS Y12) in general reduces the binding to SH3 domain interacting partners [28]. The implication is that CAS phosphorylation on tyrosine 12 by Src can inhibit the binding to vinculin and hence prevent the mechanical extension of the CAS substrate domain. This raises the possibility that Src both initiates and terminates CAS-mediated mechanotransduction in a negative feedback loop (Fig. 10).

The CAS substrate domain tyrosine phosphorylation and phosphorylation of tyrosine 12 exhibit significantly different dynamics (Fig. 6c). While the substrate domain phosphorylation is rapid and returns to basal levels 30 min after the onset of stretch, phosphorylation on tyrosine 12 is gradual and becomes noticeably elevated only 20 min after the onset of stretch. The faster dynamics of tyrosine phosphorylation in the mechanically extended substrate domain versus phosphorylation of tyrosine 12 could reflect that the latter is a much weaker phosphorylation motif for Src kinase and also less accessible. The observation of different dynamics of substrate domain and tyrosine 12

phosphorylation supports the notion of a dual role of Src in CAS-mediated mechanotransduction. Mechanical stretch of the cell is transmitted through focal adhesions to the CAS substrate domain, which becomes physically extended, undergoes phosphorylation by Src, and subsequently leads to the activation of CAS-mediated mechanotransduction pathways. Later, the loss of CAS–vinculin association after tyrosine 12 eventually becomes phosphorylated (Fig. 6c) releases the SH3-mediated anchoring of CAS to focal adhesions and reverse the CAS substrate domain to its unextended state. This in turn can be expected to inhibit CAS-mediated signaling either by gradual loss of substrate domain phosphorylation, or by making the substrate domain inaccessible for downstream signaling proteins. Hence, a Src-mediated negative feedback loop would imply that CAS signaling during a static mechanical stretch is only transient.

Materials and methods

Cell transfection and culture

CAS^{-/-} and FAK^{-/-} MEFs were obtained from Steven Hanks (Vanderbilt University, Nashville). Wild-type MEFs and Vin^{-/-} cells were a kind gift from Dr. W.H. Ziegler, University of Leipzig. CAS^{-/-} MEFs stably re-expressing CAS Tyr12 variants (WT, Y12E, Y12F), were prepared using pIRES3-puro-CAS vector variants as described previously [27]. All transfections were carried out according to the manufacturer's protocol using Jet Prime (Polyplus Transfection). CAS^{-/-} were transfected with pEGFP-C1 CAS [27] or pcDNA3.1-EGFP-*vinculin* [62]. Vin^{-/-} MEFs were transfected with pcDNA3.1-EGFP-*vinculin* and pCS2-wtCAS-*venus* [22]. FAK^{-/-} cells were transfected with pCS2-wtCAS-*venus*. All cell lines were cultivated in full DMEM (Life Technologies) with 4.5 g/l L-glucose, L-glutamine, and pyruvate, supplemented with 10 % fetal bovine serum (Sigma-Aldrich, St. Louis, MO, USA), 2 % antibiotic-antimycotic (Life Technologies), and 1 % MEM non-essential amino acids (Life Technologies). To abrogate the PKPP CAS SH3-binding motif in vinculin, we mutagenized the vinculin cDNA using QuikChange II Kit (Stratagene). The resulting construct was verified by sequencing.

Immunoblotting and immunoprecipitation

Subconfluent cell cultures were washed with phosphate-buffered saline (PBS) and lysed in modified RIPA buffer (0.15 M NaCl; 50 mM Tris-HCl, pH 7.4; 1 % Nonidet P-40; 0.1 % SDS; 1 % sodium deoxycholate; 5 mM EDTA; 50 mM NaF). Protein concentrations in lysates were

determined using the DC Protein Assay (Bio-Rad, Hercules, CA, USA). Protein lysates were diluted in Laemmli sample buffer (0.35 M Tris-HCl, pH 6.8; 10 % SDS; 40 % glycerol; 0.012 % Bromophenol blue). For immunoblotting, samples were separated on 10 % SDS-polyacrylamide gels and transferred onto nitrocellulose membranes. Non-specific activity was blocked by incubating membranes for 45 min at room temperature in Tris-buffered saline containing 5 % non-fat dry milk. Membranes were then incubated overnight at 4 °C with primary antibodies, washed extensively with Tris-buffered saline with Tween-20 (TTBS), and incubated for 1 h at room temperature with horseradish peroxidase (HRP)—conjugated secondary antibodies. After extensive washing in TTBS, the blots were developed using the LAS-1000 Single System (Fujifilm, Tokyo, Japan). The monoclonal antibody against CAS (clone 24) was obtained from BD Transduction Laboratories. Anti-*vinculin* monoclonal antibodies were from Sigma Aldrich. Anti-FAK polyclonal rabbit antibodies (FAK C-20), anti-GFP (sc8334), and HRP-conjugated anti-mouse and anti-rabbit immunoglobulin G were purchased from Santa Cruz Biotechnology. Phospho-specific antibodies against CAS phosphotyrosine 410 were bought from Cell Signaling Technology. Antibody against CAS phosphotyrosine 12 was developed recently [27]. Quantification of Western blots was carried out using ImageJ software (<http://rsbweb.nih.gov/ij/>).

For immunoprecipitations, cells were lysed in NP-40 lysis buffer (50 mM Tris, pH 7.4, 150 mM NaCl, 1 % NP-40, 5 mM EDTA, 50 mM NaF). Lysates containing 500 mg of proteins were incubated overnight on ice with 1 µg of primary antibody (monoclonal anti-GFP antibody; Molecular Probes, Invitrogen), and immune complexes were collected by additional 2-h incubation with protein A-Sepharose (20 µl of 50 % slurry; Zymed, San Francisco, CA, USA). The immunoprecipitates were washed five times with 1 ml of ice-cold NP-40 lysis buffer, resuspended in 2× SDS-PAGE sample buffer, and processed for immunoblotting.

Far-Western-blot analysis

Cell lysates were prepared from Vinculin^{-/-} MEFs re-expressing Vinculin WT tagged with GFP in a NP-40 lysis buffer (50 mM Tris, pH 7.4, 150 mM NaCl, 1 % NP-40, 5 mM EDTA, 50 mM NaF). Protein samples were prepared as described under “Immunoprecipitations”. After SDS-PAGE, proteins were transferred to nitrocellulose membrane and far-Western-blot analysis was carried out by incubating the protein blots with the recombinant protein probe at 1.2 µg/ml and anti-GST antibody (Sigma, 1:4000) in 1 % BSA in TTBS overnight. After extensive washing with TTBS, blots were treated with horseradish peroxidase-conjugated secondary antibodies and the blots were

developed using the LAS-1000 Single System (Fujifilm, Tokyo, Japan).

GST pull-downs and MS analysis

CAS SH3 domain and mutational variants with either the non-phosphorylatable Y12F substitution or a negative control phospho-mimicking Y12E substitution were N-terminally fused with glutathione-S-transferase. The recombinant protein was purified and incubated with HeLa cell lysate by applying an affinity chromatography strategy. The interacting proteins were separated by SDS-PAGE, and proteins differentially bound by both WT and Y12F CAS-SH3 domain variants were identified by peptide mass fingerprinting using a 4800 Plus MALDI TOF/TOF (AB SCIEX) mass spectrometer.

Cell lysates were incubated with glutathione Sepharose 4B beads with immobilized GST or GST-CAS-SH3 variants at 4 °C for 2 h. The beads were washed extensively and boiled in Laemmli sample buffer, and proteins were detected by SDS-PAGE and immunoblotting.

Immunofluorescence microscopy

Cells were seeded either on coverslips or on PDMS membranes (for stretching), both coated with human 5 µg/ml fibronectin (Invitrogen, Carlsbad, CA, USA). Cells seeded on coverslips were grown for 24–48 h, and subsequently fixed in 4 % paraformaldehyde, permeabilized in 0.5 % Triton X-100, washed extensively with PBS, and blocked in 3 % bovine serum albumin. Cells attached to PDMS membranes were stretched for 10 min at 0.25 Hz and 20 % peak-to-peak amplitude, immediately fixed in 4 % paraformaldehyde, permeabilized in 0.5 % Triton X-100, washed with PBS, and blocked in 3 % bovine serum albumin. PDMS membranes with cells were then mounted on coverslips. The cells (both on coverslips and PDMS membranes) were sequentially incubated with primary antibodies for 2 h, secondary antibodies for 60 min, and if needed with Dy-405 phalloidin (Dyomics) for 15 min, and extensive washing between each step. The primary antibodies were as follows: anti-vinculin (Jackson Biotechnology), anti-paxillin (BD Transduction Laboratories). The secondary antibodies were as follows: anti-rabbit (Alexa 546) and anti-mouse (Alexa 594, Alexa 633; Molecular Probes). Images were acquired with a TCS SP2 microscope system (Leica, Wetzlar, Germany) equipped with a Leica 63×/1.45 oil objective.

Fluorescence recovery after photobleaching

FRAP studies were conducted on live cells expressing either venus-tagged CAS or GFP-tagged vinculin. The cells were placed on glass-bottom dishes (MatTek, Ashland,

MA, USA) coated with 10 µg/ml fibronectin and cultured for 24 h before the experiment. Measurements were performed in DMEM at 37 °C and 5 % CO₂ and 12–18 focal adhesions from different cells, expressing CAS-venus or GFP-vinculin were analyzed. After a brief measurement for monitoring baseline intensity (488 nm), a high-energy beam was used to bleach 40–80 % of the intensity in the spot. The intensity of recovery of the bleached region was extracted from the images series, and curves were fitted to a single-exponential using SigmaPlot (SYSTAT Software). The characteristic fluorescence recovery time was extracted from the FRAP curves as described by Tolde et al. [63].

Cell stretcher

Stretch experiments were carried out either on flexible polydimethylsiloxane (PDMS, Sylgard) substrates that were molded into the shape of a cell culture well or on commercial silicone chambers (B Bridge International) all with 4.0 cm² internal surface [64]. The stretchers for both types of chambers consist of a linear stage for uniaxial stretch and are driven by a computer controlled stepper motor. The substrates were then coated with 5 µg/ml fibronectin in PBS overnight at 4 °C, and 10,000 cells were seeded 24 h prior to experiments. Uniaxial stretch was performed in the incubator under normal cell culture conditions (37 °C, 5 % CO₂, 95 % humidity) for 10 min at 20 % stretch amplitude (peak-to-peak) [65].

Traction microscopy

Traction measurements were performed on 7.0 % acrylamide/bisacrylamide (ratio 29:1) gels (Young's modulus 18.0 kPa, thickness 300 µm) with 1.0 µm red fluorescent beads embedded at the top surface [66, 67]. Gels were coated with 5 µg/ml fibronectin at 4 °C overnight. Cells were seeded on the gels at a density of 5,000 cells per cm² and incubated under normal growth conditions overnight. During measurements, the cells were maintained at 37 °C and 5 % CO₂ in a humidified atmosphere. Cell tractions were computed by an unconstrained fast Fourier traction cytometry method [40] and measured before and after the cells were treated with 80 µM cytochalasin D to relax the traction forces.

Magnetic tweezers experiments

We used high-force magnetic tweezers as described in [68]. For measurements, 30,000 cells were seeded overnight in a 35-mm tissue culture dish. Thirty minutes prior to experiments, cells were incubated with 4.5-µm fibronectin-coated superparamagnetic beads (Invitrogen, Karlsruhe, Germany). The tip of the magnetic tweezers was then placed

at a distance of 20–30 μm from a bead bound to a cell. Transfected cells were identified in fluorescence mode. During measurements, bright field images were taken at 40 \times magnification (NA 0.6) with a CCD camera (ORCA ER, Hamamatsu) at a rate of 40 frames/s. The bead position was tracked using an intensity-weighted center-of-mass algorithm. Measurements on multiple beads per well were performed at 37 $^{\circ}\text{C}$ for a maximum duration of 30 min.

Statistical analysis

Statistical analysis was performed with an unpaired two-tailed Student's *t* test. Numbers indicate actual *p* value for particular test.

Acknowledgments We thank Marie Charvátová, Navid Bonakdar, Astrid Mainka, and Michael Kuhn for their help with experiments. This work was supported by grants from the Grant Agency of the Czech Republic (Grant# 13-24851J), Czech Ministry of Education, Youth and Sport (MSM0021620858), Bayerische Forschungssallianz, Deutscher Akademischer Austauschdienst, and Deutsche Forschungsgemeinschaft.

Open Access This article is distributed under the terms of the Creative Commons Attribution License which permits any use, distribution, and reproduction in any medium, provided the original author(s) and the source are credited.

References

- Defilippi P, Di Stefano P, Cabodi S (2006) p130Cas: a versatile scaffold in signaling networks. *Trends Cell Biol* 16:257–263
- Brabek J, Constancio BS, Shin NY, Pozzi A, Weaver AM, Hanks SK (2004) CAS promotes invasiveness of Src-transformed cells. *Oncogene* 23:7406–7415
- Brabek J, Constancio SS, Siesser PF, Shin NY, Pozzi A, Hanks SK (2005) Crk-associated substrate tyrosine phosphorylation sites are critical for invasion and metastasis of Src-transformed cells. *Mol Cancer Res* 3:307–315
- Brinkman A, van der Flier S, Kok EM, Dorssers LCJ (2000) BCAR1, a human homologue of the adapter protein p130Cas, and antiestrogen resistance in breast cancer cells. *J Natl Cancer Inst* 92:112–120
- Dorssers LCJ, Grebenchtchikov N, Brinkman A, Look MP, Klijn AGM, Geurts-Moespot A, Span PN, Foekens JA, Sweep CGJ (2004) Application of a newly developed ELISA for BCAR1 protein for prediction of clinical benefit of tamoxifen therapy in patients with advanced breast cancer. *Clin Chem* 50:1445–1447
- Ruest PJ, Shin NY, Polte TR, Zhang X, Hanks SK (2001) Mechanisms of CAS substrate domain tyrosine phosphorylation by FAK and Src. *Mol Cell Biol* 21:7641–7652
- Shin NY, Dise RS, Schneider-Mergener J, Ritchie MD, Kilkenny DM, Hanks SK (2004) Subsets of the major tyrosine phosphorylation sites in Crk-associated substrate (CAS) are sufficient to promote cell migration. *J Biol Chem* 279:38331–38337
- Fonseca PM, Shin NY, Brabek J, Ryzhova L, Wu J, Hanks SK (2004) Regulation and localization of CAS substrate domain tyrosine phosphorylation. *Cell Signal* 16:621–629
- Klemke RL, Leng J, Molander R, Brooks PC, Vuori K, Cheresch DA (1998) CAS/Crk coupling serves as a “molecular switch” for induction of cell migration. *J Cell Biol* 140:961–972
- Honda H, Nakamoto T, Sakai R, Hirai H (1999) p130(Cas), an assembling molecule of actin filaments, promotes cell movement, cell migration, and cell spreading in fibroblasts. *Biochem Biophys Res Commun* 262:25–30
- Cho SY, Klemke RL (2000) Extracellular-regulated kinase activation and CAS/Crk coupling regulate cell migration and suppress apoptosis during invasion of the extracellular matrix. *J Cell Biol* 149:223–236
- Huang JH, Hamasaki H, Nakamoto T, Honda H, Hirai H, Saito M, Takato T, Sakai R (2002) Differential regulation of cell migration, actin stress fiber organization, and cell transformation by functional domains of Crk-associated substrate. *J Biol Chem* 277:27265–27272
- Polte TR, Hanks SK (1995) Interaction between focal adhesion kinase and Crk-associated tyrosine kinase substrate P130(Cas). *Proc Natl Acad Sci USA* 92:10678–10682
- Li X, Earp HS (1997) Paxillin is tyrosine-phosphorylated by and preferentially associates with the calcium-dependent tyrosine kinase in rat liver epithelial cells. *J Biol Chem* 272:14341–14348
- Harte MT, Hildebrand JD, Burnham MR, Bouton AH, Parsons JT (1996) p130(Cas), a substrate associated with v-Src and v-Crk, localizes to focal adhesions and binds to focal adhesion kinase. *J Biol Chem* 271:13649–13655
- Garton AJ, Burnham MR, Bouton AH, Tonks NK (1997) Association of PTP-PEST with the SH3 domain of p130(cas); a novel mechanism of protein tyrosine phosphatase substrate recognition. *Oncogene* 15:877–885
- Kirsch KH, Georgescu MM, Hanafusa H (1998) Direct binding of p130(Cas) to the guanine nucleotide exchange factor C3G. *J Biol Chem* 273:25673–25679
- Liu F, Sells MA, Chernoff J (1998) Transformation suppression by protein tyrosine phosphatase 1B requires a functional SH3 ligand. *Mol Cell Biol* 18:250–259
- Kirsch KH, Georgescu MM, Ishimaru S, Hanfusa H (1999) CMS: an adapter molecule involved in cytoskeletal rearrangements. *Proc Natl Acad Sci USA* 96:6211–6216
- Nakamoto T, Yamagata T, Sakai R, Ogawa S, Honda H, Ueno H, Hirano N, Yazaki Y, Hirai H (2000) CIZ, a zinc finger protein that interacts with p130(cas) and activates the expression of matrix metalloproteinases. *Mol Cell Biol* 20:1649–1658
- Polte TR, Hanks SK (1997) Complexes of focal adhesion kinase (FAK) and Crk-associated substrate (p130(Cas)) are elevated in cytoskeleton-associated fractions following adhesion and Src transformation—requirements for Src kinase activity and FAK proline-rich motifs. *J Biol Chem* 272:5501–5509
- Donato DM, Ryzhova LM, Meenderink LM, Kaverina I, Hanks SK (2010) Dynamics and mechanism of p130Cas localization to focal adhesions. *J Biol Chem* 285:20769–20779
- Nakamoto T, Sakai R, Honda H, Ogawa S, Ueno H, Suzuki T, Aizawa S, Yazaki Y, Hirai H (1997) Requirements for localization of p130(cas) to focal adhesions. *Mol Cell Biol* 17:3884–3897
- Sawada Y, Tamada M, Dubin-Thaler BJ, Cherniavskaya O, Sakai R, Tanaka S, Sheetz MP (2006) Force sensing by mechanical extension of the Src family kinase substrate p130Cas. *Cell* 127:1015–1026
- Sawada Y, Nakamura K, Doi K, Takeda K, Tobiume K, Saitoh M, Morita K, Komuro I, De Vos K, Sheetz M, Ichijo H (2001) Rap1 is involved in cell stretching modulation of p38 but not ERK or JNK MAP kinase. *J Cell Sci* 114:1221–1227
- Tamada M, Sheetz MP, Sawada Y (2004) Activation of a signaling cascade by cytoskeleton stretch. *Dev Cell* 7:709–718
- Janostiak R, Tolde O, Bruhova Z, Novotny M, Hanks SK, Rosel D, Brabek J (2011) Tyrosine phosphorylation within the SH3 domain regulates CAS subcellular localization, cell migration, and invasiveness. *Mol Biol Cell* 22:4256–4267

28. Tatarova Z, Brabek J, Rosel D, Novotny M (2012) SH3 domain tyrosine phosphorylation—sites, role and evolution. *PLoS One* 7: Article ID e36310
29. Coutu MD, Craig SW (1988) cDNA-derived sequence of chicken-embryo vinculin. *Proc Natl Acad Sci USA* 85:8535–8539
30. Bubeck P, Pistor S, Wehland J, Jockusch BM (1997) Ligand recruitment by vinculin domains in transfected cells. *J Cell Sci* 110:1361–1371
31. Demali KA, Barlow CA, BurrIDGE K (2002) Recruitment of the Arp2/3 complex to vinculin: coupling membrane protrusion to matrix adhesion. *J Cell Biol* 159:881–891
32. Geiger B, Bershadsky A, Pankov R, Yamada KM (2001) Transmembrane extracellular matrix-cytoskeleton crosstalk. *Nat Rev Mol Cell Biol* 2:793–805
33. Subauste MC, Pertz O, Adamson ED, Turner CE, Junger S, Hahn KM (2004) Vinculin modulation of paxillin-FAK interactions regulates ERK to control survival and motility. *J Cell Biol* 165:371–381
34. Giannone G, Ronde P, Gaire M, Beaudouin J, Haiech J, Ellenberg J, Takeda K (2004) Calcium rises locally trigger focal adhesion disassembly and enhance residency of focal adhesion kinase at focal adhesions. *J Biol Chem* 279:28715–28723
35. Cluzel C, Saltel F, Lussi J, Paulhe F, Imhof BA, Wehrle-Haller B (2005) The mechanisms and dynamics of alpha v beta 3 integrin clustering in living cells. *J Cell Biol* 171:383–392
36. Goetz JG (2009) Bidirectional control of the inner dynamics of focal adhesions promotes cell migration. *Cell Adh Migr* 3:185–190
37. Möhl CC, Kirchgessner N, Schafer C, Kupper K, Born S, Diez G, Goldmann WH, Merkel R, Hoffmann B (2009) Becoming stable and strong: the interplay between vinculin exchange dynamics and adhesion strength during adhesion site maturation. *Cell Motil Cytoskeleton* 66:350–364
38. Mierke CT, Kollmannsberger P, Zitterbart DP, Smith J, Fabry B, Goldmann WH (2008) Mechano-coupling and regulation of contractility by the vinculin tail domain. *Biophys J* 94:661–670
39. Wang N, Tolic-Norrelykke IM, Chen JX, Mijailovich SM, Butler JP, Fredberg JJ, Stamenovic D (2002) Cell prestress. I. Stiffness and prestress are closely associated in adherent contractile cells. *Am J Physiol Cell Physiol* 282:C606–C616
40. Butler JP, Tolic-Norrelykke IM, Fabry B, Fredberg JJ (2002) Traction fields, moments, and strain energy that cells exert on their surroundings. *Am J Physiol Cell Physiol* 282:C595–C605
41. Zhang JH, Li X, Yao B, Shen WQ, Sun HB, Xu C, Wu JH, Shi YY (2007) Solution structure of the first SH3 domain of human vinexin and its interaction with vinculin peptides. *Biochem Biophys Res Commun* 357:931–937
42. Huttelmaier S, Mayboroda O, Harbeck B, Jarchau T, Jockusch BM, Rudiger M (1998) The interaction of the cell-contact proteins VASP and vinculin is regulated by phosphatidylinositol-4,5-bisphosphate. *Current Biol* 8:479–488
43. Kioka N, Sakata S, Kawauchi T, Amachi T, Akiyama SK, Okazaki K, Yaen C, Yamada KM, Aota S (1999) Vinexin: a novel vinculin-binding protein with multiple SH3 domains enhances actin cytoskeletal organization. *J Cell Biol* 144:59–69
44. Webb DJ, Donais K, Whitmore LA, Thomas SM, Turner CE, Parsons JT, Horwitz AF (2004) FAK-Src signalling through paxillin, ERK and MLCK regulates adhesion disassembly. *Nat Cell Biol* 6:154–161
45. Kanchanawong P, Shtengel G, Pasapera AM, Ramko EB, Davidson MW, Hess HF, Waterman CM (2010) Nanoscale architecture of integrin-based cell adhesions. *Nature* 468:580–584
46. Carisey A, Tsang R, Greiner AM, Nijenhuis N, Heath N, Nazgiewicz A, Kemkemmer R, Derby B, Spatz J, Ballestrem C (2013) Vinculin regulates the recruitment and release of core focal adhesion proteins in a force-dependent manner. *Curr Biol* 23:271–281
47. Saunders RM, Holt MR, Jennings L, Sutton DH, Barsukov IL, Bobkov A, Liddington RC, Adamson EA, Dunn GA, Critchley DR (2006) Role of vinculin in regulating focal adhesion turnover. *Eur J Cell Biol* 85:487–500
48. Fernandez JLR, Geiger B, Salomon D, BenZeev A (1993) Suppression of vinculin expression by antisense transfection confers changes in cell morphology, motility, and anchorage-dependent growth of 3T3-cells. *J Cell Biol* 122:1285–1294
49. Goldmann WH, Schindl M, Cardozo TJ, Ezzell RM (1995) Motility of vinculin-deficient F9 embryonic carcinoma-cells analyzed by video, laser confocal, and reflection interference contrast microscopy. *Exp Cell Res* 221:311–319
50. Ilic D, Furuta Y, Kanazawa S, Takeda N, Sobue K, Nakatsuji N, Nomura S, Fujimoto J, Okada M, Yamamoto T (1995) Reduced cell motility and enhanced focal adhesion contact formation in cells from FAK-deficient mice. *Nature* 377:539–544
51. Humphries JD, Wang P, Streuli C, Geiger B, Humphries MJ, Ballestrem C (2007) Vinculin controls focal adhesion formation by direct interactions with talin and actin. *J Cell Biol* 179:1043–1057
52. Diez G, Kollmannsberger P, Mierke CT, Koch TM, Vali H, Fabry B, Goldmann WH (2009) Anchorage of vinculin to lipid membranes influences cell mechanical properties. *Biophys J* 97:3105–3112
53. Ezzell RM, Goldmann WH, Wang N, Parashurama N, Ingber DE (1997) Vinculin promotes cell spreading by mechanically coupling integrins to the cytoskeleton. *Exp Cell Res* 231:14–26
54. Cross SE, Jin YS, Rao J, Gimzewski JK (2007) Nanomechanical analysis of cells from cancer patients. *Nat Nanotechnol* 2:780–783
55. Swaminathan V, Myhre K, O'Brien ET, Berchuck A, Blobe GC, Superfine R (2011) Mechanical stiffness grades metastatic potential in patient tumor cells and in cancer cell lines. *Cancer Res* 71:5075–5080
56. Wakatsuki T, Schwab B, Thompson NC, Elson EL (2001) Effects of cytochalasin D and latrunculin B on mechanical properties of cells. *J Cell Sci* 114:1025–1036
57. Beningo KA, Hamao K, Dembo M, Wang YL, Hosoya H (2006) Traction forces of fibroblasts are regulated by the Rho-dependent kinase but not by the myosin light chain kinase. *Arch Biochem Biophys* 456:224–231
58. Zhang X, Jiang G, Cai Y, Monkley SJ, Critchley DR, Sheetz MP (2008) Talin depletion reveals independence of initial cell spreading from integrin activation and traction. *Nat Cell Biol* 10:1062–1068
59. Dey T, Mann MC, Goldmann WH (2011) Comparing mechano-transduction in fibroblasts deficient of focal adhesion proteins. *Biochem Biophys Res Commun* 413:541–544
60. Mierke CT, Kollmannsberger P, Zitterbart DP, Diez G, Koch TM, Marg S, Ziegler WH, Goldmann WH, Fabry B (2010) Vinculin facilitates cell invasion into three-dimensional collagen matrices. *J Biol Chem* 285:13121–13130
61. Tang DD, Tan J (2003) Role of Crk-associated substrate in the regulation of vascular smooth muscle contraction. *Hypertension* 42:858–863
62. Diez G, Auernheimer V, Fabry B, Goldmann WH (2011) Head/tail interaction of vinculin influences cell mechanical behavior. *Biochem Biophys Res Commun* 406:85–88
63. Tolde O, Rosel D, Janostiak R, Vesely P, Brabek J (2012) Dynamics and morphology of focal adhesions in complex 3D environment. *Folia Biol* 58:177–184
64. Faust U, Hampe N, Rubner W, Kirchgessner N, Safran S, Hoffmann B, Merkel R (2011) Cyclic stress at mHz frequencies aligns fibroblasts in direction of zero strain. *PLoS One* 6:e28963
65. Bonakdar N, Luczak J, Lautscham L, Czonstke M, Koch TM, Mainka A, Jungbauer T, Goldmann WH, Schroder R, Fabry B

- (2012) Biomechanical characterization of a desminopathy in primary human myoblasts. *Biochem Biophys Res Commun* 419:703–707
66. Pelham RJ, Wang YL (1998) Cell locomotion and focal adhesions are regulated by substrate flexibility (vol 94, pg 13661, 1997). *Proc Natl Acad Sci USA* 95:12070–12070
67. Raupach C, Zitterbart DP, Mierke CT, Metzner C, Muller FA., Fabry B (2007) Stress fluctuations and motion of cytoskeletal-bound markers. *Phys Rev* 76: Article ID 011918
68. Kollmannsberger P, Fabry B (2007) High-force magnetic tweezers with force feedback for biological applications. *Rev Sci Instrum* 78: Article ID 114301


5.2. The 2nd publication

Gemperle, J., Hexnerová, R., Lepšík, M., Tesina, P., Dibus, M., Novotný, M., Brábek, J., Veverka, V., and Rosel, D.

Structural characterization of CAS SH3 domain selectivity and regulation reveals new CAS interaction partners.

Sci. Rep. (2017), 7: 1–18.

SCIENTIFIC REPORTS



OPEN

Structural characterization of CAS SH3 domain selectivity and regulation reveals new CAS interaction partners

Jakub Gemperle¹, Rozálie Hexnerová², Martin Lepšík², Petr Tesina², Michal Dibus¹, Marian Novotný¹, Jan Brábek¹, Václav Veverka² & Daniel Rosel¹

CAS is a docking protein downstream of the proto-oncogene Src with a role in invasion and metastasis of cancer cells. The CAS SH3 domain is indispensable for CAS-mediated signaling, but structural aspects of CAS SH3 ligand binding and regulation are not well understood. Here, we identified the consensus CAS SH3 binding motif and structurally characterized the CAS SH3 domain in complex with ligand. We revealed the requirement for an uncommon centrally localized lysine residue at position +2 of CAS SH3 ligands and two rather dissimilar optional anchoring residues, leucine and arginine, at position +5. We further expanded the knowledge of CAS SH3 ligand binding regulation by manipulating tyrosine 12 phosphorylation and confirmed the negative role of this phosphorylation on CAS SH3 ligand binding. Finally, by exploiting the newly identified binding requirements of the CAS SH3 domain, we predicted and experimentally verified two novel CAS SH3 binding partners, DOK7 and GLIS2.

Mammalian Crk-associated substrate (CAS), a major substrate of Src kinase, plays an important role in oncogenic transformation mediated by the *v-crk* and *v-src* oncogenes (reviewed by ref. 1). Tyrosine phosphorylated CAS is enriched in focal adhesions and podosome rosettes^{2,3}. In Src-transformed cells, CAS expression is required to promote cell invasiveness and lung metastasis⁴. Furthermore, increased levels of the human ortholog of CAS, BCAR1, are associated with exacerbated prognosis in breast cancer patients⁵.

CAS serves as an adaptor protein in multiprotein signaling complexes. CAS consists of an N-terminal Src Homology 3 (SH3) domain, a large central substrate domain (SD) formed by 15 repeats of the YxxP motif followed by a serine-rich domain, and a C-terminal part composed of binding sites for the SH2 and SH3 domains of Src (YDYVHL and RPLPSP, respectively) and a CAS-family C-terminal homology domain (reviewed in ref. 1). The SD domain contains multiple tyrosine phosphorylation sites and is essential for the invasive and metastatic properties of CAS⁴. The phosphorylation of tyrosines in SD by Src family kinases enables CAS interactions with the Crk and Nck adapters^{6,7}. The extent of this phosphorylation is regulated by the CAS SH3 domain, which mediates the interaction of CAS with polyproline motifs of various kinases (FAK, PYK2/RAFTK, FRNK), phosphatases (PTP1B, PTP-PEST), and other proteins (C3G, CMS, CIZ and Vinculin)^{8–15}. The CAS SH3 domain is indeed important for tyrosine phosphorylation of the SD, as experiments with truncated CAS lacking the SH3 domain showed a decreased level of SD tyrosine phosphorylation^{4,16}. The tyrosine phosphorylation of SD can be enhanced by mechanical extension¹⁷, and this finding suggested a mechanism allowing CAS to function as a primary mechanosensor¹⁸. Notably, the critical role of CAS SH3 in mechanosensing and SD phosphorylation-mediated mechanotransduction was described recently¹⁹. Finally, signaling mediated by the CAS SH3 domain may be regulated by changing the affinity of the SH3 domain to its ligands through phosphorylation of Tyr12 within the SH3 domain^{20,21}.

The SH3 domain is a small protein interaction module of approximately 60 amino acids. Its conserved β -sandwich architecture is composed of five antiparallel β strands connected by three loops (n-Src loop, RT loop, and Distal loop) and a short 3_{10} helix. The minimal consensus sequence for SH3 domain ligands is represented

¹Department of Cell Biology, Faculty of Science, Charles University, Vinicna 7, Prague, Czech Republic. ²Institute of Organic Chemistry and Biochemistry of the Czech Academy of Sciences, Flemingovo nam. 2, Prague, Czech Republic. Correspondence and requests for materials should be addressed to V.V. (email: veverka@uochb.cas.cz) or D.R. (email: rosel@natur.cuni.cz)

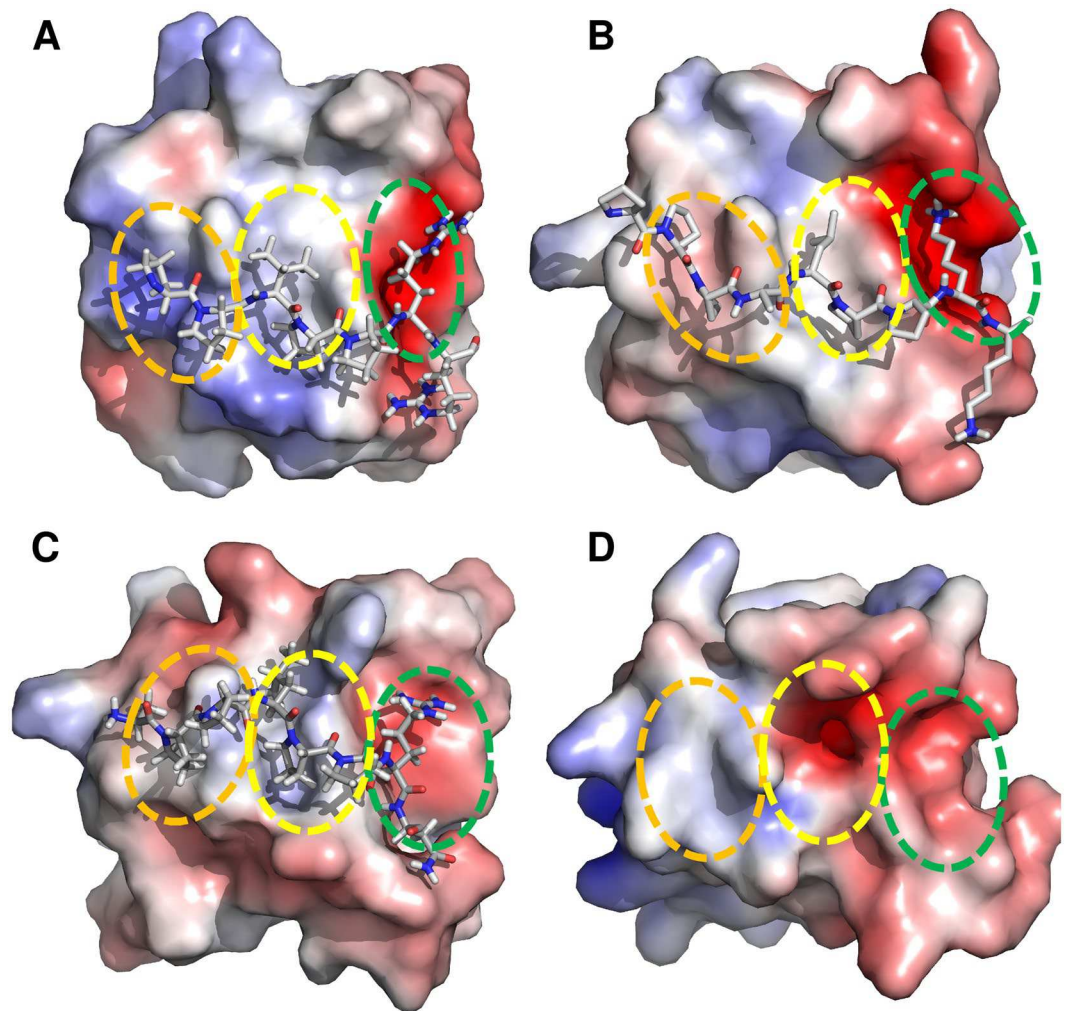


Figure 1. SH3 domains of proteins involved in the CAS signaling circuit. (A) (Grb2, PDB code 1AZE), (B) (Crk, PDB code 1CKA), (C) (Src, PDB code 1QWE), (D) (CAS, PDB code 1WYX). The first and second xP dipeptide-binding pockets are highlighted with orange and yellow circles, respectively. The third pocket/zone is highlighted with a green circle. SH3 domains are shown in electrostatic potential surface representation (APBS colored in the range from -5 to $+5$).

by the PxxP binding motif, which interacts with two xP dipeptide binding pockets formed on the SH3 surface. The SH3 domain binding specificity is further defined by a negatively charged third cleft called the specificity zone/pocket, which binds a positively charged residue that is usually present at the N- or C-terminus of the pseudo-symmetrical PxxP motif and drives ligands on the SH3 domain either in an N-to-C (Class II ligands) or C-to-N (Class I ligands) orientation²². Flanking residues, also known as short distance elements (SDEs), that bind to less conserved portions of the SH3 surface can additionally increase the binding specificity and affinity²³.

SH3 domains generally bind to their targets with a relatively low affinity ($K_d = 5\text{--}100\ \mu\text{M}$) and moderate specificity²⁴. Comparison of the CAS SH3 domain with SH3 domains of proteins involved in the same signaling circuit, such as the well-defined SH3 domains of Crk, Src, and Grb2, reveals a difference in the hydrophobicity of the second xP dipeptide-binding pocket (Fig. 1). While the second binding pocket in all these SH3 domains is mostly hydrophobic, the CAS SH3 domain also includes a negatively charged Glu17 residue. The presence of this unusual negatively charged cleft could contribute to the CAS SH3 domain specificity, perhaps recognizing unusual polyproline rich sequences. However, a systematic screen for CAS SH3 domain ligand preferences has not yet been performed, and despite the known structure of the CAS SH3 domain, the structural determinants of its regulation are not well understood.

By using a multidisciplinary approach combining molecular and structural biology, biophysics, bioinformatics, and computational modeling, we determined the CAS SH3 binding motif and obtained solution structures for the CAS SH3 domain in complex with its natural peptide ligands^{8,10}. These structural data, together with characterization of thermodynamic parameters by isothermal titration calorimetry (ITC) and modeling, allowed us to investigate the affinity contributions from the indispensable centrally located lysine and conserved (arginine) and unusual (leucine) anchoring amino acids in the binding peptides. Based on the structural data, we predicted the

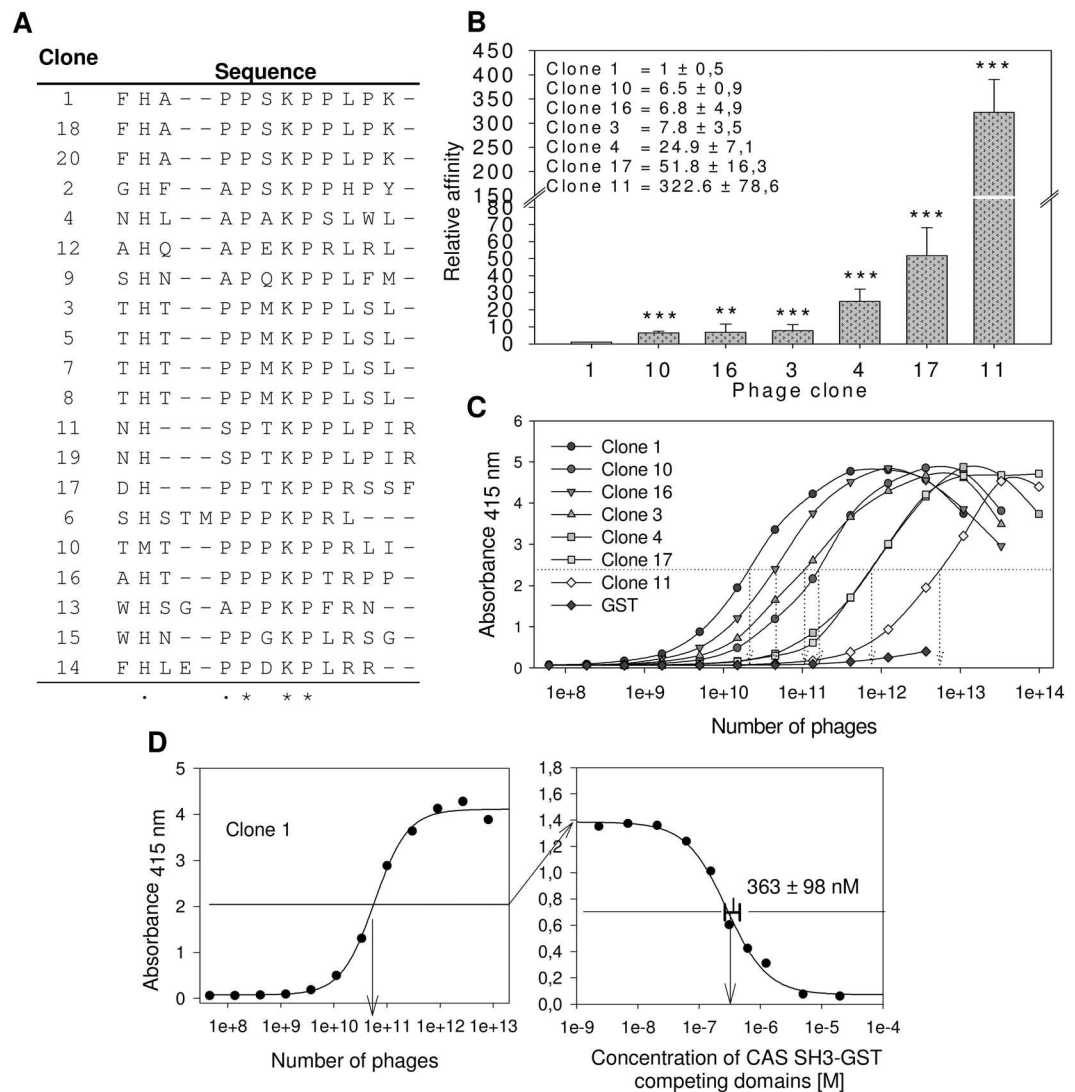


Figure 2. Screening of the CAS SH3 domain binding motif using phage display. **(A)** Sequences of 20 aligned clones. **(B)** ELISA quantification of the relative affinities of seven phage-displayed peptides towards the GST-fused CAS SH3 domain. Relative affinities were calculated based on the binding affinity of clone 1 (the tightest binder). The data are expressed as average \pm standard deviation from five independent experiments. Statistical significance (** $p < 0.01$, *** $p < 0.001$) was determined on log-transformed data by one-way repeated-measures ANOVA followed by Tukey's post-hoc test. **(C)** Representative curves of relative affinities of seven phage-displayed peptides towards the GST-fused CAS SH3 domain. GST alone with clone 1 was used as a negative control. **(D)** Representative graph for the EC_{50} value ($363 \pm 98 \text{ nM}$) for clone 1 binding obtained from seven independent experiments.

effect of Tyr12 phosphorylation. Furthermore, based on the determination of the high-affinity consensus motif, we identified novel CAS SH3 binding partners, DOK7 and GLIS2, and confirmed their interactions in living cells.

Results

The CAS SH3 domain recognizes an unconventional class II SH3 binding motif. The indispensable role of the CAS SH3 domain for CAS/BCAR1-mediated signaling is well-documented. However, to date the CAS SH3 domain-binding motif has not been precisely defined. To identify the binding motif, we performed phage display with a library composed of 10^{12} M13 phages carrying 12-amino-acid degenerate oligopeptides. For the peptide binding selection, GST-fused CAS SH3 was immobilized on GSH-agarose beads and used for bio-panning. After four rounds of panning, 20 phages were isolated and sequenced. This procedure yielded 14 unique sequences encoding CAS SH3 binding peptides (Fig. 2A). The interaction specificity was confirmed by phage ELISA, and qualitative determination of relative binding affinities was performed for seven clones (Fig. 2B,C). We determined an EC_{50} value of 363 nM for clone 1 (FHAPPSKPPLPK), which showed the highest relative affinity (Fig. 2D). This corresponds to an almost 6-fold higher affinity than that previously reported for the interaction

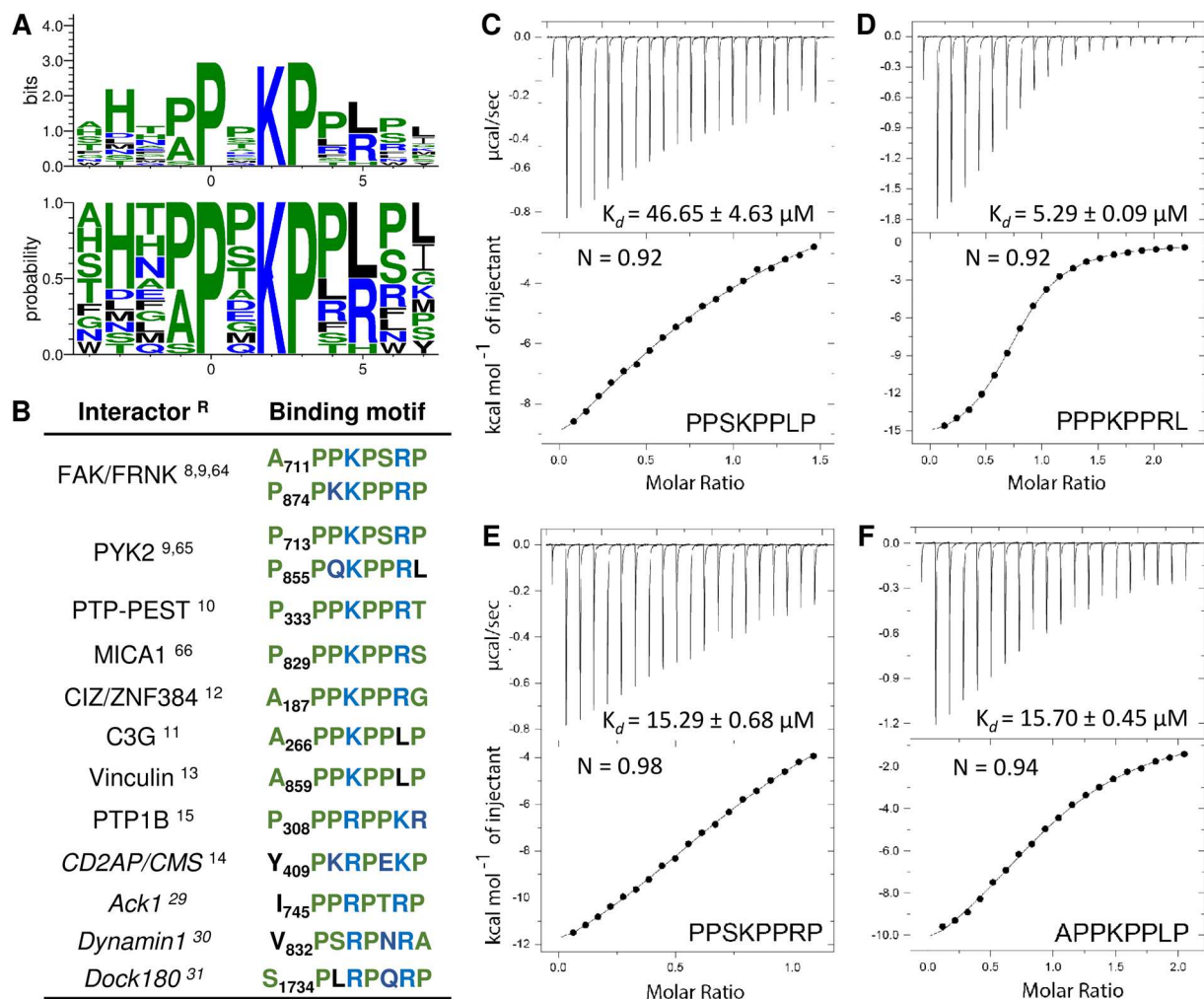


Figure 3. (A) The CAS SH3 binding motif based on the 14 unique sequences obtained from phage display. The x-axis shows the residue position relative to proline (position 0)^{64–66}. (B) The CAS SH3 domain binding interaction partners with their respective binding motifs. Interactors with small differences in binding motif are in italics. References^(R) are superscripted. (C–E) Isothermal titration calorimetry (ITC) data obtained for the interaction of CAS SH3 with four synthetic peptides.

of the CAS SH3 domain with FAK-derived peptide²⁵, suggesting that we discovered a high-affinity ligand for the CAS SH3 domain.

Based on the phage display and phage ELISA results, we determined the CAS SH3 domain high-affinity binding motif as an eight-amino-acid sequence: (A/P)₋₁P₀ ×₁K₂P₃ ×₄(L/R)₅Z₆ (Fig. 3A, Z stands for L/P/S/T). This motif is a class II ligand due to the N-to-C orientation in which position +2 is usually occupied by a hydrophobic residue. Surprisingly, we observed a clear preference for lysine at this central position in all the clones. Alanine or proline are tolerated at position -1, while serine (clone 11) showed a clear negative effect on CAS SH3 binding. We then compared this binding motif to sequences of the 12 known CAS SH3-interacting partners (Fig. 3B). Most of them are in good agreement with the identified motif, with the exception of an arginine to leucine substitution at position +5 (arginine found in 10 cases, leucine only in two). Clearly, there is a strong preference for a positively charged residue.

To analyze amino acid variations at positions -1 and +5 in the binding motif in more detail, we synthesized four octapeptides and determined their thermodynamic parameters of binding using ITC. Two of the peptides corresponded to the core binding motif of two clones with the highest affinities (clones 1 and 10, peptides PPSKPLP and PPPKPPRL, respectively), one peptide corresponding to clone 1 but with the arginine to leucine substitution at position +5 (PPSKPPRP) and one corresponding to the binding site of CAS on Vinculin (APPKPLP), which is closely related to both clone 1 and 10 peptides with alanine at position -1 (Fig. 3C–F). All the tested peptides formed equimolar complexes with CAS SH3. However, the obtained dissociation constants (K_d) revealed significant differences in their affinities towards CAS SH3. The PPPKPPRL peptide showed the highest affinity of all tested peptides ($K_d = 5.29 \pm 0.09 \mu\text{M}$). The APPKPLP and PPSKPPRP peptides exhibited lower but comparable affinities ($K_d = 15.70 \pm 0.45 \mu\text{M}$ and $K_d = 15.29 \pm 0.68 \mu\text{M}$, respectively), while the PPSKPLP peptide was identified as the weakest CAS SH3 ligand of all tested peptides ($K_d = 46.65 \pm 4.63 \mu\text{M}$). Based on these

results, we conclude that arginine at position +5 is more favorable for CAS SH3 binding than leucine at the same position, whereas the affinity contribution of alanine and proline at position -1 is indistinguishable.

Structure of the CAS SH3 domain in complex with its physiological ligands provides insight into the binding interface. With the exceptions of C3G¹¹ and the recently identified Vinculin¹³, no other binding partner of CAS harbouring leucine at position +5 has been identified to date. Our results, however, suggest that leucine is not only permitted at this position but also contributes considerably to the binding (see Fig. 2A–C). Moreover, despite the known X-ray structure of the free CAS SH3 domain²⁵, the structural aspects of CAS SH3 binding domain regulation are not well understood. We thus sought to analyze the structural basis of the CAS SH3 domain binding to its physiological ligands.

We prepared¹⁵N/¹³C-labeled CAS SH3 domain and determined its solution structure. The complete resonance assignments and high quality 3D¹⁵N- and ¹³C-edited NOESY spectra were used for structural calculation (Supplementary Table S1). The conformation of the solution structure is highly similar to that obtained by X-ray (PDB code 1WYX; backbone RMSD of 0.52 Å for residues 7–65), but unexpectedly and in contrast to the dimeric X-ray structure, the CAS SH3 domain remained monomeric in solution even at ~1 mM concentration. A more detailed analysis revealed that the crystallographic dimer is stabilized by crystal contacts that stimulate the formation of an additional two-stranded β -sheet at the dimer interface that is unambiguously absent in solution (Supplementary Figure S1).

Next, we attempted to structurally characterize complexes of CAS SH3 with Vinculin and PTP-PEST derived molecules using isotopically labeled recombinant protein and unlabeled synthetic peptides. The Vinculin and PTP-PEST binding peptides were chosen as known physiological ligands representing both variants of the binding sequence, with either arginine (PTP-PEST) or leucine (Vinculin) at position +5. Although we obtained complete resonance assignments for the peptide-bound protein, the polyproline character of the peptides prevented their unambiguous resonance assignment required for the comprehensive structural characterization of the complexes. To determine the structure of the CAS SH3 domain with peptide ligands containing a high number of repetitive prolines using NMR, we designed two chimeras with the peptide sequences located at the C-terminus of the SH3 domain. The CAS-Vinculin and CAS-PTP-PEST chimeras contained the sequences corresponding to residues 854–870 and 327–343, respectively. In both chimeras, the binding peptide was fused to the SH3 domain through a Gly/Ser-rich linker peptide. This allowed us to obtain a high overall percentage of assigned resonances (>98%) and complete assignments within the peptide region (Supplementary Table S1). In addition, the spectra of the peptide-bound protein were highly similar to those obtained for chimeras, except for a subset of signals from the peptide portion of the fusion proteins (Supplementary Figure S2). The minimal differences in signal positions can be attributed to the increased binding affinity between the protein and peptide regions in chimeras relative to the two individual molecules.

The NMR analysis of the CAS SH3-peptide ligand chimeras allowed for a detailed characterization of the binding interface between the CAS SH3 domain and the studied peptides (Fig. 4A). As expected, the binding of the peptides does not involve a major conformational rearrangement in the CAS SH3 domain (backbone RMSD of 0.97 Å for Vinculin and 0.98 Å for PTP-PEST, for residues 7–65). Comparison of the free CAS SH3 domain structure and the chimera structures revealed a subtle repositioning of the RT loop, allowing the peptide to maintain contacts with both the RT loop residues (i.e., Asn14, Glu17, Glu21, and Asp20) and residues from the core β -sheet (i.e., Asn58 and Trp43) (Fig. 4B,C). Moreover, the changes in the positions of Asn14, Glu17, and Glu21 and a subtle repositioning of side chain residues situated in the short 3_{10} helix (Val55 and Arg59) were evident from relative chemical shift perturbation analysis of CAS SH3 induced by binding of PTP-PEST or Vinculin peptide (Supplementary Figure S3). The bound structures of the peptides differed in their flexibility. For PTP-PEST, Arg338-Leu343 (positions 5–10) was very flexible, and for Vinculin, the flexible part extended between Glu867 and Val870 (positions 7–10) (Fig. 4A).

We utilized the PISA protein interface tool to describe the binding interface of all the NMR generated structural states²⁶ (Supplementary Tables S2–7). Both peptides form contacts with the same CAS SH3 residues (specifically Tyr12, Asn14, Glu17, Glu21, Trp43, Pro56, Asn58, and Arg59) mainly *via* lysine (Lys335 in PTP-PEST, Lys862 in Vinculin) as a central anchoring amino acid (K_2) followed by two proline residues positioned around the Trp43 side chain (Fig. 5). The interaction of CAS SH3 with the PTP-PEST peptide is further stabilized by hydrogen bonds formed between the Arg338 (R_5) side chain and one of the side chain oxygens of Glu21, Ser18, Glu17, or Asp20 of CAS SH3 (Fig. 5, Supplementary Tables S2–4). In Vinculin peptide, this position is occupied by hydrophobic Leu865 (L_5) oriented towards Trp43, Ile54, and Leu40 of CAS SH3 (Fig. 5, Supplementary Tables S5–7). The contacts of the peptide ligands with the Tyr12 side chain of SH3 domain are mediated by the main chain Pro332 (P_{-1}) and Pro333 (P_0) in PTP-PEST and by Ala859 (A_{-1}) and Pro860 (P_0) in Vinculin.

CAS SH3 domain binds to short distance elements. As described previously, the binding specificity and affinity of the ligand can be further increased by binding of the flanking ligand residues (SDEs) to the SH3 domain surface located in the vicinity of the third binding pocket (i.e., C-terminally from the core peptide)²³. Because our chimeric constructs also included nine amino acids corresponding to the sequence surrounding the core binding sequence on both sides, we were able to assess the potential effect of these flanking sequences on binding. At the C-terminal side of the anchoring Arg338 (R_5), there were variable H-bond interactions between Arg340 (R_7) and Gly39, Gln38, or Asp41 of CAS SH3 bound to PTP-PEST (Supplementary Tables S2–4). Interestingly, the N-terminal SDEs formed interactions with the region proximal to the first binding pocket. In PTP-PEST, Asp330 (D_{-3}) formed a transient H-bond (with 21–50% occupancy) with Lys26, which alternated with a weak H-bond between Glu327 (E_{-6}) and Arg25 (Supplementary Tables S2–4, visualized in Fig. 5). In the case of Vinculin (Supplementary Tables S5–7, visualized in Fig. 5), there was one strong, conserved H-bond

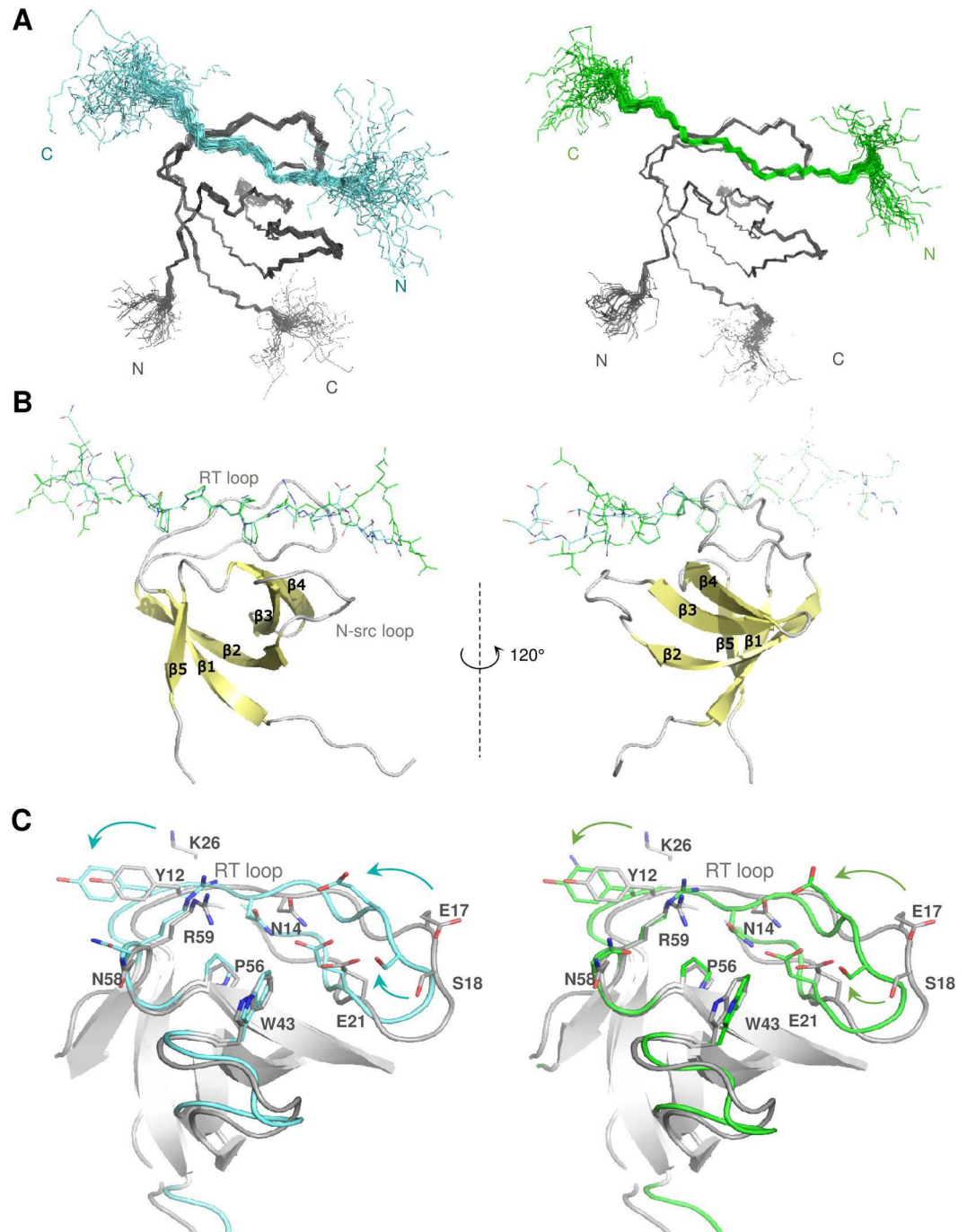


Figure 4. Solution structures of the CAS SH3 domain complexes. **(A)** Set of 40 converged structures of CAS SH3 (dark grey) with PTP-PEST- (cyan, left) and Vinculin-derived peptide (green, right). **(B)** A cartoon representation of the complexes. **(C)** Superimposition of the free CAS SH3 domain (grey) and PTP-PEST- (cyan) and Vinculin-bound (orange) CAS SH3 domains. The β -sheets are in grey.

(Lys26...Glu857/E₋₃). In addition, Lys26 established irregular weak H-bonds with Thr855 (T₋₅) and Asp856 (D₋₄).

These findings are supported by the results of a sequence alignment of the CAS SH3 domain binding partners. The alignment revealed an enrichment of negatively charged amino acid residues localized N-terminal to the polyproline core, although their exact position is not conserved (Supplementary Figure S4). Similar interactions of negatively charged SDEs with region proximal to the first binding pocket have not been described before; however, a lysine residue corresponding to Lys26 is conserved in 35.6% of human SH3_1 domains within the PFAM database, suggesting that other SH3 domains might utilize a similar mechanism to extend the ligand specificity and binding affinity.

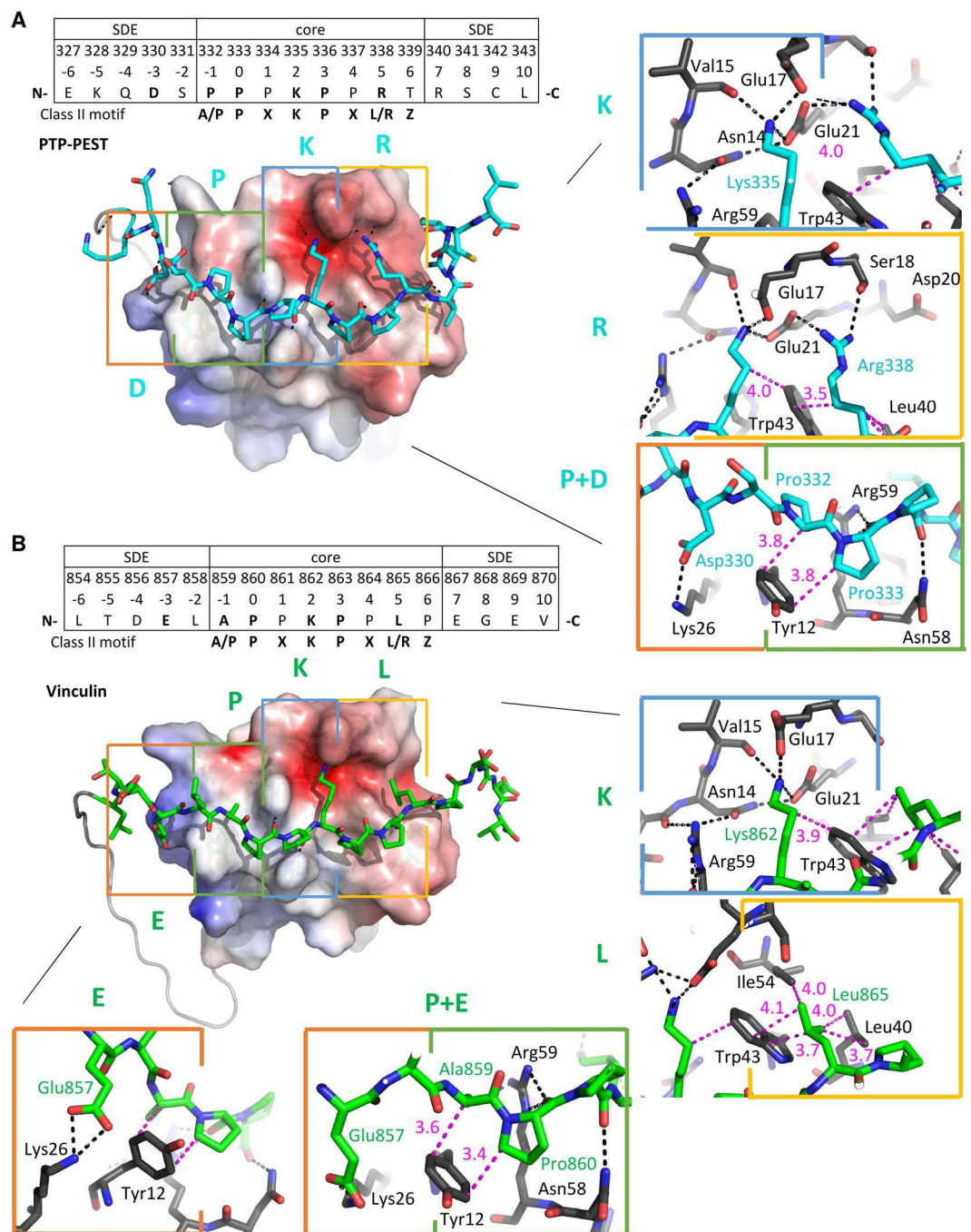


Figure 5. Key interactions between the PTP-PEST- and Vinculin- derived peptides and CAS SH3 domain. (A) PTP-PEST- and (B) Vinculin-derived peptides are shown in stick representation. The CAS SH3 parts of the complexes are shown by electrostatic potential surface representation (APBS). Four binding pockets are highlighted with rectangles (orange - zero pocket/upstream SDE, green - 1st pocket, blue - 2nd pocket, yellow - 3rd pocket), and the interaction interface is shown on the right in detail (PTP-PEST in cyan, Vinculin in green, CAS SH3 in gray). Capital letters E/D, P, K, L/R represent the key ligand amino acid residue in each CAS SH3 binding pocket. The distances between a pair of residues involved in hydrophobic interaction are shown in pink; hydrogen bonds are represented by black dotted lines.

Binding energy and sequence conservation analysis point to determinants of the CAS SH3 domain complex formation.

To understand the mechanism of the CAS SH3 domain ligand binding in energetic terms, we performed MM-GBSA analysis (see Methods) on all the NMR models. The affinities of the PTP-PEST and Vinculin extended peptides (corresponding to residues 327–343 and 854–870, respectively) towards the CAS SH3 domain were estimated as -57.0 ± 1.6 and -57.8 ± 0.8 kcal.mol⁻¹, respectively. This suggests comparable binding affinity, in agreement with the experimentally determined affinities for the PTP-PEST and Vinculin core peptides (332–339 and 859–866) of 5.3 and 15.7 μ M, respectively. All energy contributions

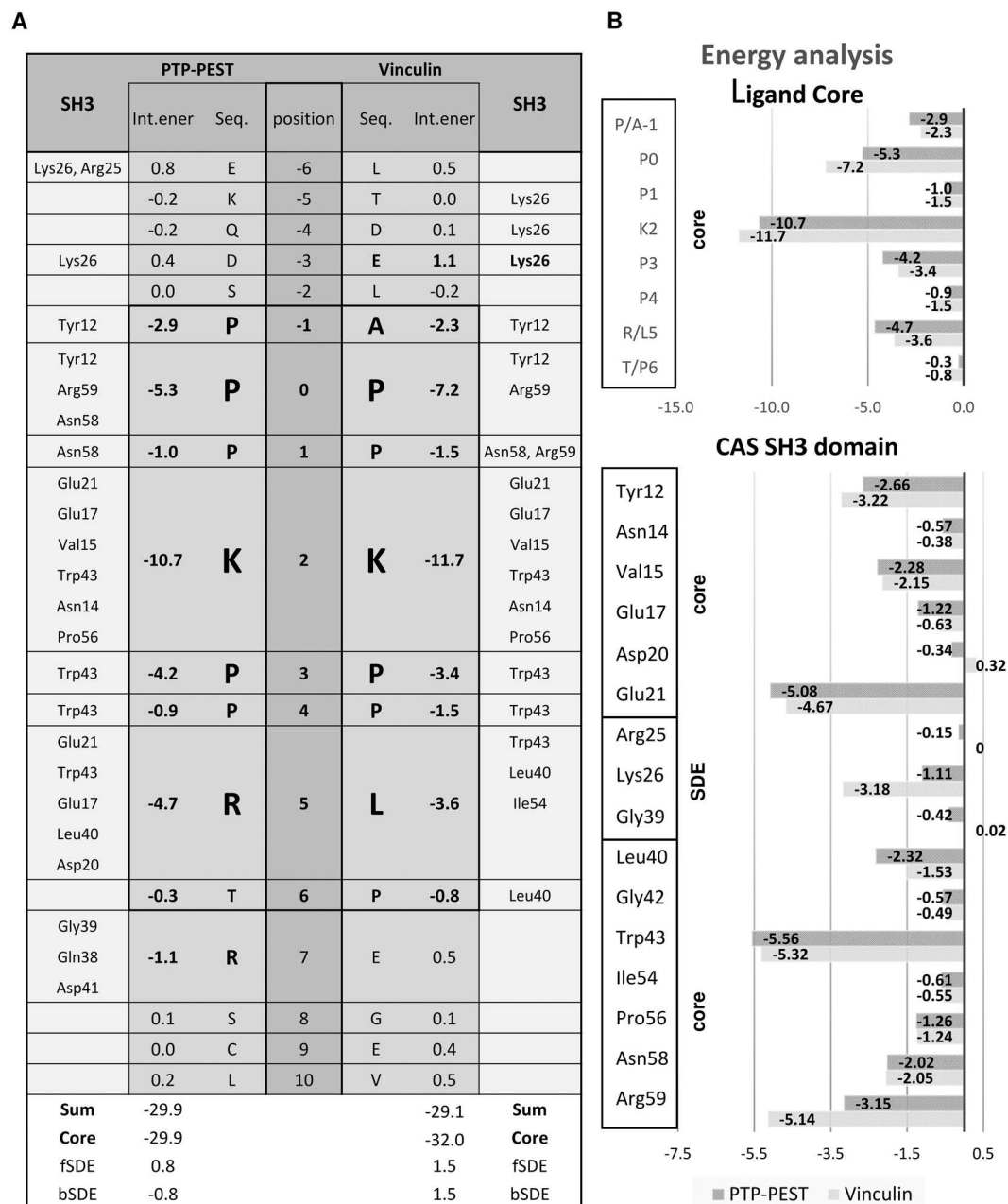


Figure 6. The attractive MM-GBSA energy contributions of individual protein and peptide residues toward binding (in kcal/mol). **(A)** Energy contribution of binding sequences of PTP-PEST or Vinculin to the CAS SH3 domain in fragmented CAS SH3 domain NMR structures. The peptide binding core is highlighted (-1 to 6). **(B)** Upper graph shows the CAS SH3 domain ligand-core binding energy contributions. Lower graph shows the energy contributions of CAS SH3 amino acid residues to binding Vinculin or PTP-PEST. fSDE: N-terminal SDE; bSDE: C-terminal SDE.

for PTP-PEST/Vinculin were determined in kcal.mol⁻¹ (Fig. 6A,B). The sums of the interaction contributions from the peptide residues (positions -6 to 10) were -29.9/-29.1. Nearly the entire interaction strength comes from the peptide core residues (positions -1 to 6; the energy sums were -29.9/-32.0). The largest contributions come from K₂ (-10.7/-11.7; Lys335/862), followed by P₀ (-5.3/-7.2; Pro333/860), R/L₅ (-4.7/-3.6; Arg338/Leu865), and P₃ (-4.2/-3.4; Pro336/Pro863). The MM-GBSA analysis of the core peptide binding is consistent with the PISA interaction interface analysis (Supplementary Tables S2-7). In contrast, the MM-GBSA analysis of the contribution of SDE elements to the binding confirmed only the stabilizing role of the C-terminal SDE, specifically Arg340 (R₇) in PTP-PEST. For the N-terminal SDE, MM-GBSA analysis suggests repulsive rather than attractive forces at position -3. However, it should be noted that the repulsive contribution of Glu857/E₋₃ in Vinculin of 1.1 kcal.mol⁻¹ may result from an improper partitioning of interaction energy and that, summing

up with the favorable contribution of Lys26 of $-3.2 \text{ kcal.mol}^{-1}$, this conserved salt bridge contributes $-2.0 \text{ kcal.mol}^{-1}$ toward binding.

The MM-GBSA energies suggest that strong attractive interactions are derived from the SH3 domain residues Trp43, Glu21, Arg59, and Tyr12 for both PTP-PEST and Vinculin, followed by weaker contributions from Leu40, Val15, Asn58, Pro56, Glu17, and Lys26 (Fig. 6B). These favorable contributions can be linked to individual hydrogen bonds (mediated by Arg59 and Asn58) including salt bridges (Glu21, Glu17, Lys26) as well as nonpolar (dispersion) interactions (Trp43, Tyr12, Leu40, Val15, and Pro56) and are conserved in both PTP-PEST and Vinculin. Glu21 forms a strong salt bridge with K_2 (Lys335/862), which is in turn locked by a bidentate interaction with the Asn14 side chain (Fig. 5). Arg59 forms conserved bidentate H-bonds *via* its side chain with the backbone of P_0 (Pro333/860). Asn58 serves as a donor to a less conserved H-bond with P_1 (Pro334/861) backbone of the ligands. The Glu17 side chain forms a conserved salt bridge with K_2 (Lys335/862) and a much less conserved salt bridge with the anchoring R_5 (Arg338) of PTP-PEST. The major contributor toward nonpolar stabilization is Trp43, which establishes many hydrophobic contacts with the nonpolar parts of the side chains of K_2 (Lys335/862), P_3 (Pro336/Pro863), and R/L_5 (Arg338/Leu865). Furthermore, the phenol ring of Tyr12 packs against the side chains of A/P_{-1} (Pro332/Ala859) and P_0 (Pro333/860). Pro56 is involved in dispersion contacts with the nonpolar parts of the side chains of K_2 (Lys335/862) and P_3 (Pro336/Pro863). The role of Leu40 is different in PTP-PEST and Vinculin. In PTP-PEST, due to the flexibility of R_5 (Arg338) and T_6 (Thr339), variable nonpolar contacts are formed with the nonpolar parts of their side chains. In Vinculin, however, due to the stability of L_5 (Leu865) and P_6 (Pro866), nonpolar interactions with Leu40, Trp43, and Ile54 are conserved.

In most known structures of SH3 domains, at least two out of three ligand binding pockets have hydrophobic/aromatic character, resulting in low binding specificity and therefore relatively high ligand promiscuity. In contrast, the CAS SH3 domain is more polar, due in part to the presence of Glu17 in the second binding pocket. We used PFAM alignment of all human SH3 domains to study the abundance of Glu/Asp residues at the position corresponding to Glu17 in CAS, which permits the binding of the centrally located lysine in the ligand. Within 506 sequences of human SH3_1 domains in the PFAM database, we identified only 12 unique SH3 domains that are likely to bind a centrally located lysine in a manner similar to CAS (Supplementary Figure S5). Of these, seven SH3 domains have glutamate and five have aspartate at the position corresponding to Glu17. The alignment of all human SH3 domains also showed that Leu40, which is important for CAS binding to the ligand, is a CAS-specific feature of the SH3 domain and does not occur in any other human SH3 domain. Interestingly, SH3 domains found by the PFAM search contain two highly conserved aromatic residues localized at the base of the second binding pocket that are substituted with charged amino acids in the CAS SH3 domain (see Supplementary Figure S5; Tyr/Phe to Asn14 and Tyr/Phe to Arg59). This further highlights the uniqueness of the CAS SH3 domain and is potentially responsible for the higher selectivity and affinity of CAS SH3 for ligands with a centrally located lysine.

CAS SH3 ligand binding is regulated by Src-dependent phosphorylation of Tyr12. As we previously suggested²⁰, CAS SH3 domain binding and signaling is negatively regulated by phosphorylation of Tyr12. At the structural level, our data indicate that the aromatic ring of Tyr12 is involved in nonpolar interactions with P_{-1}/A_{-1} and P_0 of PTP-PEST/Vinculin (Fig. 5), while its hydroxyl group remains solvent-exposed. The MM-GBSA energy decomposition suggests that Tyr12 is an important stabilizing element of the interaction of CAS SH3 with PTP-PEST/Vinculin (Fig. 6B). We probed the effects of Tyr12 phosphorylation and mutation by molecular dynamics and quantum mechanics (QM). The introduction of the phosphate group adds a -2 charge to the site, and by formation of a salt bridge with Lys26, it disrupts the native Tyr12 to P_0 and P/A_{-1} CH/ π interactions. This is corroborated by QM calculations, which show drops in interaction energy of 21 kcal.mol^{-1} for both PTP-PEST and Vinculin complexes with CAS SH3 upon modification of Tyr12 to phosphorylated Tyr12 (Supplementary Table S8). Furthermore, phosphorylated Tyr12 weakens or displaces the native salt bridges of Lys26 with the conserved Glu857 (E_{-3}) for Vinculin and transient Asp330 (D_{-3}) for PTP-PEST (Fig. 7A,B), highlighting the importance of acidic upstream SDEs to modulate the effect of phosphorylation on ligand binding.

Though the experimental evidence for the importance of Tyr12 phosphorylation in CAS SH3 binding capacity and CAS signaling is strong, it is based on *in vitro* phosphorylation of isolated SH3 domains or the use of “phosphomimicking” glutamate to substitute Tyr12 (Y12E)^{13,20}. To confirm that Src phosphorylation of CAS on Tyr12 inhibits the SH3 domain-mediated binding capacity of CAS in cells, we compared the binding affinities of CAS to FAK and Vinculin in mouse embryonic fibroblasts (MEFs) and MEFs overexpressing constitutively active Src (MEFs SrcF). Co-immunoprecipitation of Vinculin and partly FAK with endogenous CAS was significantly decreased in MEFs SrcF compared to MEFs (Fig. 7C,D). In addition, inactivation of Src in MEFs SrcF using the Src inhibitor Saracatinib restored the binding of CAS to Vinculin to a similar level as in MEFs. Surprisingly, this inhibition simultaneously stimulated the interaction between CAS and FAK, with over 9-fold higher levels than in MEFs (Fig. 7C,D). Overall, these results confirm that the Src-dependent phosphorylation of Tyr12 serves as a negative regulatory mechanism of the CAS SH3 domain binding.

We also tested the effect of Tyr12 substitution on ligand binding using a phage ELISA approach. For this analysis, we chose phage clones 10 (TMTPPPKPRLI) and 16 (AHTPPPKPTRPP) because they closely match the sequences of CAS SH3 physiological ligands PTP-PEST and FAK, respectively. As expected, the introduction of the phosphomimicking Y12E mutation led to complete disruption of ligand binding (Fig. 7E,F). This is supported by QM calculations that show a $10\text{--}11 \text{ kcal.mol}^{-1}$ drop in interaction energy upon Y12E mutation. The small delocalized system of Glu12 carboxylate is not able to form the same CH/ π interactions as Tyr12. Surprisingly, however, we found that CAS SH3 Y12F mutant binds to clone 10 with a slightly reduced affinity and to clone 16 with a markedly decreased affinity compared to CAS WT (2- and 37-fold, respectively). The QM data support this observation, as the interaction energies drop by 14 and 1 kcal.mol^{-1} for PTP-PEST and Vinculin, respectively (Supplementary Table S5). The reason for the decrease is likely primarily electronic, i.e., the decrease in dipole

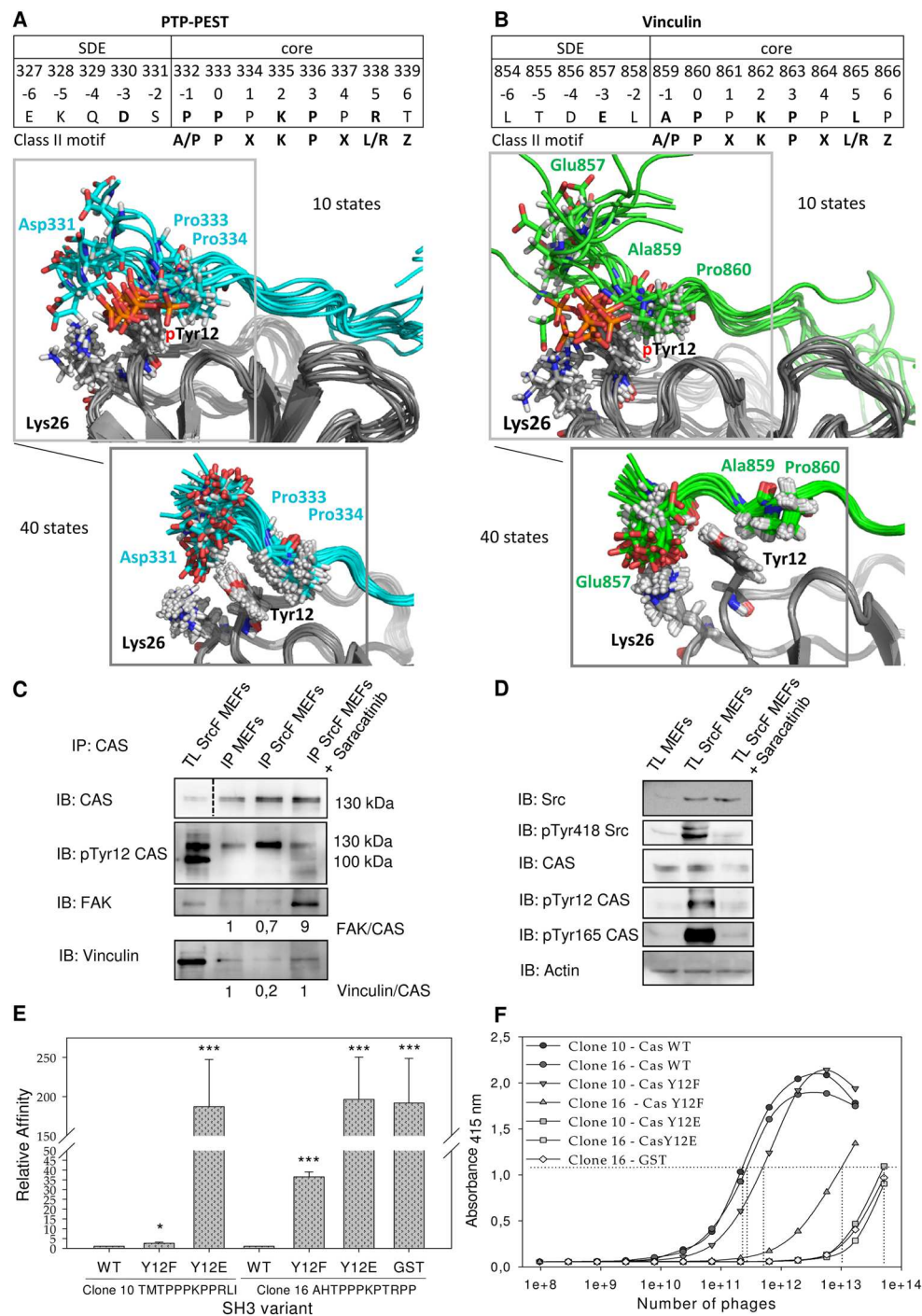


Figure 7. Src phosphorylation of CAS on Tyr12 inhibits CAS binding to FAK and Vinculin. Ten structures from molecular dynamics of phosphoTyr12 CAS SH3 with (A) PTP-PEST peptide (cyan) and (B) Vinculin peptide (green) are shown. These are compared with 40 NMR structures of unphosphorylated CAS SH3 complexes. (C) Co-precipitation analysis of the effect of Src activity on CAS binding capacity. CAS was immunoprecipitated from MEFs and from SrcF-transformed (SrcF) MEFs (in presence or absence of 5 μ M saracatinib), and the amount of co-precipitated FAK and vinculin was analyzed. Numbers indicate the fold-change in ratio of FAK or Vinculin coimmunoprecipitated with CAS. (D) Immunoblot analysis of the effect of Src activity on CAS phosphorylation. (C,D) Blots were cropped from original full-size images (see Supplemental Material). (E) Quantification of phage-displayed peptides (clone 10 and clone 16) binding to CAS SH3 variants (WT, Y12F, Y12E) fused with GST or GST alone. The relative affinity represents the binding ratio relative to CAS-WT. The data are expressed as average \pm standard deviation from three independent experiments. Statistical significance (* $p < 0.05$, *** $p < 0.001$) was determined on log-transformed data by one-way repeated-measures ANOVA followed by Tukey's post-hoc test. (F) Representative curves of phage-displayed peptides (clone 10 and clone 16) binding to CAS SH3 variants (WT, Y12F, Y12E) fused to GST or GST. GST alone with phage clone 16 was used as a negative control.

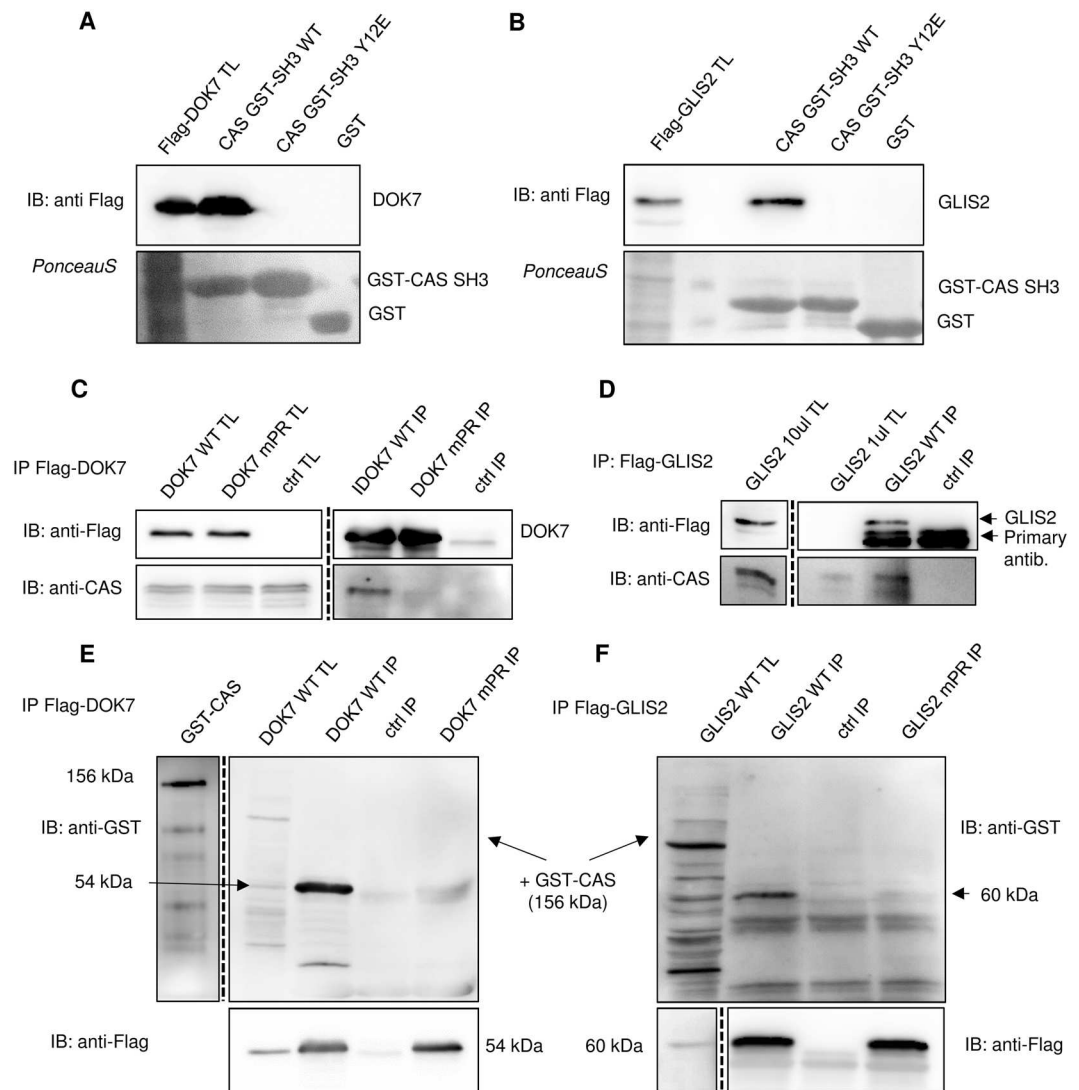


Figure 8. CAS/BCAR1 interacts with DOK7 and GLIS2. **(A,B)** Pull-down assays. Binding of **(A)** Flag-DOK7 or **(B)** Flag-GLIS2, expressed from transiently transfected MDA-MB-231 cells, to purified CAS SH3 domain variants (WT, Y12E, and Y12F) fused with GST was analyzed by pull-down assays. Pulled-down proteins were immunoblotted with anti-Flag antibody, and GST-SH3 domains were stained with Ponceau-S. **(C,D)** MDA-MB-231 cells were transfected with **(C)** Flag-DOK7 or **(D)** Flag-GLIS2 followed by immunoprecipitations using anti-Flag sepharose and for DOK7 elution with glycine, pH 3.5. Co-immunoprecipitated CAS/BCAR1 was detected with anti-CAS antibody. In far-Western experiments **(E,F)**, Flag-DOK7 **(E)** or Flag-GLIS2 **(F)** was immunoprecipitated from transfected MDA-MB-231 cells and eluted with glycine pH 3,5 (DOK7) or by 6x Laemmli sample buffer (GLIS2). Eluted Flag-DOK7 (WT, mPR) or Flag-GLIS2 (WT, mPR) were then transferred to nitrocellulose membrane and incubated with recombinant CAS/BCAR1-GST. The binding CAS/BCAR1-GST was detected with anti-GST antibody. TL: total cell lysate; IP: immunoprecipitation; Ctrl: control samples prepared from untransfected MDA-MB-231 cells. Blots were cropped from original full-size images (see Supplemental Material).

moment upon Y12F mutation. The dipole was pinpointed as an important stabilizing contribution for the analogous Trp-Pro interaction²⁷.

DOK7 and GLIS2 are CAS interaction partners. To increase understanding of CAS signaling, we scanned the identified $(A/P)_{-1}P_0 \times K_2P_3 \times (L/R)_5Z_6$ CAS SH3 binding motif in the UNIPROT SWISSPROT human/mouse protein database using PATTINPROT and BLASTP programs and identified 10 potential new interacting partners of CAS (Supplementary Figure S6A). After using published data to conduct a thorough evaluation of 10 potential partners for their possible connection to signaling processes involving CAS/BCAR1²⁸ (Supplementary Figure S6B,C), we selected **DOK7**, which contains the high affinity $P_{509}PPKPLRP$ motif, and **GLIS2**, with an anchoring leucine at position +5 ($P_{333}PPKPPLP$), as the most promising candidates. To analyze the interactions of CAS SH3 with DOK7 and GLIS2, we performed a pull-down assay with GST-fused Tyr12

variants of the CAS SH3 domain. We confirmed that both DOK7 and GLIS2 interact with the CAS SH3 domain and that these interactions are blocked by substituting Tyr12 with a phosphomimicking glutamate (Fig. 8A,B). Co-immunoprecipitation experiments suggested that DOK7 and GLIS2 bind full-length CAS (Fig. 8C,D). In addition, we mutated the CAS SH3 binding motifs in DOK7 and GLIS2 to PAPVALR or PAPVAPLP, respectively, and performed co-immunoprecipitation for DOK7 and far-Western experiments for both DOK7 and GLIS2 (Fig. 8C,E,F). These experiments confirmed that the CAS-DOK7 and CAS-GLIS2 interactions are direct and require intact CAS SH3 binding motifs.

Discussion

We used a combination of experimental and computational methods to reveal the ligand preferences of the CAS SH3 domain. Using phage display, we described the CAS SH3 high affinity binding motif as $A/P_{-1}P_0 \times {}_1K_2P_3 \times {}_4L/R_5Z_6$. This motif, which requires an uncommonly localized lysine residue at position +2 and either leucine or arginine at position +5, is present in nearly all known CAS SH3 ligands (Fig. 3B). In addition, several proteins, including PTP1B¹⁵, CD2AP¹⁴, Ack1²⁹, Dynamin1³⁰, and Dock180³¹, are annotated to bind the CAS SH3 domain *via* a centrally located arginine (position +2) instead of lysine. Therefore, it seems that arginine at position +2 is also acceptable, although our phage display did not identify it, perhaps due to its less effective binding contribution than lysine.

To understand the molecular basis of the CAS SH3 domain ligand specificity and regulation of binding, we determined solution structures of the chimeric CAS SH3 domain fused *via* a flexible linker to PTP-PEST or Vinculin-derived binding peptides. Both interactions are functionally well-described and their core 8-amino-acid binding sequences differ in the anchoring residue at position +5, with arginine in PTP-PEST and leucine in Vinculin^{10,13}. Binding of PTP-PEST/Vinculin peptides to the CAS SH3 domain leads to repositioning of the RT loop (i.e., Asn14, Glu17, Glu21, and Asp20) towards the ligand (Fig. 4B,C). The NMR chemical shift perturbation data revealed differences in induced changes for Glu17 and Asp20 of PTP-PEST compared to Vinculin (Supplementary Figure S3) that can be explained by a less restricted movement of Glu17 and increased stability of Asp20 in the case of PTP-PEST. The contributions of Glu17 and to some extent Glu21 for PTP-PEST binding are more prominent than for Vinculin because they bind not only the central lysine but also an anchoring arginine (Figs 5 and 6). In summary, our data suggest that the presence of the centrally located lysine in CAS SH3 ligands and its binding to Glu17 and 21 undermines the anchoring role of arginine and consequently allows for its effective substitution by leucine.

High-affinity binding ligands featuring a central lysine are unique for CAS SH3. A centrally located lysine has also been observed in a Vinculin-derived peptide bound to the SH3 domain of CAP protein³²; however, it displayed a markedly lower (17-fold) binding affinity compared with Vinculin bound to the CAS SH3 domain.

Although lysine from Vinculin is in contact with Asp881 of CAP SH3, the distance and orientation of interacting residues is less favorable than in the case of lysine binding to Glu17 in CAS SH3. However, a detailed analysis of the ligand binding to CAS and CAP suggests that the presence of glutamate or aspartate at the position equivalent to Glu17 in CAS permits binding of a centrally located lysine in ligands. Our analysis of human SH3 domains showed that there are only 13 unique SH3 domains with glutamate or aspartate at the position corresponding to Glu17 out of the 506 sequences of human SH3_1 domains in the PFAM database (Supplementary Figure S5). None of them possesses the other CAS SH3 specific amino acids (Asn14, Arg59, Leu40) that are potentially critical for the CAS SH3 domain binding specificity. Asn14 locks Glu21 and Arg59 *via* intramolecular bidentate H-bonds into an optimal position for ligand binding and is likely responsible for the tolerance of Arg59 close to the centrally located lysine residue at +2, which forms salt bridges with Glu17 and Glu21 (Fig. 5, Supplementary Tables S4 and S7).

Identification of an extended binding surface on CAS SH3. In addition to amino acids that interact with the typical SH3 binding pockets, other residues contribute significantly to CAS SH3-Vinculin and CAS SH3-PTP-PEST binding. Negatively charged amino acids preceding the polyproline ligand core form salt bridges or H-bonds with Lys26 (Supplementary Tables S4 and S7). Interestingly, the N-terminal SDEs from the CAS SH3 domain interaction partners are often enriched with Glu or Asp residues (Supplementary Figure S4). In our structures, Lys26 forms salt bridges in more than 90% of converged structures with Glu857 at position -3 from Vinculin, while the incidence of H-bonds between Asp330 from PTP-PEST at the same position is lower (23% of structures) (Supplementary Tables S2-7). This is in an agreement with the MM-GBSA energy calculations that attributed a higher attractive energy contribution to Lys26 for CAS SH3-Vinculin binding than CAS SH3-PTP-PEST (Fig. 6B). In the PTP-PEST chimera, the C-terminal SDE also contributes to the binding (Fig. 6A, Supplementary Tables S2-4). In particular, Arg340 forms salt bridges and H-bonds with Gly39, Gln38, or Asp41 (Supplementary Table S4) that are analogous to interactions observed in the complex of Src-SH3 with the high affinity peptide APP12 (PDB code 4RTY, ref. 33). A C-terminal extension of the core APPLPPR motif by NRPR (class II ligand) leads to a 20-fold increase in affinity³³.

New model for Src-mediated phosphorylation of CAS. Previous work suggested that CAS SH3 domain signaling is regulated by phosphorylation of Tyr12²⁰. By manipulating the levels of Src kinase expression and its activity, we confirmed that phosphorylation of Tyr12 in cells is mediated by Src and that this phosphorylation correlates with a reduction of CAS-FAK and CAS-Vinculin binding (Fig. 7C,D). We found that FAK binding to CAS is significantly increased after Src inhibition, which can be explained by a modified combination of two mechanisms of Src-mediated phosphorylation of CAS³⁴: (i) an indirect Src/FAK cooperative mechanism in which

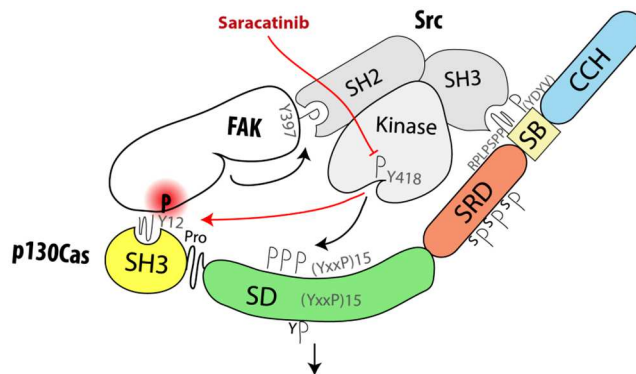


Figure 9. Model of Src-mediated regulation of CAS-FAK association. Upon activation, Src associates with both FAK and CAS through its SH2 and SH3 domains, respectively. This brings Src kinase domain into close contact with CAS SD, leading to its phosphorylation and activation of downstream signaling. With lower dynamics¹³, Src also phosphorylates Tyr12 (Y12) within CAS SH3 domain, which prevents its further binding to FAK and potentially leads to dissociation of the ternary CAS-FAK-Src complex. In contrast, when Src kinase is inhibited, the formation/stabilization of the ternary complex is enhanced.

CAS bound *via* its SH3 domain to FAK becomes phosphorylated by Src bound to FAK *via* its SH2 domain³⁵, and (ii) direct binding of Src mediated mainly by its SH3 domain to the CAS Src-binding domain³⁴. We propose that CAS, FAK, and Src can form a ternary complex mediated by: (i) CAS SH3 domain binding to FAK, (ii) Src SH2 domain binding to FAK, and (iii) Src SH3 domain binding to CAS (see model in Fig. 9). Formation of the ternary complex explains our observation that in Src-transformed MEFs, the CAS-FAK association, unlike the CAS-Vinculin interaction, is enhanced by Src kinase inhibition to levels over nine-fold higher than in untreated MEFs (see Fig. 7C). The inhibition of Src kinase prevents CAS-FAK dissociation induced by CAS Tyr12 phosphorylation, and at the same time the presence of Src stabilizes the CAS-FAK association by formation of the ternary complex. Therefore, Tyr12 phosphorylation in the CAS SH3 domain appears to be a key regulator of CAS signaling, determining the dynamics and sustainability of CAS-mediated signals. However, Src is likely not the only kinase responsible for Tyr12 CAS SH3 phosphorylation. Bmx kinase also has been shown to phosphorylate Tyr12 *in vitro*²⁰.

The role of CAS in DOK7 and GLIS2 signaling. We performed a proteome-wide search for CAS SH3 binding motifs and identified DOK7 and GLIS2 as novel putative CAS SH3 binding partners (Supplementary Figure S6A). The CAS-binding sequences of DOK7 and GLIS2 differ only at the anchoring amino acid at position +5 (leucine and arginine for DOK7 and GLIS2, respectively). Both DOK7 and GLIS2 were predicted to play a role together with CAS/BCAR1 within the same protein-protein interaction and functional network (Supplementary Figure S6B,C). While CAS is ubiquitous in all tissues, DOK7 is preferentially expressed in skeletal muscle and heart, and its binding to Crk is important for neuromuscular synapse formation³⁶. Crk binding to either DOK7 or CAS is phosphorylation dependent^{36,37}. DOK7 also has been implicated in the exercise-stimulated expansion of muscle fibers, which could be related to the mechanosensing function of CAS³⁸.

Analysis of the potential functional interactions between CAS/BCAR1 and GLIS2 showed that both are implicated in kidney function regulation and may regulate kidney cell planar polarity^{39,40}. GLIS2, also referred to as Nephrocystin 7, is a zinc finger transcription factor. Loss of GLIS2 function in humans and mice leads to development of nephronophthisis, a recessive cystic kidney disease⁴⁰ caused by a mutation in one of the nine nephrocystin genes. Interestingly, Nephrocystin 1 and 4 interact with CAS^{39,41}. In contrast to CAS, GLIS2 is mainly localized in the nucleus, but in cytosol it interacts with p120catenin and promotes p120catenin nuclear localization⁴². Similarly, CAS has previously been shown to bind nucleocytoplasmic zing finger protein CIZ¹².

Conclusions

We determined the consensus CAS SH3 binding motif and analyzed in detail structural aspects of the CAS SH3 domain binding. We revealed the requirement for an uncommon centrally localized lysine residue at position +2 of CAS SH3 binding peptides and two optional anchoring residues with different properties (leucine or arginine) at position +5. We further expanded the knowledge of CAS SH3 ligand binding regulation by Src-mediated phosphorylation of Tyr12 and confirmed its negative role in ligand binding. Finally, we identified two novel CAS SH3 binding partners, DOK7 and GLIS2.

Materials and Methods

Protein expression and purification. The CAS SH3 domain variants were expressed as fusion proteins with glutathione S-transferase from a pGEX-2TK expression system in *Escherichia coli* BL21 (DE3). Bacteria were grown in LB medium with 100 mg/ml ampicillin, and protein expression was induced with 0.4–1 mM isopropyl-b-thiogalactopyranoside (IPTG) at 25 °C overnight or 37 °C for 1.5 h. Uniformly¹⁵N and/or¹³C-labeled GST-fused CAS SH3 domain was grown in minimal medium supplemented with 1 g/l (¹⁵NH₄)₂SO₄ and/or 4 g/l ¹³C glucose (Cambridge Isotope Laboratories). Bacterial pellets were suspended in PBS, pH 7.4, containing 0.05% 2-mercaptoethanol and supplemented with bacterial inhibitors MixB (SERVA) and lysed with a French pressure

cell press. Proteins were then solubilized by addition of 20% TritonX-100 to a final concentration of 1% and incubated at -20°C overnight. GST-SH3 fusion protein was purified using Pierce Glutathione Agarose (Thermo Scientific). Bound GST-SH3 was eluted with 10 mM glutathione in 50 mM Tris, pH 8.0, for ELISA experiments. The GST-fused SH3 domain concentration was determined by absorbance at 280 nm using an extinction coefficient of $58,500\text{ M}^{-1}\text{ cm}^{-1}$. Extinction coefficients were calculated using the Protparam tool (Expasy). For NMR measurements, the GST tag was removed by thrombin (Sigma) cleavage and subsequent size exclusion chromatography (Sephadex-75, Amersham Biosciences). Two additional amino acid residues remained present at the N-terminus of CAS SH3 after thrombin cleavage. PBS was subsequently exchanged for NMR buffer (25 mM sodium phosphate, pH 7.5, 100 mM NaCl, 1 mM TCEP, 0.01% NaN_3) with an Amicon Ultra-15 Centrifugal Filter Unit (3 K, EMD Millipore). The purity of the proteins was confirmed by SDS-PAGE.

Library screening (Phage display). Panning of a phage display library comprising 10^{12} M13 phages (Ph.D.TM -12 Phage Display Peptide Library Kit, New England Biolabs) carrying 12-amino-acid degenerate oligopeptides was performed according to the manufacturer's protocol. Briefly, approximately 0.5 mg purified GST-fused CAS SH3 domain (isolated from 40 ml bacterial culture) bound to Pierce Glutathione Agarose (Thermo Scientific) was incubated with blocking buffer (100 mM NaHCO_3 , pH 8.6, 5 mg/ml BSA) and then with 10^{11} infectious particles from the phage display library. After washing 10 times with TBS containing 0.1–0.5% Tween 20, the bound phages were eluted with 200 mM glycine HCl, pH 2.2. After four selection cycles, the 20 bound clones were isolated and sequenced.

Enzyme-linked immunosorbent assay (ELISA). The relative binding affinities of individual phage clones to GST-CAS SH3 were assessed by ELISA according to the manufacturer's protocol (Ph.D.TM -12 Phage Display Peptide Library Kit, New England Biolabs). Briefly, a dilution series of phage stocks was prepared in TBS with 0.5% Tween 20 (TBST, 10^{15} – 2×10^6 pfu/ml), and phages were scored for their ability to bind immobilized GST-CAS SH3 domain (100 μl of 50 $\mu\text{g}/\text{ml}$ per well) in 96-well plate. Bound phages were detected with anti-M13 antibody conjugated to HRP and quantified in a colorimetric assay (ABTS at 415 nm, Invitrogen) using Varioskan Flash (Thermo Scientific). Relative binding affinities (the affinity of the phage clone with the highest affinity was arbitrarily set to 1) were evaluated based on the number of phages required to bind the immobilized GST-fused CAS SH3 domain at 50% saturation. Curves were fitted with the standard sigmoidal function in Sigmaplot. The clones with highest affinities were selected for further analyses (e.g., binding to immobilized 5 μg of CAS SH3 variants per well).

The EC_{50} for phage clone 1 (FHAPPSKPPLPK, highest affinity) was determined using competitive displacement of the phage bound ($5.5 \cdot 10^{10}$ pfu) to immobilized GST-fused CAS SH3 domain (100 μl of 20 $\mu\text{g}/\text{ml}$ per well to yield the best specificity/sensitivity ratio) by serial additions of free GST-fused CAS SH3 domain in TBST (1 $\mu\text{g}/\text{ml}$ –800 $\mu\text{g}/\text{ml}$) as previously described⁴³. The amount of bound phages was assessed with anti-M13 antibody conjugated to HRP and quantified in a colorimetric assay. Displacement curves were fitted to standard sigmoidal function and EC_{50} was calculated in Sigmaplot version 11 software using a four-parameter logistic equation. Statistical significance (* $p < 0.05$, ** $p < 0.01$, *** $p < 0.001$) was determined on log-transformed data by one-way ANOVA followed by Tukey's post-hoc test.

Isothermal titration calorimetry (ITC). ITC experiments were performed using a MicroCal Auto-iTC200 System (GE Healthcare) at 25°C . The samples were prepared in PBS, pH 7.5, supplemented with 0.05% 2-mercaptoethanol. Protein and peptide concentrations were determined by amino acid analysis. Four synthetic peptides (PPPKPRL, APPKPPLP, PPSKPPLP, and PPSKPPRP) were used for titration experiments, and their concentrations in PBS were adjusted to 660 μM . For peptide–CAS SH3 complex formation, 2 μl aliquots of 660 μM peptide solution were injected stepwise into a sample cell containing 200 μl of 60 μM CAS SH3. Each assay was accompanied by a control experiment in which the binding buffer was titrated with the injected peptide alone. The dilution heat values obtained for the control titration were then subtracted from those obtained for the complex formation. All experiments were performed at least in triplicate. The association constants and stoichiometry (N) were estimated using MicroCal Origin software (GE Healthcare). Known variances of each measurement were utilized to calculate the weighted average of the dissociation constant (K_d) and stoichiometry as a maximum likelihood estimator. The standard deviation was determined from at least three independent experiments.

NMR spectroscopy and structure determination. NMR spectra were acquired at 25°C on 600 MHz and 850 MHz Bruker Avance spectrometers, both of which were equipped with a triple-resonance ($^{15}\text{N}/^{13}\text{C}/^1\text{H}$) cryoprobe. The sample volume was 0.35 ml, with a 450 μM concentration of CAS SH3 and CAS SH3 chimeras (sequences in Supplementary Figure S7) in NMR buffer (25 mM sodium phosphate, pH 7.5, 100 mM NaCl, 1 mM TCEP, 0.01% NaN_3), 5% $\text{D}_2\text{O}/95\%$ H_2O . A series of double- and triple-resonance spectra^{44,45} were recorded to determine essentially complete sequence-specific resonance backbone and side-chain assignments. Constraints for ^1H – ^1H distance required to calculate the structure of the CAS SH3 domain and CAS SH3 chimeras were derived from 3D $^{15}\text{N}/^1\text{H}$ NOESY-HSQC and $^{13}\text{C}/^1\text{H}$ NOESY-HMQC, which were acquired using a NOE mixing time of 100 ms.

The families of converged structures for the CAS SH3 domain and CAS SH3 chimeras were initially calculated using Cyana 2.1⁴⁶. The combined automated NOE assignment and structure determination protocol was used to automatically assign the NOE cross-peaks identified in NOESY spectra and to produce preliminary structures. In addition, backbone torsion angle constraints, generated from assigned chemical shifts using the TALOS+ program⁴⁷ were included in the calculations. Subsequently, five cycles of simulated annealing combined with redundant dihedral angle constraints were used to produce sets of converged structures with no significant restraint violations (distance and van der Waals violations $< 0.2 \text{ \AA}$ and dihedral angle constraint violation $< 5^{\circ}$), which were further refined in explicit solvent using the YASARA software with the YASARA forcefield⁴⁸. The structures with the lowest total energy were selected. Analysis of the family of structures obtained was carried out using the

Protein Structure Validation Software suite (www.nesg.org) and Molmol⁴⁹. The statistics for the resulting structures are summarized in Supplementary Table S1. Chemical shift perturbations divided by standard deviation (relative CSP) were plotted against amino acid sequence to highlight the differences between PTP-PEST and Vinculin complexes (Supplementary Figure S3).

Analyses of NMR structures. *Interface analysis.* Hydrogen bonds and nonpolar contacts between Cas SH3 and its ligands were assessed with PISA²⁶ with default settings. Prior to analysis, the linker sequence (residues 75–83) were removed from the chimeric proteins. All structure figures were generated using PyMOL (Schrödinger, LLC).

Interaction energies – Molecular mechanics. Energy contributions of CAS SH3 and PTP-PEST/Vinculin residues toward binding were calculated using the MM-GBSA method⁵⁰ in AMBER14⁵¹ on 40 fragmented NMR structures for each ligand. AMBER ff14SB force field⁵² was used for the protein and ligands. The generalized Born model of Tsui and Case (igb = 1) was used for the polar solvation energies⁵³, and a solvent-accessible surface-area-dependent term with SURFTEN = 0.0072 and SURFOFF = 0.0 parameters was employed for nonelectrostatic solvation free energies^{53,54}. Debye-Hückel screening with 150 mM ionic strength was used. The interaction energies were decomposed on a per-residue basis so that 1–4 interactions were added to electrostatic and van der Waals contributions.

Interaction energies – Quantum mechanics. Tyr12-mutated variants of CAS SH3 in complex with PTP-PEST and Vinculin were derived from the first NMR models with the linker removed. The side chains were modeled with the LEaP module of AMBER14⁵¹, and the entire complexes were optimized using PM6-D3H4, a semiempirical quantum mechanical (SQM) method corrected for dispersion and hydrogen bonding⁵⁵, and the COSMO implicit solvent model with $\epsilon_r = 78.4$ to mimic the solvent⁵⁶. The MOPAC2016 program with the MOZYME linear scaling algorithm was employed⁵⁷. The interaction energy was calculated on the optimized structures as the difference between the energy of the complex and the sum of the energies of the constituents. The calculations were performed within the Cuby4 framework⁵⁸.

Molecular dynamics. The first fragmented NMR model for each PTP-PEST and Vinculin was turned into a Tyr12-phosphorylated variant by automatic building in the LEaP module of AMBER14⁵¹ using published phosphotyrosine parameters⁵⁹. The system was prepared and run according to a published protocol⁶⁰ with the following changes: the numbers of Cl⁻/Na⁺ counterions added to neutralize the system and match the physiological concentration of 0.15 M were 15/15 and 13/18, respectively, and the production run was 50 ns.

Motif definition and sequence alignment. The precomputed sequence alignment of all human SH3_1 domains from the PFAM database⁶¹ was filtered for obsolete entries and manually edited to identify conserved positions relevant to ligand binding. Sequences from phage display or from known high-affinity CAS SH3 domain binding ligands were aligned using CLUSTAL 2.1 multiple sequence alignment⁶². The alignments were further analyzed to describe sequence motifs using WebLogo version 3.0⁶³.

Plasmid construction. pEGFP-C1 CAS and pGEX-CAS-SH3 domain constructs were prepared previously²⁰. The chimeric CAS SH3 domains with the binding peptide were prepared by fusion of mouse CAS SH3 domain with a flexible spacer sequence (SGGSGSG) and binding peptides derived from PTP-PEST (327–343 of mouse PTP-PEST, UniProtKB accession number P35831) or Vinculin (854–870 of mouse Vinculin, UniProtKB accession number Q64727). cDNA coding for the flexible peptides with the binding peptides was commercially synthesized (geneArt, Life technologies) and inserted in frame at the 3' end of the CAS SH3 domain using *Bam*HI/*Eco*RI sites. The constructs were verified by sequencing. DOK7 cDNA was PCR-amplified from cDNA isolated from MCF7 human breast carcinoma cells using a forward primer (5'-TACTCGAGATGGACTACAAAGACGATGACGACAAGAAGATGACCGAGGCGCG-3') that includes a sequence coding for Flag epitope and a reverse primer (5'-TAGAATTCTCAGTCTCAAGGAGGGGGTTTACC-3'). In parallel, GLIS2 cDNA was prepared from the BLM melanoma cell line and amplified by PCR using the following primers: forward 5'-TACTCGAGATGGACTACAAAGACGATGACGACAAGCACTCCCTGGACGAGCCG-3', reverse 5'-TAGAATTCTCAGTTCACCACAGCCGGT-3'. The PCR-amplified DOK7 and GLIS2 cDNA were cleaved with *Xho*I/*Eco*RI and inserted into *Xho*I/*Eco*RI-cleaved pIRES2-EGFP (Addgene), resulting in plasmids pIRES2-FLAG-DOK7 and pIRES2-FLAG-GLIS2. Constructs were verified by sequencing.

Site-directed mutagenesis of DOK7 and GLIS2 was performed by whole plasmid synthesis using Q5 polymerase (New England Biolabs) with respective primers (DOK7 mPR: forward 5'-TGGTGGGTGCCTCAAGGCCAGCACCGGTAGCGCTGCGTCCGCGG-3', reverse 5'-CCGCGGACGCAGCGCTACCGGTGCTGGCCTTGAGGCACCCACCA-3'; GLIS2 mPR: forward 5'-CTCCTGCAGCTGCGCCAGCACCGGTAGCGCCACTGCCCGCC-3', reverse 5'-GGCGGGCAGTGGCGCTACCGGTGCTGGGCGCAGCTGCAGGAG-3'). pIRES2-FLAG-DOK7 and pIRES2-FLAG-GLIS2 were used as templates. After PCR, 5U of *Dpn*I were added to each reaction and incubated for 1.5 h at 37 °C. Individual mutated clones were selected for the presence of a newly introduced *Age*I site, and final constructs were verified by sequencing.

Cell transfection and culture. MDA-MB-231 cells (provided by RNDr. Zadinova from Charles University) were cultivated in full DMEM (Sigma) with 4.5 g/l glucose, L-glutamine, and pyruvate, supplemented with 10% fetal bovine serum (Sigma). The cells were transfected with pIRES2-FLAG-DOK7 WT/mPR, pIRES2-FLAG-GLIS2 WT/mPR, or pEGFP-C1 CAS constructs using a PEI transfection reagent (Polysciences) according to the manufacturer's protocol.

Far-Western-blot analysis, immunoprecipitation, and GST pull-downs. MDA-MB-231 cells transiently transfected with pIRES2-FLAG-DOK7 or pIRES2-FLAG-GLIS2 were lysed in a Triton lysis buffer (50 mM Tris HCl, pH 7.4, with 150 mM NaCl and 1% TRITON X-100). Protein concentrations in lysates were determined using the DC Protein Assay (Bio Rad). Lysates containing 750 µg proteins were incubated overnight (4 °C) with 35 µl of an anti-FLAG M2 affinity gel (Sigma) and washed 3 times with 1 ml ice-cold TBS buffer. Complexes were eluted using 0.1 M glycine, pH 3.5. The eluted proteins were immediately re-equilibrated to neutral pH with 1 M Tris, pH 9.2, and mixed with 6x Laemmli sample buffer and processed for SDS-PAGE. After SDS-PAGE, proteins were transferred onto a nitrocellulose membrane. The membranes were usually cut after the transfer to enable probing for up to 3 proteins of different molecular mass (e.g. 1–2 proteins of interest and a loading control). Nonspecific activity was blocked by incubating the membranes for 90 min at room temperature in TBS containing 4% bovine serum albumin. Membranes were then incubated overnight at 4 °C with a primary antibody, washed extensively with TBS with 0.05% Tween 20 (TBST), incubated for 1 h at room temperature with HRP-conjugated secondary antibody, washed extensively in TBST, and developed using an AI600 System (GE Healthcare). For far-Western-blot analysis, the protein blots were incubated with 2 µg/ml recombinant protein probe (recombinant human BCAR1, Abcam) in 1% BSA in TBST overnight followed by washing with TBST and incubation (2 h, 4 °C) with anti-GST antibody (Sigma). After extensive washing with TBST, blots were treated with HRP-conjugated secondary antibodies and developed using the AI600 System.

The GST-CAS SH3 domain and mutational variants were expressed in bacteria and affinity purified as described above (see “Protein expression and purification” section). Cell lysates from MDA-MB-231 cells transiently transfected with pIRES2-FLAG-DOK7 or pIRES2-FLAG-GLIS2 were incubated with 20 µg of GST or GST-CAS SH3 variants immobilized on Glutathione Agarose (Thermo Scientific) for 2 h at 4 °C. The agarose beads were washed extensively with LB1 buffer (50 mM HEPES, pH 7.4, 150 mM NaCl), boiled in 6x SDS-PAGE sample buffer, and processed for immunoblotting. The nitrocellulose membrane was stained with Ponceau S (for SH3 domain loading); destained and pulled-down DOK7 was detected with anti-Flag antibody.

Immunoprecipitations from lysates of MEFs or MEFs transfected with SrcF were performed similarly as described above. To immunoprecipitate CAS proteins, protein-A sepharose (GE-Healthcare) and anti-CAS antibody (BD Transduction Laboratories) were used. To inhibit Src kinase, cells were treated with 5 µM Saracatinib for 3 h. After transferring proteins onto nitrocellulose membrane and blocking, the membranes were incubated with anti CAS, Src, FAK, Vinculin, CAS Tyr12, CAS pTyr165, Src pTyr418 or actin antibody.

Antibodies. Anti-M13 fused to HRP (phage display library kit, New England Biolabs), anti-CAS (BD Transduction Laboratories, mouse monoclonal clone 21), anti-GST (G7781, Sigma, rabbit polyclonal), anti-FLAG (Sigma, mouse monoclonal clone M2), anti-FAK (C-20, Santa Cruz Biotechnology, rabbit), anti-v-Src (Ab-1, Calbiochem, mouse monoclonal clone 327), anti-Vinculin (Sigma, mouse monoclonal clone V284), anti-CAS pY165 (#4015, Cell Signaling Technology, rabbit polyclonal), anti-Src pY418 (#2101, Cell Signaling Technology, rabbit polyclonal), anti-Actin (C-11, Santa Cruz, goat polyclonal), and secondary antibody/ies fused to HRP (Abcam) were used as purchased. Anti-CAS Y12 antibody was prepared as previously described²⁰.

References

- Defilippi, P., Di Stefano, P. & Cabodi, S. p130Cas: a versatile scaffold in signaling networks. *Trends Cell Biol* **16**, 257–263 (2006).
- Fonseca, P. M. *et al.* Regulation and localization of CAS substrate domain tyrosine phosphorylation. *Cell Signal* **16**, 621–629 (2004).
- Brábek, J. *et al.* CAS promotes invasiveness of Src-transformed cells. *Oncogene* **23**, 7406–7415 (2004).
- Brábek, J. *et al.* Crk-associated substrate tyrosine phosphorylation sites are critical for invasion and metastasis of Src-transformed cells. *Mol. Cancer Res.* **3**, 307–315 (2005).
- Dorssers, L. C. *et al.* The prognostic value of BCAR1 in patients with primary breast cancer. *Clin Cancer Res* **10**, 6194–6202 (2004).
- Schlaepfer, D. D., Broome, M. A. & Hunter, T. Fibronectin-stimulated signaling from a focal adhesion kinase-c-Src complex: involvement of the Grb2, p130cas, and Nck adaptor proteins. *Mol Cell Biol* **17**, 1702–1713 (1997).
- Sakai, R. *et al.* A novel signaling molecule, p130, forms stable complexes *in vivo* with v-Crk and v-Src in a tyrosine phosphorylation-dependent manner. *EMBO J* **13**, 3748–3756 (1994).
- Polte, T. R., Hanks, S. K. & Polte Hanks, S. K. T. R. Interaction between focal adhesion kinase and Crk-associated tyrosine kinase substrate p130Cas. *Proc Natl Acad Sci USA* **92**, 10678–10682 (1995).
- Li, X. & Earp, H. S. Paxillin is tyrosine-phosphorylated by and preferentially associates with the calcium-dependent tyrosine kinase in rat liver epithelial cells. *J Biol Chem* **272**, 14341–14348 (1997).
- Garton, A. J., Burnham, M. R., Bouton, A. H. & Tonks, N. K. Association of PTP-PEST with the SH3 domain of p130(cas); A novel mechanism of protein tyrosine phosphatase substrate recognition. *Oncogene* **15**, 877–885 (1997).
- Kirsch, K. H., Georgescu, M. M. & Hanafusa, H. Direct binding of p130(Cas) to the guanine nucleotide exchange factor C3G. *J. Biol. Chem.* **273**, 25673–25679 (1998).
- Nakamoto, T. *et al.* CIZ, a zinc finger protein that interacts with p130(cas) and activates the expression of matrix metalloproteinases. *Mol Cell Biol* **20**, 1649–1658 (2000).
- Janoštiak, R. *et al.* CAS directly interacts with vinculin to control mechanosensing and focal adhesion dynamics. *Cell. Mol. Life Sci.* **71**, 727–44 (2014).
- Kirsch, K. H., Georgescu, M. M., Ishimaru, S. & Hanafusa, H. CMS: an adapter molecule involved in cytoskeletal rearrangements. *Proc Natl Acad Sci USA* **96**, 6211–6216 (1999).
- Liu, F., Hill, D. E. & Chernoff, J. Direct binding of the proline-rich region of protein tyrosine phosphatase 1B to the Src homology 3 domain of p130(Cas). *J Biol Chem* **271**, 31290–31295 (1996).
- Tazaki, T. *et al.* Functional analysis of Src homology 3-encoding exon (exon 2) of p130Cas in primary fibroblasts derived from exon 2-specific knockout mice. *Genes Cells* **13**, 145–157 (2008).
- Sawada, Y. *et al.* Force sensing by mechanical extension of the Src family kinase substrate p130Cas. *Cell* **127**, 1015–1026 (2006).
- Janoštiak, R., Pataki, A. C., Brábek, J. & Rösel, D. Mechanosensors in integrin signaling: The emerging role of p130Cas. *European Journal of Cell Biology* **93**, 445–454 (2014).
- Braniš, J. *et al.* The role of focal adhesion anchoring domains of CAS in mechanotransduction. *Sci. Rep.* **7**, 46233 (2017).
- Janoštiak, R. *et al.* Tyrosine Phosphorylation within the SH3 domain Regulates CAS Subcellular Localization, Cell Migration, and Invasiveness. *Mol Biol Cell.* **22**, 4256–67 (2011).

21. Tatárová, Z., Brábek, J., Rösel, D. & Novotný, M. SH3 domain tyrosine phosphorylation-sites, role and evolution. *PLoS One* **7**, e36310 (2012).
22. Saksela, K. & Permi, P. SH3 domain ligand binding: What's the consensus and where's the specificity? *FEBS Lett.* **586**, 2609–14 (2012).
23. Musacchio, A. How SH3 domains recognize proline. *Adv. Protein Chem.* **61**, 211–68 (2002).
24. Mayer, B. J. SH3 domains: complexity in moderation. *J Cell Sci* **114**, 1253–1263 (2001).
25. Wisniewska, M. *et al.* The 1.1 angstrom resolution crystal structure of the p130cas SH3 domain and ramifications for ligand selectivity. *J. Mol. Biol.* **347**, 1005–1014 (2005).
26. Krissinel, E. & Henrick, K. Inference of Macromolecular Assemblies from Crystalline State. *J. Mol. Biol.* **372**, 774–797 (2007).
27. Biedermannova, L., Riley, E., Berka, K., Hobza, K. P. & Vondrasek, J. Another role of proline: stabilization interactions in proteins and protein complexes concerning proline and tryptophane. *Phys. Chem. Chem. Phys.* **10**, 6350 (2008).
28. Szklarczyk, D. *et al.* STRING v10: protein-protein interaction networks, integrated over the tree of life. *Nucleic Acids Res.* **43**, D447–52 (2015).
29. Modzelewska, K., Newman, L. P., Desai, R. & Keely, P. J. Ack1 mediates Cdc42-dependent cell migration and signaling to p130Cas. *J Biol Chem* **281**, 37527–37535 (2006).
30. Kang, Y. S. *et al.* P130Cas attenuates epidermal growth factor (EGF) receptor internalization by modulating EGF-triggered dynamin phosphorylation. *PLoS One* **6**, e20125 (2011).
31. Hsia, D. A. *et al.* Differential regulation of cell motility and invasion by FAK. *J Cell Biol* **160**, 753–767 (2003).
32. Zhao, D. *et al.* Structural investigation of the interaction between the tandem SH3 domains of c-Cbl-associated protein and vinculin. *J. Struct. Biol.* **187**, 194–205 (2014).
33. Feng, S. B., Kasahara, C., Rickles, R. J. & Schreiber, S. L. Specific interactions outside the proline-rich core of two classes of Src homology 3 ligands. *Proc. Natl. Acad. Sci. USA* **92**, 12408–12415 (1995).
34. Pellicena, P. & Miller, W. T. Processive phosphorylation of p130Cas by Src depends on SH3-polyproline interactions. *J. Biol. Chem.* **276**, 28190–28196 (2001).
35. Ruest, P. J., Shin, N. Y., Polte, T. R., Zhang, X. & Hanks, S. K. Mechanisms of CAS substrate domain tyrosine phosphorylation by FAK and Src. *Mol Cell Biol* **21**, 7641–7652 (2001).
36. Hallock, P. T. *et al.* Dok-7 regulates neuromuscular synapse formation by recruiting Crk and Crk-L. *Genes Dev* **24**, 2451–2461 (2010).
37. Vuori, K., Hirai, H., Aizawa, S. & Ruoslahti, E. Introduction of p130cas signaling complex formation upon integrin-mediated cell adhesion: a role for Src family kinases. *Mol Cell Biol* **16**, 2606–2613 (1996).
38. Haramizu, S. *et al.* Habitual exercise plus dietary supplementation with milk fat globule membrane improves muscle function deficits via neuromuscular development in senescence-accelerated mice. *Springerplus* **3**, 339 (2014).
39. Donaldson, J. C. *et al.* Crk-associated substrate p130(Cas) interacts with nephrocystin both proteins localize to cell-cell contacts of polarized epithelial cells. *Exp. Cell Res.* **256**, 168–178 (2000).
40. Attanasio, M. *et al.* Loss of GLIS2 causes nephronophthisis in humans and mice by increased apoptosis and fibrosis. *Nat Genet* **39**, 1018–1024 (2007).
41. Mollet, G. *et al.* Characterization of the nephrocystin/nephrocystin-4 complex and subcellular localization of nephrocystin-4 to primary cilia and centrosomes. *Hum. Mol. Genet.* **14**, 645–656 (2005).
42. Hosking, C. R. *et al.* The transcriptional repressor Glis2 is a novel binding partner for p120 catenin. *Mol Biol Cell* **18**, 1918–1927 (2007).
43. Clackson, T. & Lowman, H. B. *Phage Display: A Practical Approach* (Oxford University Press, 2004).
44. Renshaw, P. S. *et al.* Letter to the Editor: Sequence-specific assignment and secondary structure determination of the 195-residue complex formed by the Mycobacterium tuberculosis proteins CFP-10 and ESAT-6. *J. Biomol. NMR* **30**, (225–226 (2004).
45. Veverka, V. *et al.* NMR assignment of the mTOR domain responsible for rapamycin binding. *J. Biomol. NMR* **36**(Suppl 1), 3 (2006).
46. Herrmann, T., Güntert, P. & Wüthrich, K. Protein NMR structure determination with automated NOE assignment using the new software CANDID and the torsion angle dynamics algorithm DYANA. *J. Mol. Biol.* **319**, 209–27 (2002).
47. Shen, Y., Delaglio, F., Cornilescu, G. & Bax, A. TALOS+: a hybrid method for predicting protein backbone torsion angles from NMR chemical shifts. *J. Biomol. NMR* **44**, 213–23 (2009).
48. Harjes, E. *et al.* GTP-Ras disrupts the intramolecular complex of C1 and RA domains of Nore1. *Structure* **14**, 881–8 (2006).
49. Koradi, R., Billeter, M. & Wüthrich, K. MOLMOL: a program for display and analysis of macromolecular structures. *J. Mol. Graph.* **14**(51–5), 29–32 (1996).
50. Kollman, P. A. *et al.* Calculating structures and free energies of complex molecules: combining molecular mechanics and continuum models. *Acc. Chem. Res.* **33**, 889–97 (2000).
51. Case, D. A. *et al.* AMBER14. University of California, San Francisco. <http://www.ambermd.org> (2014).
52. Hornak, V. *et al.* Comparison of multiple Amber force fields and development of improved protein backbone parameters. *Proteins Struct. Funct. Bioinforma.* **65**, 712–725 (2006).
53. Tsui, V. & Case, D. A. Calculations of the Absolute Free Energies of Binding between RNA and Metal Ions Using Molecular Dynamics Simulations and Continuum Electrostatics. *J Phys Chem B* **105**, 11314–11325 (2001).
54. Still, W. C., Tempczyk, A., Hawley, R. C. & Hendrickson, T. Semianalytical treatment of solvation for molecular mechanics and dynamics. *J. Am. Chem. Soc.* **112**, 6127–6129 (1990).
55. Řezáč, J. & Hobza, P. Advanced Corrections of Hydrogen Bonding and Dispersion for Semiempirical Quantum Mechanical Methods. *J. Chem. Theory Comput.* **8**, 141–151 (2012).
56. Klamt, A. & Schüürmann, G. COSMO: a new approach to dielectric screening in solvents with explicit expressions for the screening energy and its gradient. *J. Chem. Soc., Perkin Trans. 2*, 799–805 (1993).
57. Stewart, J. MOPAC2009. *Stewart Computational Chemistry, Colorado Springs*. <http://www.openmopac.net> (2009).
58. Řezáč, J. Cuby: An integrative framework for computational chemistry. *J. Comput. Chem.* **37**, 1230–1237 (2016).
59. Homeyer, N., Horn, A. H. C., Lanig, H. & Sticht, H. AMBER force-field parameters for phosphorylated amino acids in different protonation states: phosphoserine, phosphothreonine, phosphotyrosine, and phosphohistidine. *J. Mol. Model.* **12**, 281–9 (2006).
60. Zakova, L. *et al.* Structural Integrity of the B24 Site in Human Insulin Is Important for Hormone Functionality. *J. Biol. Chem.* **288**, 10230–10240 (2013).
61. Finn, R. D. *et al.* The Pfam protein families database: towards a more sustainable future. *Nucleic Acids Res.* **44**, D279–D285 (2016).
62. Larkin, M. A. *et al.* Clustal W and Clustal X version 2.0. *Bioinformatics* **23**, 2947–2948 (2007).
63. Crooks, G. E., Hon, G., Chandonia, J.-M. & Brenner, S. E. WebLogo: A Sequence Logo Generator. *Genome Res.* **14**, 1188–1190 (2004).
64. Harte, M. T., Hildebrand, J. D., Burnham, M. R., Bouton, A. H. & Parsons, J. T. p130Cas, a substrate associated with v-Src and v-Crk, localizes to focal adhesions and binds to focal adhesion kinase. *J Biol Chem* **271**, 13649–13655 (1996).
65. Ohba, T., Ishino, M., Aoto, H. & Sasaki, T. Interaction of two proline-rich sequences of cell adhesion kinase beta with SH3 domains of p130(Cas)-related proteins and a GTPase-activating protein. *Graf. Biochem. J.* **330**, 1249–1254 (1998).
66. Suzuki, T. *et al.* MICAL, a novel CasL interacting molecule, associates with vimentin. *J Biol Chem* **277**, 14933–14941 (2002).

Acknowledgements

We thank Marie Charvatova for technical help. This work was funded by the Grant Agency of the Czech Republic (15-07321 S, 15-17419 S, and P208/12/G016), Charles University Grant Agency (1510-243-250404) and the

Ministry of Education of the Czech Republic (LQ1604, LO1304, IT4Innovations National Supercomputing Center – LM2015070 and BIOCEV CZ.1.05/1.1.00/02.0109). Institutional support was provided by project RVO 61388963 of the Academy of Sciences of the Czech Republic.

Author Contributions

J.G., R.H., M.L., P.T., and M.D. performed the experiments and analyzed the results. M.N., V.V., and D.R. analyzed the results. J.G., J.B., V.V., and D.R. conceived the experiments and wrote the manuscript. All authors reviewed the manuscript.

Additional Information

Supplementary information accompanies this paper at doi:[10.1038/s41598-017-08303-4](https://doi.org/10.1038/s41598-017-08303-4)

Competing Interests: The authors declare that they have no competing interests.

Publisher's note: Springer Nature remains neutral with regard to jurisdictional claims in published maps and institutional affiliations.



Open Access This article is licensed under a Creative Commons Attribution 4.0 International License, which permits use, sharing, adaptation, distribution and reproduction in any medium or format, as long as you give appropriate credit to the original author(s) and the source, provide a link to the Creative Commons license, and indicate if changes were made. The images or other third party material in this article are included in the article's Creative Commons license, unless indicated otherwise in a credit line to the material. If material is not included in the article's Creative Commons license and your intended use is not permitted by statutory regulation or exceeds the permitted use, you will need to obtain permission directly from the copyright holder. To view a copy of this license, visit <http://creativecommons.org/licenses/by/4.0/>.

© The Author(s) 2017

5.3. The 3rd publication/preprint

Koudelkova, L., Pataki, C., Tolde, O., Pavlik, V., Nobis, M., **Gemperle, J.**, Anderson, K., Brábek, J., Rosel, D.

Novel FRET-Based Src Biosensor Reveals Mechanisms of Src Activation and Its Dynamics in Focal Adhesions.

SSRN. <https://ssrn.com/abstract=3206266> (Preprint posted July 2, **2018**).

Under revision at Cell Chemical Biology journal.

Novel FRET-based Src biosensor reveals mechanisms of Src activation and its dynamics in focal adhesions

Lenka Koudelkova¹⁺, Andreea Csilla Pataki¹⁺, Ondřej Tolde¹, Vojtech Pavlik^{1,2}, Max Nobis³, Jakub Gemperle¹, Kurt Anderson^{3,4}, Jan Brábek¹, Daniel Rosel^{1*}

¹ Charles University, Faculty of Science - BIOCEV, Department of Cell Biology, Vestec 252 50, Czech Republic

² Current address: Contipro, Dolní Dobrouč 561 02, Czech Republic

³ Cancer Research UK, Beatson Institute, Glasgow G611BD, Scotland

⁴ Current address: The Francis Crick Institute, London NW11AT, UK

⁺ Contributed equally to this work

^{*}Correspondence: rosel@natur.cuni.cz

SUMMARY

Src kinase plays an important role in a multitude of fundamental cellular processes, and is often found deregulated in tumors. Active Src adopts an open conformation whereas inactive Src is characterized by very compact structure stabilized by inhibitory intramolecular interactions. Taking advantage of this spatial regulation, we constructed a FRET-based Src biosensor and analyzed conformational changes of Src following Src activation and the spatio-temporal dynamics of Src activity in cells. We found that activatory mutations either in regulatory or kinase domains induce opening of Src structure. Surprisingly we discovered that Src inhibitors differ in their effect on the Src structure, some counterintuitively inducing opened conformation. Finally, we analyzed the dynamics of Src activity in focal adhesions by FRET imaging and found that Src is rapidly activated during focal adhesions assembly, its activity remains steady and high throughout the focal adhesions life cycle and decreases during focal adhesions disassembly.

KEYWORDS

Src, biosensor, FRET, structure, inhibitors, focal adhesions

INTRODUCTION

The product of the *c-src* proto-oncogene, Src kinase, is the founding member of the Src family nonreceptor tyrosine kinases. Src plays crucial roles in migration, mechanosensing, mitogenic and anti-apoptotic signaling, thus precise control of Src activation is necessary to avoid tumor transformation (Yeatman, 2004; Frame et al., 2002; Yeatman, 2004; Frame et al., 2002; Playford and Schaller, 2004). Despite the mechanisms of negative control, enhanced expression and/or activation of Src is commonly observed in various tumors (e.g. colon carcinomas, breast carcinomas, pancreatic carcinomas) (Irby and Yeatman, 2000; Giaccone and Zucali, 2008). Under the circumstances of elevated or aberrant Src kinase activity, numerous Src substrates become phosphorylated. These Src phosphorylated substrates have been implicated in induction of tumorigenesis and development of malignant cell phenotype (Yeatman, 2004; Frame et al., 2002; Yeatman, 2004; Frame et al., 2002; Playford and Schaller, 2004). Even though the vast number of Src kinase substrates have been already identified, the exact mechanism of Src-mediated transformation has not been decidedly elucidated.

Seven functionally and structurally important regions can be described in Src. From N-terminus it is the SH4 domain, unique domain, SH3 domain, SH2 domain, CD linker, catalytic domain and C-terminal tail containing a key regulatory residue Y527 (chicken Src numbering). SH3 and SH2 domains serve not only for binding of signaling partners (e.g. p130Cas, FAK, paxillin, STAT3), but they also play an important role in downregulating Src kinase activity (Superti-Furga et al., 1993). Structural studies have shown that active Src adopts an open conformation whereas inactive Src is characterized by very compact structure, with the SH3 and SH2 domains turned inwards, and packed against the catalytic domain on the side opposite to the catalytic cleft (Xu et al., 1997). The compact and inactive conformation of Src is maintained by three main intramolecular interactions: i) SH2 domain binding of phosphorylated Y527, ii) binding of SH3 domain to a part of the CD linker, iii) binding of SH3 domain to the N-terminal lobe of the catalytic domain (Brabek et al., 2002; Cooper et al., 1986; Xu et al., 1999; Brabek et al., 2002; Cooper et al., 1986; Xu et al., 1997). The release of the intramolecular regulatory interaction of SH2 domain with phosphorylated Y527 leads to the opening of Src structure and the kinase domain adopts an active conformation (Cowan-Jacob et al., 2005). The mechanism of SH3 domain-mediated negative regulatory interactions and especially their effect on Src structure remains less understood.

The current model for Src regulation proposes a correlation between structural condensation of the protein backbone and catalytic activity (Cowan-Jacob et al., 2005). Upon external stimuli or mutagenesis, intramolecular regulatory interactions are disturbed, the conformation loosens and Src kinase domain becomes activated. Taking advantage of these conformational changes, we constructed a genetically encoded intramolecular FRET-based Src biosensor and analyzed conformational changes of Src following Src activation induced by Src mutagenesis or upon external chemical or mechanical stimulation of cells. Using FRET imaging we further analyzed the spatio-temporal dynamics of Src activation in focal adhesions.

RESULTS

Design and construction of Src-FRET biosensor

According to known structures of active and inactive Src, the greatest spatial distance between any two parts of Src molecule after its activation is the distance between C-terminus and SH2 domain (Cowan-Jacob et al., 2005, Fig. 1 A, B). We thus decided to insert the FRET pair of fluorescence proteins in this area of Src. The donor fluorophore was inserted in the loop between β D and β E strands of SH2 domain (Xu et al., 1997). This loop is oriented outwards of the compact structure of Src and is on the opposite side to the SH2 ligand binding site. To minimize potential disrupting effect of the fluorescence protein insertion on the SH2 domain fold, two highly flexible linker peptides (8, 11 amino acids) were added to the donor fluorescence protein inserted to SH2 domain. The acceptor fluorescence protein was inserted at the very C-terminus of Src molecule (7 amino acids long linker peptide). To minimize dimerization artifacts, monomeric versions of fluorescent proteins mCFP and mCitrine (mCit) were chosen as donor and acceptor fluorophores, respectively.

Given to the proposed design, the following constructs were prepared: the full-length chicken *c-src* gene with mCFP inserted into the SH2 domain (Src-CFP), chicken *c-src* with mCit linked to the C-terminus of Src (Src-YFP), complete biosensor construct with both mCFP and mCit inserted (Src-FRET), complete biosensor construct where Src kinase was activated by mutation of Tyr527 to Phe (Y527F, Src-FRET527F) and positive control construct (PC, Fig. 1C). The constructs were expressed in HEK cells and the relative levels of an activatory phosphorylation of Tyr416 within the activation loop were determined (Boerner et al., 1996). None of the constructs with WT-Src showed any significant difference ($p > 0.45$) in relative phosphorylation of Tyr416, which suggests that the insertion of the fluorophores has no effect on basal activity of Src kinase (Fig. 2A). In contrast, the biosensor construct with activated Src exhibits a significant increase (approximately 2-fold) of relative Tyr416 phosphorylation, confirming its activated status.

In the prepared biosensor variants, the FRET between the incorporated fluorophores was measured with a FRET steady-state approach (Fig. 2B). Fluorescence spectra were recorded in fresh cell lysates at an excitation wavelength of 433 nm, which excites the mCFP donor, and FRET ratio was calculated as ratio of fluorescence intensity at 480 nm (mCFP emission peak) and 525 nm (mCit emission peak). FRET ratio of Src-FRET construct in average reached approximately 73% of the maximum FRET within the theoretical range, given by the difference in FRET ratio between the positive control and Src-CFP, and was significantly ($p < 0.0001$) different from FRET ratio of Src-FRET527F reaching approximately 33% of the maximum FRET. This shows that the dynamic range of the Src-FRET biosensor is at least 40% of the theoretical dynamic range for the FRET of the mCFP and mCit pair, indicating that Src-FRET biosensor can effectively monitor structural changes following Src activation. Importantly, the fluorescence spectra from cells transfected simultaneously by Src-CFP and Src-YFP constructs closely resemble spectra from cells transfected by Src-CFP only, confirming that the FRET observed in Src-FRET and Src-FRET527 is a result of an intramolecular FRET (Fig. 2B).

Src FRET biosensor is responsive to interaction-based activation

The inactive structure of Src is maintained by intramolecular interactions mediated by SH2 and SH3 domains (Xu et al., 1997; Xu et al., 1999). It was previously shown that cooperative binding of peptides derived from Src interactor Sin to Src SH2 and SH3 domains can activate Src (Alexandropoulos and Baltimore, 1996). The Src-FRET biosensor represents an excellent tool to test the effect of peptides competing with intramolecular binding sequences on compactness of Src structure. We thus analyzed the effect of purified variants of Sin-derived peptides on FRET of the Src-FRET biosensor in vitro. In agreement with the study of Alexandropoulos and Baltimore, our results showed that Sin peptide carrying both SH2 and SH3 binding sites (SinWT) effectively promotes the decrease in FRET ratio of the Src biosensor, whereas the Sin peptides mutated either in SH2 (SinY), SH3 (SinR) or both SH2 and SH3 binding sites (SinRY), have no effect (Fig. 2 C, D).

Src FRET biosensor reveals the effect of Src mutations on compactness of Src structure

Large number of mutations activating the oncogenic potential of Src were described throughout the history of Src protooncogene analysis, however, the effect of many of these mutation on the overall structure/compactness of Src is not known. This is especially true for mutations affecting SH3-mediated intramolecular interactions. To this end, we introduced several mutations known to affect Src activity into the biosensor and analyzed their effect on FRET and kinase activity. We prepared 3 biosensor variants carrying activatory mutations affecting the SH3-mediated regulation of Src: i) Src-FRET-RT biosensor with mutation in RT loop of SH3 domain inhibiting its interaction with kinase domain (Thr96/Ile + Arg95/Trp, (Miyazaki et al., 1999)); ii) Src-FRET-nSrc with mutation in n-Src loop of SH3 domain inhibiting its interaction with kinase domain (Asp117/Asn, (Miyazaki et al., 1999)); iii) Src-FRET-CD with mutation in the CD linker inhibiting its binding to SH3 domain (Pro250/Gly, Lys249/Asp, (Gonfloni et al., 1997)). In addition, we prepared a biosensor variant Src-FRET-CA carrying mutation within the kinase domain (Glu381(376)/Gly) shown to constitutively activate Src, though the mechanism of the activation is unknown (Bjorge et al., 1995), and two double mutant variants combining the activatory Tyr527 to Phe mutation uncoupling the SH2-mediated regulations with either RT loop or CD linker mutations (Src-FRET-FRT and Src-FRET-FCD, respectively).

The mutated variants of the biosensor were transiently expressed in U2OS cells and the effect of the mutations on FRET and Src kinase activity was analyzed. All mutated variants have shown significantly lower FRET ($p < 0.001$) than the non-mutated biosensor (Fig. 3A, B). When compared to FRET ratio of the SH2-activated Src-FRET527F, the biosensors show 4 different levels of FRET. First, there is a group not significantly different ($p > 0.323$) from Src-FRET527F which includes Src-FRET527F itself and Src-FRET-CD variants. The Src-FRET-CA and the double mutated Src-FRET-FRT and Src-FRET-FCD variants form a group of biosensors with FRET significantly lower ($p < 0.004$) than Src-FRET527F. The biosensor variants with activating mutations directly within SH3 domain exhibit intermediate level of FRET decrease. The Src-FRET-RT exhibits FRET levels close, but significantly higher ($p < 0.001$), than that of Src-FRET527F group. The mutations within nSrc-loop, the Src-FRET-nSrc variant, has the lowest effect on compactness of Src structure as its FRET is significantly higher than even of the Src-FRET-RT ($p < 0.001$). In addition to FRET, the effect of the mutations on Src kinase activity was evaluated using a kinetic kinase assay. The sensitivity of the assay was not

sufficient to confirm the 4 different levels of the Src activity, as indicated by the FRET analysis. When compared to kinase activity of Src-FRET527F, only Src-FRET-CA has shown significantly higher kinase activity ($p=0.009$) and Src-FRET-WT together with Src-FRET-nSrc exhibited significantly lower kinase activity ($p<0.001$ and $p=0.013$, respectively). The kinase activities of individual Src-FRET variants, however, exhibited, in an inverse manner, similar trends as the FRET (Fig. 3C, Supp. Fig. 1).

Taken together, these data show that the biosensor can effectively monitor even small changes in activity of Src and that mutations affecting SH3-mediated intramolecular interactions of Src also result in the opening of Src structure.

Src FRET biosensor is functionally equivalent to Src

The initial testing of the biosensor has shown that the biosensor expressed in HEK and U2OS cells can monitor structural changes of Src following activation via mutation of regulatory Y527 or using a SH2-SH3 competing peptide. HEK and U2OS cells express low but not negligible amount of endogenous Src and thus are not optimal for testing functional relevance of the biosensor for Src signaling. Therefore, we stably expressed the Src-FRET biosensor in SYF fibroblasts (nulls for Src-family kinases, Src, Yes and Fyn (Klinghoffer et al., 1999)) and analyzed the effect of Src-FRET biosensor activation on phosphorylation of Src substrates p130Cas and paxillin. The phosphorylation of both p130Cas and paxillin was virtually absent in untransfected SYFs. In contrast, expression of Src-FRET biosensor in SYFs resulted in substantial phosphorylation of both p130Cas and paxillin. This phosphorylation was significantly increased upon stimulation of the cells with EGF or LPA and, conversely, inhibited when treated with Src kinase inhibitor dasatinib (Fig. 4A). These results indicate that Src-FRET biosensor effectively phosphorylates known Src substrates and responds both to physiological signals activating Src and to inhibition by Src inhibitor.

Src activation dynamics upon mechanical stimulation

P130Cas, an adaptor protein and Src substrate, was shown to function as a mechanosensor. Its substrate domain can be mechanically stretched, and this exposes tyrosine residues within the domain for Src-mediated phosphorylation (Janostiak et al., 2014b; Sawada et al., 2006). Interestingly, static mechanical stretch of cells induces bi-phasic tyrosine phosphorylation of p130Cas with maximum at 15 and 45 minutes after the stretch (Branis et al., 2017; Janostiak et al., 2014a). However, the role of Src in tension-mediated phosphorylation was not clearly addressed. We stretched SYFs expressing Src-FRET biosensor and analyzed Src activity in the cells by monitoring the total level of FRET and phosphorylation of p130Cas. We found that FRET of the biosensor is significantly decreased 15 minutes and 45 minutes after the stretch (Fig. 4B, C). The dynamics of Src activation upon static stretch thus reflects the bi-phasic dynamics of p130Cas phosphorylation and shows that mechanical stimulation of cells activates Src.

The effect of inhibitors on Src structure

Having established that the Src-FRET biosensor functions effectively as Src in cells and responds to mechanical stimuli, we then examined the effect of LPA, EGF and compounds known to inhibit Src on FRET ratio of the Src-FRET biosensor in cells. The treatment of SYFs expressing the Src-FRET biosensor with both EGF and LPA resulted in

significant decrease of FRET ratio, indicating and confirming activation of the biosensor in the cells upon EGF and LPA treatments (Fig. 5 A, B; compare with Fig. 4A). Surprisingly, treatment with dasatinib induced significant decrease of FRET indicating open conformation of Src, despite inactivating Src kinase activity (Fig. 5, Supp. Fig. 2). It was previously shown for Hck and Src kinases that binding of specific ligands targeting ATP-binding pocket results in increased accessibility of SH2 and SH3 domains to intermolecular binding which could be responsible for the observed dasatinib-induced opening of Src structure (Leonard et al., 2014). Therefore, we decided to analyze a panel of Src inhibitors for the effect on compactness of Src-FRET biosensor. All kinase inhibitors tested effectively inhibited the Src kinase (Supp. Fig. 2). Along with dasatinib, bosutinib and UM-164 also significantly lowered ($p < 0.05$) the FRET ratio of the biosensor. In contrast, treatment of the cells with saracatinib and SKI-1 had no effect on FRET (Fig. 5 C, D). We also tested the effect of Sodium Orthovanadate, which inhibits Src kinase activity by preventing P-Tyr527 dephosphorylation (Ryder and Gordon, 1987), and found that it significantly increases the FRET ratio of the biosensor (Fig. 5 C, D). This is consistent with the increased Tyr527 phosphorylation and subsequent induction of closed conformation of Src.

When analyzing the effect of inhibitors on the FRET ratio of the Src FRET biosensor we noticed a substantial difference in pattern of Src FRET biosensor localization in the cells. Strikingly, the inhibitors which induced opened conformation of the Src FRET biosensor (dasatinib, UM-164, bosutinib) showed high enrichment in focal adhesions resembling the localization of the 527F activated Src (Fig. 6, (Fincham and Frame, 1998)). In contrast, treatment of cells with inhibitors not affecting the FRET ratio of the Src FRET biosensor (SKI-1, saracatinib) and with Sodium Orthovanadate did not visibly changed the localization pattern of the Src FRET biosensor, which remained mostly cytoplasmic. This indicates that opened conformation of Src and not its kinase activity is required for its targeting to focal adhesions.

Analysis of Src activation using FRET imaging

The new Src-FRET biosensor proofed its potential in analyzing Src activity upon Src mutagenesis and activation/inhibition of the cells by chemical and mechanical cues. Because of its design it can provide not only information about Src activity but also about Src intracellular localization dynamics. Therefore, we next focused on monitoring Src activation dynamics in cells. To overcome the higher demand for the donor fluorophore stability and brightness in long-term live imaging experiments we replaced mCFP in the Src-FRET construct for mTurquoise2 (Goedhart et al., 2012). When expressed in cells, the resulting Src-FRET(T) construct monitored Src activation status after the treatment with LPA or EGF in a similar manner as its mCFP counterpart, though when compared to maximum FRET of positive control (mTurquoise2-mCit), its dynamic range was somehow smaller than of the mCFP variant of the biosensor (Supp. Fig. 3). The Src-FRET(T) biosensor exhibited, however, much brighter and stable donor fluorescence effectively enabling us to monitor dynamics of Src activation status in live cells.

To analyze the dynamics of Src activation in focal adhesions, U2OS cells were transiently co-transfected with the Src-FRET(T) biosensor and mCherry-FAT (focal adhesion targeting domain of FAK) or mCherry-vinculin constructs. The cells were seeded onto fibronectin-coated cover glass to allow cell adhesion, and FRET and mCherry signals were analyzed live by TIRF microscopy during later stages of cell

spreading. The focal adhesions were detected using the mCherry signal of the mCherry-FAT or mCherry-vinculin fusion constructs. The cell body was detected as the mCit signal of the Src-FRET(T) biosensor. The FRET was analyzed by sensitized emission approach and quantified as nF/I_{CFP} according to (Xia and Liu, 2001). In average we found that FRET in focal adhesions is about 20% lower than in surrounding cytoplasm showing highly significant ($p < 2 \times 10^{-26}$) and localized activation of Src in focal adhesions (Fig. 7 D). In fact, in the cell area illuminated by the TIRF evanescent field, the active Src conformation was detected almost exclusively in focal adhesions (Supp. Video 1). Analysis of Src activation dynamics revealed that, during the initial phase of focal adhesion formation, characterized by increasing intensity signal of mCherry-FAT or mCherry-vinculin, the FRET is high at the beginning but decreases progressively reaching its minimal values mostly before the mCherry signal reaches its maximum intensity (Fig. 7, Supp. Fig. 4). The FRET remains low throughout the mature stage of focal adhesion, characterized by stable intensity of the mCherry signal, and gradually increases during focal adhesion disassembly (Fig. 7 B, C).

Even though, Src is locally activated in focal adhesions we did not observe any enrichment of Src, detected as mCit signal, in any stage of focal adhesion life cycle (Fig. 7 B, C). This indicates high dynamics of Src in focal adhesions. FRAP analysis revealed that Src-FRET(T) biosensor dynamics in focal adhesions is indeed very high with average half-time recovery 0.90 ± 0.57 s (Supp. Fig. 5). This is well in agreement with single-molecule analyses showing 1 s residency time of Src in focal adhesions (Machiyama et al., 2015).

DISCUSSION

Understanding the precise regulation of Src in living cells is the key to understanding Src-dependent signal transduction and to development of effective therapeutic approaches targeting Src. To monitor Src activity in cells, several attempts were already made, including FRET based substrate biosensors (Ting et al., 2001; Wang et al., 2005), biosensor based on a monobody targeting the SH3 domain of Src (Gulyani et al., 2011) or biarsenical dyes staining of tetracysteine motif introduced into SH2 domain (Irtegun et al., 2014). All approaches provided valuable information about Src activity in the cells. However, and unlike our biosensor, they don't provide combined information about the activity and intracellular localization of diverse subpopulations of Src molecules at one time. An approach similar to ours was adopted to monitor the activation of Src family kinase Lck (Paster et al., 2009; Stirnweiss et al., 2013). The authors designed a FRET biosensor consisting of full backbone of Lck with enhanced yellow fluorescent protein inserted at the very C-terminus and enhanced cyan fluorescent protein inserted either between SH3 and SH2 domains (Paster et al., 2009) or between the unique and SH3 domain (Stirnweiss et al., 2013). Our Src-FRET biosensor uses the same insertion site for the acceptor fluorophore (the very C-terminus of Src) but differs in insertion site of donor fluorophore. Insertion into the linker between SH3 and SH2 domains could not be used for Src, since the linker is critical to couple communication between SH3 and SH2 domains and mutation of this linker leads to activation of Src (Young et al., 2001). Insertion between SH3 and unique domain is in our opinion less optimal than our solution, as it is sterically more distant from the C-terminus than our insertion into the SH2 domain, and would lead to less efficient FRET. In agreement with these assumptions,

in the *in-vitro* steady-state FRET measurements (ratio of relative FRET and CFP fluorescence) our biosensor exhibits higher dynamic range than that of Lck (Stirnweiss et al., 2013).

New insights in Src regulation: correlation between mutations and compactness of Src structure, the role of SH3 domain in regulation of Src

Throughout the 40 years history of studying Src kinase, many mutations activating Src were described. The crystallographic data have come with clear evidence that mutations affecting SH2-mediated intramolecular interactions lead to the opening of Src structure (Cowan-Jacob et al., 2005). However, there was no clear evidence on the effect of SH3-mediated intramolecular interactions or activatory mutations in the kinase domain on Src structure. Our data show that mutations inhibiting SH3-CD linker interaction leads to opening of the Src structure to a similar extent as the Tyr527 to Phe mutation uncoupling the SH2-mediated regulation. Mutations affecting the interaction of SH3 domain with N-terminal lobe of kinase domain also effectively induced opening of Src structure but to a lesser extent. Importantly, the effect of the mutations inhibiting the SH2- and SH3-mediated intramolecular interactions is additive, indicating high degree of independency of these negative intramolecular interactions in regulation of Src kinase. Surprisingly the activatory mutation within the kinase domain Glu381(376)/Gly opens the Src structure to a level similar of the analyzed double mutants. The Glu381(376) is located at the C-terminus of αE helix in the C-lobe of kinase domain and is in no contact with either SH2 or SH3 domain in closed inactive conformation of Src (Xu et al., 1997). Therefore, the effect of Glu381(376)/Gly substitution on opening of the Src structure is indirect. To conclude, the data suggest that activated conformation of the kinase domain negatively affects intramolecular SH2- and SH3-binding to kinase domain and forces the opened conformation of Src.

Differential effect of Src inhibitors on Src structure

Src kinase inhibition has long been an important target for cancer therapy (Rosel et al., 2013). The known small-molecule Src kinase inhibitors are ATP competitive inhibitors and according to their binding mode are generally classified as type I or type II inhibitors; type I bind active and type II bind inactive kinase (Dar and Shokat, 2011). The classification of the inhibitors relies mostly on the position of conserved DFG motif at the beginning of activation segment. "DFG-in" position, specific for type I inhibitors, represents an active state of the kinase with aspartate of the DFG motif oriented inward toward the active site. When this aspartate is directed out-ward (DFG-out, type II inhibitors) the phenylalanine of DFG is directed into the active site and the kinase is in inactive conformation (Roskoski, Jr., 2016). Besides the position of the DFG, αC helix orientation is also associated with active (αC -in) and inactive (αC -out) state of the kinase (Leonard et al., 2014).

The inhibitors analyzed exhibited two distinct phenotypes of action on Src. The first group represented by dasatinib, bosutinib and UM-164 induced opened conformation of Src and enrichment of the Src-FRET biosensor in focal adhesions. This phenotype closely resembled the phenotype 527F activated Src, indicating that the phenotype is associated with active rather than inactive conformation of Src. The second group represented by saracatinib and SKI-1 had no effect on either compactness of Src structure or Src-FRET biosensor localization to focal adhesions. Dasatinib and bosutinib

represent type I Src inhibitors binding Src in DFG-in, α C-in conformation (Leonard et al., 2014; Roskoski, Jr., 2016; Tong et al., 2017). UM-164 (DAS-DFGO2) and saracatinib are type II inhibitors (DFG-out) which differ in their effect on α C-helix position, UM-164 binding Src with α C-in and saracatinib with α C-out conformation (Roskoski, Jr., 2016; Tong et al., 2017). For SKI-1 we could not ascertain its binding mode to Src in the literature. The common denominator of the effect of all three inhibitors promoting the opened structure of Src is induction of α C-in conformation. Similarly, it was shown that inhibitors stabilizing α C-in active conformation of kinase domain greatly increase accessibility of Src SH3 domain for intramolecular interactions, indicating a potential opening of Src structure (Leonard et al., 2014). Taken together, our data show that conformation of Src kinase domain affects the overall compactness of Src structure: namely kinase domain in active conformation characterized by α C helix-in orientation induces global opening of Src. In agreement with this, activatory mutation in kinase domain (Glu381(376)/Gly) promotes Src structure opening (Fig. 3). Finally, our results show that the Src-FRET biosensor could be used as a tool to distinguish between the modes of binding/action of new inhibitors without the need for resolving the structure of the Src-inhibitor complex. In this sense, we can conclude that SKI-1 inhibitor binds Src in its inactive conformation with α C-out orientation of α C helix.

The Src-FRET biosensor unraveled two classes of Src inhibitors differing in their effect on the Src structure and subcellular localization. Conceivably, biological activity of inactivated Src kinase would differ for inactivated Src with opened conformation, with both SH2 and SH3 domains unrestricted for binding their targets, and inactivated Src in closed conformation. Therefore, the two classes of Src inhibitors would have different effect on intracellular signaling and thus potentially divers therapeutic outcome.

Src as a potential mechanosensor

The Src-FRET biosensor monitors Src activity through conformational changes, opening of the compact structure of inactive Src, following Src activation. It is thus intriguing that mechanical stimulation of cells leads to opening of the Src structure. The dynamics of Src “opening” upon mechanical stretching of the cells follows the pattern of p130Cas phosphorylation. P130Cas was shown to function as a primary mechanosensor; upon mechanical stretch its substrate domain unfolds and exposes cryptic tyrosines that are subsequently phosphorylated by Src (Sawada et al., 2006). The spatio-temporal resolution achieved in our cell stretching experiments didn’t allow to distinguish whether the Src opening precedes p130Cas phosphorylation or vice versa. However, the cellular stretch-mediated opening of Src indicates that Src could act as a primary mechanosensor which is directly mechanically activated by local forces. Interestingly, the substrate-based Src biosensors revealed that local Src activation in response to mechanical perturbation can be very fast, which is in agreement with the concept of Src being a sensor of local mechanical tension (Wang et al., 2005; Na et al., 2008). In this context, our experimental setup relies on average status of the biosensor molecules in cell populations. Therefore, it could not detect fast local mechanical tension-mediated activation of the molecules but is rather dependent on accumulation of the activated molecules in time. The live cell FRET imaging with the Src-FRET biosensor under controlled exertion of local mechanical forces on the cells is needed to further ascertain the function of Src as a mechanosensor.

Src role in focal adhesions

It has been well established that Src has mostly uniform distribution in cells, with significant fraction localized on membrane, and that activated Src is enriched in focal adhesions (Machiyama et al., 2015). Src localization to focal adhesions requires intact SH2 domain and is mediated by FAK (Klinghoffer et al., 1999; Machiyama et al., 2015; Wu et al., 2016). This mechanism of Src focal adhesion targeting implies a requirement for opened conformation of Src which we have confirmed with our biosensor. Surprisingly, no enrichment of Src was observed in any stage of focal adhesion life cycle. This raises a question about the mechanism of Src activation in focal adhesions. We envision three potential mechanisms of Src structure opening in focal adhesions. First, local dephosphorylation of tyrosine 527 would release the intramolecular SH2 binding and allow for its intermolecular bindings (e.g. to phosphorylated FAK). This would induce opened conformation of Src and activate the kinase. Second, and analogical to our observation with Sin-derived peptides, simultaneous binding of SH2 and SH3 domain to their target sites within focal adhesion proteins opens Src and activates the kinase. Third, opened conformation of Src is achieved by direct mechanical tension. We propose that the opening of Src structure could be achieved by dynamic mechanical tension in focal adhesions which is transmitted to Src molecules, anchored on N-terminus to plasma membrane, through intermolecular SH2 domain binding. This tension would release the SH3-mediated intramolecular interaction and forced the full activation of the kinase. Interestingly, we found that Src is extremely dynamic in focal adhesions. This is inconsistent with the model of Src targeting through simultaneous binding of SH2 and SH3 domains to focal adhesion proteins, which would be expected to stabilize Src in focal adhesions. On the contrary, Src exhibits high dynamics and localized activation in focal adhesions without detectable enrichment. This is in line with the hypothesis of tension-mediated opening of Src.

Dynamics of Src activation in focal adhesions was previously analyzed using substrate-based FRET biosensors (Wu et al., 2016). The data suggested that assembly of focal adhesions and Src activation is practically concurrent and that focal adhesion disassembly is preceded by another wave of Src activation. We don't see waves of Src activation in focal adhesions but rather a steady activation level of Src throughout the mature, stable phase of focal adhesions life cycle and rapid activation or gradual inhibition during focal adhesion assembly and disassembly, respectively. Both biosensors differ in their mode of action. Our biosensor relies on correlation between compactness of Src structure and its activity, which we have confirmed under all experimental setups tested. Nevertheless, we cannot rule out specific condition in live cells where opened conformation is not strictly reflected by higher kinase activity. In contrast the substrate biosensors monitor the kinase activity through the level of specific substrate phosphorylation. This, however, depends on local combination of kinase and counteracting phosphatases activities. Putting both observations together we propose the following model of Src role in focal adhesions life cycle. Src is locally and rapidly activated during focal adhesion assembly and phosphorylates its substrates. Its activity remains high during the mature stage of focal adhesion cycle but is counteracted by phosphatases which stabilize the level of phosphorylation of the Src substrates in focal adhesions. The disassembly is potentially initiated by decreased phosphatases' activity, inducing hyperphosphorylation of Src targets and subsequent disassembly of focal adhesions (Supp. Fig. 6).

There are several indirect evidences that increased Src-dependent phosphorylation destabilizes localization of proteins in focal adhesion or even destabilizes the focal adhesions themselves (Sup. Fig. 6). Among others, it was shown that: i) cells lacking the tyrosine phosphatase Shp2 exhibited increased turnover of focal adhesions (von Wichert et al., 2003); ii) increased tyrosine phosphorylation of paxillin is associated with more dynamic focal adhesions and is absent from stable fibrillar adhesions (Zaidel-Bar et al., 2007) or that iii) Src phosphorylation of ARHGAP42 on tyrosine 376 increases dynamics of focal adhesions (Luo et al., 2017). In addition, Src was shown to phosphorylate with slow dynamics p130Cas of Tyr12 within the SH3 domain, inhibiting its binding capacity and SH3-mediated anchoring of p130Cas to focal adhesions (Branis et al., 2017; Gemperle et al., 2017; Janostiak et al., 2011). The mutational analysis of Tyr12 further suggested that its phosphorylation destabilizes focal adhesions and induces migratory phenotype of cell (Janostiak et al., 2011). Besides phosphorylation-dependent loss of binding to focal adhesions, Src phosphorylation-stimulated p130Cas ubiquitination and its subsequent degradation was shown as another mechanism regulating focal adhesion's dynamics (Teckchandani et al., 2014).

SIGNIFICANCE

We constructed a genetically encoded intramolecular FRET-based Src biosensor and analyzed conformational changes of Src following Src activation and the spatio-temporal dynamics of Src activity in cells. We found that activatory mutations affecting SH3 domain-mediated intramolecular interactions and activating mutation in kinase domain induce opening of Src structure. We discovered that Src inhibitors exhibit two distinct phenotypes of action on Src. First group of inhibitors, characterized by inducing α C-helix-out conformation of kinase domain, has no effect on Src structure or localization. Second group, inducing α C-helix-in conformation, surprisingly and counterintuitively leads to opened conformation of Src and its localization to focal adhesions. Finally, we analyzed the dynamics of Src activity in focal adhesions by FRET imaging. Based on these results we propose a new model for the role of Src-dependent phosphorylation in focal adhesions, according to which Src-dependent tyrosine phosphorylation of focal adhesion proteins drives the assembly phase of focal adhesions. It remains stable during maturation of focal adhesions due to counteracting activity of tyrosine phosphatases. Hyperphosphorylation of the Src targets in focal adhesions, potentially due to decrease of phosphatases activity, induces focal adhesions' disassembly and is followed by Src inactivation.

FIGURE LEGENDS

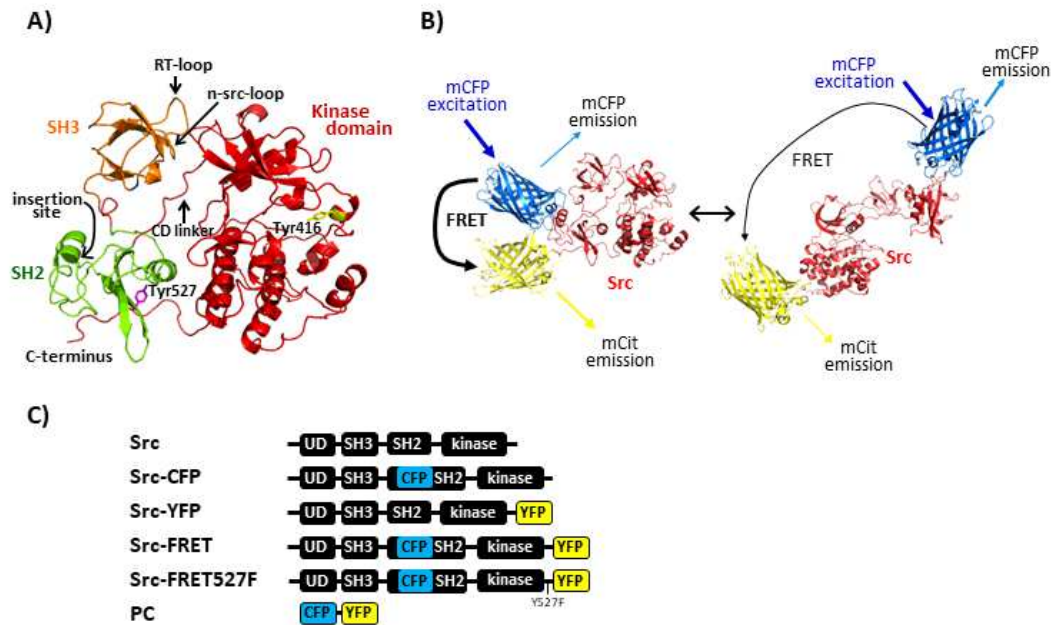


Fig. 1. Design of Src-FRET biosensor. A) Structure of inactive Src with critical residues and motives depicted. B) Model of Src biosensor action. Compact, inactive conformation of Src biosensor gives high FRET between inserted mCFP and mCit fluorophores (left). Upon activation, the Src structure loosens and the FRET decreases (right). Linkers between the fluorophores and the kinase are not depicted. The structure models were created according to PDB structures 1FMK, 1Y57, 2H5P, 1F0B. C) Schematic representation of the different Src and control constructs used in this study. UD – unique domain, CFP – mECFP/(mTurquoise2), YFP – mCit.

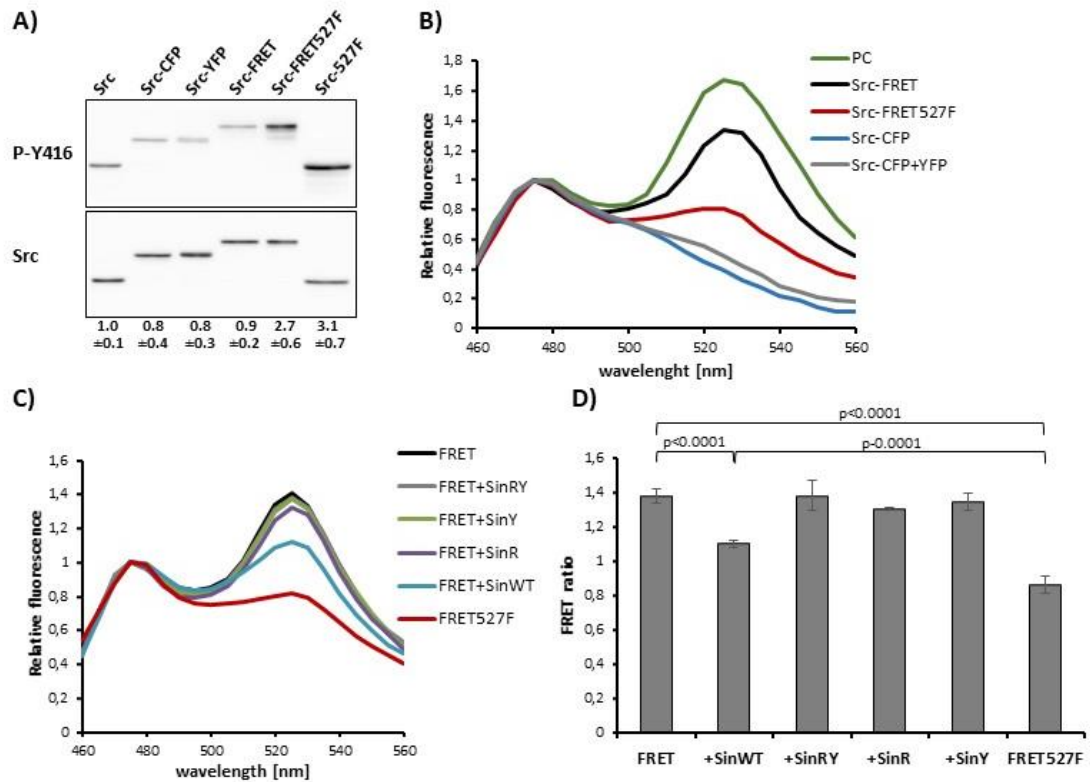


Fig. 2. Insertion of the fluorophores into Src has no significant effect on Src activation. HEK293TF cells were transiently transfected with Src constructs, lysed and analyzed for Tyr416 phosphorylation and emission spectra. A) Representative matched pair of blots showing detection of activated Src (P-Y416 antibody) and total Src. Numbers indicate ratio of Try416 phosphorylation and Src signal (mean \pm standard deviation, out of minimum 5 independent experiments) normalized to unmanipulated Src. B) Representative emission spectra normalized to emission maximum of mCFP. C, D) The biosensor variants were transfected into HEK293FT cells and native cell lysates were supplemented with purified GST-SinWT (FRET+SinWT), GST-SinY (FRET+SinY), GST-SinR (FRET+SinR), GST-SinRY (FRET+SinRY) or GST alone (FRET, FRET527F). After 30 min of incubation fluorescence emission spectra were recorded. C) Representative emission spectra normalized to emission maximum of mCFP. D) Bar graph represents ratio of normalized mCit (525 nm) and mCFP (475 nm) emission. The data are shown as mean \pm standard deviation out of minimum 3 independent experiments performed in triplicates. P values indicate statistical significance calculated by one-way ANOVA and followed by Tukey's post-hoc test.

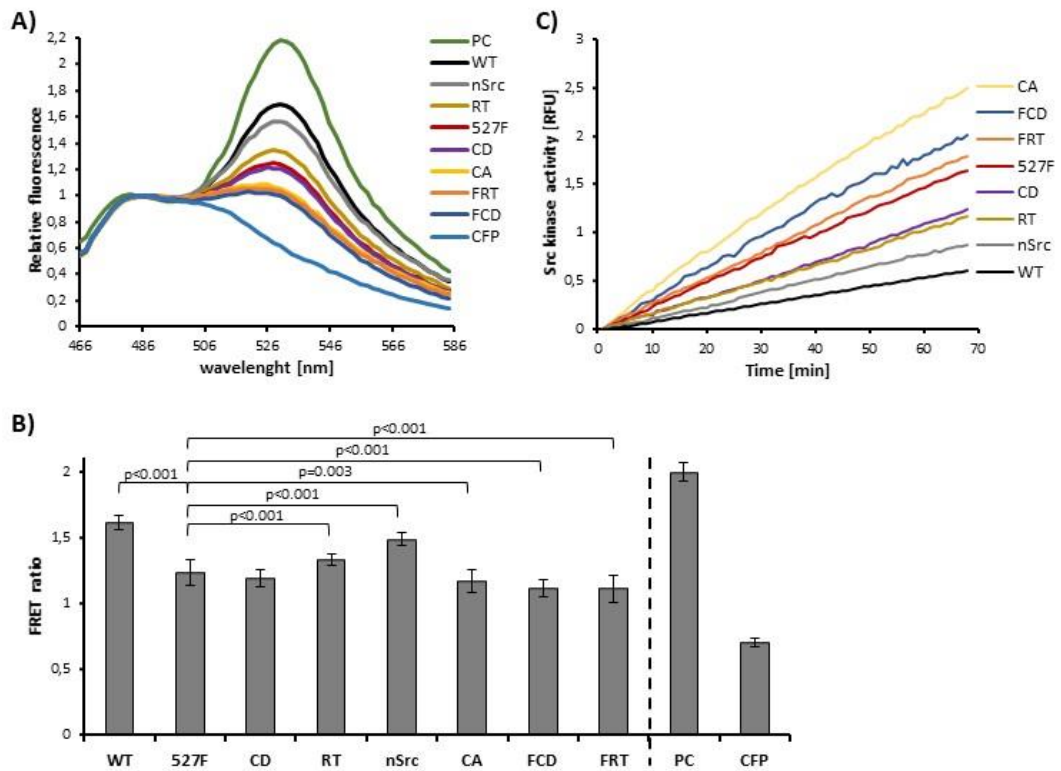


Fig. 3. Src FRET biosensor is responsive to activatory mutations. The biosensor variants were transfected into U2OS cells and the fluorescence emission spectra were recorded. A) Representative emission spectra normalized to emission maximum of mCFP. B) Bar graph represents ratio of normalized mCit (530 nm) and mCFP (480 nm) emission. The data are shown as mean \pm standard deviation out of minimum 3 independent experiments performed in triplicates. P values indicate statistical significance compared to FRET ratio of Src-FRET527F (527F) variant of the biosensor as calculated by one-way ANOVA and followed by Tukey's post-hoc test. C) Kinetic analysis of kinase activity of the biosensor variants using Omnia kinase assay. Representative graph is shown.

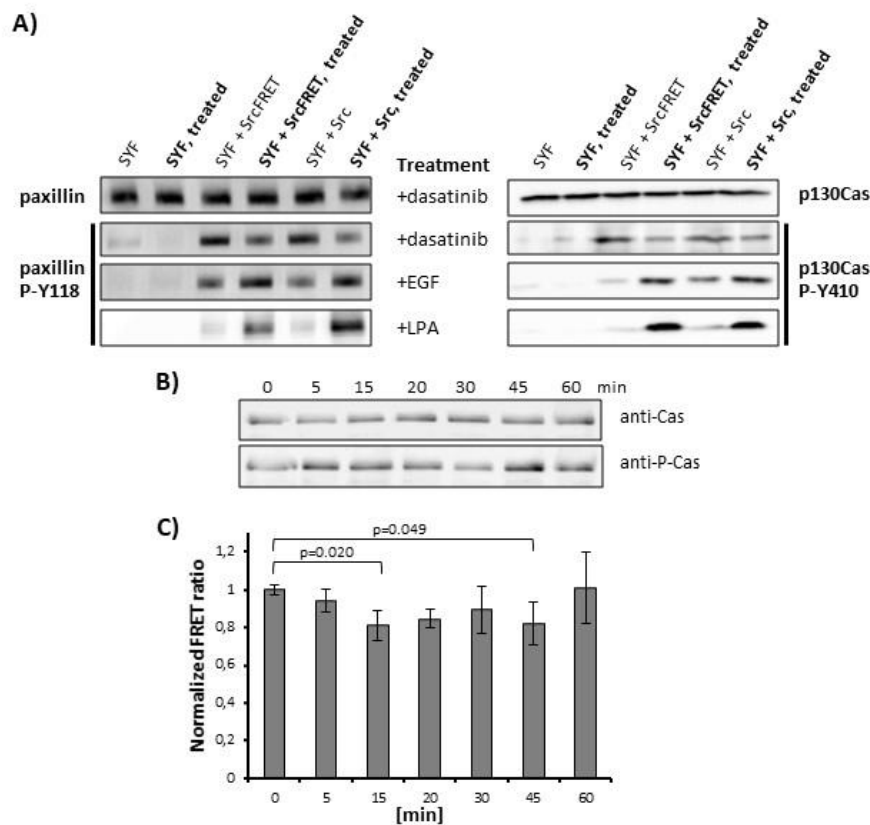


Fig. 4. Src-FRET biosensor responds physiological signals activating Src. A) SYF cells and SYFs stably expressing Src-FRET biosensor (SrcFRET) or c-Src (Src) were incubated for 30 min +/- 150nM dasatinib, for 12 hours +/- 100 ng/ml EGF or for 2 hours +/- 10 μ M LPA. Cells were then lysed and analyzed for expression and phosphorylation of Src substrates paxillin and p130Cas. Representative blots from three independent experiments are shown. B, C) SYF cells stably expressing SrcFRET-WT biosensor were seeded on fibronectin coated flexible membrane, incubated for 24 h, and then subjected to 20% static stretch for indicated times. B) Cells were lysed and analyzed by Western blotting against phosphorylated Y410 in the p130Cas (anti-P-Cas) substrate domain. Representative blot from three independent experiments is shown. C) Cells were lysed and in native cell lysates the FRET was analyzed as a ratio of FRET fluorescence intensity (λ ex 433, λ em 530) and fluorescence intensity of mCFP (λ ex 433, λ em 480). FRET ratio of unstretched cells (0 min) was arbitrary set to 1. The data are shown as mean +/- standard deviation out of minimum 3 independent experiments performed in triplicates. P values indicate statistical significance compared to unstretched cells (0 min) as calculated by one-way ANOVA and followed by Tukey's post-hoc test.

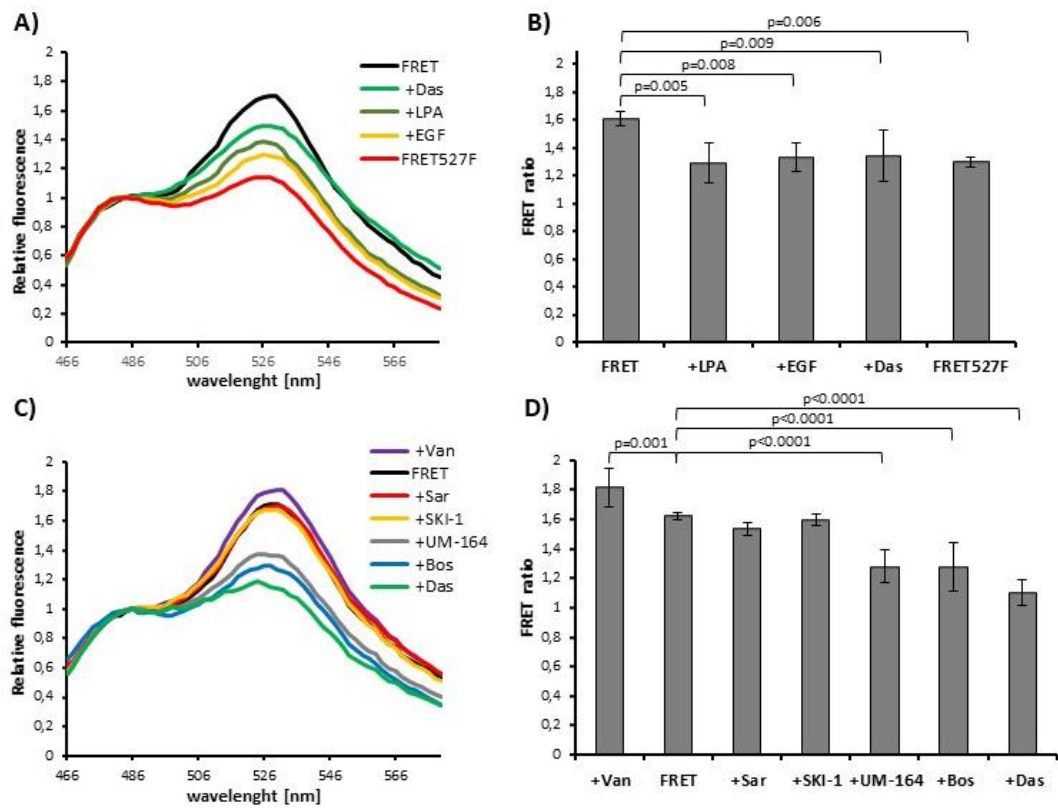


Fig. 5. Src FRET biosensor is responsive to activatory and inhibitory treatments in cells. SrcFRET biosensor (FRET) and biosensor with activating Tyr527 to Phe mutation (FRET527F) were stably expressed in SYF cells. SYFs expressing the FRET-WT biosensor were incubated for 10 min with 10 μ M LPA (serum starved, +LPA), 24 hours with 100 ng/ml EGF (serum starved, +EGF), 60 min with 500 μ M Sodium Orthovanadate (+Van), or for 60 min with Src kinase inhibitors: 100nM dasatinib (+Das), 4 μ M saractinib (+Sar), 1 μ M bosutinib (+Bos), 100nM UM-164 (+UM-164), or 10 μ M SKI-1 (+SKI-1). A, C) Representative emission spectra. Relative fluorescence represents fluorescence intensity normalized to emission maximum of mCFP. B, D) Bar graph represents ratio of normalized mCit (530 nm) and mCFP (480 nm) emission. The data are shown as mean \pm standard deviation out of minimum 3 independent experiments performed in triplicates. P values indicate statistical significance compared to FRET ratio from untreated cells (FRET) as calculated by one-way ANOVA and followed by Tukey's post-hoc test.

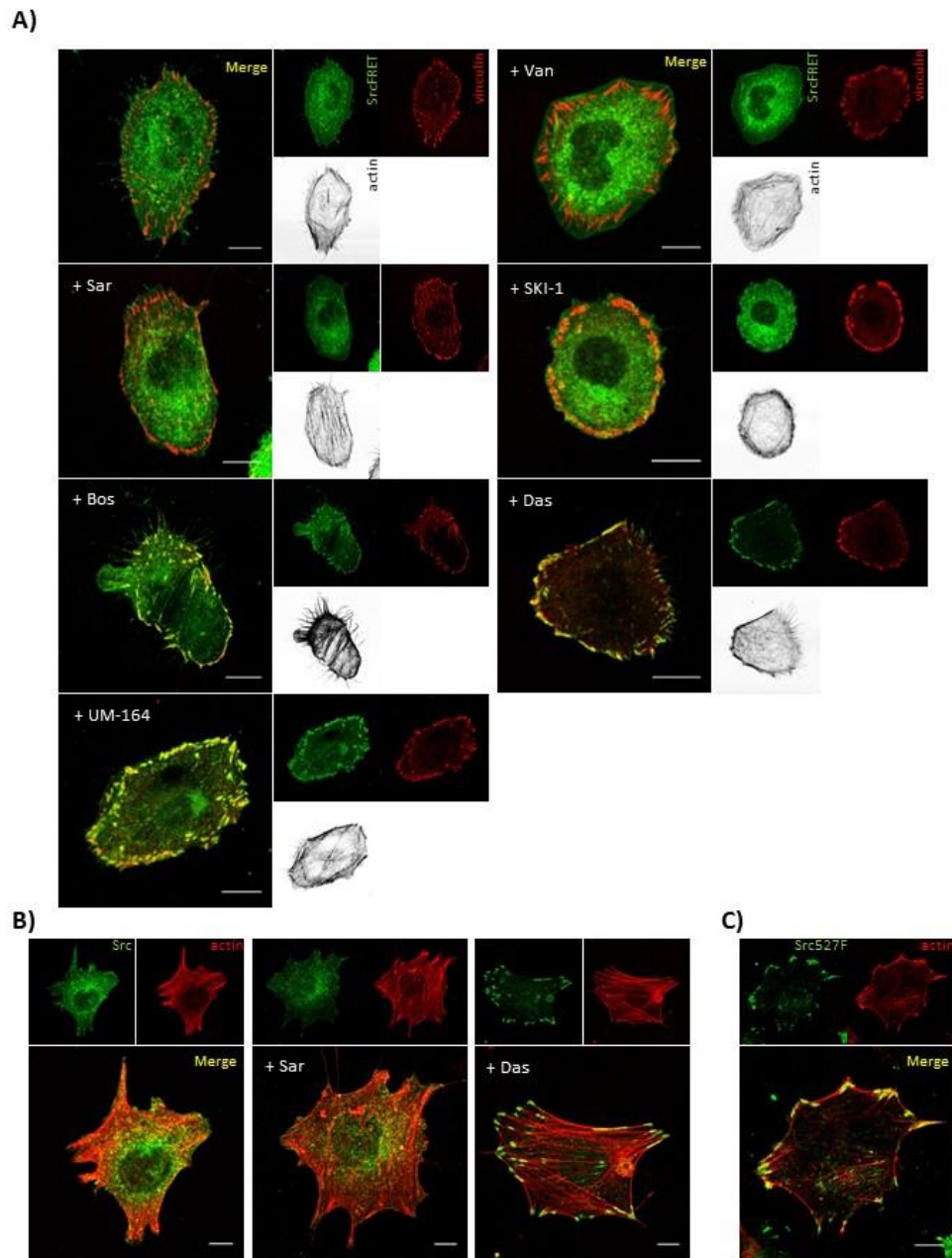


Fig. 6. The effect of Src inhibitors on Src FRET biosensor localization. SYF cells stably expressing SrcFRET-WT biosensor (A), c-Src (B) or activated Src (Src527F, C) were directly stained or incubated for 60 min with 500 μ M Sodium Orthovanadate (+Van), or for 60 min with Src kinase inhibitors: 100nM dasatinib (+Das), 4 μ M saractinib (+Sar), 1 μ M bosutinib (+Bos), 100nM UM-164 (+UM-164), or 10 μ M SKI-1 (+SKI-1). Cells were then fixed and stained for vinculin (focal adhesions marker, red (A)), F-actin (grey (A) or red (B, C)) or Src (mCit fluorescence (A) or anti-Src antibody (B, C), green). Scale bar 10 μ m.

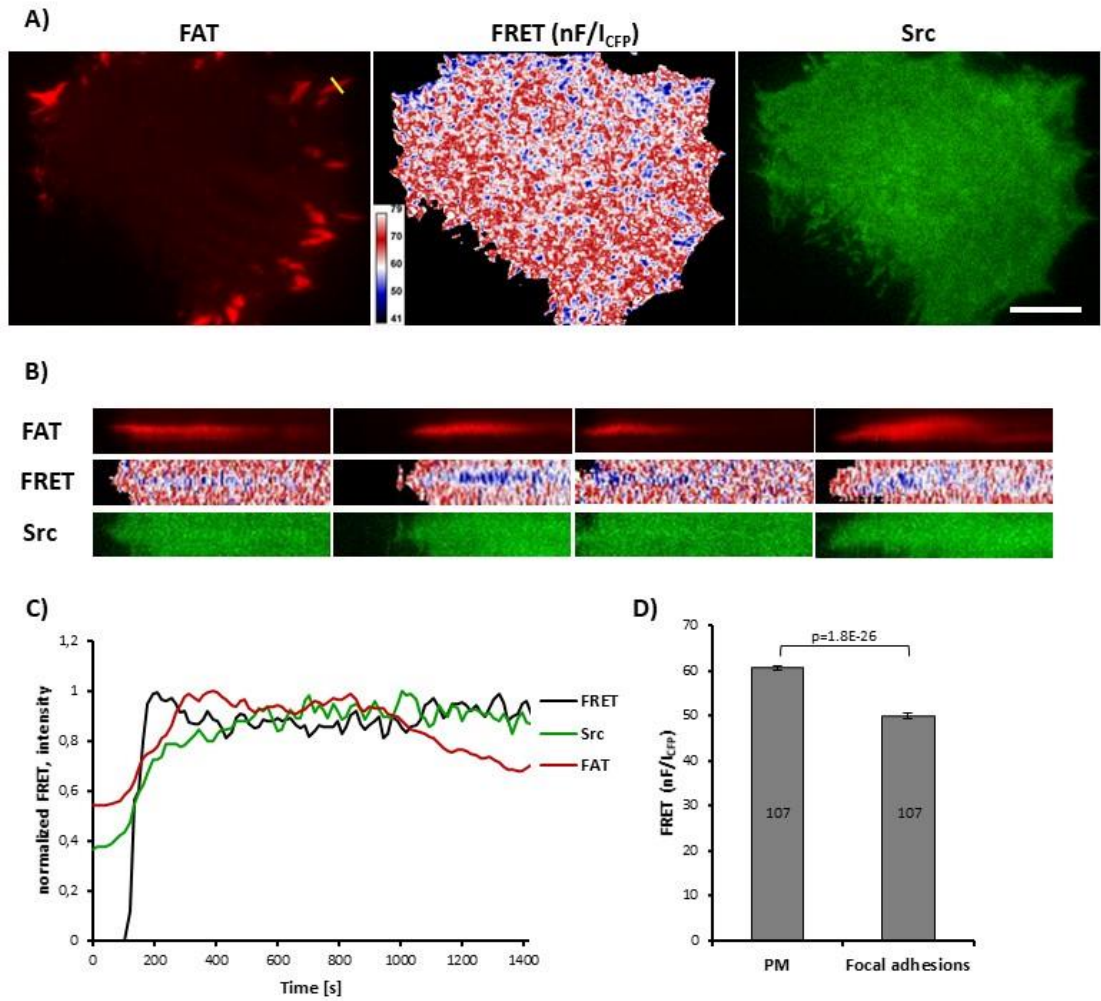


Fig. 7. Src activity in focal adhesions. U2OS cells transiently co-expressing mTurquoise2-based Src-FRET(T) and mCherry-FAT were imaged in life. A) Representative cell image showing focal adhesions (FAT - mCherry signal, red), Src activity map (FRET (nF/I_{CFP})) and Src-FRET(T) localization (Src - mCherry signal, green). Scale bar 10 μ m. B) Representative kymographs (out of 20) of FAT, Src-FRET(T) localization and Src-FRET(T) activity dynamics in focal adhesions. C) Representative graph showing dynamics of mCherry-FAT (FAT), Src-FRET(T) (Src) localization and Src-FRET(T) activity (FRET (nF/I_{CFP})) dynamics in focal adhesion. The data correspond to the first (left) kymograph in B and are normalized to maximum values. D) The bar graph shows average FRET (nF/I_{CFP}) \pm standard error in focal adhesions and random regions of plasma membrane (PM) of similar size as the focal adhesions. Number in the bar graphs indicates number of individual measurements. P value indicates statistical significance as calculated by one-way ANOVA.

METHODS

Cell culture and transfection

All cell lines were cultured in full DMEM (Life Technologies) with 4.5 g/l L glucose, L glutamine, and pyruvate, supplemented with 10% fetal bovine serum (Sigma Aldrich), 2% antibiotic–antimycotic (Life Technologies), and 1% MEM non-essential amino acids (Life Technologies). Cell transfections were carried out using Lipofectamine® 2000, jet PRIME, or polyethylenimine according to manufacturer instructions. SYFs stably expressing Src biosensor variants were prepared via retrovirus infection using the Src biosensor variants cloned in pMSCV-puro vector and the Phoenix retroviral packaging lineage followed by sorting of cell by FACS for YFP.

Cell Lines

SYF, HEK293FT and U2OS cells were kind gift from Tomas Vomastek (Institute of Microbiology, Czech Republic).

DNA constructs

To generate Src-FRET biosensor, full length chicken Src cDNA was PCR amplified from a source vector (Brabek et al., 2002) using the forward primer (5'-GGATCCATGGGTAGTAGCAAGAGC) and the reverse primer (5'-GAATTCTAGGTTCTCTCCAGGCTGG), and cloned in pYES2 vector. The AatII insertion site for donor fluorophore was created using QuikChange II mutagenesis kit (Stratagene), using the forward (5'-CAAGATCCGCAAGCTGGACGTCAGCGGCGGCTTCTACATC) and reverse (5'-GATGTAGAAGCCGCCGCTGACGTCCAGCTTGCGGATCTTG) primers. The mCFP cDNA was PCR amplified from a source vector (gift from Professor Cerny; PrF UK, Czech Republic) using the forward (5'-GACGTCGGAAGCGGAGGTAGTGGTGGAATGGTGAGCAAGGGCG) and reverse (5'-GACGTCACCTCCACTGCCGCTACCACTTCCGCCGAGAGTGATCCCG) primers, both included sequence coding for the linker peptides (underlined), and cloned into AatII site in the Src cDNA. The mCit cDNA was PCR amplified from a source vector (gift from Professor Cerny) using the forward primer (5'-GAATTCGGTGGCAGTGGAGGGATGGTGAGCAAGGGCG; underlined sequence coding for the linker peptide) and reverse primer (5'-GAATTCCTACTTGTACAGCTCGTCCATGC), and cloned into EcoRI site in the Src cDNA. To generated mutated versions of the Src-FRET biosensor, the resulted Src-FRET biosensor was first cloned into pBlueScript SK+ using BamHI/NotI restriction sites and was subsequently mutagenize using QuikChange II mutagenesis kit (Stratagene). The primers used for the mutagenesis were as follows: for Tyr527 to Phe (forward: 5'-CGACAGAGCCCCAGTTCCAGCCTGGAGAGAAC, reverse: 5'-GTTCTCTCCAGGCTGGAAGTGGGGCTCTGTCTG), for RT loop mutagenesis (forward: 5'-TCCTGGATTGAAACGGACTTGTCTTC, reverse: 5'-CTCGTAGTCGTAGAGAGCCAC), for n-Src loop mutagenesis (forward: 5'-GAAGGTAAGTGGTGGCTGGCTCATT, reverse: 5'-CGTGTGTTGACAATCTGCAGGC), for CD linker mutagenesis (forward: 5'-GTCCGGCGACCAGACCCAGGGACTCG, reverse: 5'-GTGGGGCAGACGTTGGTCTAG), for kinase domain mutagenesis (forward: 5'-GTGGGGAGGATGAACTACGTGCACC, reverse: 5'-ATAGGCCATGCCGGATGCAATC). The resulted Src-FRET biosensors variants were cloned to expression pRESpuro3 and pMSCV

puro vectors using BamHI/NotI and BamHI/EcoRV restriction sites, respectively. The mTurquoise2 cDNA with linkers and AatII cloning sites, corresponding to mCFP sequence in the Src-FRET biosensor, was prepared by DNA synthesis (GeneArt, Life Technologies) and after digestion with AatII it was cloned to replace mCFP in the AatII site of Src-FRET constructs. For FRET positive control constructs, both mCFP and mTurquoise2 were PCR amplified from corresponding Src-FRET constructs using the same set of primers (forward: 5'-GAATTCCACCATGGTGAGCAAGGGCG, reverse 5'-GGATCCAGATCTGAGTCGGACTTGTACAGCTCGTCCATGC) and cloned into EcoRI/BamHI sites of pRESpuro3. The mCit was PCR amplified using the forward (5'- GGATCCATGGTGAGCAAGGGCG) and reverse (5'- GCGGCCGCCTTGTACAGCTCGTCCATGC) primers and cloned into BamHI/NotI sites next to the inserted mCFP or mTurquoise2.

To generate mCherry-FAT construct, FAT domain of mouse FAK PCR amplified from a source vector (Fonseca et al., 2004) using the forward primer (5'- GGATCCATGGGTGCAAGCTTCAGCC) and reverse (5'- AGATCTGTGTGGCCGTGTCTGC), and cloned in frame to BglII site in pmCherry-C1 vector.

All the constructs were verified by sequencing.

Immunoblotting

Subconfluent cells were washed on ice with 1 x PBS and lysed, using RIPA buffer (0.15M NaCl; 50mM Tris-HCl, pH 7.4; 1% Nonidet P-40; 0.1% SDS; 1% sodium deoxycholate; 5mM EDTA; 50mM NaF). Protein concentration of lysates were determined by using the DC Protein Assay (Bio-Rad). Protein lysates were diluted in Laemmli sample buffer (0.35M Tris-HCl, pH 6.8; 10% SDS, 40% glycerol; 0.012% bromophenol blue) with 1mM DTT. Protein samples were separated on 10% SDS-polyacrylamide gels and transferred onto nitrocellulose membranes. The membranes were usually cut after the transfer to enable probing for up to 3 proteins of different molecular mass (e.g. 1-2 proteins of interest and a loading control). Membranes were then blocked in Tris-buffered saline, containing 5% non-fat dry milk (or 4% bovine serum albumin depending on the antibody) for 1 h at room temperature to prevent non-specific activity. After blocking, membranes were incubated overnight at 4°C with a primary antibody, washed properly with Tris-buffered saline with 0.1% Tween-20, and incubated for 1 h with a secondary antibody conjugated with horseradish peroxidase. After washing with TTBS, membranes were developed by using the LAS 1000 Single System (Fujifilm).

List of antibodies

Src (monoclonal, Invitrogen, cat. no. AH01152), Src pY418 (polyclonal, Sigma, cat. no. S1940), p130Cas (monoclonal, BD Transduction Laboratories, cat. no. 610272), p130Cas pY410 (polyclonal, Cell Signaling, cat. no. 4011), paxillin (monoclonal, BD Transduction Laboratories, cat. no. 610051), paxillin pY118 (polyclonal, Cell Signaling, cat. no. 2541), vinculin (monoclonal, Sigma, cat. no. V9131).

Kinase assay

Kinase activity of Src variants was measured using Omnia® Y Peptide 2 Kit (ThermoFisher Scientific). The assay is based on detection of fluorescence increase after kinase-specific substrate phosphorylation. Specifically, substrate peptide is attached to the

chelation-enhanced fluorophore Sox. Upon phosphorylation of the peptide by the kinase, Mg^{2+} is chelated to form a bridge between the Sox moiety and the incorporated phosphate group on the tyrosine within the substrate peptide, which consequently causes increase in fluorescence. Kinase assays were performed according to the manufacturer's protocol. Briefly, cells were washed with PBS and lysed in HEPES-Triton buffer (50mM HEPES, pH 7.4; 1% Triton X-100, 1mM DTT, 6mM $MgCl_2$, 6mM $MnCl_2$, protease inhibitors, phosphatase inhibitors). Lysates were clarified by centrifugation. Kinase reactions (in quadruplicates for each variant) was assembled by adding cell lysate, kinase reaction buffer, 0.2mM DTT, 1mM ATP and 10 μ M peptide substrate. Using plate reader (TECAN 200Pro), reactions were incubated at 30 °C and fluorescence intensity was measured (λ_{ex} 360 \pm 10 nm / λ_{em} 485 \pm 20 nm) at 60 second intervals for 1 hour. The slope of fluorescence intensity increase was determined and normalized to amount of Src construct in a sample (mCit signal, 500/530 nm).

Cell stretching

Cell stretching experiments were carried out on 10 cm² stretchable PDMS chambers (STREX Inc.). The substrates of chambers were coated with 5 μ g/ml fibronectin (Invitrogen). Cells were seeded on fibronectin-coated substrates and cultured overnight at 37°C with 5% CO₂. Uniaxial static stretching was performed in the incubator under regular cell culture conditions, using a manual stretcher (STREX Inc.). Cells were stretched for various time intervals (0 min, 5 min, 15 min, 20 min, 30 min, 45 min and 60 min) at an amplitude of 20 % and then immediately lysed in Tris-buffered saline with 1% tritonX-100 with protease and phosphatase inhibitors (SERVA). The lysis buffer has been used as a reference for FRET measurements. The lysate was split in two parts, one was immediately used for FRET measurement, second for immunoblot analysis after adding Laemmli sample buffer (0.35M Tris-HCl, pH 6.8; 10% SDS, 40% glycerol; 0.012% bromophenol blue) with 1mM DTT.

FRET steady state analysis

Cells expressing the biosensor variants were treated for 10 min with 10 μ M LPA (after overnight serum starvation), 24 hours with 100 ng/ml EGF (after overnight serum starvation), 60min with either 500 μ M Sodium Orthovanadate, 100nM dasatinib (LC Laboratories), 4 μ M saractinib (BioVision), 1 μ M bosutinib (LC Laboratories), 100nM UM-164 (Sigma), or 10 μ M SKI-1 (Abcam). After the treatment cells were lysed in HEPES-Triton buffer (50mM HEPES, pH 7.4; 1% Triton X-100, 1mM DTT, 6mM $MgCl_2$, 6mM $MnCl_2$, protease inhibitors, phosphatase inhibitors, 100 μ M ATP), and the FRET signal of each sample was determined using a Varioskan Flash (Fig. 2; Thermo Scientific) or Tecan 200Pro (all spectral scanning and direct FRET data except Fig. 2; PTI, Edison, NJ) spectral scanning fluorescence plate readers. To record FRET fluorescence spectra, the cell lysates were excited at an excitation wavelength of mCFP (433 \pm 5 nm Varioskan Flash, 433 nm \pm 10 nm Tecan 200Pro) and the fluorescence emission spectra 460-580 nm was recorded (in 5 nm or 2 nm steps for Varioskan Flash and Tecan 200Pro, respectively). For FRET ratio determination, after background subtraction, emission ratios of mCit (525 \pm 12 nm Varioskan Flash, 530 \pm 20 nm Tecan 200Pro) and mCFP (475 \pm 12 nm Varioskan Flash, 480 \pm 20 nm Tecan 200Pro) were calculated. In samples with bosutinib, bosutinib autofluorescence was subtracted by calculating the difference in

fluorescence intensities between the cell lysates of bosutinib-treated cells expressing and not expressing SrcFRET biosensor.

For FRET analysis in cell lysates after stretch, the fluorescence spectra could not be reliably recorded due to low amount of sample material and, as a consequence, low fluorescence intensities in the spectral mode measurements. Instead, FRET was measured as a ratio of FRET fluorescence intensity ($\lambda_{\text{ex}} 433 \pm 9 \text{ nm}$, $\lambda_{\text{em}} 530 \pm 20 \text{ nm}$) and the fluorescence intensity of mCFP ($\lambda_{\text{ex}} 433 \pm 9 \text{ nm}$, $\lambda_{\text{em}} 480 \pm 20 \text{ nm}$). In order to compare in-between independent experiments, the data were normalized with respect to the FRET ratio of unstretched cells which was arbitrary set to 1. In all FRET steady state measurements, the gating for each experimental cohort was set to same value, which was computed from sample with the highest fluorescence intensity within the cohort.

Fluorescence microscopy

Cell immunostaining and confocal microscopy

Cells were seeded on coverslips coated with 10 $\mu\text{g}/\text{ml}$ fibronectin (Invitrogen) and grown for 12 - 24 h. Subsequently, the cells were fixed in 4% paraformaldehyde, permeabilized using 0.3% Triton X-100, washed with PBS and blocked in 3% bovine serum albumin in PBS. Samples were then sequentially incubated with primary antibodies for 3 h, secondary antibodies for 1 h, phalloidin for 15 min, and extensively washed with PBS between each step. The slides were mounted in Mowiol 4–88 (Millipore) containing 1,4-diazobicyclo-[2.2.2]-octane (Sigma). The secondary antibodies were anti-rabbit-IgG Alexa Fluor 546 and anti-mouse-IgG Alexa Fluor 633 (Invitrogen). F-actin was probed with phalloidin conjugated with Alexa Fluor 405 (Dyomics) or Alexa Fluor 555 (Life Technologies). Images were acquired using Leica TCS SP8 microscope system equipped with a Leica 63 \times / 1.45 NA oil objective.

FRET sensitized emission analysis

U2OS cells were transiently co-transfected with the Src-FRET(T) biosensor and mCherry-FAT or mCherry-vinculin using polyethylenimine transfection agents (Sigma). Prior imaging the cells were trypsinized and allowed to attach on 35 mm dishes with glass bottom coated with fibronectin (MatTek, MA) and imaged in a window 30-60 min after seeding. FRET experiments were performed using Nikon Ti-E microscope with Nikon CFI HP Apo TIRF 100 \times Oil, NA 1.49. The microscope was equipped with two cameras, Andor iXon Ultra DU897 (Andor Technologies, UK) for acquisition of images excited with 445 nm and 488 nm laser beams, and Hamamatsu ORCA 4.0 V2 (Hamamatsu Photonics, Japan) for acquisition of images excited with 561 nm laser beam. Image splitter (DualView DV2, Photometrics, AZ) with filter cube splitting the beam at 505 nm was inserted in the light path preceding the Andor camera. Obtained dual images were processed using ImageJ. FRET, corrected for spectral bleed-throughs and normalized to donor fluorescence, was calculated as nF/I_{CFP} according to (Xia and Liu, 2001) in ImageJ using PixFRET plug-in (Feige et al., 2005).

Fluorescence recovery after photobleaching (FRAP)

U2OS cells were transiently co-transfected with the Src-FRET(T) biosensor and mCherry-vinculin using polyethylenimine transfection agents (Sigma). Prior imaging the cells were trypsinized and allowed to attach for 4 hours on 35 mm dishes with glass bottom coated with fibronectin (MatTek, MA). FRAP experiments were performed using Leica SP8 confocal microscope with a 63 \times /1.45 NA oil immersion objective. White light

laser set to 512 nm was used to excite mCit and to 584 nm to excite mCherry. The focal adhesion was detected according to mCherry-FAT signal and in the selected focal adhesion the mCit signal was bleached using a high energy beam. The image acquisition started 5 s before bleaching and continued for approximately 30 s (one frame every 1.301 s). The recovery curves of the bleached regions were calculated from extracted image series using LAS X software (Leica), and the recovery halftime values were calculated from the FRAP curves by nonlinear regression analysis as described in (Tolde et al., 2012).

Quantification and statistical analysis

All the data were presented as mean \pm standard deviation or \pm standard error from at least three independent experiments. The significance of differences was analyzed with one-way ANOVA followed by Tukey's honest significant difference test using GraphPad Prism software (version 6.07, GraphPad Software Inc.). Statistical significance was defined as $p < 0.05$. FRAP data fitting was performed in Excel using Solver add-in (Microsoft).

ACKNOWLEDGMENTS

We gratefully acknowledge Dr. Xuehua Xu and Dr. Joseph Brzostowski for help with FRET sensitized emission protocol, Dr. Tomas Vomastek for gift of SYF, HEK293FT and U2OS cell lines and Dr. Katerina Kuzelova for gift of SKI-1 inhibitor. This work was funded by Czech Science Foundation grant 15 07321S, by the Ministry of Education, Youth and Sports of CR within the LQ1604 National Sustainability Program II (Project BIOCEV FAR) and by the project „BIOCEV“ (CZ.1.05/1.1.00/02.0109). We acknowledge the IMCF at BIOCEV, institution supported by the MEYS CR (LM2015062 Czech Bioluminescence Imaging). Part of the study was performed by the equipment for metabolomics and cell analyses (Grant no. CZ.1.05/2.1.00/19.0400) supported by the Research and Development for Innovations Operational Program, co-financed by the European regional development fund and the state budget of the Czech Republic.

AUTHOR CONTRIBUTIONS

LK, ACP performed most of the experiments and analyzed the results. OT performed the FRET imaging experiments. VP performed the original cloning and analyses in HEK cells. JG, MN analyzed the results. DR, JB, and KA conceived the experiments and wrote the manuscript. All authors reviewed the manuscript.

DECLARATION OF INTERESTS

Daniel Rosel and Jan Brabek have filed Czech Republic patent application on the SrcFRET biosensor. The authors have no other financial or non-financial competing interests.

REFERENCES

- Alexandropoulos,K. and Baltimore,D. (1996). Coordinate activation of c-Src by SH3- and SH2-binding sites on a novel p130Cas-related protein, Sin. *Genes Dev.* *10*, 1341-1355.
- Bjorge,J.D., Bellagamba,C., Cheng,H.C., Tanaka,A., Wang,J.H., and Fujita,D.J. (1995). Characterization of two activated mutants of human pp60c-src that escape c-Src kinase regulation by distinct mechanisms. *J. Biol. Chem.* *270*, 24222-24228.
- Boerner,R.J., Kassel,D.B., Barker,S.C., Ellis,B., DeLacy,P., and Knight,W.B. (1996). Correlation of the phosphorylation states of pp60c-src with tyrosine kinase activity: the intramolecular pY530-SH2 complex retains significant activity if Y419 is phosphorylated. *Biochemistry* *35*, 9519-9525.
- Brabek,J., Mojzita,D., Novotny,M., Puta,F., and Folk,P. (2002). The SH3 domain of Src can downregulate its kinase activity in the absence of the SH2 domain-pY527 interaction. *Biochem. Biophys. Res. Commun.* *296*, 664-670.
- Branis,J., Pataki,C., Sporrer,M., Gerum,R.C., Mainka,A., Cermak,V., Goldmann,W.H., Fabry,B., Brabek,J., and Rosel,D. (2017). The role of focal adhesion anchoring domains of CAS in mechanotransduction. *Sci. Rep.* *7*, 46233.
- Cooper,J.A., Gould,K.L., Cartwright,C.A., and Hunter,T. (1986). Tyr527 is phosphorylated in pp60c-src: implications for regulation. *Science* *231*, 1431-1434.
- Cowan-Jacob,S.W., Fendrich,G., Manley,P.W., Jahnke,W., Fabbro,D., Liebetanz,J., and Meyer,T. (2005). The crystal structure of a c-Src complex in an active conformation suggests possible steps in c-Src activation. *Structure.* *13*, 861-871.
- Dar,A.C. and Shokat,K.M. (2011). The evolution of protein kinase inhibitors from antagonists to agonists of cellular signaling. *Annu. Rev. Biochem.* *80*, 769-795.
- Feige,J.N., Sage,D., Wahli,W., Desvergne,B., and Gelman,L. (2005). PixFRET, an ImageJ plug-in for FRET calculation that can accommodate variations in spectral bleed-throughs. *Microsc. Res. Tech.* *68*, 51-58.
- Fincham,V.J. and Frame,M.C. (1998). The catalytic activity of Src is dispensable for translocation to focal adhesions but controls the turnover of these structures during cell motility. *EMBO J.* *17*, 81-92.
- Fonseca,P.M., Shin,N.Y., Brabek,J., Ryzhova,L., Wu,J., and Hanks,S.K. (2004). Regulation and localization of CAS substrate domain tyrosine phosphorylation. *Cell Signal.* *16*, 621-629.
- Frame,M.C., Fincham,V.J., Carragher,N.O., and Wyke,J.A. (2002). v-Src's hold over actin and cell adhesions. *Nat. Rev. Mol. Cell Biol.* *3*, 233-245.

- Gemperle,J., Hexnerova,R., Lepsik,M., Tesina,P., Dibus,M., Novotny,M., Brabek,J., Veverka,V., and Rosel,D. (2017). Structural characterization of CAS SH3 domain selectivity and regulation reveals new CAS interaction partners. *Sci. Rep.* 7, 8057.
- Giaccone,G. and Zucali,P.A. (2008). Src as a potential therapeutic target in non-small-cell lung cancer. *Ann. Oncol.* 19, 1219-1223.
- Goedhart,J., von,S.D., Noirclerc-Savoie,M., Lelimosin,M., Joosen,L., Hink,M.A., van,W.L., Gadella,T.W., Jr., and Royant,A. (2012). Structure-guided evolution of cyan fluorescent proteins towards a quantum yield of 93%. *Nat. Commun.* 3, 751.
- Gonfloni,S., Williams,J.C., Hattula,K., Weijland,A., Wierenga,R.K., and Superti-Furga,G. (1997). The role of the linker between the SH2 domain and catalytic domain in the regulation and function of Src. *EMBO J.* 16, 7261-7271.
- Gulyani,A., Vitriol,E., Allen,R., Wu,J., Gremyachinskiy,D., Lewis,S., Dewar,B., Graves,L.M., Kay,B.K., Kuhlman,B., Elston,T., and Hahn,K.M. (2011). A biosensor generated via high-throughput screening quantifies cell edge Src dynamics. *Nat. Chem. Biol.* 7, 437-444.
- Irby,R.B. and Yeatman,T.J. (2000). Role of Src expression and activation in human cancer. *Oncogene* 19, 5636-5642.
- Irtegun,S., Wood,R., Lackovic,K., Schweiggert,J., Ramdzan,Y.M., Huang,D.C., Mulhern,T.D., and Hatters,D.M. (2014). A biosensor of SRC family kinase conformation by exposable tetracysteine useful for cell-based screening. *ACS Chem. Biol.* 9, 1426-1431.
- Janostiak,R., Brabek,J., Auernheimer,V., Tatarova,Z., Lautscham,L.A., Dey,T., Gemperle,J., Merkel,R., Goldmann,W.H., Fabry,B., and Rosel,D. (2014a). CAS directly interacts with vinculin to control mechanosensing and focal adhesion dynamics. *Cell Mol. Life Sci.* 71, 727-744.
- Janostiak,R., Pataki,A.C., Brabek,J., and Rosel,D. (2014b). Mechanosensors in integrin signaling: the emerging role of p130Cas. *Eur. J. Cell Biol.* 93, 445-454.
- Janostiak,R., Tolde,O., Bruhova,Z., Novotny,M., Hanks,S.K., Rosel,D., and Brabek,J. (2011). Tyrosine phosphorylation within the SH3 domain regulates CAS subcellular localization, cell migration, and invasiveness. *Mol. Biol. Cell* 22, 4256-4267.
- Klinghoffer,R.A., Sachsenmaier,C., Cooper,J.A., and Soriano,P. (1999). Src family kinases are required for integrin but not PDGFR signal transduction. *EMBO J.* 18, 2459-2471.
- Leonard,S.E., Register,A.C., Krishnamurty,R., Brighty,G.J., and Maly,D.J. (2014). Divergent modulation of Src-family kinase regulatory interactions with ATP-competitive inhibitors. *ACS Chem. Biol.* 9, 1894-1905.
- Luo,W., Janostiak,R., Tolde,O., Ryzhova,L.M., Koudelkova,L., Dibus,M., Brabek,J., Hanks,S.K., and Rosel,D. (2017). ARHGAP42 is activated by Src-mediated tyrosine phosphorylation to promote cell motility. *J. Cell Sci.* 130, 2382-2393.

- Machiyama,H., Yamaguchi,T., Sawada,Y., Watanabe,T.M., and Fujita,H. (2015). SH3 domain of c-Src governs its dynamics at focal adhesions and the cell membrane. *FEBS J.* **282**, 4034-4055.
- Miyazaki,K., Senga,T., Matsuda,S., Tanaka,M., Machida,K., Takenouchi,Y., Nimura,Y., and Hamaguchi,M. (1999). Critical amino acid substitutions in the Src SH3 domain that convert c-Src to be oncogenic. *Biochem. Biophys. Res. Commun.* **263**, 759-764.
- Na,S., Collin,O., Chowdhury,F., Tay,B., Ouyang,M., Wang,Y., and Wang,N. (2008). Rapid signal transduction in living cells is a unique feature of mechanotransduction. *Proc. Natl. Acad. Sci. U. S. A* **105**, 6626-6631.
- Paster,W., Paar,C., Eckerstorfer,P., Jakober,A., Drbal,K., Schutz,G.J., Sonnleitner,A., and Stockinger,H. (2009). Genetically encoded Förster resonance energy transfer sensors for the conformation of the Src family kinase Lck. *J. Immunol.* **182**, 2160-2167.
- Playford,M.P. and Schaller,M.D. (2004). The interplay between Src and integrins in normal and tumor biology. *Oncogene* **23**, 7928-7946.
- Rosel,D., Brabek,J., Vesely,P., and Fernandes,M. (2013). Drugs for solid cancer: the productivity crisis prompts a rethink. *Onco. Targets. Ther.* **6**, 767-777.
- Roskoski,R., Jr. (2016). Classification of small molecule protein kinase inhibitors based upon the structures of their drug-enzyme complexes. *Pharmacol. Res.* **103**, 26-48.
- Ryder,J.W. and Gordon,J.A. (1987). In vivo effect of sodium orthovanadate on pp60c-src kinase. *Mol. Cell Biol.* **7**, 1139-1147.
- Sawada,Y., Tamada,M., Dubin-Thaler,B.J., Cherniavskaya,O., Sakai,R., Tanaka,S., and Sheetz,M.P. (2006). Force sensing by mechanical extension of the Src family kinase substrate p130Cas. *Cell* **127**, 1015-1026.
- Stirnweiss,A., Hartig,R., Gieseler,S., Lindquist,J.A., Reichardt,P., Philipsen,L., Simeoni,L., Poltorak,M., Merten,C., Zuschratter,W., Prokazov,Y., Paster,W., Stockinger,H., Harder,T., Gunzer,M., and Schraven,B. (2013). T cell activation results in conformational changes in the Src family kinase Lck to induce its activation. *Sci. Signal.* **6**, ra13.
- Superti-Furga,G., Fumagalli,S., Koegl,M., Courtneidge,S.A., and Draetta,G. (1993). Csk inhibition of c-Src activity requires both the SH2 and SH3 domains of Src. *EMBO J.* **12**, 2625-2634.
- Teckchandani,A., Laszlo,G.S., Simo,S., Shah,K., Pilling,C., Strait,A.A., and Cooper,J.A. (2014). Cullin 5 destabilizes Cas to inhibit Src-dependent cell transformation. *J. Cell Sci.* **127**, 509-520.
- Ting,A.Y., Kain,K.H., Klemke,R.L., and Tsien,R.Y. (2001). Genetically encoded fluorescent reporters of protein tyrosine kinase activities in living cells. *Proc. Natl. Acad. Sci. U. S. A* **98**, 15003-15008.

- Tolde,O., Rosel,D., Janostiak,R., Vesely,P., and Brabek,J. (2012). Dynamics and morphology of focal adhesions in complex 3D environment. *Folia Biol. (Praha)* 58, 177-184.
- Tong,M., Pelton,J.G., Gill,M.L., Zhang,W., Picart,F., and Seeliger,M.A. (2017). Survey of solution dynamics in Src kinase reveals allosteric cross talk between the ligand binding and regulatory sites. *Nat. Commun.* 8, 2160.
- von Wichert,G., Haimovich,B., Feng,G.S., and Sheetz,M.P. (2003). Force-dependent integrin-cytoskeleton linkage formation requires downregulation of focal complex dynamics by Shp2. *EMBO J.* 22, 5023-5035.
- Wang,Y., Botvinick,E.L., Zhao,Y., Berns,M.W., Usami,S., Tsien,R.Y., and Chien,S. (2005). Visualizing the mechanical activation of Src. *Nature* 434, 1040-1045.
- Wu,Y., Zhang,K., Seong,J., Fan,J., Chien,S., Wang,Y., and Lu,S. (2016). n-situ coupling between kinase activities and protein dynamics within single focal adhesions. *Sci. Rep.* 6, 29377.
- Xia,Z. and Liu,Y. (2001). Reliable and global measurement of fluorescence resonance energy transfer using fluorescence microscopes. *Biophys. J.* 81, 2395-2402.
- Xu,W., Doshi,A., Lei,M., Eck,M.J., and Harrison,S.C. (1999). Crystal structures of c-Src reveal features of its autoinhibitory mechanism. *Mol. Cell* 3, 629-638.
- Xu,W., Harrison,S.C., and Eck,M.J. (1997). Three-dimensional structure of the tyrosine kinase c-Src. *Nature* 385, 595-602.
- Yeatman,T.J. (2004). A renaissance for SRC. *Nat. Rev. Cancer* 4, 470-480.
- Young,M.A., Gonfloni,S., Superti-Furga,G., Roux,B., and Kuriyan,J. (2001). Dynamic coupling between the SH2 and SH3 domains of c-Src and Hck underlies their inactivation by C-terminal tyrosine phosphorylation. *Cell* 105, 115-126.
- Zaidel-Bar,R., Milo,R., Kam,Z., and Geiger,B. (2007). A paxillin tyrosine phosphorylation switch regulates the assembly and form of cell-matrix adhesions. *J. Cell Sci.* 120, 137-148.

5.4. The 4th publication/preprint

Gemperle, J., Dibus, M., Koudelková, L., Rosel, D., Brábek, J.

The interaction of PKN3 with p130Cas promotes malignant growth.

BioRxiv. <https://doi.org/10.1101/334425> (Preprint posted June 29, 2018).

Under revision at Molecular Oncology journal.

The interaction of p130Cas with PKN3 promotes malignant growth

Short title: p130Cas and PKN3 interaction promotes malignancy

Jakub Gemperle, Michal Dibus, Lenka Koudelková, Daniel Rosel, and Jan Brábek

p130Cas and PKN3 interaction promotes malignancy

Department of Cell Biology, Faculty of Science - Biocev, Charles University, 12843 Prague 2, Czech Republic

Correspondence to Jan Brábek: Department of Cell Biology, Faculty of Science - Biocev, Charles University, Vinicna 7, 12843 Prague 2, Czech Republic: jan.brabek@natur.cuni.cz

Abstract

Protein p130Cas constitutes an adaptor protein mainly involved in integrin signaling downstream of Src kinase. Owing to its modular structure, p130Cas acts as a general regulator of cancer cell growth and invasiveness induced by different oncogenes. However, other mechanisms of p130Cas signaling leading to malignant progression are poorly understood. Here, we show a novel interaction of p130Cas with Ser/Thr kinase PKN3, which is implicated in prostate and breast cancer growth downstream of phosphoinositide 3-kinase. This direct interaction is mediated by the p130Cas SH3 domain and the centrally located PKN3 polyproline sequence. PKN3 is the first identified Ser/Thr kinase to bind and phosphorylate p130Cas and to colocalize with p130Cas in cell structures that have a pro-invasive function. Moreover, the PKN3-p130Cas interaction is important for mouse embryonic fibroblast growth and invasiveness independent of Src transformation, indicating a mechanism distinct from that previously characterized for p130Cas. Together, our results suggest that the PKN3-p130Cas complex represents an attractive therapeutic target in late-stage malignancies.

Keywords: PKN3, p130Cas, BCAR1, CAS, Src, SH3

Introduction

p130Cas (Crk associated substrate, CAS) is a molecular scaffold involved in the regulation of several processes, such as cell survival, migration, invasivity, and proliferation in both normal and pathological cells (Cabodi, del Pilar Camacho-Leal, et al., 2010; Tikhmyanova et al., 2010). Owing to its modular structure, p130Cas plays a crucial role in signaling originating from many mutated or amplified oncogenes (Nikonova et al., 2014; Tornillo et al., 2014; Tikhmyanova et al., 2010). It has been reported that knockdown of p130Cas leads to proliferative arrest in breast cancer cell lines carrying oncogenic mutations in *BRAF*, *KRAS*, *PTEN*, or *PIK3CA* (Pylayeva et al., 2009). Moreover, its involvement in Src-mediated tumorigenesis has been clearly demonstrated. For example, Src-transformed mouse embryonic fibroblasts (MEFs) exhibit increased ability to invade through Matrigel and induce metastases in mice in a p130Cas-dependent manner (Honda et al., 1998; Brábek et al., 2004, 2005). Other studies in vivo have shown that p130Cas also drives the growth, aggressiveness, and progression of ErbB2-overexpressing breast tumors, including metastatic colonization of the lungs (Cabodi et al., 2010b, 2006). Correspondingly, elevated expression of p130Cas in human patients is associated with early disease recurrence and poor prognosis in several cancer types, including lung, prostate, pancreas, ovarian, and mammary cancers (Fromont and Cussenot, 2011; Fromont et al., 2007; Defilippi et al., 2006; Nick et al., 2011; Tikhmyanova et al., 2010; Nikonova et al., 2014; Cabodi et al., 2010a) and is associated with hormone deprivation-mediated resistance to anti-tumor drugs (standard therapeutics) such as adriamycin (doxorubicin) and tamoxifen (Ta et al., 2008; Dorssers et al., 2001). Taken together, such evidence clearly underlines a role for p130Cas as a general regulator of cancer cell growth and metastasis as induced by different oncogenes.

The structure of p130Cas consists of an N-terminal SRC homology 3 (SH3) domain, substrate domain (SD), and serine-rich domain (SRD) followed by Src and PI3K binding regions and terminated by a CAS-family C-terminal homology domain (CCH) (Cabodi, del Pilar Camacho-Leal, et al., 2010). The majority of known p130Cas downstream signaling is attributed to tyrosine phosphorylation of a repeated YXXP motif within the p130Cas SD domain (Cabodi et al., 2010a; Defilippi et al., 2006). The level of p130Cas tyrosine phosphorylation is mainly dependent on the binding capacity of its SH3 domain, which facilitates direct interaction of p130Cas with the polyproline motif of various phosphatases (e.g., PTP1B, PTP-PEST) and kinases (FAK, PYK2) or mediates indirect association with Src via a FAK (PYK2) bridge (Fonseca et al., 2004; Ruest et al., 2001; Astier et al., 1997). Specifically, association of p130Cas via the p130Cas SH3 domain with FAK and Src at focal adhesions transmits signals that induce lamellipodia and cell migration, support cell proliferation and cell invasiveness, and block anoikis (Donato et al., 2010; Tazaki et al., 2008; Ruest et al., 2001; Nikonova et al., 2014; Defilippi et al., 2006; Brábek et al., 2005). p130Cas has also been shown to be phosphorylated at serine residues, which correlates with an invasive cell phenotype and is partially dependent on the p130Cas SH3 domain; however, responsible serine/threonine kinases have not yet been identified (Makkinje et al., 2009). In addition, p130Cas has been shown to interact with 14-3-3 proteins in a phosphoserine-dependent manner, which occurs mainly at

lamellipodia during integrin-mediated cell attachment to the extracellular matrix (ECM) (Garcia-Guzman et al., 1999).

In a screen for new interaction partners of the p130Cas SH3 domain, we recently predicted a list of candidates and verified p130Cas SH3 binding to the polyproline motifs of GLIS2 and DOK7 (Gemperle et al., 2017). Among other predicted candidates, serine/threonine PKN3 kinase, with the polyproline motif P₅₀₀PPKPPRL, constitutes a member of the PKN family, which is part of the protein kinase C (PKC) superfamily of serine/threonine kinases. The role of PKN3 in tumorigenesis was identified in early reports, which showed that *PKN3* mRNA is scarce in normal human adult tissues but abundantly expressed in numerous cancer cell lines (Oishi et al., 1999). In contrast, the other members of the PKN family, PKN1 and PKN2, exhibit ubiquitous expression in human and rat tissues (Hashimoto et al., 1998; Mukai and Ono, 1994; Quilliam et al., 1996). PKN3, but not PKN1 or PKN2, has been shown to regulate malignant prostate cell growth downstream of activated phosphoinositide 3-kinase (PI3K) independent of Akt (Leenders et al., 2004) and, moreover, only PKN3 possess the polyproline sequence in its central portion that we have predicted as a potential p130Cas SH3 domain binding site (Gemperle et al., 2017). In addition, when stimulated in a fatty-acid dependent manner, the catalytic activity of PKN3 was less responsive in comparison to PKN1 and PKN2, thereby highlighting the differences in function of PKN isoforms, as well as their regulation (Oishi et al., 1999).

Using orthotopic mouse tumor models, the effect of PKN3 on cancer growth was shown by conditional reduction of PKN3 expression in tumors. In all cases, downregulation of PKN3 protein impaired primary prostate and breast tumor growth and blocked metastasis (Unsal-Kacmaz et al., 2011; Leenders et al., 2004). Correspondingly, overexpression of exogenous PKN3 in breast cancer cells further increased their malignant behavior in vitro (Unsal-Kacmaz et al., 2011). Although PKN3 KO mice appeared indistinguishable from their WT counterparts, this model also indicated the role of host stromal PKN3 in tumor progression (Mukai et al., 2016). Stromal PKN3 is enriched in primary endothelial cells as well as in osteoclasts (Uehara et al., 2017), being apart from tumor cells among the few normal cell types with significant amount of PKN3; this is consistent with the usually invasive features of endothelial cells in particular (Aleku et al., 2008). Accordingly, systemic administration of siRNA-lipoplex (Atu027) directed against PKN3 and targeting mainly the stromal compartment rather than the pathologically defined tumor entity, prevented lung metastasis in lung experimental and spontaneous breast metastasis models in a dose-dependent manner (Santel et al., 2010).

In mammalian tissues, the PKN family underlies some of the main Rho GTPase-associated protein kinase activities (Mellor et al., 1998; Vincent and Settleman, 1997; Lim et al., 2008). Specifically, Unsal-Kacmaz et al. demonstrated that PKN3 physically interacts with Rho-family GTPases, and preferentially with RhoC, a known mediator of tumor invasion and metastasis in epithelial cancers (Unsal-Kacmaz et al., 2011). However, additional molecular mechanisms by which PKN3 contributes to malignant growth and tumorigenesis are not well understood.

In this study, we have shown that PKN3 directly interacts with p130Cas and phosphorylates it in vitro and potentially in vivo. Furthermore, we have demonstrated the

importance of the PKN3–p130Cas interaction for PKN3-stimulated cell growth and invasiveness in vitro and tumor growth in vivo.

Results

p130Cas directly interacts with PKN3

To confirm the predicted PKN3-p130Cas interaction, we first analyzed the potential of p130Cas SH3 domain variants to pull-down PKN3. The scheme of p130Cas and PKN3 mutagenesis is shown in Fig. 1 A. As predicted, only the p130Cas SH3 WT, but not phosphomimicking mutant variant (Y12E), showed strong association with PKN3 WT. Correspondingly, p130Cas SH3 WT was not able to effectively pull-down a PKN3 variant in which the target polyproline motif was mutated to P₅₀₀APSAPRL (PKN3 mPR; Fig. 1 B; 10–50× decrease compared to WT; $p = 0.003$). Notably, a kinase-inactivating mutation in the catalytic domain of mouse PKN3 (KD; K577E; Figs. 1 A and S1 A) also caused significant decrease (4–20×; $p = 0.007$) of PKN3–p130Cas SH3 interaction (Fig. 1 B). Subsequently, we confirmed p130Cas - PKN3 interaction using co-immunoprecipitation analysis. We demonstrated that PKN3 co-precipitates with immunoprecipitated GFP-p130Cas WT and the non-phosphorylatable mutant (Y12F) (Fig. 1 C), but not with the phosphomimicking mutant (Y12E), and that p130Cas co-precipitates strongly with immunoprecipitated PKN3 WT, less with PKN3 KD, and almost not at all with PKN3 mPR (Fig. 1 D). Finally, using far-western experiments, we confirmed that the p130Cas-PKN3 interaction is direct (Fig. 1, E and F).

PKN3 colocalizes with p130Cas in lamellipodia and podosome rosettes

To further assess the p130Cas-PKN3 interaction, we analyzed the co-localization of p130Cas and PKN3 in cells. Specifically, we analyzed the dynamic localization of p130Cas and PKN3 in p130Cas^{-/-} MEFs co-expressing GFP-p130Cas, variants of mCherry-PKN3, and CFP-LifeAct. We found that both p130Cas and PKN3 were enriched in lamellipodia of MEFs (Fig. 2 A; Movies S1 and 2). Localization of the PKN3-mPR mutant to lamellipodia was slightly but significantly impaired (Fig. 2, A and B), suggesting that the polyproline sequence of PKN3 is important for its targeting to lamellipodia. However, cells expressing GFP-Flag-PKN3 KD exhibited more pronounced filopodia-like protrusions and the presence of lamellipodia was extremely rare compared to that in cells expressing other variants of PKN3, preventing quantification of PKN3 membrane localization (Fig. S1 B and Movie S3).

PKN3 has been recently shown to localize to specific actin-rich structures termed podosome rings and belts in osteoclasts (Uehara et al., 2017). Formation of similar structures, termed podosome rosettes, can be induced in MEFs when transformed by activated Src (SrcF) (Tarone et al., 1985). Notably, p130Cas was shown to be critical for their formation (Brábek et al., 2004). To investigate whether PKN3 localizes to podosome rosettes, we expressed the Flag-PKN3 variants in SrcF-transformed p130Cas^{-/-} MEFs re-expressing p130Cas (SC cells) and analyzed their localization using confocal microscopy on fixed cells. Both PKN3 WT and mPR were enriched in podosome rosettes

and co-localized there along with p130Cas and actin, suggesting that p130Cas is not responsible for PKN3 targeting to podosome rosettes (Fig. 2 C).

PKN3 activity is important for stress fiber formation

In live cell imaging/microscopy experiments, we noticed temporary co-localization of GFP-PKN3 WT or mPR with stress fibers (mCherry-LifeAct) (Fig. S1, B and C). As PKN3 downregulation in HUVEC cells leads to disruption of stress fiber formation (Möpert et al., 2012) and p130Cas expression has been previously shown to affect stress fiber morphology (Honda et al., 1998), we analyzed the importance of PKN3 activity and interaction with p130Cas on stress fiber formation. Therefore, we co-transfected p130Cas-GFP WT and mCherry-Flag-fused PKN3 variants (WT, mPR, KD) or mCherry to p130Cas^{-/-} MEFs (Fig. 3 A). Cells expressing PKN3 WT or mPR displayed prominent stress fibers, suggesting that interaction between p130Cas and PKN3 is not important for stress fiber formation. In contrast, transfection of cells by PKN3 KD greatly reduced stress fiber formation, instead inducing cortical localization of F-actin (Fig. 3 A).

p130Cas stimulates PKN3 kinase phosphorylation on Thr849 independently of p130Cas-PKN3 interaction

It has previously been shown that PKN3 turn motif site phosphorylation (human Thr860, homologous to mouse Thr849) correlates with PKN3 activity and that active PKN3 is predominantly localized in the nucleus (Unsal-Kacmaz et al., 2011; Leenders et al., 2004). To determine whether p130Cas influences PKN3 activation we analyzed the activity of endogenous mouse PKN3 using an anti-pThr849 antibody in the presence or absence of p130Cas protein. PKN3 phosphorylation on Thr849 was lower in p130Cas^{-/-} MEFs than in p130Cas^{-/-} MEFs re-expressing p130Cas or transfected by GFP-p130Cas (Fig. 3, B and C). Expression of the Y12E variant of GFP-p130Cas, which does not bind PKN3, also increased Thr849 phosphorylation of PKN3. Consistent with these findings, the PKN3 mPR mutant, which is unable to bind p130Cas, did not differ with regard to pThr849 phosphorylation status from PKN3 WT (Fig. 3, D and E). Notably, however, Thr849 phosphorylation was not increased by expression of GFP-p130Cas without the CCH domain (dCCH) (Figs. 3 A and B, and S2 D). PKN3 KD, used as a negative control for anti-pThr849 antibody specificity, was not phosphorylated, as expected (Fig. 3 D). Taken together, the data suggest that p130Cas expression induces PKN3 activation and this activation is independent of p130Cas-PKN3 interaction.

p130Cas-PKN3 co-expression and p130Cas Ser428(432) and PKN3 Thr860 phosphorylation are positively correlated in human breast (prostate) tumors

Previous studies showed positive correlation between PKN3 or p130Cas/BCAR1 protein levels and cancer progression in patients with breast or prostate cancer (Strumberg et al., 2012; Schultheis et al., 2014; Dorssers et al., 2004; Leenders et al., 2004; Oishi et al., 1999; Nikonova et al., 2014; Fromont and Cussenot, 2011). To test the assumed link between PKN3 and p130Cas signaling, we further performed cross-correlation analysis of publicly available transcriptomic data using the cBio Cancer Genomics Portal (cbioportal.org) (Gao et al., 2013). We focused on invasive breast carcinoma (1100

tumors in TCGA, provisional) and prostate adenocarcinoma studies (499 tumors, TCGA, provisional). Within these sets of RNA-Seq data, we evaluated the mRNA expression of PKN3 and p130Cas/BCAR1 and ran correlation statistical analysis (Fig. 4, A-C). This analysis showed that elevated expression of *PKN3* significantly positively correlates with the elevated expression of p130Cas/BCAR1 and vice versa in both patients with breast cancer and those with prostate cancer (Figs. 4 A and S2 A). Similarly, the level of p130Cas/BCAR1 expression increased with the level of Src kinase, signaling through which is highly associated with p130Cas/BCAR1 (Brábek et al., 2004; Fonseca et al., 2004; Figs. 4 B and S2 B). In contrast, expression of *PKN2*, which does not possess a p130Cas interaction site and therefore does not suggest crosstalk with the p130Cas/BCAR1 signaling circuit, had negative correlation to mRNA levels of p130Cas/BCAR1 (Figs. 4 C and S2 C and D).

In parallel, we analyzed the available data on protein phosphorylation levels of PKN3 and p130Cas/BCAR1 (Clinical Proteomic Tumor Analysis Consortium (CPTAC), MS analysis of 34 invasive breast carcinoma tumors). Statistical analysis revealed that phosphorylation of PKN3 at Thr860 (homologous to mouse Thr849), which reflects PKN3 activity, and p130Cas/BCAR1 at Ser428 (conserved homolog to mouse Ser432 and shown in cBioportal analysis as p130Cas/BCAR1 Ser474) exhibits strong positive correlation (Pearson test 0.42, *p* value 0.0134; Spearman test 0.434, *p* value 0.0106; Fig. 4 D). Taken together, the cross-correlation analysis of the transcriptomic and phosphoproteomic data showed a positive correlation between PKN3 and p130Cas/BCAR1 expression in invasive breast carcinoma and prostate adenocarcinoma tumors, and positive correlation between PKN3 activity and the level of p130Cas/BCAR1 phosphorylation on Ser428 in invasive breast carcinoma tumors.

PKN3 phosphorylates mouse p130Cas on Ser432

p130Cas has also been previously reported to undergo serine phosphorylation under various conditions; e.g., during mitosis or cell adhesion. However the kinase responsible for the phosphorylation has not yet been identified (Garcia-Guzman et al., 1999; Makkinje et al., 2009; Yamakita et al., 1999). Our cross-correlation analysis of the transcriptomic and phosphoproteomic data showed that phosphorylation of human p130Cas/BCAR1 on Ser428 correlates with increased PKN3 activity, indicating that PKN3 might be responsible for this phosphorylation. Human Ser428 of p130Cas/BCAR1 corresponds to mouse p130Cas Ser432, which has conserved surrounding sequence (KRLSA) and fits well to the known PKN3 phosphorylation motif (Collazos et al., 2011). As for the majority of p130Cas potential Ser/Thr phosphorylation sites, Ser432 is localized in the p130Cas SRD domain. To test the assumed ability of PKN3 to phosphorylate p130Cas, we prepared a GFP-fused p130Cas mutant for Ser432 (S432A) and p130Cas mutated in SRD in such a manner that all 15 Ser/Thr sites were substituted with Ala or Asn (15AN). The substitution of several Ser/Thr to Asn, instead of more common substitution to Ala, was used with the aim to preserve the helical structure of the SRD. To determine whether PKN3 could phosphorylate p130Cas in the SRD domain we performed kinase assays in vitro with precipitated Strep-Flag-PKN3 and newly prepared GFP-p130Cas variants (WT, 15AN, and S432A) in the presence of ATP γ S followed by

detection with a specific antibody against anti-thiophosphate ester (Fig. 4 E). GFP-p130Cas WT exhibited the highest thiophosphorylation compared to GFP-p130Cas 15AN and Ser432, which were thiophosphorylated to a similar extent. Partial thiophosphorylation of GFP-p130Cas 15AN indicated that PKN3 could phosphorylate p130Cas also outside SRD domain (Fig. 4 A). Notably, PKN3 autophosphorylation was also observed (Fig. S2 E). These results verified the presence of a PKN3 phosphorylation motif in the sequence surrounding Ser432 and indicated that PKN3 phosphorylates p130Cas on Ser432 *in vitro*.

Protein p130Cas, similarly to Nedd9 (another member of the p130Cas family; HEF1), exists in cells in two main isoforms, which are attributed to different Ser/Thr phosphorylation (Hivert et al., 2009; Makkinje et al., 2009). Depending on the cell type, p130Cas protein is present upon SDS-PAGE as a single protein or detected as a doublet with the increased proportional representation of the upper band correlating with cell aggressive properties (Janoštiak et al., 2011; Makkinje et al., 2009). To test the biological relevance of p130Cas Ser432 phosphorylation in cells, we prepared lysates from p130Cas^{-/-} MEFs with reintroduced GFP-p130Cas mutants with or without overexpression of mCherry-PKN3 WT and examined the p130Cas migration profile after separation on SDS-PAGE using an acrylamide/bisacrylamide ratio of 30:0.2 (Fig. 4 F), which improves the separation of Ser/Thr phosphorylation-induced gel shifts, similarly to Hivert et al. (Hivert et al., 2009). GFP-p130Cas WT migrated as 4 bands with the most pronounced form migrating the slowest. GFP-p130Cas Y12E displayed a shift of the p130Cas protein content from the slowest migrating band toward faster migrating forms. In comparison, the 15 Ser/Thr mutations (15AN) migrated only in the form of two faster bands, similarly to the single mutation of Ser432 (S432A mutant), and was not changed by PKN3 overexpression (Fig. 4 F). Furthermore, GFP-p130Cas without the CCH domain also migrated in the form of two faster bands. We concluded that p130Cas SH3 and CCH domains are important for p130Cas Ser/Thr phosphorylation and that the presence of the slowest migration form of p130Cas is associated with Ser432 phosphorylation. However, we failed to promote a switch of the slower migrating p130Cas (WT) isoform to faster ones by serum starvation (Fig. 4 F) or by maintaining the cells in suspension (Fig. S2 F); therefore, we could not demonstrate the change of p130Cas WT SDS-PAGE migration pattern by PKN3 overexpression.

PKN3 overexpression regulates the growth of MEFs in a PKN3–p130Cas interaction-dependent manner

Both PKN3 and p130Cas have been implicated in the regulation of malignant cell growth (Cabodi et al., 2010b, 2006; Leenders et al., 2004). Although PKN3 is scarce in normal human adult tissues except in endothelial cells (HUVECs) (Aleku et al., 2008), a recent study showed that PKN3 is also present in moderate levels in MEFs, supporting these cells as a physiologically relevant model (Mukai et al., 2016). To investigate whether PKN3 regulates cell proliferation in MEFs and whether this is dependent on p130Cas, we prepared stable MEF cells with doxycycline (Dox) inducible mCherry-fused PKN3 WT or mCherry alone in the p130Cas null background with or without re-expression of p130Cas (Fig. 5 A). mCherry-PKN3 WT expression started from 5 h and reached

saturation within 24 h post-treatment with Dox (Fig. 5 B). Cell morphology was unaffected by mCherry-PKN3 WT expression; however, starting 5 h after adding Dox, MEFs re-expressing p130Cas exhibited increased growth rate compared to non-induced controls (Fig. 5 C). Induction of mCherry alone as an additional control had no effect and the growth rate of p130Cas^{-/-} MEFs was not affected by PKN3 expression (Fig. 5, D and E), indicating that the PKN3-mediated regulation of cell growth was p130Cas-dependent.

To investigate whether PKN3-mediated induction of cell growth rate required PKN3 interaction with p130Cas, we prepared stable cell lines of p130Cas^{-/-} MEFs re-expressing p130Cas with Dox-inducible Flag-fused PKN3 variants (WT, mPR, KD) (Fig. 5 F). Only the induction of expression of PKN3 WT, but not mPR or KD, led to the increase of cell growth compared to that in non-induced controls (Fig. 5 G). Increase of cell proliferation induced by PKN3 variants was also verified by AlamarBlue assay (Fig. S3 A) with similar outcome.

To test whether PKN3 promoted cell growth of MEFs by phosphorylation of the p130Cas SRD domain, we reintroduced GFP-p130Cas variants (WT, 15AN) or GFP as control to p130Cas^{-/-} MEFs with Dox-inducible mCherry-PKN3 (Fig. S3 B). Both GFP-p130Cas WT and 15AN, but not GFP alone, changed cell morphology, as characterized by an increased number of cell protrusions (Fig. S3 C). This morphology was not changed by Dox-inducible mCherry-PKN3, although Dox treatment increased the growth of cells expressing GFP-p130Cas WT and 15AN compared to that of non-induced controls (Fig. S3 D). Therefore, the effect of PKN3 on cell growth was probably independent of p130Cas SRD domain phosphorylation.

To investigate which signaling pathways are involved in the accelerated cell growth induced by PKN3, we analyzed the activation status of STAT3, ERK, Akt, MLC, mTOR, and Src signaling (Fig. S4 A). In agreement with previous studies, we did not find any significant changes (Leenders et al., 2004). Only Src activity was slightly increased by PKN3 expression in a p130Cas-dependent manner, which is consistent with a recent study demonstrating that PKN3 could promote Src activity in osteoclasts (Fig. S4, A and B) (Uehara et al., 2017). Taken together, these results indicated that PKN3 regulates the growth of MEFs and that this effect requires PKN3-p130Cas interaction independently of p130Cas SRD domain phosphorylation.

Interaction of p130Cas with PKN3 is required for PKN3-dependent increase of invasiveness

The localization of PKN3 in lamellipodia suggests its importance in cell migration. In p130Cas^{-/-}MEFs re-expressing p130Cas, we analyzed the effect of inducible expression of PKN3 on 2D migration using a wound healing assay. We found that PKN3 expression has no effect on the 2D migration on either plastic or fibronectin (FN) (Fig. 6, A and B). These results are consistent with a study of Lachmann et al. (Lachmann et al., 2011) where only siRNA anti-PKN1 or anti-PKN2, but not anti-PKN3, had an effect on wound healing closure of 5637 bladder tumor cells.

Next, we investigated the potential role of PKN3 in invasive cell migration in 3D collagen. To analyze the effect of PKN3 on cell invasiveness, we utilized a 3D cell-zone

exclusion assay as characterized in Van Troys et al. (Van Troys et al., 2018). In this assay, a monolayer of cells grown on a thick layer of collagen is wounded and then the system is overlaid with another layer of collagen. The cells migrating into the wound adopt the morphology and mechanisms of movement of cells migrating in 3D but can be monitored in one focal plane and their movement can be easily tracked and analyzed as in 2D (details described in Methods). p130Cas^{-/-} MEFs re-expressing p130Cas clearly moved faster and more individually compared to p130Cas^{-/-} MEFs (Fig. 6, C and D, and Movie S4 versus 5). Induced expression of PKN3 in p130Cas^{-/-} MEFs (Fig. 6, C and D, and Movie S5) was not sufficient to increase cell migration or to promote individual cell movement. In contrast, activation of PKN3 expression in p130Cas^{-/-} MEFs re-expressing p130Cas led to an increase of cell speed and invading distance compared to that in non-induced cells but did not change cell directionality (Fig. 6, C-E, and Movie S4). Notably, induced expression of PKN3 mPR and KD variants did not induce invasiveness of p130Cas^{-/-} MEFs re-expressing p130Cas (Fig. 6, F-G) but rather had the opposite effect, suggesting that PKN3-p130Cas interaction and PKN3 activity are important for PKN3-induced cell invasiveness of MEFs in collagen.

To test whether PKN3 promotes the invasiveness of MEFs by phosphorylation of the p130Cas SRD domain, we performed the 3D cell-zone exclusion assay with p130Cas^{-/-} MEFs re-expressing GFP-p130Cas variants (WT, 15AN) or GFP as control with or without Dox to induce mCherry-PKN3. Re-expression of GFP-p130Cas (WT or 15AN) caused an increase of cell invasive capability in 3D collagen (Fig. S4 C). Cell treatment by Dox further slightly increased the migration velocity of cells re-expressing both GFP-p130Cas WT and GFP-p130Cas 15AN in collagen compared to that of non-induced controls (Fig. S4, C and D), indicating that phosphorylation of p130Cas in the SRD domain by PKN3 is not involved in the PKN3-dependent increase of MEF invasiveness. Taken together, our results suggest that PKN3 expression increases cell invasiveness of MEFs and that this induced invasiveness is dependent on p130Cas. Furthermore, the PKN3 activity and its ability to interact with p130Cas is required for PKN3-induced cell invasiveness of MEFs, but is independent of PKN3-mediated phosphorylation of the p130Cas SRD domain.

PKN3 regulates growth and invasiveness of Src-transformed MEFs in a 3D environment through interaction with p130Cas

Having established the importance of the PKN3-p130Cas interaction for cell proliferation and cell migration in a 3D environment, we next analyzed whether this interaction also influences the growth and invasive behavior of SrcF-transformed cells. We first analyzed the effect of SrcF-induced transformation on the level of endogenous PKN3. We found that PKN3 expression is significantly increased in MEFs transformed by activated Src (almost 2×; $p < 0.009$) and that this increase is dependent on the presence of p130Cas (Figs. 7 A and S5 A). To reduce the contribution of endogenous PKN3 in subsequent experiments, we inactivated PKN3 in SrcF p130Cas^{-/-} MEFs re-expressing p130Cas (SC cells) using CRISPR/CAS9 system (Methods; Fig. 7 B). All PKN3 KO clones (SCpkn3^{-/-}) tested exhibited significantly reduced proliferation compared to the parental cells (Fig. 7 C). Consistent with this, reintroduction of PKN3 (mCherry-Flag fused), but

not PKN3 mPR or mCherry alone, under a Dox-controlled promoter (Fig. 7 D) led to rescue of cell growth in SCpkn3^{-/-} cells when Dox was supplemented to the medium (Figs. 7 E and S5 B).

To mimic the tumor environment, we further examined the growth of SCpkn3^{-/-} cell lines in a 3D environment, similarly as reported in Unsal-Kacmaz et al. ([Unsal-Kacmaz et al., 2012](#)). Induced expression of PKN3 in SCpkn3^{-/-} cells promoted a more aggressive behavior characterized by the appearance of a larger number of multicellular clusters in 3D Matrigel when compared to that in uninduced cells (Fig. 7, F and G). In contrast, inducible expression of PKN3 mPR did not significantly change cell growth. To further confirm our results that PKN3 supports aggressive cell behavior of SrcF-transformed MEFs in Matrigel, we also established stable SC cell line inducibly expressing shRNA anti-endogenous PKN3 (Fig. 7, F-H). Consistent with the previous findings, the enhanced growth of parental SC cells compared to that of SCpkn3^{-/-} cells was reduced by Dox-induced shRNA anti-PKN3 to a basal level of SCpkn3^{-/-} cells (Fig. 7 G). Taken together, these results suggested that PKN3 supports a more malignant phenotype in SrcF MEFs and that interaction of PKN3 with p130Cas may at least partly mediate this effect.

p130Cas has been previously shown to be crucial for invasion of SrcF-transformed MEFs (Brábek et al., 2004). To investigate whether PKN3 could influence the migration of SrcF-transformed MEFs in a 3D environment, we used the 3D cell-zone exclusion assay. In agreement with the results obtained in untransformed MEFs, in SCpkn3^{-/-} cells, induction of PKN3 but not PKN3 mPR expression led to an increase of cell invasion (Fig. 8, A and B). Consistent with this, inducible downregulation of PKN3 in parental SC cells by shRNA led to a decrease of cell migration in collagen (Fig. 8, A and B).

p130Cas and Src are critical components of podosome-like structures, which are involved in degradation of the ECM (Brábek et al., 2004). As we had shown that PKN3 is also localized to podosome-like structures, we next tested whether the increased invasiveness of PKN3 overexpressing cells was due to their elevated ECM degradation activity. We analyzed the podosome-associated proteolytic activity by gelatin degradation assay and found that gelatin degradation in SCpkn3^{-/-} cells is not affected by the expression of PKN3 (Fig. 8 C). These results indicated that the induced invasiveness of SCpkn3^{-/-} cells expressing PKN3 was reflective of a PKN3-induced migratory phenotype rather than increased degradation of ECM.

Nevertheless, PKN3 was recently demonstrated to be necessary for the bone degradation/resorption activity of osteoclasts, similar to that found for p130Cas (Nagai et al., 2013; Uehara et al., 2017). In both cases, an intact polyproline sequence of PKN3 and the p130Cas SH3 domain were required, as we had validated for PKN3-p130Cas binding, and both sequences were implicated in osteoclast function through an association with Src. We thus hypothesized that the Src-PKN3 interaction is indirect and mediated by p130Cas and tested this by co-immunoprecipitation experiments from SrcF-transformed p130Cas^{-/-} MEFs with or without p130Cas re-expression. As predicted, we found that Src failed to co-precipitate with PKN3 in the absence of p130Cas, confirming that the Src-PKN3 interaction is indirect (Fig. 8 D).

Interaction of p130Cas with PKN3 is required for PKN3 dependent tumor growth in vivo

As both PKN3 and p130Cas enhance cell proliferation in vitro and can contribute to various stages of tumor development in vivo (Tornillo et al., 2014; Unsal-Kacmaz et al., 2011; Leenders et al., 2004) and to expand our results showing in vitro functional relevance of the PKN3–p130Cas interaction to in vivo analysis, we subcutaneously injected SCpkn3^{-/-} cells stably engineered for inducible expression of either PKN3 WT or PKN3 mPR fused to mCherry, or mCherry alone, into nu/nu mice (total 48). As a positive control, a parental line of SC cells inducibly expressing mCherry was used. The animals were split into four groups (12 per group), all treated with Dox to induce the expression of mCherry-fused PKN3 variants or mCherry alone. The primary tumors were surgically removed at days 21 and 22 after inoculation for the SCpkn3^{-/-} cell lines (+PKN3 WT, +mCherry, and +PKN3 mPR, respectively) and at day 16 in parental SC cells inducibly expressing mCherry owing to large tumor sizes (Fig. 8, E and F). The tumors from parental SC cells with inducible mCherry reached the highest weight despite the shorter period of time. The SCpkn3^{-/-} cells expressing mCherry induced the smallest tumors among all groups. Re-expression of PKN3 WT, but not PKN3 mPR, in SCpkn3^{-/-} cells led to significant increase of tumors weight when compared to that for unmodified SCpkn3^{-/-} cells (Fig. 8, C and D). Even though the tumors from SCpkn3^{-/-} cells re-expressing PKN3 mPR were removed one day later than those from SCpkn3^{-/-} re-expressing PKN3 WT, their statistical comparison (ANOVA on ranks, Tukey's post hoc test) yielded an almost significant *p* value of 0.059, indicating that PKN3 likely promotes tumor growth from SCpkn3^{-/-} cells and that the PKN3–p130Cas interaction may be important in this promotion.

We further analyzed individual tumors for expression of mCherry as a reporter for Dox induced expression in the tumor cells by dot blot analysis (Fig. S5 C). Despite the comparable PKN3 mPR and WT protein level produced by Dox-induced cells in vitro, the majority of mCherry-PKN3 mPR-expressing tumors exhibited significantly increased mCherry signal compared to tumors with mCherry-PKN3 WT. This increase, however, did not lead to comparable tumor growth.

As p130Cas (Brábek et al., 2005) as well as PKN3 (Unsal-Kacmaz et al., 2011) expression is able to promote metastasis, we also evaluated the presence of lung metastases after 14 days post-surgery in animals injected with the parental SC cells, and after 21 days for all SCpkn3^{-/-} cells, as schematically represented in Fig. 5 D. Metastases were clearly observed only in 3 out of 5 surviving mice injected with the parental SC cell line (Fig. S5 E), suggesting that 21 days post-surgery (total 42 days) was not a sufficient time period for the formation of detectable metastases in mice injected with SCpkn3^{-/-} cells.

Discussion

In this study, we have, for the first time, shown and characterized PKN3–p130Cas interaction and provided new insight into the molecular mechanism of the regulation of tumor-promoting kinase PKN3 and p130Cas-mediated signaling. In particular, we demonstrated that PKN3-p130Cas interaction is necessary for PKN3 to promote malignant growth and invasiveness of SrcF-transformed MEFs. The interaction between mouse p130Cas and mouse PKN3 is mediated by binding of the p130Cas SH3 domain and PKN3 central polyproline region (P₅₀₀PPKPPRL; Fig. 1, A-F). The dynamics of this interaction is potentially regulated similarly as that of other p130Cas SH3 ligands by Src-dependent phosphorylation of the p130Cas SH3 domain on Tyr12, which in its non-phosphorylated state contributes significantly to p130Cas SH3 ligand binding (Gemperle et al., 2017).

The PKN3-p130Cas interaction represents new crosstalk within PI3K–integrin signaling. p130Cas was previously shown to be in complex with PI3K to support anti-estrogenic drug-resistant cell growth (Cabodi et al., 2004). The connection of PKN3 to integrin signaling was indicated by a study showing that PKN3 KO decreased chemotaxis of MEFs toward FN and caused a glycosylation defect of integrin β 1 and integrin α 5 (Mukai et al., 2016). Moreover, PKN3 promotes osteoclasts to resorb bone matrix via stimulation of integrin effector kinase-Src kinase (Uehara et al., 2017). This effect was strongly dependent on the PKN3 polyproline region that we showed to be responsible for p130Cas binding. Here, we were able to demonstrate that the PKN3-Src association is indeed mediated by p130Cas (Fig. 8 D). Furthermore, consistent with the effect in osteoclasts, we observed a slight activity increase for integrin effector kinase-Src kinase induced by PKN3 overexpression in MEFs (Figs. 7 A, and S4 A and B).

We found PKN3 to co-localize with p130Cas in pro-invasive structures: lamellipodia of MEFs and podosome rosettes of Src-transformed MEFs (Fig. 2, A and B). Notably, PKN3 was not detected at focal adhesions, which are highly redundant in terms of protein composition with podosome rosettes, whereas p130Cas is present in both structures. As PKN family kinases are implicated in cell migration, we investigated the role of PKN3 in cell migration and invasiveness. MEF migration as measured by wound healing assay (2D) was not affected by PKN3 overexpression (Fig. 6, A and B). In contrast, we observed increased cell velocity in collagen (3D) upon induction of PKN3 expression, but not expression of a kinase inactive PKN3 variant (KD) or a PKN3 variant unable to bind p130Cas (mPR). Moreover, the effect of PKN3 expression on migration in 3D was dependent on p130Cas expression (Figs. 6 C-G and 8, A and B). Our results are consistent with independent studies wherein the invasiveness of SrcF-transformed MEFs through Matrigel was greatly decreased in the absence of p130Cas (Brábek et al., 2005) and where MEF PKN3 KO cells exhibited lower migratory activity induced by various treatments than that of MEFs with endogenous PKN3 (Mukai et al., 2016). Similarly, Leenders et al. indicated that PC3 cells with downregulated PKN3 failed to migrate to form network-like structures on Matrigel (Leenders et al., 2004). Although we have not elucidated the exact molecular mechanisms by which PKN3 promotes cell

migration, we observed PKN3 binding to actin in a p130Cas-dependent manner (Fig. S5 F) and temporal colocalization of PKN3 with stress fibers (Figs. 3 A and S1, B and C). Given the binding of PKN3 also to regulators of actin dynamics-Rho GTPases (Unsal-Kacmaz et al., 2011), we predict that PKN3 affects intracellular actin dynamics with the co-involvement of p130Cas.

PKN3 is the first kinase documented to phosphorylate p130Cas on Ser/Thr residues (Fig. 4 E), which are abundantly present on p130Cas and yield a dynamic phosphorylation pattern (Makkinje et al., 2009). One of these p130Cas residues, Ser432 (homologous to human Ser428), is abundantly phosphorylated in breast carcinoma tumors (Fig. 4 D) and represents one of the major Ser/Thr phosphorylation sites in MEFs cultivated in vitro (Fig. 4 F). Notably, some phosphoproteomic studies have shown that this phosphorylation is enriched in response to insulin, which is also a potent activator for PKN3 (PhosphoSite database, Leenders et al., 2004)), and correlates with PKN3 activity in breast carcinoma tumors (Fig. 4 D). The effects of this phosphorylation as well as that of p130Cas in the SRD domain are still unknown, as p130Cas^{-/-} MEFs with reintroduced GFP-p130Cas 15AN increased cell growth and invasiveness similarly as GFP-p130Cas WT in a PKN3-dependent manner (Figs. S3 D, S4 C and D).

Notably, a p130Cas paralog termed Nedd9 was found to be phosphorylated on Ser369, which is homologous to p130Cas Ser432. Mutation of Ser369 to alanine, similarly to mutation of p130Cas Ser432, induces p130Cas mobility shift upon SDS-PAGE from 4 bands to two faster migrating bands. Although the kinase responsible for Nedd9 Ser369 phosphorylation is unknown, this modification was shown to induce Nedd9 proteasomal degradation (Hivert et al., 2009). Protein p130Cas, however, is stable during the cell cycle and exhibits a constant expression pattern in cells. Therefore, the effect of p130Cas Ser432 phosphorylation is likely different from that of Ser369 in Nedd9.

Furthermore, transformation of MEFs by a constitutive active Src led to an increase of PKN3 endogenous protein levels in cells grown on plastic, which was dependent on the presence of p130Cas (Figs. 7 A and S5 A). Similarly, PKN3 levels were shown to be elevated by its activators PI3K (Leenders et al., 2004) and RhoA/C (Unsal-Kacmaz et al., 2011), and by the oncogenic form of Ras (Leenders et al., 2004). This suggests that PKN3 functions as an effector of various signal transduction pathways that mediate cell growth and transformation.

Several studies have presented evidence for the significant contribution of PKN3 and p130Cas to tumor growth as well as metastasis formation (Kang et al., 2015; Brábek et al., 2005; Unsal-Kacmaz et al., 2011; Leenders et al., 2004; Tornillo et al., 2014). Our data support these results and furthermore suggest that binding of PKN3 to p130Cas is important for PKN3-induced tumor growth. We hypothesize that targeting p130Cas, PKN3, and their co-operation may be exploited in cancer therapy and, based on our insight in PKN3 signaling in osteoclasts, potentially in pathophysiological signaling related to bone disease such as osteoporosis, rheumatoid arthritis, and periodontal disease as well. Moreover, a therapeutic agent that targets PKN3 by RNA interference (siRNA Atu027) has already completed Phase I clinical trials in a study with patients exhibiting different solid advanced and metastatic tumors, showing very promising results without

any adverse effects (Schultheis et al., 2014), further supporting the validity of this strategy.

Conclusion

In this study, we characterized PKN3 as a direct p130Cas binding protein using molecular, functional, and microscopic analyses in vitro and in vivo. Notably, we show that PKN3 phosphorylates p130Cas, colocalizes with p130Cas to pro-invasive cell structures and PKN3-p130Cas interaction is required for increased cell invasiveness and malignant growth. In summary, we suggest that aberrantly expressed PKN3 and p130Cas can cooperate in cancer progression and tumor growth and therefore may represent an attractive target for therapeutic intervention.

Figures

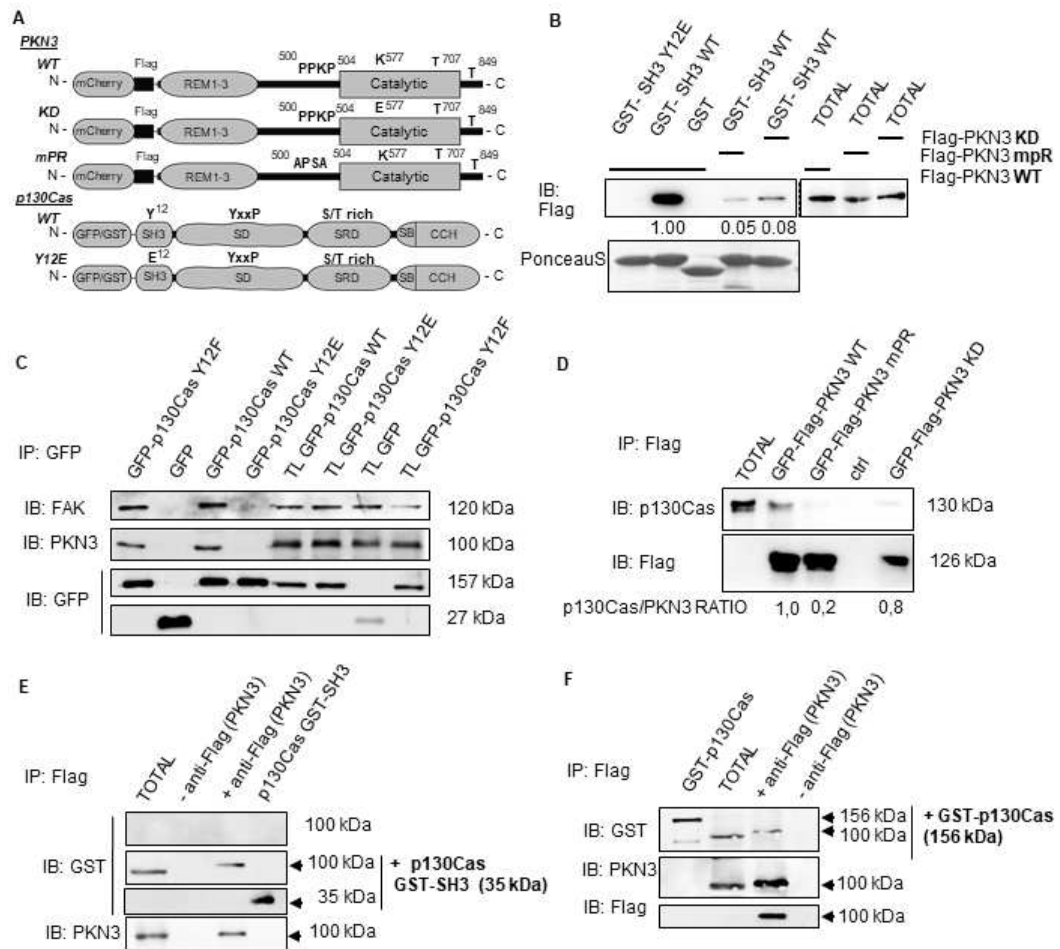


Figure 1. p130Cas directly interacts with PKN3 **A)** Schematic representation of PKN3 and p130Cas domains, important residues and their mutagenesis. **B)** Purified GST-fused p130Cas SH3 variants (WT, Y12E) were used to pull-down Flag-PKN3 variants (WT, mPR, KD), expressed in mouse embryonic fibroblasts (MEFs). Pulled-down proteins were immunoblotted with anti-Flag antibody, and GST-SH3 domains were stained with Ponceau-S. GST with lysate from Flag-PKN3 WT was used as a negative control. **C-D)** Binding of PKN3 to full-length p130Cas was verified by co-immunoprecipitations. **C)** The MDA-MB-231 cells were transiently transfected with indicated mouse GFP-p130Cas variants or GFP alone followed by immunoprecipitations using anti-GFP antibody. Co-immunoprecipitated PKN3 and FAK (as a positive control) were detected using anti-PKN3 antibody or anti-FAK, respectively. **D)** The MDA-MB-231 cells were transiently transfected with mouse Flag and GFP-fused PKN3 variants (WT, mPR, KD) followed by immunoprecipitations using anti-Flag sepharose and co-immunoprecipitated p130Cas was detected by anti-p130Cas antibody. In far western experiments **E-F)** Flag-PKN3 was immunoprecipitated from transfected MDA-MB-231 cells, transferred to nitrocellulose membrane and incubated with **E)** recombinant GST-p130Cas SH3 domain or **F)** whole GST-p130Cas followed by detection with anti-GST antibody. The membrane was then stripped and both endogenous (endo PKN3) as well as exogenous PKN3 (exo Flag-PKN3) were detected by anti-PKN3 and anti-Flag antibody, respectively. The upper membrane in fig. E was not incubated with recombinant GST-p130Cas SH3 domain and represents a negative control for anti GST antibody. As a positive control for GST cross-reactivity a purified GST-p13Cas SH3 in **E)** or whole GST-p130Cas in **F)** was ran alongside.

TL or TOTAL: total cell lysate; IP: immunoprecipitation; Ctrl: control samples prepared from untransfected MDA-MB-231 cells.

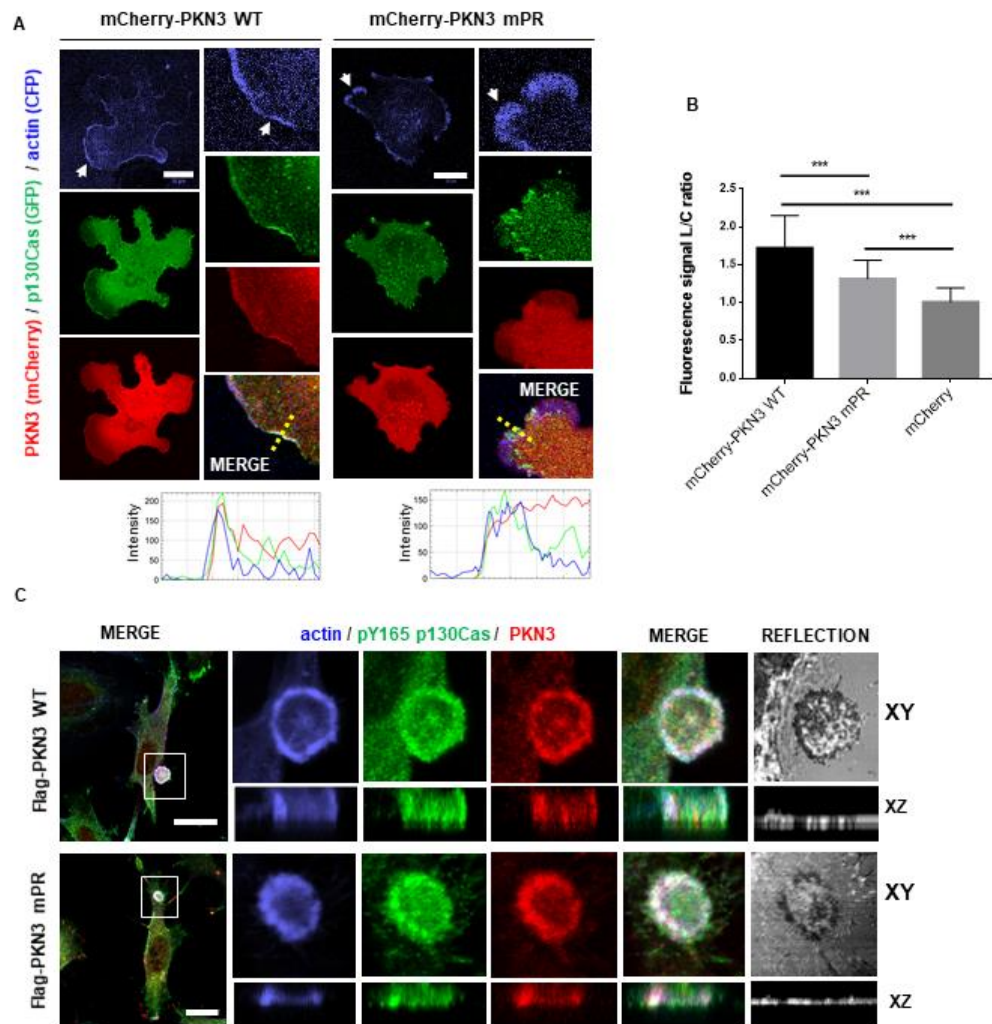


Figure 2. PKN3 colocalizes with p130Cas in lamellipodia and podosome rosettes. Representative images are shown. **A)** p130Cas^{-/-} MEFs plated on fibronectin (FN) were transfected by GFP-p130Cas, CFP-LifeAct and mCherry-PKN3WT or mCherry-PKN3 mPR and imaged live 24 h after transfection. White arrow indicates lamellipodia. Histogram of dotted straight line is shown. **B)** Quantification of mCherry-PKN3 WT, mCherry-PKN3 mPR and mCherry localization to lamellipodia (LifeAct as marker) was calculated as described in methods (values are mean \pm SD from three independent experiments, n>50 measurements – 3 per cell; *P<0,001, one-way ANOVA on ranks followed by Dunn’s post-hoc test). **C)** Src-transformed p130Cas^{-/-} MEFs co-expressing p130Cas (SC) and mouse Flag tagged PKN3 WT or Flag-PKN3 mPR are shown. Cells were grown on FN-coated coverslips for 48 h, fixed and stained for p130Cas by anti-pTyr165 p130Cas antibody (pY165 p130Cas; 2nd 405), for actin by Phalloidin 488 and for Flag-PKN3 by anti-Flag antibody (2nd 633). Reflection (670 nm) indicates fibronectin degradation. All scale bars represent 20 μ m. Cell were imaged by Leica TCS SP8 microscope system equipped with Leica 63x/1.45 oil objective.

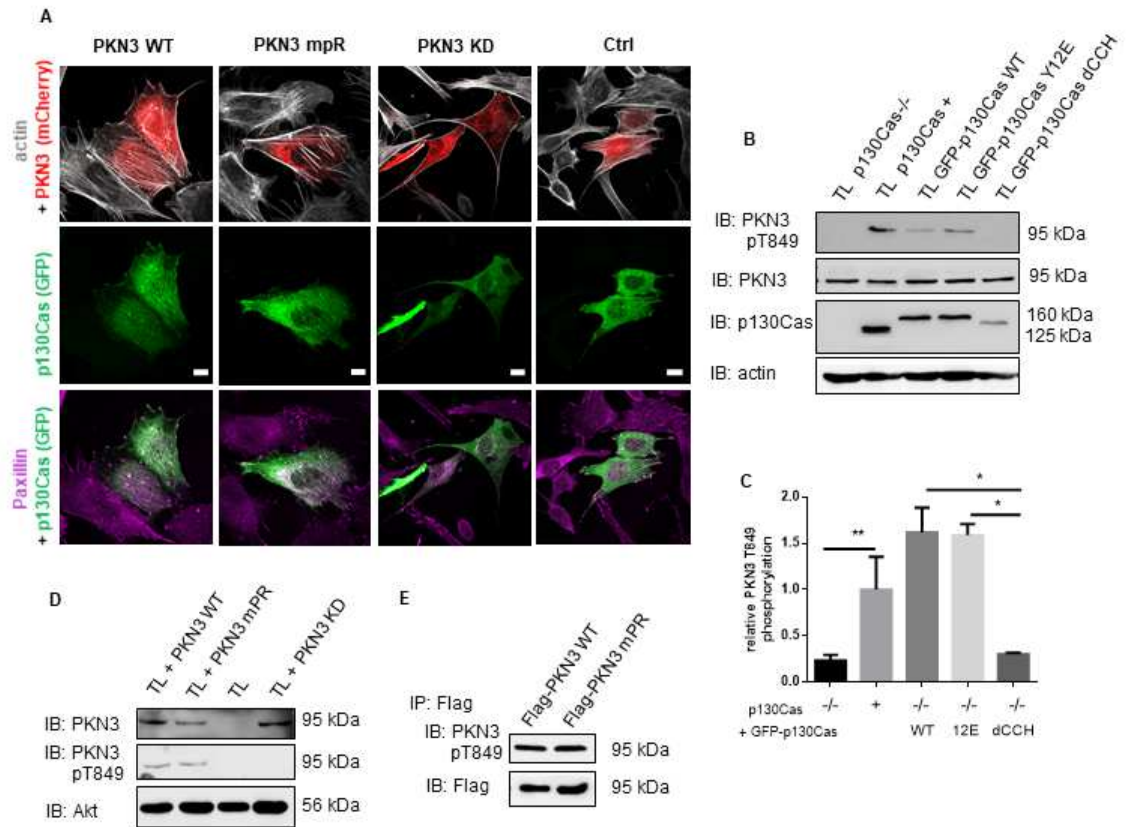


Figure 3. PKN3 activity is important for stress fibers formation and is stimulated by expression of p130Cas. **A)** p130Cas^{-/-} MEFs growing on FN-coated cover slips were co-transfected by GFP-p130Cas and mCherry-PKN3 fusion variant (WT, mpR, KD) or mCherry. After 48 h cells were fixed and imaged by Leica TCS SP2 microscope (63x/1.45 oil objective). Stress fibers were visualized by Phalloidin (405) and focal adhesions by anti-Paxillin staining (2nd 633). Representative images are shown. Scale bars represent 20 μ m. **B)** p130Cas^{-/-} MEFs or p130Cas^{-/-} MEFs re-expressing p130Cas or transfected by GFP-fused p130Cas variants (WT, YE, dCCH) were lysed in RIPA buffer, blotted to nitrocellulose membrane and analyzed for endogenous PKN3 activity by antibody anti-phosphoThr849 of PKN3 (pT849 PKN3). Expression of p130Cas mutants was verified by anti-p130Cas antibody and loading by anti-PKN3 and anti-actin antibody. **C)** Densitometric quantification of PKN3 activity (pT849 PKN3 phosphorylation). Error bars indicate means \pm SD from three independent experiments. Statistical significance was evaluated by one-way repeated ANOVA followed by Turkey's post-hoc test. **D)** Lysates or **E)** immunoprecipitates (by Flag-sepharose) from p130Cas^{-/-} MEFs re-expressing p130Cas and overexpressing PKN3 variants (WT, mpR, KD) were immunoblotted by anti-PKN3, anti-pT849 PKN3 and anti-Akt antibodies (loading control).

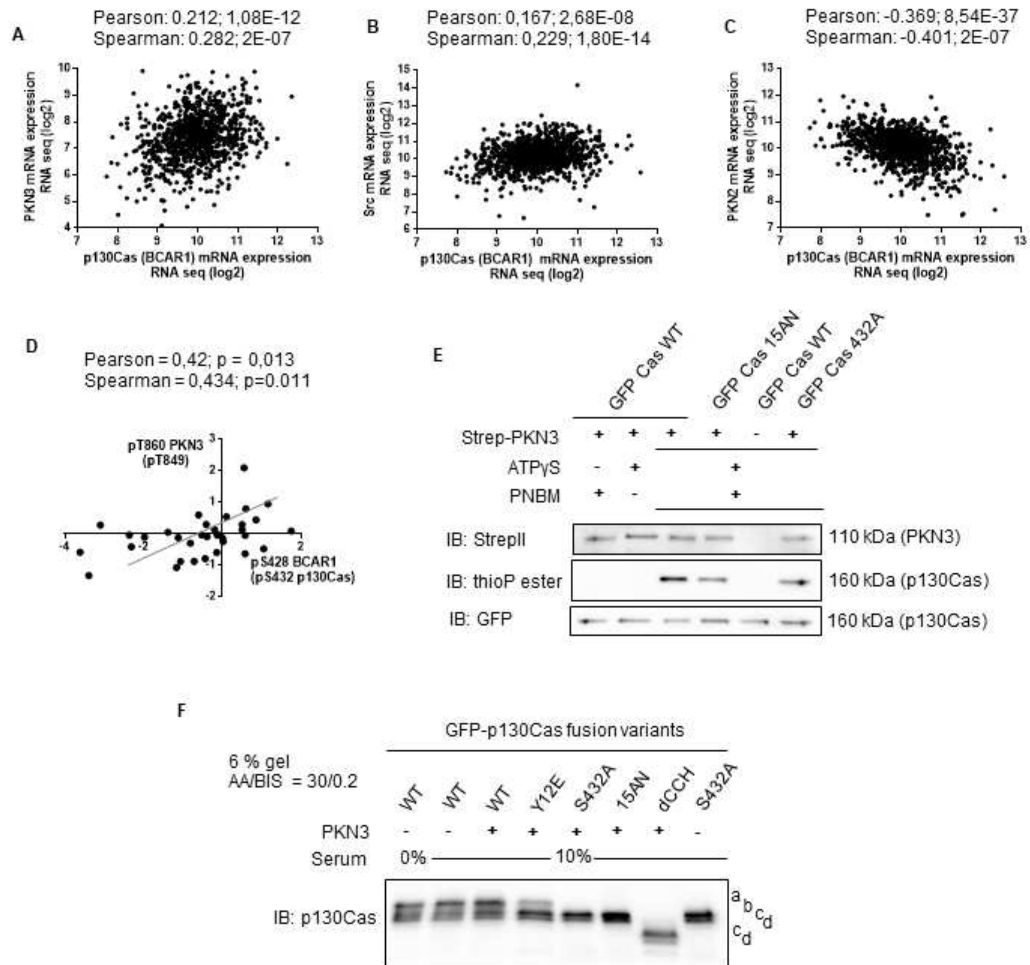


Figure 4. PKN3 phosphorylates p130Cas and PKN3 activity correlates with p130Cas phosphorylation in human breast carcinomas. **A-C)** Correlation statistics (graphs) of publicly available RNA seq data of co-expression of **A)** human p130Cas/BCAR1 and PKN3; **B)** p130Cas/BCAR1 and Src; **C)** p130Cas/BCAR1 and PKN2 or graph **D)** showing positive linear dependency of protein phosphorylation levels (log ratio values) of PKN3 Thr860 and p130Cas/BCAR1 Ser428 in invasive human breast tumors. **E)** Kinase reactions in vitro with precipitated Strep-PKN3 and GFP fusion p130Cas variants (shown as Cas). Reactions were carried out in the presence of ATPyS followed by alkylation with PNBM and detection with specific anti-thiophosphate esters (thioP ester) antibody. Combinations of PNBM (alkylation reagent) or ATPyS were facilitated to exclude false positive signals. Antibodies anti-StrepII and GFP were used to detect PKN3 kinase or GFP-fused p130Cas variants, respectively. Representative blots are shown. **F)** Lysates from p130Cas^{-/-} MEFs re-expressing GFP-fused p130Cas variants with or without mCherry-PKN3 overexpression were run on SDS-PAGE using an acrylamide/bisacrylamide ratio of 30:0.2 followed by immunoblotting and detection by anti-p130Cas antibody. a-d refers to different GFP-p130Cas isoforms.

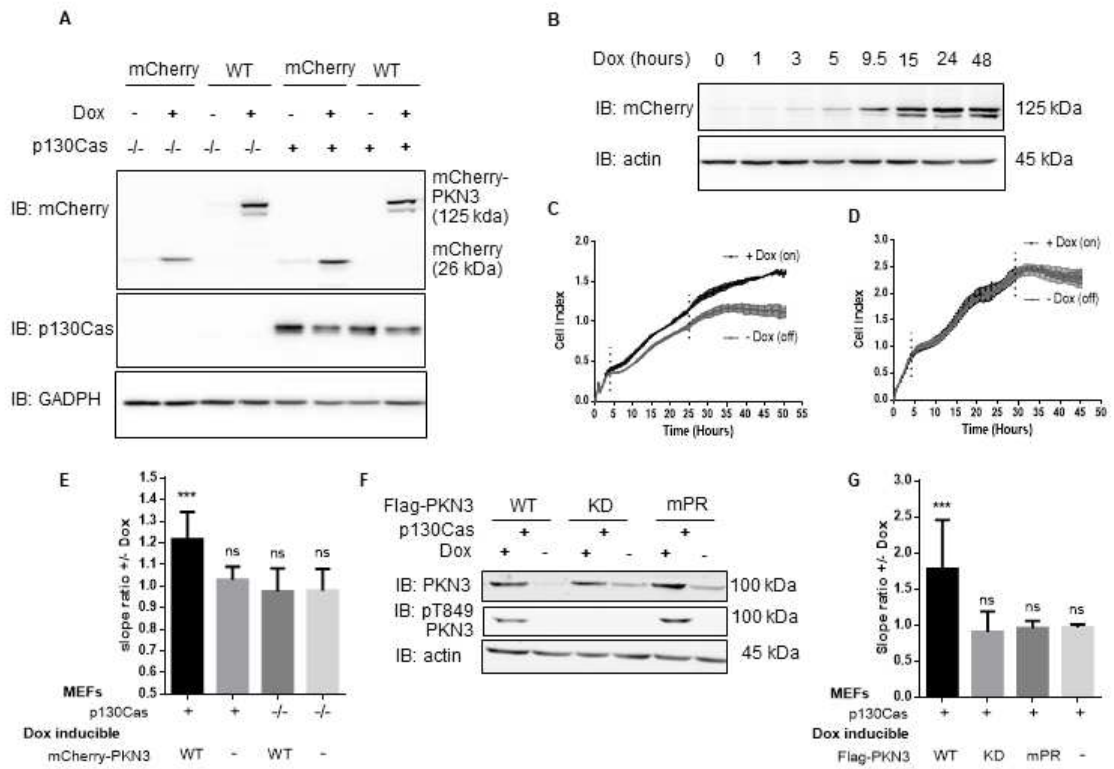


Figure 5. PKN3 overexpression regulates growth of MEFs and this effect requires PKN3 – p130Cas interaction. **A)** Immunoblotted lysates from MEFs p130Cas^{-/-} or MEFs p130Cas^{-/-} re-expressing p130Cas (p130Cas⁺) treated by Doxycycline (Dox) to induce expression of mCherry-PKN3 or mCherry alone. p130Cas presence was detected by anti-p130Cas antibody and mCherry epitope by anti-mCherry antibody. **B)** Dynamics of mCherry-PKN3 expression after supplementation with Dox shown by immunoblot with anti-mCherry antibody. **C-E)** Effect of induced mCherry-PKN3 expression on cell growth. Representative graphs showing growth of MEFs p130Cas^{-/-} re-expressing p130Cas (p130Cas⁺) **C)** or MEFs p130Cas^{-/-} **D)** measured in real-time using the xCELLigence RTCA (real-time cell analysis) system instrument. **E)** Quantification of cell growth change induced by mCherry-PKN3 expression (“-” indicates inducible mCherry expression used as negative control). Slope ratios reflecting cell growth were calculated from the log growth phase of cell growth (indicated by dotted lines; see C and D). **F)** Immunoblotted lysates from MEFs p130Cas^{-/-} re-expressing p130Cas (p130Cas⁺) treated or not treated by Dox which induced expression of Flag-fused PKN3 variants (WT, mPR, KD, empty vector). Stimulated overexpression of PKN3 was detected by anti-PKN3 antibody and its activity by antibody anti-pT849 PKN3. **G)** Quantification of cell growth change stimulated by Dox-inducible expression of Flag-fused PKN3 variants (WT, mPR, KD) in MEFs p130Cas^{-/-} re-expressing p130Cas (p130Cas⁺).

All error bars indicate means \pm SD calculated from 3-5 independent experiments (each in triplicates). Statistical significance was always calculated between induced and non-induced cells and evaluated by one-way repeated ANOVA followed by Turkey post-hoc test (***P < 0.001).

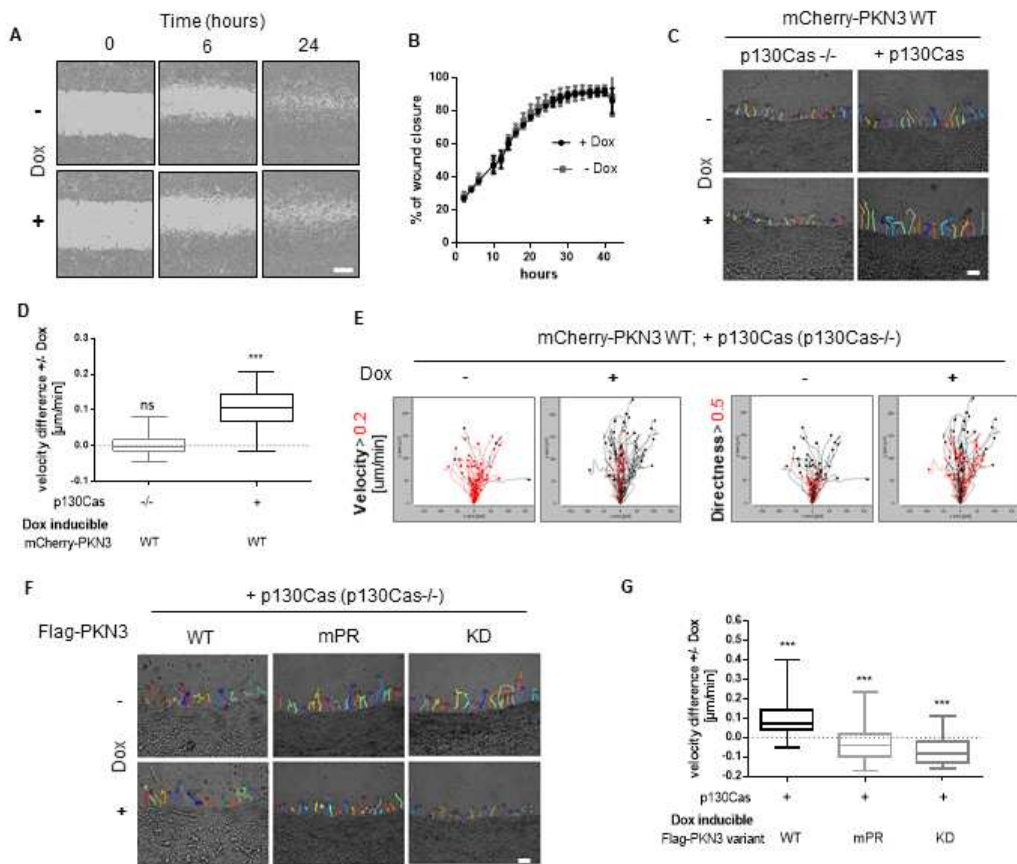


Figure 6. The interaction of p130Cas with PKN3 is required for PKN3-dependent increase of invasiveness but not 2D migration. **A-B)** 2D migration analyzed by wound healing assay. **A)** Representative images of MEFs p130Cas^{-/-} re-expressing p130Cas with or without 24 h pre-induced for Flag-PKN3 expression at the time of wounding (0 h), after 6 and 24 h are shown (scale bar 300 μ m). **B)** Representative graph. **C-G)** Cell invasiveness analyzed by 3D cell-zone exclusion assay. Cell migration into collagen was recorded using time-lapse video microscopy with frames being collected every 5 min for 18 h, starting 2 h after collagen scratch, with or without Dox supplementation. Expression of different constructs was pre-induced day before. **C)** Representative tracking maps of cells (MEFs p130Cas^{-/-} or MEFs p130Cas^{-/-} re-expressing p130Cas) migrating into collagen supplemented with or without Dox for induction of mCherry-PKN3 expression (scale bar 100 μ m). Relevant supplemental movies S4-5 are included. **D)** Quantification of cell migration velocity difference induced by Dox-inducible mCherry-PKN3 expression in the p130Cas null background with or without re-expression of p130Cas. **E)** Migration maps comparing the velocity and directionality of cells described in D). The boxed traces represent the length (above 0.2 μ m black, below red) and directionality (above 0.5 black, below red) of cell movement of each individually tracked cell plotted from the same point of origin. **F)** Representative tracking maps of MEFs p130Cas^{-/-} re-expressing p130Cas migrating into collagen supplemented with or without Dox for induction of Flag-PKN3 variant expression as indicated (scale bar 100 μ m) and their quantification **G)**.

Box and whisker graphs show quantification of cell migration into collagen out of 3 independent experiments (n=60 cells). Statistical significance comparing induced and non-induced cells was evaluated by one-way ANOVA or one-way ANOVA on ranks followed by Turkey post-hoc test (***P < 0.001).

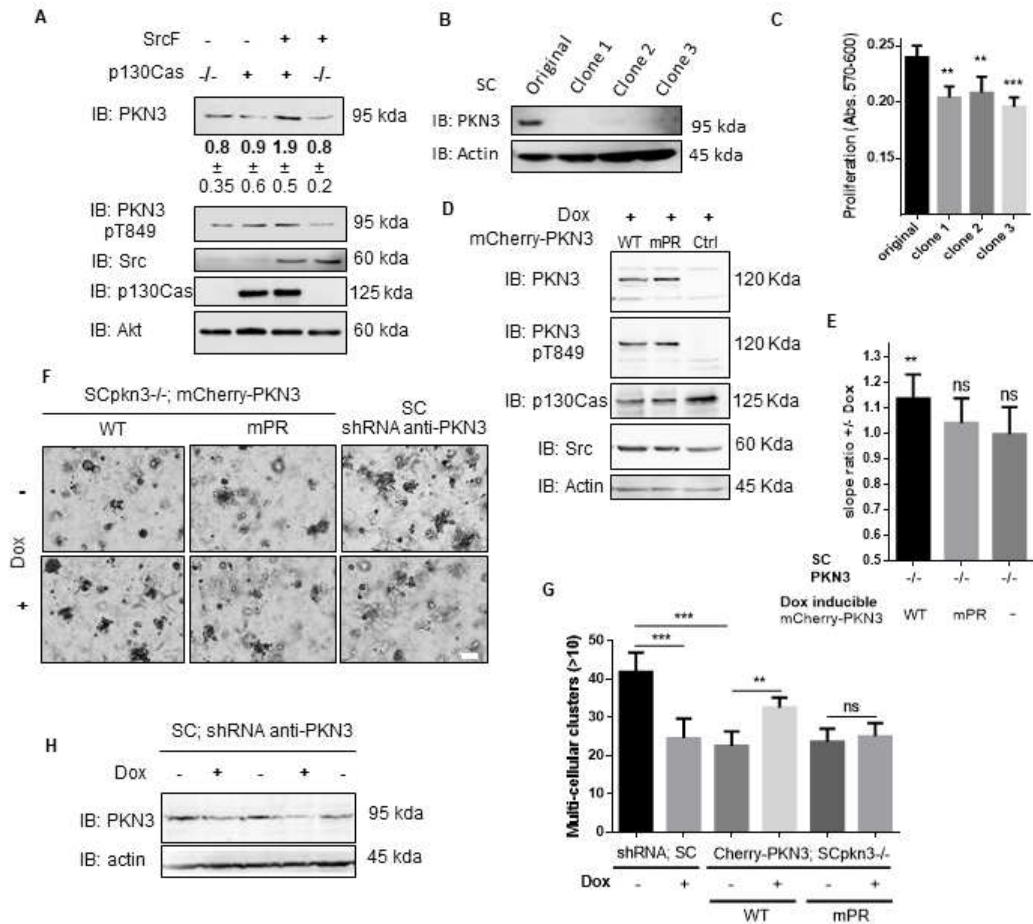


Figure 7. PKN3 regulates growth in 2D and in 3D environment of Src-transformed MEFs through interaction with p130Cas. **A)** Immunoblotted lysates from MEFs p130Cas^{-/-} re-expressing p130Cas with or without transformation by constitutively active Src (SrcF, SC cells). Src and p130Cas were detected by corresponding antibodies anti-Src or anti-p130Cas, respectively. Antibodies anti-PKN3 or anti-pT849 PKN3 were used for PKN3 and anti-Akt served as loading control. Densitometric quantification of protein PKN3 amount is indicated below. **B)** Immunoblot of SC cells and SC cells with *PKN3* gene inactivated using CRISPR/CAS9 (SCpkn3^{-/-}). Inactivation of PKN3 expression is visualized by antibody anti-PKN3. Antibody anti-actin was used as loading control. **C)** Quantification of SC cells proliferation rate with or without inactivated *PKN3* gene cassette by AlamarBlue method (72 h after cell seeding). The graph shows mean absorbance measurement at 570 nm with reference at 600 nm corrected for the initial deviations of cell seeding counts. **D)** Immunoblotted lysates from SCpkn3^{-/-} cells treated by Dox to induce expression of mCherry-PKN3, mCherry-PKN3 mPR or mCherry alone. PKN3 constructs were detected by anti-PKN3 and anti-pT849 PKN3 antibodies. Src and p130Cas were detected by anti-Src or anti-p130Cas antibodies, respectively. Antibody anti-actin served as loading control. **E)** Quantification of cell growth change induced by Dox-inducible mCherry, mCherry-PKN3 WT or mCherry-PKN3 mPR expression in SCpkn3^{-/-} cells measured by xCELLigence RTCA system. Slope ratios reflecting cell growth were calculated from the log growth phase of cell growth (representative curves are shown in supplementary figure S5B). **F)** SC and SCpkn3^{-/-} cells stably expressing mCherry-PKN3 WT, mPR or shRNA anti-PKN3 in Dox-dependent manner were embedded into Matrigel. Photographs were taken on day 7, scale bar represents 100 μ m; enlarged image for each sample is shown with subtracted background using ImageJ. **G)** Multi-cellular clusters (>10 cells) indicating proliferating cells were quantified relative to individual cells or small cell aggregates on day 7. Average mean is shown. **H)** Immunoblot analysis showing effectiveness of PKN3 knockdown in SC cells. Antibody anti-actin was used as loading control. All error bars indicate means \pm SD calculated from 3-5 independent experiments (each in triplicates C, E); in duplicates G). Statistical significance comparing induced and non-induced cells (E, G) was evaluated by one-way repeated ANOVA followed by Turkey post-hoc test (**P < 0.01), among variants/groups (C, G) by one-way ANOVA followed by Turkey post-hoc test (**P < 0.01; ***P < 0.001).

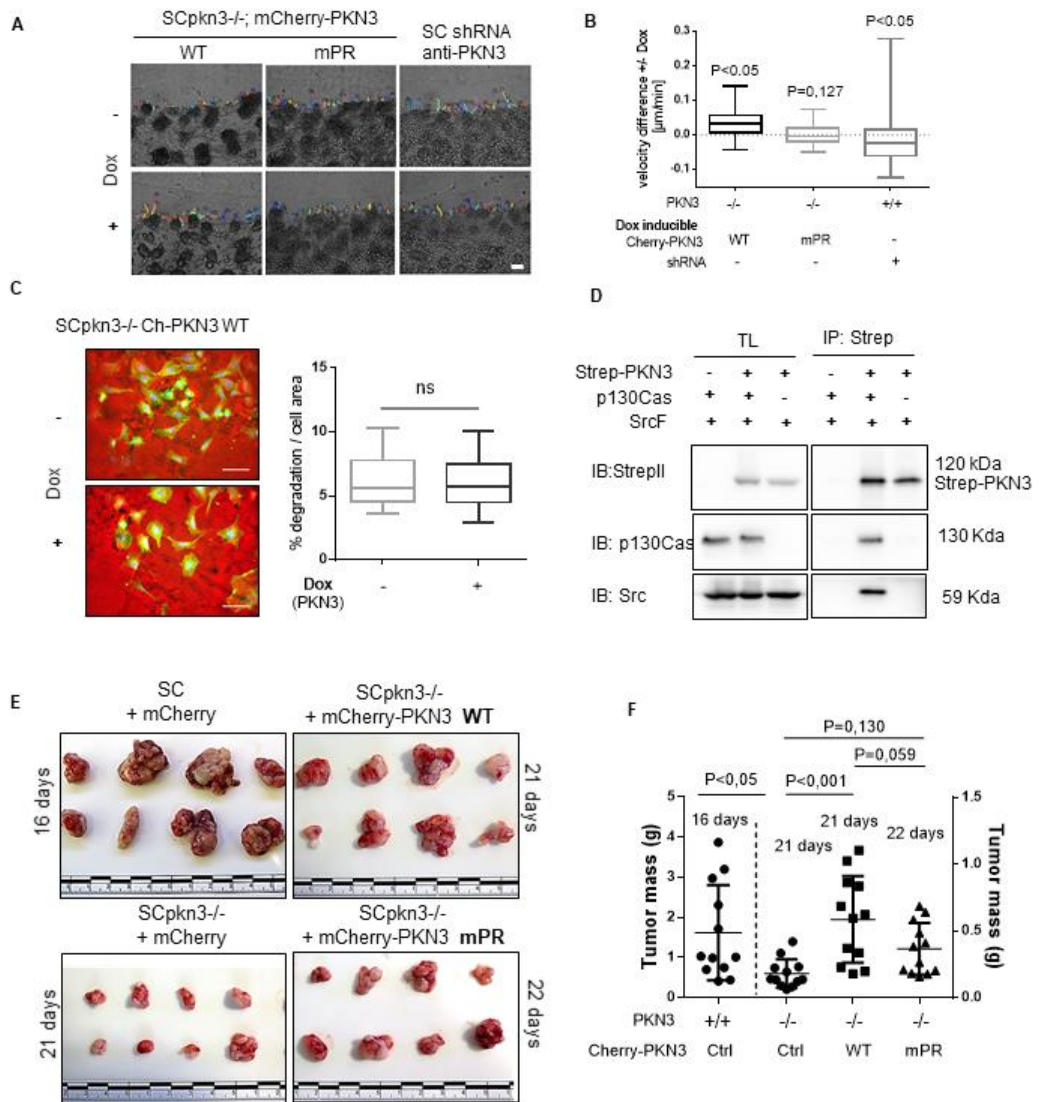


Figure 8. PKN3 regulates cell migration in 3D environment of SrcF-transformed MEFs and tumor growth in vivo through interaction with p130Cas. **A)** Representative tracking maps of SC or SCpkn3^{-/-} cells stably expressing mCherry-PKN3 WT, mPR or shRNA anti-PKN3 in Dox-dependent manner as indicated are shown (scale bar 100 μ m). Cells migrated into collagen with or without Dox supplementation. **B)** Quantification of cell velocity difference between induced and non-induced controls. Statistical significance was evaluated from 3-5 independent experiments by one-way ANOVA on ranks followed by Turkey post-hoc test. **C)** Gelatin degradation (Cy3-labeled) of SCpkn3^{-/-} cells expressing Dox-inducible mCherry-PKN3. Representative images are shown (on the left). Scale bar represents 100 μ m. Quantification calculated as % degraded area related to total cell area stained by phalloidin 488 (on the right). **D)** Association of PKN3 with Src in p130Cas-dependent manner is shown by co-immunoprecipitations. SrcF-transformed cells with or without p130Cas were transfected by Strep-PKN3 and PKN3 was precipitated by Strep-Tactin[®] Superflow[®] resin followed by western blotting and detection by anti-StrepII antibody. Coimmunoprecipitated p130Cas and Src were detected using appropriate antibodies (anti-p130Cas, anti-Src). **E)** 8 representative tumors of SC or SCpkn3^{-/-} cells with Dox-induced mCherry, mCherry-PKN3 or mCherry-PKN3 mPR are shown with the same scale (units in cm). **F)** Their respective quantification expressed as tumor mass weight at defined timescale as indicated. Statistics were evaluated by ANOVA on Ranks Dunn's Method. TL: total cell lysate; IP: immunoprecipitation; Ctrl: control sample prepared from SC cells.

Material and methods

Antibodies and reagents

The following antibodies were used: Akt (rabbit pAb, #9272S), phospho-Akt (Ser473, rabbit mAb D9E, #4060S), phospho-p130Cas (Tyr165, rabbit pAb), p44/42 MAPK (i.e., Erk1/2, rabbit mAb 137F5, #4695), phospho-Src family (Tyr416, rabbit pAb, #2101S), Stat3 (rabbit mAb D3Z2G, #12640), Phospho-Stat3 (Tyr705, mouse mAb 3E2, #9138S), Phospho-Myosin Light Chain 2 (Ser19, mouse mAb, #3675), Phospho-S6 Ribosomal Protein (Ser235/236, rabbit mAb 2F9, #4856), Phospho-GSK-3 α/β (Ser21/9, Rabbit mAb 37F11, #9327) (Cell Signaling Technology); p130Cas (mouse mAb 24), Paxillin (mAb 349) (BD Transduction Laboratories); Src (Calbiochem, mouse mAb 327, Ab-1); FAK (rabbit pAb, C-20), Actin (goat pAb, C-11) (Santa Cruz Biotechnology); MAPK (i.e., Erk1/2, mouse mAb V114A, Promega); GST (rabbit pAb, G7781; Sigma Aldrich); PKN3 (rabbit pAb, NBP-130102), mCherry (rabbit pAb, NBP2-25157), StrepII (mAb 517, NBP2-43735) (NOVUS Biologicals); PKN3 (rabbit pAb, AP14628A; Abgent); and phospho-PKN3 (human Thr860 = mouse Thr849) (Pfizer, Oncology). Immunoprecipitations were carried out using a Flag antibody (mouse mAb M2, Sigma Aldrich) and GFP antibody (Abcam, rabbit polyclonal ab290). Secondary antibodies fused to HRP (Abcam) were used as recommended by the manufacturer. The secondary antibodies for fluorescence imaging were: anti-rabbit (Alexa-546) and anti-mouse (Alexa-594, Alexa-633; Molecular Probes).

The reagents used were doxycycline hydrochloride, blasticidin, and puromycin (Sigma Aldrich), glutathione (reduced, LOBA Chemie), Phalloidin 405 (Thermo Fisher Scientific), FN (Invitrogen), collagen R solution (SERVA), Matrigel (Corning), Strep-Tactin® Superflow® resin (IBA Lifesciences), nProtein A Sepharose 4 Fast Flow (GE Healthcare), anti-Flag M2 affinity resin (Sigma), and p-nitrobenzyl mesylate (Abcam).

Cell lines and culture conditions (shRNAs, transfection, retrovirus, and lentivirus preparation)

p130Cas^{-/-} MEFs were obtained from Steven Hanks (Vanderbilt University, Nashville). p130Cas^{-/-} MEFs expressing constitutively active mouse Src Y527F (SrcF cells) or both p130Cas WT and Y527F (SC cells) were prepared using the LZRS-MS-IRES-GFP retroviral vector and the Phoenix E packaging line as described previously (Brábek et al., 2004).

To generate SC PKN3 null, cells were transiently transfected by sgRNA anti-PKN3 (sequence provided in Table S2) and a puromycin resistance-expressing CRISP-CAS9 plasmid. Cells were selected by puromycin for 2–3 days followed by clonal isolation. Success of CRISPR targeting was analyzed by PCR and Surveyor nuclease assay as published (Ran et al., 2013) and by western blots. Sequences around the CRISPR modification site were amplified by PCR from three selected mammalian clones, cloned into pJET1.2/blunt using a CloneJET PCR Cloning Kit (ThermoFisher), and sequenced (at least six from each). Sequencing revealed that CRISPR nicking most frequently caused frameshift -1 bp or + 49/+37 bp. Potential off-targets were predicted

(<http://tools.genome-engineering.org>) and the three most potent tested by Surveyor assay (results negative, primer sequences provided in Table S2). SC cells with Dox-inducible PKN3 shRNA (see plasmid construction, below) were prepared similarly as described previously (Leenders et al., 2004; Czauderna et al., 2003).

To stably deliver Flag-fused or mCherry-Flag-fused constructs, retroviral pMSCV-puro or lentiviral pLVX-Tet-On Advanced system (Clontech) was used. In brief, cells were infected with viral supernatant generated in transfected Phoenix E packaging cells (pMSCV system) or produced in HEK293T cells co-transfected by pVSV-G and psPAX2 plasmids together with pLVX-Tet-On in the first round or with pLVX-tight-puro in the second. All cells were then selected with puromycin (2.5 µg/ml) or/and blasticidin (2–4 µg/ml) and alternatively sorted by FACS (1–3 rounds) after transient (24 h) induced expression by Dox. Cells without fluorescent protein were cloned and tested by western blot. SC $pkn3^{-/-}$ cells from clone 1 were used for reintroduction of PKN3 (mCherry-Flag fused constructs).

To re-introduce GFP fused p130Cas variants to p130Cas $^{-/-}$ MEFs, a retroviral pBabe system was used. After infection of p130Cas $^{-/-}$ MEFs by viral supernatants prepared in HEK293T cells co-transfected by pVSV-G, Gag-Pol, and pBabe plasmids, respectively, GFP positive cells were selected by FACS.

MDA-MB-231 cells were provided by Dr. Marie Zadinova from Charles University. All transfections were carried out according to the manufacturer's protocol using Jet Prime (Polyplus Transfection) or PEI transfection reagent (Polysciences). All cells were cultivated in full DMEM (Sigma) with 4.5 g/l L-glucose, L-glutamine, and pyruvate, supplemented with 10% FBS (Sigma) and ciprofloxacin (0.01 mg/ml) at 37 °C and 5% CO₂. Cells were confirmed as being negative for mycoplasma contamination by PCR.

Plasmid construction

cDNAs coding for p130Cas SRD domain variants (WT, 15AN; sequences provided in Table S1) were commercially synthesized and cloned into the pMA-T vector (geneArt, Life Technologies). The 15AN variant was generated by mutation of all 15 Ser/Thr to Ala or Asn. Mutant variant S432A (KRLS to KRLA) was created subsequently by whole plasmid synthesis using Q5 polymerase (New England Biolabs) and respective site-directed mutagenesis primers (listed in Table S2). Following PCR, 5U of DpnI was added to each reaction and incubated for 1.5 h at 37 °C. Individual mutated clones were screened by sequencing. Sequences of all SRD variants were then switched with the original p130Cas SRD domain cassette within the p130Cas sequence (pUC19 vector) using Bpu10I/SacII sites. pEGFP-C1 p130Cas variants and pGEX-p130Cas-SH3 domain constructs were prepared similarly as described previously (Janoštiak et al., 2011; Braniš et al., 2017). GFP-fused p130Cas variants were introduced into the pBABE retroviral expression vector by EcoRI and blunt end (generated by BamHI/AgeI restriction followed by fill in by Klenow) cloning. All constructs were verified by sequencing. To prepare the GSK3-derived peptide fused to GST, a pair of phosphorylated oligonucleotides (see Table S2) was annealed and inserted in frame at the 3' end of the GST (pGEX vector) using BamHI/EcoRI sites. Production of GST fused proteins (SH3, GSK3) from the pGEX

system were carried out as in Gemperle et al. (Gemperle et al., 2017). Oligos for sgRNA construction and primers for CRISPR off-target screening were designed and plasmids constructed (LentiCRISPR, BsmBI site) as published (Ran et al., 2013) and are listed in Table S2. PKN3 shRNA was cloned into a lentivirus-adapted vector system allowing Dox-inducible expression of shRNAs (Czauderna et al., 2003) via PCR followed by ligation and DpnI mediated cleavage of template DNA. Primers are listed in Table S2. Correct insertion of the shRNA sequence was confirmed first by restriction analysis to confirm the reintroduced BsrGI restriction site, and then with DNA sequence analysis.

cDNAs coding for whole mouse PKN3 with added sequence for Flag epitope and shorter sequence with mutations to create mPR and KD variants (sequences provided in Table S1) were commercially synthesized and cloned into pMK-RQ or in pMA-T vectors, respectively (geneArt, Life Technologies). The mPR mutant was created to abrogate binding to p130Cas (motif P₅₀₀PPKPPR to PAPSAPR) similarly as suggested in Gemperle et al. (Gemperle et al., 2017). The KD mutation was designed as published for human PKN3 (Leenders et al., 2004). Sequence for mPR was swapped within whole PKN3 in the pMK-RQ vector using NdeI/HindIII sites, and that for KD by NdeI/BamHI followed by cloning PKN3 variants (WT, mPR, KD) to other corresponding vectors: mCherryC1/eGFP C1 (BsrGI/EcoRI), pMSCV-Puro (XhoI/EcoRI), and pLVX-Tight-Puro (BsrGI/EcoRI). A lentiviral expression vector pLVX-Tight-Puro allowing Dox-inducible gene expression was also prepared with mCherry-fused PKN3 variants via NheI/EcoRI and XbaI/EcoRI sites. Flag-fused mCherry control was prepared similarly, except prior to cloning to the pLVX-Tight-Puro system, Flag sequence was inserted in frame in front of mCherry in mCherry C1 vector by annealing the phosphorylated oligonucleotides described in Table S2 and digested NheI/HindIII vector sites. Prior to kinase reactions in vitro, Flag-PKN3 was also cloned to the StrepII pcDNA3 vector using blunt end ligation (AfeI/EcoRV vector sites, Flag-PKN3 cleaved from pMSCV-puro by BsrGI/EcoRI and filled in by Klenow). CFP or mCherry-fused LifeAct was prepared as published (Riedl et al., 2008). All constructs were verified first by restriction analysis and then by sequencing.

Preparation of cell extracts and immunoblotting

Cell were lysed in RIPA (total lysates; composition: 150 mM NaCl; 50 mM Tris-HCl, pH 7.4, 1 % Nonidet P-40, 0.1 % SDS, 1 % sodium deoxycholate, 5 mM EDTA, 50 mM NaF) or in 1% Triton lysis buffer (immunoprecipitations, pull downs; composition: 50 mM Tris HCl [pH 7.1], with 150 mM NaCl and 1% TRITON X-100) supplemented with protease (MixM; SERVA) and phosphatase inhibitors (MixII; SERVA) followed by immunoblotting as described previously (Janoštiak et al., 2014). In brief: protein extracts were separated using SDS-PAGE under denaturing conditions (6–15 % gels) and were transferred to nitrocellulose membrane (Bio-Rad Laboratories). Membranes were blocked with 4 % BSA or 3% milk-TBST (Tris-buffered saline and 0.05% Tween 20), incubated with the indicated primary antibodies overnight at 4 °C, and then incubated with HRP-linked secondary antibodies at RT for 1 h, washed extensively in TBST, and developed using an AI600 System (GE Healthcare). To improve the separation of p130Cas by SDS-PAGE, a ratio of acrylamide/bisacrylamide 30:0.2 was used.

Immunoprecipitations (see kinase assays, below), pull-downs, and far western experiments were carried out similarly as in Gemperle et al. and Janoštiak et al. (Gemperle et al., 2017 and Janoštiak et al., 2014). For far-western-blot analysis, the protein blots were incubated with 2 $\mu\text{g/ml}$ recombinant human GST-p130Cas/BCAR1 (Abcam) or purified mouse GST-p130Cas SH3 diluted in 1 % BSA in TBST overnight followed by washing with TBST and incubation (2 h, 4 °C) with anti-GST antibody (Sigma). After extensive washing with TBST, blots were treated with HRP-conjugated secondary antibodies and developed using the AI600 System. Band intensity was determined using Fiji (ImageJ; National Institutes of Health; Schindelin et al., 2012).

Kinase assays

Cells were transfected with either Flag- or StrepII-fused mouse PKN3 (WT or KD) using the PEI transfection reagent (Polysciences) according to manufacturer instructions. After 48 h, cells were washed with PBS and lysed in standard lysis buffer (50 mM Tris-HCl [pH 7.1], 150 mM NaCl, 1 % Triton-X-100) with protease and phosphatase inhibitors (SERVA) and 10 mM glycerol-2-phosphate (Sigma). Proteins were immunoprecipitated with anti-Flag M2 affinity resin (Sigma) and eluted with Flag peptide as described previously (Unsal-Kacmaz et al., 2011). StrepII-fused PKN3 was precipitated with Strep-Tactin® Superflow® resin (IBA Lifesciences) and eluted with 1 \times Buffer E (Strep-Tactin Elution Buffer, IBA Lifesciences). Kinase assays were carried out in conditions described previously (Unsal-Kacmaz et al., 2011; Leenders et al., 2004). GFP-fused p130Cas variants (WT, 15AN, S432A; see plasmid construction section, above) were immunoprecipitated from transiently transfected cells using anti-GFP 3E6 antibody (Invitrogen) and nProtein A Sepharose 4 Fast Flow (GE Healthcare). Subsequently, immobilized p130Cas was dephosphorylated using Lambda protein phosphatase (New England Biolabs) as specified by the manufacturer. Phosphatase was inactivated by two washes with TBS containing 10 mM sodium orthovanadate and 20 mM EDTA and two washes with TBS and p130Cas variants were eluted with 0.1 M glycine pH 3.5 for 10 min in RT. After elution, pH was equilibrated by adding the corresponding volume of 1 M Tris pH 9.2 and proteins were used as a substrate in reaction with 1 mM ATP γ S (Sigma). After 45 min in 35 °C, reactions were stopped with EDTA to a final concentration of 20 mM and alkylated with 50 mM p-nitrobenzyl mesylate (Abcam) at RT for 2 h. Samples were resolved using SDS-PAGE and immunoblotted using anti-thiophosphate ester antibody (clone 51-8, Abcam). GSK3-derived peptide fused to GST was prepared and used as a positive control for PKN3 activity as described previously (Unsal-Kacmaz et al., 2011) and its phosphorylation detected by anti-Phospho-GSK-3 α/β antibody. For autoradiography, kinase reactions were performed similarly, with 5 μCi [γ -³²P] ATP added to the reaction. The samples were heated for 10 min at 95 °C, resolved using SDS-PAGE, and subjected to autoradiography.

2D and 3D migration assays

Scratch-based migration assays in 2D were carried out using an IncuCyte automated imaging system (Essen BioScience). Briefly, MEFs with Dox-inducible PKN3 WT were seeded onto 96-well plates (Corning) at a density of 100,000 cells/well (10% serum in

DMEM) and half of the wells were supplemented with Dox (final 250 ng/ml). After 24 h, monolayers of cells were scratched using a scratching apparatus that produced strongly identical scratches in each well. The IncuCyte system was programmed to obtain real-time phase-contrast images of the wounds every 2 h for 2 days. Cell migration was automatically quantified and expressed as relative wound density, which indicates the ratio of sharpness of the wounded area and of the adjacent non-wounded area. The IncuCyte imaging system was then used to automatically calculate the area of each wound at each time point up to the point of complete closure of the wound from an average of the quadruplicate.

3D cell zone exclusion assays were carried out using the JuLI™ Br (NanoEnTek) system with two microscopes situated in the incubator. Collagen R solution (4 mg/ml, SERVA) was diluted to the final mix: 1 mg/ml collagen, 1 % serum (to decrease the effect of proliferation), 1× DMEM, 15 mM HEPES (750 mM), 8.5 mM NaOH (1 M), 0.4 % NaHCO₃ (7.5 %, Sigma), and 5 µg/ml folic acid. Next, 40 µl of the collagen mix was then added into each well (total 6) of two 96-well plates and let to polymerize at 37 °C. Cell suspension (100 µl; 1 × 10⁶ cells/ml) non-induced or 24 h Dox-preinduced cells were added on top of the collagen gel. After cell attachment (4 h), the medium was removed and scratch was performed. Immediately after removal of the rest of media in the generated wound, another layer of collagen mix (100 µl) was added (schema of the experiment is shown in Van Troys et al. (Van Troys et al., 2018)). Collagen was allowed to polymerize for 15 min at RT to prevent formation of bubbles in the collagen interface, then for another 15 min at 37 °C. Finally, 100 µl of DMEM with 1 % serum supplemented with or without Dox (500 ng/ml) was added on the top of each well and CellTracker software (Piccinini et al., 2015) was used to manually track at least 60 random (fastest) (top) migrating cells across the cell/collagen interface in the main focal plane from three independent replicates. To create cell migration/tracking maps the “Chemotaxis And Migration Tool” version 2.0 (Ibidi) was used.

2D proliferation and 3D cultures in Matrigel

To determine the difference in cell proliferation capacity among individual clones, an AlamarBlue assay was used. For this, 10,000 cells per well were seeded in a 96-well plate and after cell attachment (4 h), medium was removed and replaced by a culture medium solution containing 10 % AlamarBlue. The plates were further incubated for 2 h at 37 °C prior to initial cell mass measurement followed by replacing with standard medium (± Dox if required). Cell growth was then measured again after 72 h using a culture medium solution containing 10 % AlamarBlue to assess the increment of cell mass. Absorbance was measured at 570 nm (with reference at 600 nm) using an Infinite M200 PRO microplate reader. As a control, AlamarBlue was added to the cell growth medium without cells. The assay was performed in triplicates and was repeated three times.

xCELLigence RTCA technology, which provides highly standardized experimental conditions, was used to study cell proliferation. The cells were counted (100,000/ml) and then separated to supplement one part with Dox (final 250 ng/ml) and one part without. Subsequently, 10,000 cells with or without Dox were seeded per well of an xCELLigence E-plate in triplicate, left to sit for 30 min at RT, and then transferred to the xCELLigence

RTCA device. Data were collected every 30 min for 48–72 h. All data were recorded using RTCA Software version 2.0, which generated curve-slope values reflecting the speed of cell growth. Cell growth was calculated from the log growth phase of the curve starting 4–9 h post Dox-induction followed by processing in MS Excel and comparison to non-induced controls. E-plates were recycled to remove cells and used repeatedly up to three times.

SC cells were embedded into Matrigel (Corning) as previously published (Unsal-Kacmaz et al., 2011). In brief, cells grown in 6-cm dishes with or without Dox for 24 h were detached from culture dishes and suspended in Matrigel solution (per well: 80 μ l of Matrigel and 20 μ l of medium with 10 % serum and 20 ,000 cells) at 4 °C. Then, 100 μ l of this Matrigel-embedded cell suspension was overlaid on 40 μ l of Matrigel in a 96-well plate. The plate was allowed to solidify at 37 °C in the incubator. After 30 min, DMEM \pm Dox (500 ng/ml) was added and replaced every 2–3 days. After 7 days, multicellular clusters were imaged using differential interference contrast (DIC) microscopy (Nikon-Eclipse TE2000-S) and analyzed from duplicated wells. Quantification was based on at least three independent experiments.

Microscopy and immunostaining

Confocal images/movies were acquired using a Leica TCS SP2 or SP8 confocal microscope system equipped with a Leica 63 \times /1.45 oil objective (two HyD detectors and two standard PMT detectors, Leica LAS-AF software) followed by processing in Fiji.

Cells were seeded on cover slips coated with human FN 10 μ g/ml (Invitrogen), grown for 24 to 48 h, and subsequently fixed in 4 % PFA, permeabilized in 0.5 % TritonX-100, washed extensively with PBS, and blocked in 3 % BSA. The cells were then sequentially incubated with primary antibody (dilution according to manufacturer protocol) for 2 h, secondary antibody for 60 min, and Alexa Fluor 594 phalloidin (Molecular Probes) for 15 min, with extensive washing between each step. In addition, slides were mounted with Mowiol 4–88 (475904; EMD Millipore) containing 2.5 % 1,4-diazobicyclo-[2.2.2]-octane (D27802; Sigma-Aldrich) in the presence or absence of DAPI for nuclear staining and imaged at RT.

Colocalization analyses of PKN3 with p130Cas and actin in lamellipodia were conducted on live cells co-transfected by mCherry-PKN3 variants (mPR, WT, –), GFP-p130Cas and CFP fused LifeAct. Alternatively, GFP-PKN3 variants and mCherry-LifeAct were used. The cells were placed on glass-bottom dishes (MatTek,) coated with 10 μ g/ml FN, transfected, and cultured for 24 h before the experiment. Movies were acquired of cells in DMEM without phenol red supplemented with 10 % Serum at 37 °C and 5 % CO₂ using a Leica TCS SP2 or SP8 confocal microscope (63 \times /1.45 oil objective). Quantification of mCherry-PKN3 WT, mCherry-PKN3 mPR, and mCherry localization to lamellipodia (lifeActin as marker) was calculated by measuring the signal ratio of mCherry fluorescence in lamellipodium versus in cytosol (5 μ m from lamellipodium). A total of 160 measurements (50 living cells) gathered in three independent experiments were performed using Fiji.

Gelatin degradation assay was performed according to the manufacturer instructions (QCM™ Gelatin Invadopodia Assay, Merck Millipore). Cells were seeded on gelatin supplemented with DMEM, 10 % serum with or without Dox, and gelatin degradation was assessed after 48 h using a Nikon-Eclipse TE2000-S (10×/0.25 or 20×/0.40 Nikon objective) followed by processing in Fiji.

Lung metastases on the lung parenchyma were visualized using a Carl Zeiss AxioZoom.V16 fluorescence microscope followed by processing in Fiji.

Subcutaneous mouse tumor models

Nu/nu mice (total 48, n = 12 per group), 8-week old, were subcutaneously injected with 1×10^6 GFP-positive SC cells (200 μ l of suspension in PBS) that either expressed endogenous PKN3 (group 1) or lacked PKN3 expression (group 2, 3, and 4). These cells expressed mCherry vector (group 1 and 2), mCherry-fused Flag-PKN3 WT (group 3), or mCherry-fused Flag-PKN3 mPR (group 4) induced by doxycycline hydrochloride, which was administered via Dox pellets (200 mg/kg) on the day of cell injection. After 16 (group 1, faster tumor growth) or 21–22 days (within groups 2–4), tumors were surgically removed under total body anesthesia and their weight was determined, followed by disruption by a tissue tearor in RIPA lysis buffer containing protease inhibitors (Serva) and preclearance by centrifugation at 16,000 g at 4 °C for 30 min. Tissue lysates were normalized to GFP level (Infinite M200 PRO) and analyzed by immunoblotting (SDS-PAGE separation or dot blot) as described in Janoštiak et al. (Janoštiak et al., 2014). Post-operation, doxycycline hydrochloride was administered via drinking water at 0.2 mg/ml and supplemented with 1 % sucrose. Animals in group 1 were killed 14 days post-surgery, and in groups 2–4 at 21 days post-surgery, and their lungs were collected. Immediately at sacrifice the right lungs were washed in PBS and viewed under a fluorescence microscope to analyze GFP and mCherry-positive metastases grown on the surface, as well as within the lung parenchyma. Right lungs were fixed for 72 h in 4 % PFA for immunohistochemistry analysis. All experiments (surgery, cell transplantation, measurement of tumor weight) were performed blinded and independently by two researchers, and in compliance with the guidelines of the Ministry of Education, Youth and Sports of CR (institutional approval no.70030/2013-MZE-17214).

In silico analysis

Data of invasive breast carcinoma (1100 tumors in TCGA, provisional) and prostate adenocarcinoma studies (499 tumors, TCGA, provisional) were retrieved from and analyzed using the cBio Cancer Genomics Portal (cbioportal.org) (Gao et al., 2013) or processed using the SigmaPlot software package (Systat Software, Inc., Point Richmond, CA). The available data on protein phosphorylation levels of p130Cas/BCAR1 were renumbered from isoform 6 (Ser474) to isoform 1 (corresponding to Ser432)

Statistical analysis

Statistical analyses were performed using the SigmaPlot software package (Systat Software, Inc.). Data with a normal distribution were subjected to one-way ANOVA, whereas data failing the normality test were analyzed by one-way ANOVA on ranks

followed by Dunn's post hoc comparison. All compared groups passed an equal variance test. Where not indicated differently, the same cells treated or not treated by Dox were compared. Graphs were created using GraphPad Prism 6. Data are reported as the means \pm SD unless otherwise indicated. Correlations statistics were calculated according to the Spearman's rank and Pearson correlation methods. A p-value of 0.05 was considered as the threshold for statistical significance. P-values are indicated in the figure legends.

Online supplemental material

Fig. S1 shows confirmation of PKN3 kinase inactivity, and another western blot showing PKN3 phosphorylation on Thr849 influenced by p130Cas variant expression and that PKN3 colocalizes with stress fibers. Fig. S2 shows PKN3 autophosphorylation, the phospho-pattern of p130Cas from suspension cells, and co-expression of human p130Cas/BCAR1 and PKN3 in prostate and breast tumors. Fig. S3 shows the influence of PKN3 and GFP-p130Cas variants expression on cell morphology and proliferation. Fig. S4 shows that PKN3 induction does not change the activation status of STAT3, ERK, Akt, MLC, and mTOR signaling (only slight increase in Src activity) in cells growing on plastic and that PKN3-dependent invasiveness is independent of phosphorylation in p130Cas SRD. Fig. S5 shows that PKN3 crosstalk with Src is p130Cas dependent. Furthermore, Fig. S5 also provides additional information relevant to tumors and metastasis. Fig. S6 shows that PKN3 binds strongly to the p130Cas SH3 domain and do not bind to the p130Cas SRD domain. Movies S1–S3 show that only PKN3 WT clearly localizes to lamellipodia of p130Cas^{-/-} MEFs re-expressing p130Cas co-transfected by GFP-PKN3 variants and mCherry-LifeActin. Movies S4–S5 show (3D cell zone exclusion assay) that PKN3 increases cell migration velocity in collagen only in the presence of p130Cas. Tables S1 and S2, included as an Excel files, provide a list of synthesized cDNA sequences (geneArt) or oligonucleotides, respectively, used in this study.

Acknowledgements

This work was funded by Czech Science Foundation grants 15-17419S and 15-07321S, by the Ministry of Education, Youth and Sports of CR within the LQ1604 National Sustainability Program II (Project BIOCEV-FAR), by the project „BIOCEV“ (CZ.1.05/1.1.00/02.0109), and by the Charles University Grant Agency (224217). We acknowledge support by the MEYS CR (CZ.02.1.01/0.0/0.0/16_013/0001775 Czech-BioImaging) and support by the Imaging Methods Core Facility at BIOCEV Institution supported by the Czech-BioImaging large RI project (LM2015062 funded by MEYS CR) for their support with obtaining imaging data presented in this paper. We thank Marie Charvátová for technical help and L. Janečková for help with immunohistochemistry. We acknowledge Pfizer as the source of the materials and thank Dr. Keziban Unsal-Kacmaz by providing the anti-phospho Thr849 PKN3 antibody (human Thr860). We would like to thank Editage (www.editage.com) for English language editing.

The authors declare no competing financial interests and no conflict of interests.

Author contributions: Conceptualization, J. Gemperle, D. Rosel, and J. Brábek; methodology, J. Gemperle, M. Dibus, and L. Koudelková; investigation, J. Gemperle, M. Dibus, D. Rosel, and J. Brábek; resources, J. Brábek; writing: original draft, J. Gemperle; writing: reviewing, J. Gemperle, M. Dibus, D. Rosel, and J. Brábek; visualization, J. Gemperle; supervision, J. Brábek and D. Rosel; funding acquisition, J. Gemperle, M. Dibus, J. Brábek, and D. Rosel.

Footnotes

Abbreviations used: BCAR1 = breast cancer anti-estrogen resistance protein 1; Dox = doxycycline; FN = fibronectin; KO = knockout; mPR = mutation P₅₀₀PPKPPRL to PAPSAPRL (mouse PKN3 mutant unable to bind p130Cas); MEF = mouse embryonic fibroblast; PKN3 = protein kinase N3; p130Cas = Crk-associated substrate (size 130 kDa); RTCA = real-time cell analysis; SC = p130Cas^{-/-}; MEFs re-expressing p130Cas transformed by SrcF; SCpkn3^{-/-} = SC PKN3 KO; SrcF = constitutively active Src (Src Y527F).

References

- Aleku, M., P. Schulz, O. Keil, A. Santel, U. Schaeper, B. Dieckhoff, O. Janke, J. Endruschat, B. Durieux, N. Röder, K. Löffler, C. Lange, M. Fechtner, K. Möpert, G. Fisch, S. Dames, W. Arnold, K. Jochims, K. Giese, B. Wiedenmann, A. Scholz, and J. Kaufmann. 2008. Atu027, a liposomal small interfering RNA formulation targeting protein kinase N3, inhibits cancer progression. *Cancer Res.* 68:9788–9798.
- Astier, A., S.N. Manié, H. Avraham, H. Hirai, S.F. Law, Y. Zhang, E.A. Golemis, Y. Fu, B.J. Druker, N. Haghayeghi, A.S. Freedman, and S. Avraham. 1997. The related adhesion focal tyrosine kinase differentially phosphorylates p130Cas and the Cas-like protein, p105HEF1. *J. Biol. Chem.* 272:19719–19724.
- Brábek, J., S.S. Constancio, N.Y. Shin, A. Pozzi, A.M. Weaver, and S.K. Hanks. 2004. CAS promotes invasiveness of Src-transformed cells. *Oncogene.* 23:7406–7415.
- Brábek, J., S.S. Constancio, P.F. Siesser, N.Y. Shin, A. Pozzi, and S.K. Hanks. 2005. Crk-associated substrate tyrosine phosphorylation sites are critical for invasion and metastasis of Src-transformed cells. *Mol. Cancer Res.* 3:307–315.
- Braniš, J., C. Pataki, M. Spörrer, R.C. Gerum, A. Mainka, V. Cermak, W.H. Goldmann, B. Fabry, J. Brabek, and D. Rosel. 2017. The role of focal adhesion anchoring domains of CAS in mechanotransduction. *Sci. Rep.* 7:46233.
- Cabodi, S., L. Moro, G. Baj, M. Smeriglio, P. Di Stefano, S. Gippone, N. Surico, L. Silengo, E. Turco, G. Tarone, and P. Defilippi. 2004. p130Cas interacts with estrogen receptor alpha and modulates non-genomic estrogen signaling in breast cancer cells. *J. Cell Sci.* 117:1603–1611.
- Cabodi, S., A. Tinnirelo, P. Di Stefano, B. Bisarò, E. Ambrosino, I. Castellano, A. Sapino, R. Arisio, F. Cavallo, G. Forni, M. Glukhova, L. Silengo, F. Altruda, E. Turco, G. Tarone, and P. Defilippi. 2006. p130Cas as a new regulator of mammary epithelial cell proliferation, survival, and HER2-Neu oncogene-dependent breast tumorigenesis. *Cancer Res.* 66:4672–4680.
- Cabodi, S., M. del Pilar Camacho-Leal, P. Di Stefano, and P. Defilippi. 2010. Integrin signalling adaptors: not only figurants in the cancer story. *Nat. Rev. Cancer.* 10:858–870.
- Cabodi, S., A. Tinnirello, B. Bisaro, G. Tornillo, M. del Pilar Camacho-Leal, G. Forni, R. Cojoca, M. Iezzi, A. Amici, M. Montani, A. Eva, P. Di stefano, S.K. Muthuswamy, G. Tarone, E. Turco, and P. Defilippi. 2010. p130Cas is an essential transducer element in ErbB2 transformation. *FASEB J.* 24:3796–3808.
- Collazos, A., N. Michael, R.D. Whelan, G. Kelly, H. Mellor, L.C. Pang, N. Totty, and P.J. Parker. 2011. Site recognition and substrate screens for PKN family proteins. *Biochem. J.* 438:535–543.
- Czauderna, F., A. Santel, M. Hinz, M. Fechtner, B. Durieux, G. Fisch, F. Leenders, W. Arnold, K. Giese, A. Klippel, and J. Kaufmann. 2003. Inducible shRNA expression for application in a prostate cancer mouse model. *Nucleic Acids Res.* 31:e127.
- Defilippi, P., P. Di Stefano, and S. Cabodi. 2006. p130Cas: a versatile scaffold in signaling networks. *Trends Cell Biol.* 16:257–263.

- Donato, D.M., L.M. Ryzhova, L.M. Meenderink, I. Kaverina, and S.K. Hanks. 2010. Dynamics and mechanism of p130Cas localization to focal adhesions. *J. Biol. Chem.* 285:20769–20779.
- Dorssers, L.C., S. Van der Flier, A. Brinkman, T. van Agthoven, J. Veldscholte, E.M. Berns, J.G. Klijn, L.V. Beex, and J.A. Foekens. 2001. Tamoxifen resistance in breast cancer: elucidating mechanisms. *Drugs*, 61:1721–1733.
- Dorssers, L.C., N. Grebenchtchikov, A. Brinkman, M.P. Look, S.P. van Broekhoven, D. de Jong, H.A. Peters, H. Portengen, M.E. Meifer-van Gelder, J.G. Klijn, D.T. van Tienoven, A. Geurts-Moespot, P.N. Span, J.A. Foekens, and F.C. Sweep. 2004. The prognostic value of BCAR1 in patients with primary breast cancer. *Clin. Cancer Res.* 10:6194–6202.
- Fonseca, P.M., N.Y. Shin, J. Brábek, L. Ryzhova, J. Wu, and S.K. Hanks. 2004. Regulation and localization of CAS substrate domain tyrosine phosphorylation. *Cell Signal.* 16:621–629.
- Fromont, G., G. Vallancein, P. Validire, P. Levillain, and O. Cussenot. 2007. BCAR1 expression in prostate cancer: Association with 16q23 LOH status, tumor progression and EGFR/KAI1 staining. *Prostate.* 67:268–273.
- Fromont, G. and O. Cussenot. 2011. The integrin signalling adaptor p130CAS is also a key player in prostate cancer. *Nat. Rev. Cancer.* 11:227.
- Gao, J., B.A. Aksoy, U. Dogrusoz, G. Dresdner, B. Gross, S.O. Sumer, Y. Sun, A. Jacobsen, R. Sinha, E. Larsson, E. Cerami, C. Sander, and N. Schultz. 2013. Integrative analysis of complex cancer genomics and clinical profiles using the cBioPortal. *Sci. Signal.* 6: p11.
- Garcia-Guzman, M., F. Dolfi, M. Russello, and K. Vuori. 1999. Cell adhesion regulates the interaction between the docking protein p130(Cas) and the 14-3-3 proteins. *J. Biol. Chem.* 274:5762–5768.
- Gemperle, J., R. Hexnerová, M. Lepšík, P. Tesina, M. Dibus, M. Novotný, J. Brábek, V. Veverka, and D. Rösel. 2017. Structural characterization of CAS SH3 domain selectivity and regulation reveals new CAS interaction partners. *Sci. Rep.* 7:8057.
- Hashimoto, T., H. Mukai, T. Kawamata, T. Taniguchi, Y. Ono, and C. Tanaka. 1998. Localization of PKN mRNA in the rat brain. *Brain Res. Mol. Brain Res.* 59:143–153.
- Hivert, V., J. Pierre, and J. Raingeaud. 2009. Phosphorylation of human enhancer of filamentation (HEF1) on serine 369 induces its proteasomal degradation. *Biochem. Pharmacol.* 78:1017–1025.
- Honda, H., H. Oda, T. Nakamoto, Z. Honda, R. Sakai, T. Suzuki, T. Saito, K. Nakamura, K. Nakao, T. Ishikawa, M. Katsuki, Y. Yazaki, and H. Hirai. 1998. Cardiovascular anomaly, impaired actin bundling and resistance to Src-induced transformation in mice lacking p130Cas. *Nat. Genet.* 19:361–365.
- Janoštiak, R., O. Tolde, Z. Brůhová, M. Novotný, S.K. Hanks, D. Rösel, and J. Brábek. 2011. Tyrosine phosphorylation within the SH3 domain regulates CAS subcellular localization, cell migration, and invasiveness. *Mol. Biol. Cell.* 22:4256–4267.
- Janoštiak, R., J. Brábek, V. Auernheimer, Z. Tatárová, L.A. Lautscham, T. Dey, J. Gemperle, R. Merkel, W.H. Goldmann, B. Fabry, and D. Rösel. 2014. CAS directly

- interacts with vinculin to control mechanosensing and focal adhesion dynamics. *Cell. Mol. Life Sci.* 71:727–744.
- Kang, H., C. Kim, H. Lee, J.G. Rho, J.W. Seo, J.W. Nam, W.K. Song, S.W. Nam, W. Kim, and E.K. Lee. 2015. Downregulation of microRNA-362-3p and microRNA-329 promotes tumor progression in human breast cancer. *Cell Death Differ.* 23:484–495.
- Lachmann, S., A. Jevons, M. De Rycker, A. Cassamassima, S. Radtke, A. Collazos, and P.J. Parker. 2011. Regulatory domain selectivity in the cell-type specific PKN-dependence of cell migration. *PLoS One*, 6:e21732.
- Leenders, F., K. Möpert, A. Schmiedeknecht, A. Santel, F. Czuderna, M. Aleku, S. Penschuck, S. Dames, M. Dternberger, T. Röhl, A. Wellmann, W. Arnold, K. Giese, J. Kaufmann, and A. Klippel. 2004). KN3 is required for malignant prostate cell growth downstream of activated PI 3-kinase. *EMBO J.* 23:3303–3313.
- Lim, W.G., X. Chen, J.P. Liu, B.J. Tan, S. Zhou, A. Smith, N. Lees, L. Hou, F. Gu, X.Y. Yu, Y. Du, D. Smith, C. Verma, K. Kiu, and W. Duan. 2008. The C-terminus of PRK2/PKN γ is required for optimal activation by RhoA in a GTP-dependent manner. *Arch. Biochem. Biophys.* 479L:170–178.
- Makkinje, A., R.I. Near, G. Infusini, P. Vanden Borre, A. Bloom, D. Cai, C.E. Costello, and A. Lerner. 2009. AND-34/BCAR3 regulates adhesion-dependent p130Cas serine phosphorylation and breast cancer cell growth pattern. *Cell Signal.* 21:1423–1435.
- Mellor, H., P. Flynn, C.D. Nobes, A. Hall, and P.J. Parker. 1998. PRK1 is targeted to endosomes by the small GTPase, RhoB. *J. Biol. Chem.* 273:4811–4814.
- Möpert, K., K. Löffler, N. Röder, J. Kaufmann, and A. Santel. 2012. Depletion of protein kinase N3 (PKN3) impairs actin and adherens junctions dynamics and attenuates endothelial cell activation. *Eur. J. Cell Biol.* 91:694–705.
- Mukai, H., A. Muramatsu, R. Mashud, K. Kubouchi, S. Tsujimoto, T. Hongu, Y. Kanaho, M. Tsubaki, S. Nishida, G. Shiol, S. Danno, M. Mehruba, R. Satoh, and R. Sugirua. 2016. PKN3 is the major regulator of angiogenesis and tumor metastasis in mice. *Sci. Rep.* 6:18979.
- Mukai, H. and Y. Ono. 1994. A novel protein kinase with leucine zipper-like sequences: its catalytic domain is highly homologous to that of protein kinase C. *Biochem. Biophys. Res. Commun.* 199:897–904.
- Nagai, Y., K. Osawa, H. Fukushima, Y. Tamura, K. Aoki, K. Ohya, H. Yasuda, H. Hikiji, M. Takahashi, Y. Seta, S. Seo, M. Kurokawa, S. Kato, H. Honda, I. Nakamura, K. Maki, and E. Jimi. 2013. p130Cas, Crk-associated substrate, plays important roles in osteoclastic bone resorption. *J. Bone Miner. Res.* 28:2449–2462.
- Nick, A.M., R.L. Stone, G. Armaiz-Pena, B. Ozpolat, I. Tekedereli, W.S. Graybill, C.N. Landen, G. Villares, P. Vivas-Mejia, J. Bottsford-Miller, H.S. Kim, J.S. Lee, S.M. Kim, K.A. Baggerly, P.T. Ram, M.T. Deavers, R.L. Coleman, G. Lopez-Berenstein, and A.K. Sood. 2011. Silencing of p130cas in ovarian carcinoma: a novel mechanism for tumor cell death. *J. Natl. Cancer Inst.* 103:1596–1612.
- Nikonova, A. S., A.V. Gaponova, A.E. Kudinov, and E.A. Golemis. 2014. CAS proteins in health and disease: An update. *IUBMB Life.* 66:387–395.

- Oishi, K., H. Mukai, H. Shibata, M. Takahashi, and Y. Ona. 1999. Identification and characterization of PKNbeta, a novel isoform of protein kinase PKN: expression and arachidonic acid dependency are different from those of PKNalpha. *Biochem. Biophys. Res. Commun.* 261:808–814.
- Piccinini, F., A. Kiss, and P. Horvath. 2015. CellTracker (not only) for dummies. *Bioinformatics.* 32:955–957.
- Pylayeva, Y., K.M. Gillen, W. Gerald, H.E. Beggs, L.F. Reichardt, and F.G. Giancotti. 2009. Ras- and PI3K-dependent breast tumorigenesis in mice and humans requires focal adhesion kinase signaling. *J. Clin. Invest.* 119:252–266.
- Quilliam, L.A., Q.T. Lambert, L. Mickelson-Young, J.K. Westwick, A.B. Sparks, B.K. Kay, N.A. Jenkins, D.J. Gilbert, N.G. Copeland, and C.J. Der. 1996. Isolation of a NCK-associated kinase, PRK2, an SH3-binding protein and potential effector of Rho protein signaling. *J. Biol. Chem.* 271:28772–28776.
- Ran, F. A., P.D. Hsu, J. Wright, V. Agarwala, D.A. Scott, and F. Zhang. 2013. Genome engineering using the CRISPR-Cas9 system. *Nat. Protoc.* 8:2281–2308.
- Riedl, J., A.H. Crevenna, K. Kessenbrock, J.H. Yu, D. Neukirchen, M. Bista, F. Bradke, D. Jenne, T.A. Holak, Z. Werb, M. Sixt, and R. Wedlich-Soldner. 2008. Lifeact: a versatile marker to visualize F-actin. *Nat. Methods.* 5:605–607.
- Ruest, P.J., N.Y. Shin, T.R. Polte, X. Zhang, and S.K. Hanks. 2001. Mechanisms of CAS substrate domain tyrosine phosphorylation by FAK and Src. *Mol. Cell Biol.* 21:7641–7652.
- Santel, A., M. Aleku, N. Röder, K. Möpert, B. Durieux, O. Janke, O. Keil, J. Endruschat, S. Dames, C. Lange, M. Eisermann, K. Löffler, M. Fechtner, G. Fixch, C. Vank, U. Schaeper, K. Giese, and J. Kaufmann. 2010. Atu027 prevents pulmonary metastasis in experimental and spontaneous mouse metastasis models. *Clin. Cancer Res.* 16:5469–5480.
- Schindelin, J., I. Arganda-Carreras, E. Frise, V. Kaynig, M. Longair, T. Pietzsch, C. Rueden, S. Saalfeld, B. Schmid, J.Y. Tinevez, D. White, v. Hartenstein, K. Eliceiri, P. Tomancak, and A. Cardona. 2012. Fiji: an open-source platform for biological-image analysis. *Nat. Methods.* 9:676–682.
- Schultheis, B., D. Strumberg, A. Santel, C. Vank, F. Gebhardt, O. Keil, C. Lange, K. Giese, J. Kaufmann, M. Khan, and J. Drevs. 2014. First-in-human phase I study of the liposomal RNA interference therapeutic Atu027 in patients with advanced solid tumors. *J. Clin. Oncol.* 32:4141–4148.
- Strumberg, D., B. Schultheis, U. Traugott, C. Vank, A. Santel, O. Keil, K. Giese, J. Kaufmann, and J. Drevs. 2012. Phase I clinical development of Atu027, a siRNA formulation targeting PKN3 in patients with advanced solid tumors. *Int. J. Clin. Pharmacol. Ther.* 50:76–78.
- Ta, H.Q., K.S. Thomas, R.S. Schrecengost, and A.H. Bouton. 2008. A novel association between p130Cas and resistance to the chemotherapeutic drug adriamycin in human breast cancer cells. *Cancer Res.* 68:8796–8804.
- Tarone, G., D. Cirillo, F.G. Giancotti, P.M. Cornoglio, and P.C. Marchisio. 1985. Rous sarcoma virus-transformed fibroblasts adhere primarily at discrete protrusions of the ventral membrane called podosomes. *Exp. Cell Res.* 159:141–157.

- Tazaki, T., K. Miyazaki, E. Hiyama, T. Nakamoto, R. Sakai, N. Yamasaki, Z. Honda, M. Noda, N. Miyasaka, T. Sueda, and H. Honda. 2008. Functional analysis of Src homology 3-encoding exon (exon 2) of p130Cas in primary fibroblasts derived from exon 2-specific knockout mice. *Genes Cells*. :13:145–157.
- Tikhmyanova, N., J.L. Little, and E.A. Golemis. 2010. CAS proteins in normal and pathological cell growth control. *Cell. Mol. Life Sci.* 67:1025–1048.
- Tornillo, G., P. Defilippi, and S. Cabodi. 2014. Cas proteins: dodgy scaffolding in breast cancer. *Breast Cancer Res.* 16:443.
- Uehara, S, N. Udagawa, H. Mukai, A. Ishihara, K. Maeda, T. Yamashita, K. Murakami, M. Nishita, T. Nakamura, S. Kato, Y. Minami, and N. Takahashi. 2017. Protein kinase N3 promotes bone resorption by osteoclasts in response to Wnt5a-Ror2 signaling. *Science Signaling.* 10:ean0023.
- Unsal-Kacmaz, K., S. Rangunathan, E. Rosfjord, S. Dann, E. Upešlacis, M. Grillo, R. Hernandez, F. Mack, and A. Klippel. 2011. The interaction of PKN3 with RhoC promotes malignant growth. *Mol. Oncol.* 6:284–298.
- Van Troys, M., P. Masuzzo, L. Huyck, K. Bakkali, D. Waterschoot, L. Martens, and C. Ampe. 2018. Analysis of invasion dynamics of matrix-embedded cells in a multisample format. *Methods Mol. Biol.* 1749:79–117.
- Vincent, S., and J. Settleman. 1997. The PRK2 kinase is a potential effector target of both Rho and Rac GTPases and regulates actin cytoskeletal organization. *Mol. Cell Biol.* 17:2247–2256.
- Yamakita, Y., G. Totsukawa, S. Yamashiro, D. Fry, X. Zhang, S.K. Hanks, and F. Matsumura. 1999. Dissociation of FAK/p130(CAS)/c-Src complex during mitosis: role of mitosis-specific serine phosphorylation of FAK. *J Cell Biol.* 144:315–324.